# The Impact of Novel Sterilisation Methods on the Biological and Biomechanical Properties of Decellularised Heart Valves

**Sahirah Aslam**

Submitted in accordance with the requirements for the degree of Doctor of Philosophy

The University of Leeds

Institute of Medical and Biological Engineering

Faculty of Biological Sciences

School of Biomedical Sciences

September 2022

The candidate confirms that the work submitted is her own and that appropriate credit has been given where reference has been made to the work of others.

## Acknowledgments

I would firstly like to express my sincere gratitude to my supervisors, Dr Helen Berry, Professor Louise Jennings, Dr Amisha Desai and Dr Jennifer Edwards. Thank you for your expert guidance, encouragement and compassion throughout the past four years. Without the unwavering support that you have all individually provided, I would not have been able to complete this journey.

I would like to thank all members of the iMBE team for their contribution towards this project and my professional development. I wish to thank Dr Daniel Thomas, Mrs Nicola Conway and Dr James Warren for their infinite help, support, and patience. To my fellow peers, particularly Jacqueline Solis, Dr Patrick Lawson-Statham and Dr Kern Cowell, thank you for making this an enjoyable experience.

On a personal level, I would like to thank my wonderful family for providing me with unconditional love and support throughout my life. Especially to my beautiful nieces Anaya, Hoorain and Hareem, thank you all for melting away all of my PhD woes.

The biggest thank you goes to my darling husband, Wasim Islam. I cannot put into words how much of a positive impact you have had on me. Thank you for believing in me and supporting me always. I truly would not have made it if I did not have you by my side. I am eternally grateful for how happy and loved you make me feel.

This work is dedicated to my beloved father, Muhammad Aslam, my cherished grandmother, Jannat Bibi, and my dearest uncle, Mohammed Noor Din, who were sadly taken from us during my studies. My heart aches to see how proud you all would have been to share my joy and achievements.

## Abstract

Valvular heart disease has a major impact on patient morbidity and mortality on a global scale. Current heart valve replacement options present with numerous limitations. These can be addressed by the implementation of a novel decellularised heart valve replacement option that can meet clinical needs. However, decellularised heart valves require sterilisation prior to clinical use.

The aim of this study was to identify a novel sterilisation method that minimally impacts ECM structure and components, biochemical composition, biocompatibility, and biomechanical properties of decellularised porcine pulmonary heart valves (dPHVs).

Sterilisation of dPHVs with 1 mg/L copper chloride ($CuCl_2$) combined with 1 % hydrogen peroxide ($H_2O_2$) (pH 7) for 3 hours at 37 °C resulted in histoarchitectural alterations of the leaflets, a reduction in collagen thermal stability and a loss of tissue mechanical strength. However, the intensity of collagen IV and fibronectin immunolabelling was comparable to untreated dPHV tissue.

Supercritical carbon dioxide ($ScCO_2$) sterilisation (supplemented with 13.5 - 18.5 % [v/v] PAA and 4.5 - 6 % [v/v] $H_2O_2$) of dPHVs in Poly-Tyvek pouches resulted in the unanticipated compression of the whole dPHV macroscopic structure. $ScCO_2$ treatment of dPHVs in Poly-Tyvek pouches and dPHVs submerged in PBS resulted in a significant reduction in collagen IV immunolabelling and a reduction in collagen thermal stability in comparison to untreated dPHV controls. However, fibronectin immunolabelling was retained along with the ECM histoarchitecture, biochemical composition and tissue biomechanical properties.

$ScCO_2$ sterilisation of dPHVs submerged in PBS did not detrimentally impact valve competency, expansion characteristics and suture retention properties in comparison to untreated dPHV controls.

*In vitro* contact and extract cytotoxicity assessments demonstrated that both sterilisation methods investigated did not induce a cytotoxic response.

Overall, $ScCO_2$ sterilisation under submerged conditions may be the optimal method for the terminal sterilisation of dPHVs.

# Table of Contents

# List of Figures

# List of Tables

## List of Abbreviations

| | |
|---|---|
| AV | Atrioventricular |
| BSA | Bovine Serum Albumin |
| C.l | Confidence limits |
| CHAPS | 3-[(3-Cholamidopropyl)dimethylammonio]-1-propanesulfonate |
| DMB | 1,9-dimethylene blue |
| DMSO | Dimethyl sulfoxide |
| dPHV | Decellularised porcine pulmonary heart valve |
| DSC | Differential scanning calorimetry |
| ECM | Extracellular matrix |
| EPS | Exopolysaccharide |
| EtO | Ethylene oxide |
| FBS | Foetal bovine serum |
| FDA | Food and Drug Aministration |
| GAGs | Glycosaminoglycans |
| $H_2O_2$ | Hydrogen peroxide |
| HA | Hyaluronic acid |
| H & E | Haematoxylin and eosin |
| HCl | Hydrochloric acid |
| HLA | Human lymphocyte antigens |
| HRP | Horseradish Peroxidase |
| $MgCl_2$ | Magnesium chloride |
| MHC | Major histocompatibility complex |
| mm | Millimetre |
| MPa | Mega pascals |

| | |
|---|---|
| N | Newton |
| NaCl | Sodium Chloride |
| NaOH | Sodium hydroxide |
| NBF | Neutral buffered formalin |
| NYHA | New York Heart Association |
| PAA | Peracetic acid |
| PBS | Phosphate buffered saline |
| PERV | Porcine endogenous retrovirus |
| PGA | Polyglycolic acid |
| PHV | Pulmonary heart valve |
| PLA | Polylactic acid |
| psi | Pounds per square inch |
| ROS | Reactive oxygen species |
| RVOT | Right ventricular outflow tract |
| SAL | Sterility assurance level |
| SAVR | Surgical aortic valve replacement |
| $ScCO_2$ | Supercritical carbon dioxide |
| SDC | Sodium deoxycholate |
| SDS | Sodium dodecyl sulphate |
| SEM | Scanning electron microscopy |
| SJM | St. Jude Medical |
| SL | Semilunar |
| SMC | Smooth muscle cells |
| TAVR | Transcatheter aortic valve replacement |
| TBS | Tris-Buffered Saline |
| ToF | Tetralogy of Fallot |

| | |
|---|---|
| TPB | Tryptone phosphate broth |
| TSB | Tryptone soya broth |
| VECs | Valvular endothelial cells |
| VICs | Valvular interstitial cells |

# Chapter 1 : Introduction

## 1.1 Overview

Valvular heart disease has a major impact on patient morbidity and mortality on a global scale. The prevalence of heart valve disease is increasing internationally, and consequentially, the number of heart valve interventions is expected to increase to more than 850,000 procedures worldwide by 2050 (Yacoub and Takkenberg, 2005). Although surgical correction of the valvular aberrations is the preferred method of intervention (Yacoub and Cohn, 2004), heart valve replacement is commonly a requirement and the most beneficial option for severe valvular dysfunction. Current valve replacement options are either mechanical or biological, both of which present advantages and disadvantages. Mechanical heart valves are very durable. However, they provide a surface that encourages thrombosis, resulting in the patient requiring life-long anticoagulation therapy. The use of biological or bioprosthetic heart valves of an allogeneic or xenogeneic origin would not require anticoagulant supplementation. However, multiple reoperations may be essential throughout the patient's lifetime due to poor durability of the replacement valve (Harris et al., 2015). In consideration of these limitations, a superior novel therapeutic strategy is urgently required to improve the long-term clinical outcome of the patients.

Tissue engineering is a pioneering avenue that is being extensively explored to produce a clinically relevant heart valve that evades the limitations presented by current valve replacement options. The exposure of heart valve allografts to an effective decellularisation process removes the immunogenic components of the valve allografts. This ultimately results in decellularised valve allografts that retain inherent properties of native heart valves, with the absence of components that would otherwise induce an adverse immune response or calcification of the valve. In a study conducted by da Costa, F.D.A. et al. (2010), decellularised heart valve allografts were implanted in patients, and demonstrated stable structural integrity, low rate of calcification, and adequate haemodynamics. This demonstrates the feasibility of this approach.

In order to enhance patient safety, facilitate the translation of decellularised heart valves to commercial production, and to promote the clinical adoption of decellularised heart valves, a robust novel sterilisation method will need to be formulated and applied to the heart valve following the decellularisation process. This will provide a superior sterility assurance level and improve production efficiency. It is essential that the formulated sterilisation method does not invoke a detrimental effect on the decellularised heart valve composition, biomechanical function, biocompatibility and recellularisation potential. The sterilisation method must also hold the capacity to inactivate microbial bioburden.

## 1.2 The Human Heart

The heart works as a synchronous unit to perform its vital function of propelling blood to tissues and organs in the body. This is essential for supplying oxygen and nutrients in exchange for carbon dioxide and other waste products. Roughly the same size as a closed fist, the heart is located in the mediastinum which is an anatomical region arising from the sternum to the vertebral column. Approximately two-thirds of the mass of the heart is positioned to the left of the chest's midline.

The heart is surrounded by a protective membrane called the pericardium which is composed of two elements; the fibrous pericardium, and the serous pericardium. Composed of tough connective tissue, the superficial fibrous pericardium functions to protect the heart and to prevent overstretching. The deeper serous layer is composed of delicate tissue, and functions to prevent friction as the heart contracts (Tortora and Derrikson, 2011).

The heart is formed of four chambers, which are the left and right superior atria, and the left and right inferior ventricles (Figure 1.1). The superior atria receive blood that is being returned to the heart, whilst the inferior ventricles eject the blood from the heart. The left and right atria are partitioned by the interatrial septum, and the left and right ventricles are partitioned by the intraventricular septum. The right atrium receives blood from the superior vena cava and inferior vena cava. The received blood is passed from the right atrium to the right ventricle through the tricuspid valve. The blood is then ejected from the right ventricle

through the pulmonary valve into the pulmonary trunk, which is divided into the right and left pulmonary arteries. The blood is then transported to the lungs. The left atrium receives blood from the lungs through pulmonary veins. The received blood is passed from the left atrium to the left ventricle through the mitral valve. The blood is then ejected from the left ventricle through the aortic valve into the aorta for systemic circulation (Tortora and Derrikson, 2011).

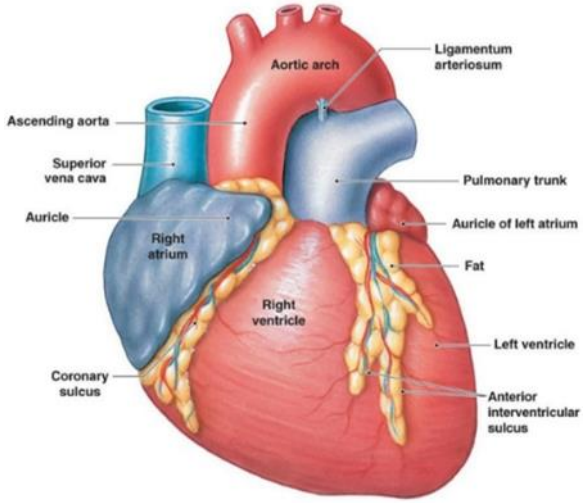


**Figure 1.1 Anterior Surface of the Human Heart.** Figure derived from Mahmoud (2018).

The thickness of the myocardium of the heart chambers is in accordance to their specific function. The atria deliver blood to the corresponding ventricles under less pressure. Therefore, the myocardium of both the left and right atria is considered thin, where the average thickness is roughly 2-3 mm. The ventricular walls are thicker than the atria walls because the ventricles eject blood over greater distances and under a higher pressure than the atria. Despite both ventricles ejecting an equal amount of blood, the right ventricle has a smaller workload than the left ventricle. The right ventricle pumps blood to the lungs under a lower pressure with less resistance to blood flow and a shorter distance. The left ventricle provides systemic circulation of blood flow to all parts of the body under a high pressure because there is a larger resistance to blood flow. Therefore, the left ventricle needs to match the cardiac output of the right ventricle by working much harder. This functional difference is demonstrated by the anatomical difference observed between the two ventricles, where the myocardium of the left ventricle is thicker than the right. The thickness of the left

ventricle is on average 10-15 mm, in comparison to 4-5 mm which is the average thickness of the right ventricle (Tortora and Derrikson, 2011).

The cardiac cycle regulates the pumping of blood into the pulmonary circulation and systemic circulation, which are two closed circuits. The cardiac cycle refers to a series of changes in pressure within the heart, driven by electrochemical changes that induce cardiac muscle contraction. This results in movement of blood through the chambers and into the circuits. The cardiac cycle can be divided into diastole and systole. Ventricular diastole represents the filling of the ventricles, where the ventricles relax and expand as blood is received. Toward the end of this phase, the left and right atria contract (atrial systole), pumping blood into the inferior corresponding ventricles. During ventricular systole, the ventricles contract vigorously while the two superior corresponding atria are relaxed (atrial diastole). The contraction of the right ventricle provides deoxygenated blood to pulmonary circulation, and the contraction of the left ventricle provides oxygenated blood to systemic circulation (Pollock and Makaryus, 2018). The outcome of one circuit becomes the input of the other.

## 1.3 Heart Valves

The contraction and relaxation of the chambers of the heart and changes in pressure cause valves to open and close in response. This is vital to ensure the unidirectional blood flow by allowing blood through, but closing to prevent the backflow. Valves are composed of extracellular matrix (ECM) that conforms to a specific anisotropic arrangement, which is populated with valvular interstitial cells (VICs) and are surrounded by a layer of valvular endothelial cells (VECs). The ECM of the valves is composed of layers rich in elastin, proteoglycan and collagen, facilitating the exertion of the intricate biomechanical properties of the valve leaflets and supporting structures (Hinton, Robert B. and Yutzey, 2011).

There are four valves that are part of the anatomy of the human heart; the tricuspid, mitral, aortic, and pulmonary valves (Figure 1.2). The tricuspid and mitral valves are termed atrioventricular (AV) valves because they are located between an atrium and a ventricle. The aortic and pulmonary valves are termed semilunar (SL) valves because they are made of distinct crescent shaped cusps.

The SL valves serve as a junction between the ventricles and the great arteries (Anderson, R. H. et al., 2000).

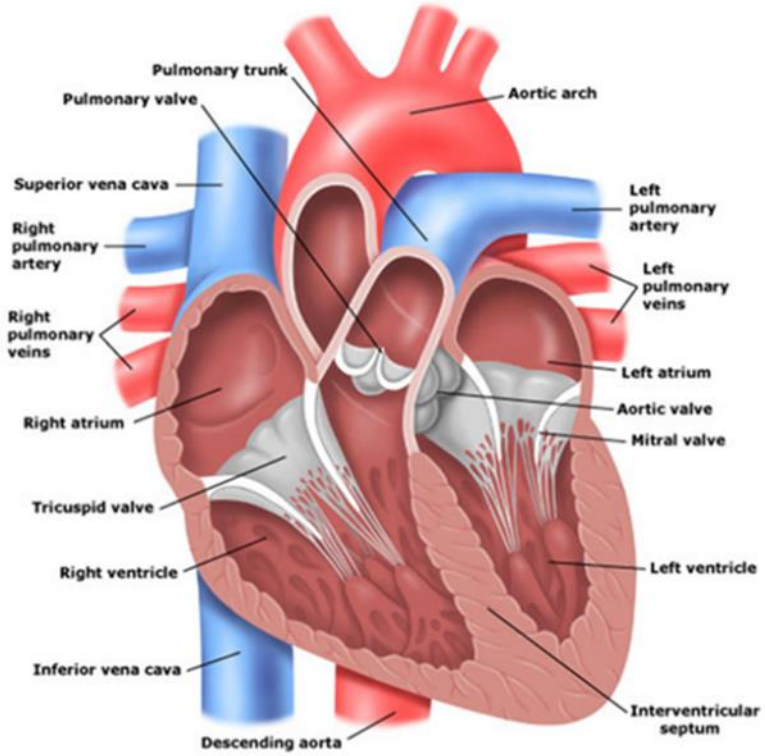


**Figure 1.2 Heart Valve Locations.** Figure derived from Schiros (2012).

Following systemic circulation, deoxygenated blood enters the right atrium, where it is pushed into the right ventricle through the tricuspid valve. During right ventricular systole, the blood is ejected from the right ventricle through the pulmonary valve into pulmonary circulation, where the blood becomes oxygenated. The oxygenated blood returns to the left atrium, where it is pushed into the left ventricle through the mitral valve. During left ventricular systole, the blood is ejected from the left ventricle through the aortic valve, where it enters systemic circulation. This essentially highlights the importance of all the heart valves in controlling unidirectional blood flow from the chambers of the heart to pulmonary and systemic circulation (de Vlaming et al., 2012).

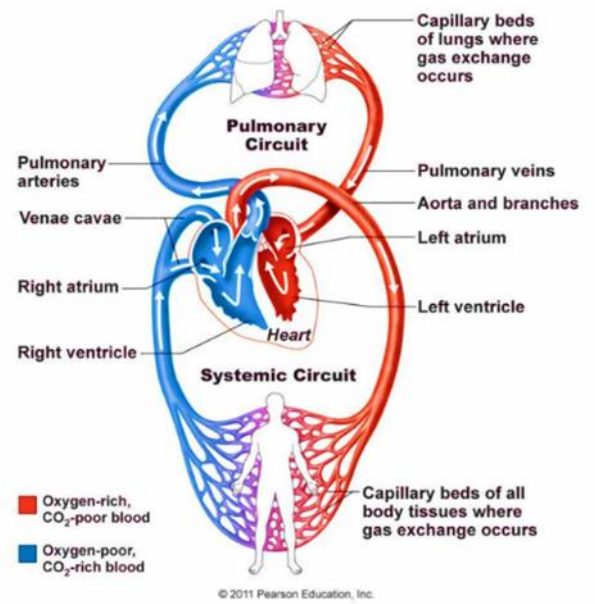


**Figure 1.3 Systemic Circulation of Blood.** Figure derived from Lawrence (2016).

### 1.3.1 Atrioventricular Valves

The AV valves function to prevent the backflow of blood from the ventricles to atria, and have a specialised support apparatus (Hinton, Robert B. and Yutzey, 2011). The AV valve complex is defined by a ring shaped annuli formed by the fibrous skeleton of the heart, and an intricate apparatus composed of chordae tendinae and papillary muscles that tether the valve to the ventricle. The annuluses adapt in shape and size in response to diastole and systole during the cardiac cycle (Bateman et al., 2013). When an AV valve opens to allow the passage of blood from the atrium into the ventricle, the rounded ends of the valve cusps propel into the ventricle. During ventricular diastole, the papillary muscles are relaxed and the chordae tendinae are limp opening the AV valves, allowing the flow of blood from the high pressure in the atria to the lower pressure in the ventricles. During ventricular systole, the increase in pressure causes the coaptation of the valve leaflets by driving the cusps upward (Figure 1.4). The regurgitation of blood back into the atria following ventricular contraction is prevented by the pulling and tightening of the chordae tendinae in response to papillary muscle contraction.

The mitral valve possesses two apposing leaflets, which are the anterior and posterior leaflets. The posterior leaflet guards around two-thirds of the valvar orifice, and the anterior leaflet guards around one-third of the valvar orifice (Anderson, Robert H. et al., 2004). The sub-valvar apparatus consist of two papillary muscles that have arising chordae tendinae which insert onto ventricular

surface of each valvar leaflet (Silver et al., 1971). The tricuspid valve possess three leaflets, which are the anterior, posterior and septal leaflets. The sub-valvar complex of tricuspid valves consists of three papillary muscles which also provide support to the septal leaflet. The mitral valve guards the left AV junction, and the tricuspid valve guards the right AV junction (Bateman et al., 2013).

Both of the AV valves share similarities within their histology. The atrial side of the leaflets consist of spongey tissue called *lamina spongiosa*, which is composed of collagen fibres, fibrocytes and histiocytes (Misfeld and Sievers, 2007). The mechanical strength required by the AV valves to endure the intense pressure adjustments during the cardiac cycle is mostly supplied by the collagen fibres. Primary sensory and autonomic innervations are innervated typically within the *lamina spongiosa* portion of the leaflets. The ventricular side of the leaflets consist of fibrous tissue called *lamina fibrosa*. The exposed surfaces of the *lamina spongiosa* and *lamina fibrosa* are enclosed by endothelial cells. Fibroblasts, smooth muscle cells and myocardial cells are also located within the leaflet tissue, which have been demonstrated to elicit contractile activities (Fenoglio et al., 1972; Filip et al., 1986; Icardo and Colvee, 1995).

### 1.3.2 Semilunar Valves

The SL valves function to allow the ejection of blood from the ventricles into their corresponding greater arteries and to prevent the backflow of blood into the ventricles during ventricular diastole. The SL valve complex is defined by three crescent shaped cusps, hence their naming of 'half-moon'. The cusps of the SL vales are attached to the arterial wall by their convex lateral lining. During ventricular systole, the pressure in the ventricles exceeds the pressure in the arteries causing the leaflets to float in the direction of blood flow from the ventricles to the greater arteries. Soon after ventricular systole but before the complete relaxation of the heart, the pressure in the ventricles drops in comparison to the pressure within the arteries. The ejected blood starts to flow back down the greater arteries toward the ventricles. However, the back-flowing of the blood fills the valve cusps, causing the free edges of the cusps to compactly coapt. This closes the junction between the arteries and the ventricles, preventing the regurgitation of blood (Figure 1.4).

The aortic valve is situated between the left ventricle and the aorta. Through the aortic valve, oxygenated blood is ejected from the left ventricle into the aorta to supply oxygenated blood for systemic circulation. It is considered to be the 'centrepiece of the heart' due to its location within the cardiac base between the tricuspid valve and mitral valve. It is thought to be the most important heart valve to facilitate the normal functioning of the heart (Piazza et al., 2008). The pulmonary valve is situated between the right ventricle and the pulmonary artery. Through the pulmonary valve, deoxygenated blood is ejected from the right ventricle into the pulmonary artery for pulmonary circulation. In a fully functioning adult heart, these valves prevent the regurgitation of blood from the greater arteries to the ventricles following ventricular systole.

The aortic valve consists of three crescent shaped leaflets, and three dilations called the sinuses of the Valsalva. It is positioned within the aortic root, which is a portion of the left ventricular outflow tract that provides support to the aortic valve leaflets (Anderson, R. H., 2007; Underwood et al., 2000). The valve base lies on the basal attachment, which is a virtual ring located below the ventriculoarterial junction (Piazza et al., 2008). The sinuses interpolate with the ascending aorta at the sinotubular junction. The sinuses have a crown-like border that runs from the basal attachment to the sinotubular junction. The crescent side of the leaflets adhere to this, creating a hinge arrangement allowing the leaflets to flex. Coronary ostia are situated within the right and left sinuses, which gives rise to the right and left coronary arteries (Rozeik et al., 2014). The naming of the cusps are in relation to the location of the coronary arteries; right coronary, left coronary, and non-coronary. A critical function of the aortic valve is to supply blood for coronary perfusion. Up to 3-5 % of the circulating blood is directed to the right and left coronary arteries whilst the aortic valve is closed in order to achieve this critical function (Bateman et al., 2013). The phases of the cardiac cycle and the associated changes in pressure within the aortic root continuously change the geometric parameters of the valvar complex (Swanson and Clark, 1974). In a study conducted by Hamdan et al. (2012), the *in vivo* deformation dynamics and mechanical properties of the aortic annulus during the cardiac cycle was assessed. It was found that the minimum diameter of a normal adult aortic valve increased by approximately 12 % during systole.

The pulmonary valve is considered to be an anatomically simpler valvar structure in comparison to the aortic valve due to its location within the distal portion of the right ventricular outflow tract, called the infundibular musculature (Bateman et al., 2013). Nonetheless, it has been reported that pulmonary valve autografts may be clinically effective for replacement of diseased aortic valves due to minimal differences between the structural and architectural elements and mechanical properties (Stradins et al., 2004). The pulmonary valve consists of three crescent shaped leaflets, united by three commissures (Jonas et al., 2016). The commissures are formed by the SL hinges ascending to attach at the sinotubular junction adjacent to each other (Dong et al., 2018). The leaflets are called the anterior cusp, the right cusp, and the left cusp relative to their location to the aortic cusps. The right pulmonary cusp is apposed to the right aortic cusp, and the left pulmonary cusp is apposed to the left aortic cusp (Gross and Kugel, 1931). The supraventricular crest of the right ventricle supports the commissure of the right and left cusps (Bateman et al., 2013). The hemodynamic ventriculoarterial junction is formed by the SL attachment of the valve leaflets (Saremi et al., 2014). The pulmonary root is part of the right ventricular outflow tract (RVOT) that supports the pulmonary valve leaflets (Stamm et al., 1998). The structures of the pulmonary root are more delicate than the structures found in the aorta due to a reduced exposure to haemodynamic forces.

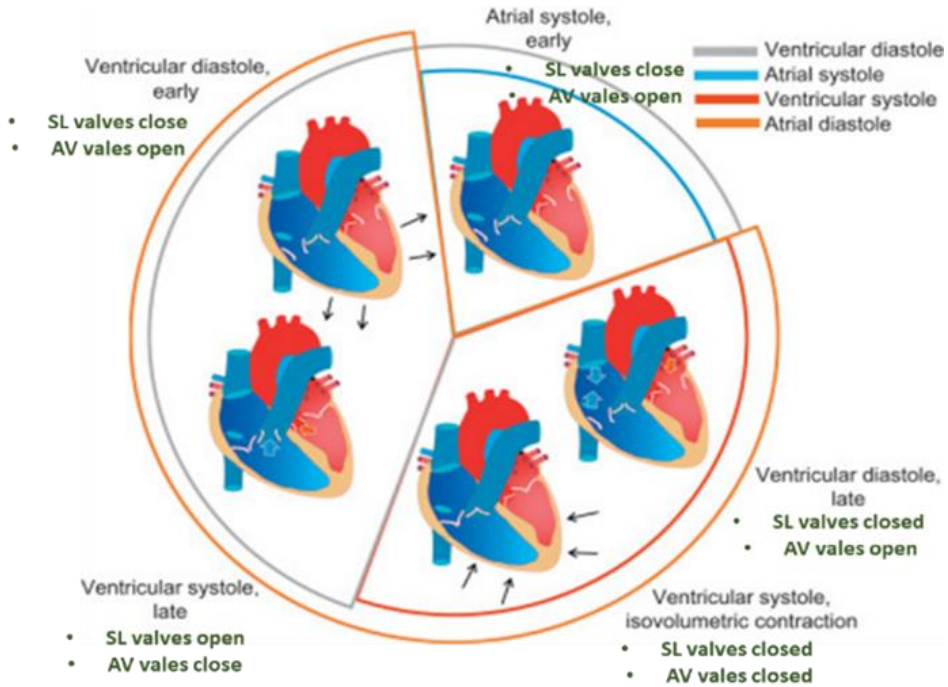


**Figure 1.4 Schematic of AV Valves During Systole and Diastole.** Figure adapted from (Athanasiou et al., 2017).

### 1.3.2.1 Layers of the Semilunar Valve leaflets

There are three distinct layers of connective tissue between the artery and ventricle surfaces of the SL valve leaflets; lamina radialis, lamina spongiosa and lamina fibrosa, respectively (Figure 1.5 A). Although, lamina ventricularis and lamina arterialis can also be included into this nomenclature (Gross and Kugel, 1931). The layer located under the ventricular endothelium is the lamina ventricularis. This layer is formed of compact network of reticular fibres featuring a sparse amount of collagenous and elastic fibres. Reticular fibres are located between the collagenous and elastic fibres, forming a layer with a thickness between 58 and 108μm (Misfeld and Sievers, 2007). The load bearing elastic and collagen fibres within the connective tissue display a preferred anisotropic orientation that resembles a honeycomb structure. This preferred arrangement is believed to aid in the maintenance of the collagen fibre geometry upon the application of external forces (Vesely, 1998). Radiating from the radialis and fibrosa layers, a looser structure of collagenous fibres, reticular fibres and elastic fibres called the lamina spongiosa is formed, with an approximate thickness between 40 and 300 μm (Misfeld and Sievers, 2007). The leaflets of the SL valves have a fibrous core termed the lamina fibrosa. Delicate sheets of elastin line the lamina fibrosa, with distinguished features on the ventricular and aortic surfaces. Circumferential collagen fibres are found in the arterial layer which transfer the load of the leaflets to the wall of the root that forms the outflow apparatus of the specific SL valves (Broom, 1978). The lamina fibrosa has a thickness of 80 to 170 μm. The layer located under the arterial endothelium is termed the lamina arterialis. A distinct network of neuronal innervation has also been found in SL leaflets. The neuronal innervation is believed to arise from the ventricular endocardial plexus (Marron et al., 1996).

The architectural configuration of the SL leaflets undergoes micro and macroscale changes during the cardiac cycle (Korossis, S., 2018). The folds in the collagen fibre layer of the fibrosa gives the corrugated appearance when the valves are fully open during ventricular systole which disappear during ventricular diastole as the leaflets fully extend (Figure 1.5 B). As the SL valves close, the radially aligned fibrosa corrugations and elastic fibres of the ventricularis layers radially expand to increase the leaflet dimensions without major stress impact. Circumferentially

aligned collagen fibres are then uncrimped as the leaflet stretches further. The collagen fibre corrugations in the fibrosa are smoothed in both the radial and circumferential directions, producing stiffened leaflets that ensure optimal leaflet coaptation when the valve is fully closed (Schoen, Frederick J. and Levy, 1999). Therefore, the multi-layered leaflet structure supports sufficient valve closure and coaptation by aiding collagen fibre extension to generate stiffened leaflet structures (Korossis, S., 2018; Schoen, Frederick J. and Levy, 1999).

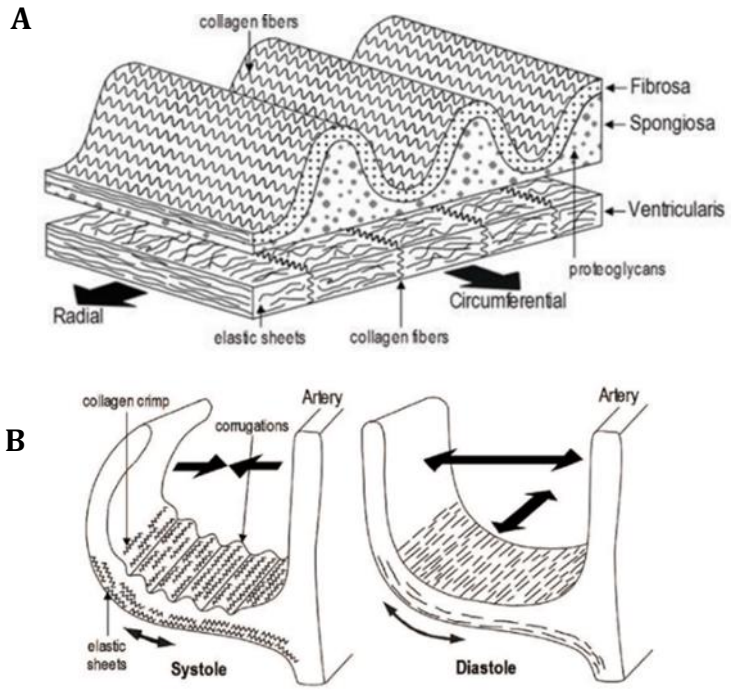


**Figure 1.5 Layers (A) and Architectural Configuration of SL Leaflets During Ventricular Systole and Ventricular Diastole (B).** Figure taken from Schoen, Frederick J. and Levy (1999) and Korossis, S. (2018).

### 1.3.2.2 Cellular Characteristics of Semilunar Valves

Resident cells of the heart valves play an important role in maintaining homeostasis in response to changes within the microenvironment induced by the cardiac cycle, via orchestrating complex signalling networks that include secretion of biochemical signals, matrix remodelling proteins and matrix proteins (Wang et al., 2014). Heart valves have VECs and VICs. CD31+ VECs line the peripheral boundaries of the leaflets, whereas VICs are dispersed throughout the layers of the leaflets. VICs often exhibit a smooth muscle cell, cardiac muscle cell, or fibroblast phenotype (Brand et al., 2006). VICs and VECs are activated in response to valve

injury or disease to mediate a mechanism to repair the valve. An example of this is VECs being able to facilitate tissue regeneration in response to injury by undergoing endothelial to mesenchymal transition. This leads to a fibroblast or myofibroblast phenotypic change that causes adjustments in micro-environmental signals (Bischoff and Aikawa, 2011). However, persistent activation of valvular cells can induce valvular disease progression by causing inappropriate remodelling of the ECM (Rajamannan et al., 2011). An example of this is aortic VICs being able to deposit fibrotic collagen and calcified matrix (Rajamannan et al., 2005). Although, Wang, H. et al. (2013) conducted a study which demonstrated that VICs maintain an inactivated fibroblast phenotype when cultured on hydrogels that resemble native ECM in comparison to being cultured on plastic plates.

In a study conducted by Simmons et al. (2005), it was demonstrated that VECs found on the arterial and ventricular surfaces of the valves exhibited different transcriptional profiles to each other, suggesting that the spatial heterogeneity of valvular endothelial phenotypes may have an influence in susceptibility of the valve to pathological developments.

ECM components such as collagen, proteoglycans, glycosaminoglycans (GAGs) and elastin play an important role in the regulation of VICs. VICs are the most prevalent cells of the heart valves and are located in all of the layers of the valve (Liu et al., 2007). Collagen may help inhibit pathogenic differentiation of VICs by inhibiting myofibroblast activation and calcific nodule formation (Gu and Masters, 2010). Collagen has been demonstrated to promote VIC adhesion, proliferation and matrix synthesis (Butcher and Nerem, 2004). Hyaluronic acid (HA) is a type of GAG. HA is a major component of heart valve ECM and serves as an important factor for the culturing and proliferation of viable VICs (Masters et al., 2005; Murata, 1981). Masters et al. (2005) demonstrated that VICs encapsulated within HA hydrogels resulted in significant elastin production, suggesting that HA and VICs have a synergistic relationship where HA is able to regulate VICs secretory properties. Elastin is a major ECM component on the flow side of the valves. It has been indicated that elastin plays an important role in regulating gene expression of VICs (Hinton, R. B. et al., 2010).

VECs and VICs are in contact with each other near the boundaries of the heart valves and communicate with each other via paracrine signals (Hinton, Robert B.

and Yutzey, 2011). Butcher and Nerem (2006) demonstrated that VECs decreased VIC proliferation, stimulated VICs to adopt a quiescent phenotype, and increased protein synthesis with shear stress. This study indicated that VECs regulate VIC phenotype and matrix synthesis.

#### 1.3.2.3 Biomechanical Properties of Semilunar Valves

The heart valves are exposed to mechanical stresses whilst carrying out their primary function of enforcing and controlling unidirectional blood flow during the cardiac cycle (Hasan et al., 2014). Heart valves have a cyclic loading of up to 30 million times a year, during which 3-5 litres of blood is pumped through the valves per minute (Butcher et al., 2011). Thus, it is imperative to understand the biomechanical properties of natural heart valves.

Uniaxial testing is a common means of assessing the mechanical properties of heart valves. The data generated from uniaxial testing is usually expressed as stress-strain behaviour, where the tensile stress is the force applied per specimen unit area and the strain is the change in length of the specimen per unit original length when the force is applied. Using this data generated, the Young's modulus, otherwise known as the elastic modulus can also be calculated as the ratio of stress and strain. The regions of a tensile-stress strain curve might be linked to the valve structures (Figure 1.6). The regions of a tensile-stress strain curve can be divided into; (i) low stress–low strain pre-transition linear elastic phase, (ii) non-linear transition phase, (iii) post-transition linear collagen phase, (iv) non-linear phase. The low stress-low strain pre-transition linear phase can be associated with the elongation of elastin fibres and straightening of collagen fibres. The non-linear transition phase can be associated with the force transfer between elastin and collagen fibres. The post-transition linear collagen phase can be associated with elastin and collagen fibre elongation. Finally, the non-linear phase can be associated with rupture of collagen and elastin fibres and complete fracture of the specimen (Hasan et al., 2014).

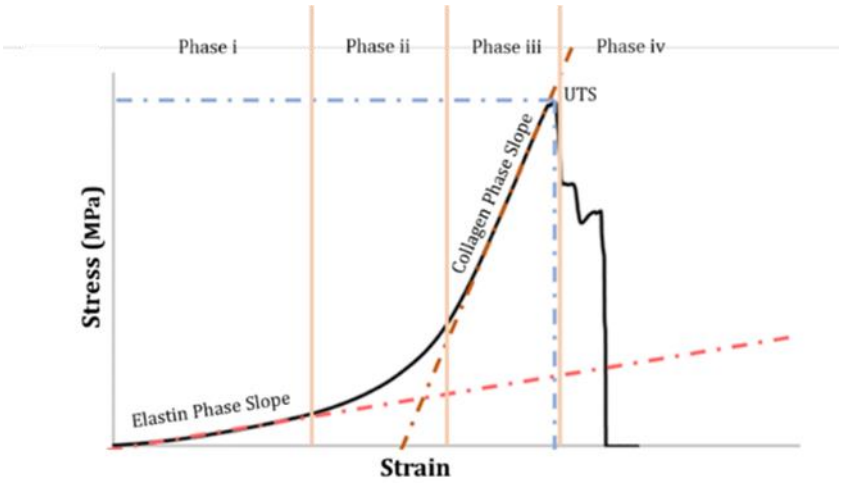


**Figure 1.6 Stress-Strain Behaviour of Heart Valve Tissue.**

Stradins et al. (2004) used uniaxial tensile investigations to compare pathologically unchanged human aortic and pulmonary valve properties. The experimental results showed that the ultimate stress in circumferential direction was higher for pulmonary valve cusps than for aortic valve, with ultimate tensile stress values of around 2.78 and 1.74 mega pascals (MPa), respectively. However, the elastic modulus of circumferentially aligned pulmonary and aortic valve cusps were similar at 16.05 ± 2.02 MPa and 15.34 ± 3.84 MPa, respectively. This data implied that human aortic and pulmonary heart valves have similar mechanical characteristics.

In a study conducted by Mavrilas and Missirlis (1991), the human aortic heart valve leaflets was demonstrated to have an elastic modulus of approximately 15 MPa in the circumferential direction, and approximately 2 MPa in the radial direction. In comparison to these values, Armeniades et al. (1973) stated that the elastic modulus of the human aortic heart valve leaflets was 8.3 MPa and 2.4 MPa in the circumferential and radial direction, respectively. The variation in this data is evident. Although variability in the biological properties of the specimens used within these studies may account for the variability, experimental variations may also be responsible. Experimental variations can arise from a number of factors and parameters, such as inconsistencies in specimen preparation, and size and dimensions of the specimen (Karimi et al., 2008). These data also show that the elastic modulus is higher in the circumferential direction than the radial direction. This corresponds to the anisotropic arrangement of the tissue of the heart valves

and demonstrates that the heart valves are inherently highly anisotropic (Hasan et al., 2014).

The circumferential expansion characteristics of the artery component of the heart valve root impacts leaflet coaptation following systole, and plays a role in transmitting stress from the leaflets to the pulmonary artery wall during systole. The artery wall therefore aids in the prevention of fatigue and structural failure of the valve leaflets (Desai et al., 2018; Hopkins, R.A., 2003; Sutton et al., 1995). Korossis, S.A. et al. (2005) therefore used dilation assessments of the aorta component of intact native and decellularised porcine aortic roots to determine the functionality of decellularised heart valves.

#### 1.3.2.4 Hydrodynamic Properties of Semilunar Heart Valves

The haemodynamic environment surrounding heart valves plays an important role in controlling the normal function of the heart valves; to ensure unidirectional blood flow with maximal flow rate and minimal flow resistance. Accordingly, the interaction between heart valves and the local haemodynamic environment is critical in our understanding of the normal function of the heart valves, in addition to valve disease progression (Sacks and Yoganathan, 2007). Hydrodynamic functional studies are also essential in assessing transvalvular pressure gradients and leakage through fully coapt leaflets of replacement heart valves (Desai et al., 2018).

The aortic valve opens during ventricular systole and closes during ventricular diastole. The flow of blood through the aortic valve during ventricular systole accelerates to a rate of $1.35 \pm 0.35\,\mathrm{m\,s^{-1}}$ (Otto, C. M., 2001). Toward the end of the deceleration phase of ventricular systole, the aortic valve closes with little regurgitated flow through the valve. The movement of aortic valve leaflets away from the sinus wall and into a closed position is facilitated by the axial pressure differences which result in vortices behind the sinuses of the aortic valve leaflets (Reul and Talukder, 1989). Although Reul and Talukder (1989) reported that axial pressure differences alone are sufficient to close the aortic valve, the vortices allow an efficient and fast closure. It should also be noted that during the cardiac cycle, the aortic valve annulus expands and contracts which also influences the aortic

valve leaflet function and facilitates the opening and closing of the leaflets (Sacks and Yoganathan, 2007).

The pulmonary valve flow profile is similar to that of the aortic valve with the exception of a lower velocity magnitude (Sacks and Yoganathan, 2007). The peak velocity at the valve outlet is measured to be $0.75 \pm 0.15\ ms^{-1}$ (Oh et al., 1997). During acceleration phase of the blood flow, the peak velocity is observed inferiorly which is shifted counter-clockwise through the remaining ejection phase. The decrease in velocity in the inferior right region of the vessel evolves into retrograde flow in the deceleration phase (Sloth et al., 1994).

*In vitro* assessments into the leakage flow rate of the closed heart valve under static back-pressure can give indication of the valve competency. Jennings (2001) used static leakage flow assessment to evaluate valvular regurgitation of closed native and glutaraldehyde fixed porcine aortic and pulmonary heart valve roots to determine valvular insufficiency.

## 1.4 Heart Valve Disease

Heart valve disease is defined as a structural or functional anomaly of the heart valves. The disruptions to the valvular anatomical integrity commonly seen in heart valve disease usually leads to valvular stenosis, valvular regurgitation, or a combination of both. The consequential surface disruptions of heart valves associated with the disruption of valvular integrity can often lead to the induction of pathologic events such as platelet aggregation and microorganism accumulation, which leads to the predisposition of thromboembolism and infective endocarditis. Valvular stenosis refers to the narrowing of the valvular orifice due to the thickening, stiffening, and/or fusion of the valve leaflets. This can obstruct the flow of blood through the valve. This essentially creates a pressure gradient between the pre and post valvular areas. The heart tries to compensate for this pressure gradient by developing a pressure hypertrophy whereby the myocardium wall thickness increases, known as concentric hypertrophy, or the chamber volume enlarges due to dilation, known as eccentric hypertrophy (Rossi and Carillo, 1991). However, this mechanism is not sufficient for the long term compensation of the reduction in the valvular orifice, and the contractile function of the specific

chambers of the heart declines. Valvular regurgitation refers to the valves becoming 'leaky' due to insufficient coaptation. This leads to the backflow of blood into the atrium or the ventricle. Valvular atresia can also occur, where the heart valve does not open sufficiently to allow the ejection of blood (Boudoulas, K.D. et al., 2013).

There are a number of pathophysiological entities that are associated with valvular heart disease. This includes heritable disorders, inflammatory triggers, myocardial diseases, degenerative processes, and iatrogenic causes of valvular heart disease. Many valvular abnormalities are associated with heritable disorders of connective tissue, such as the well-known Marfan and Ehlers-Danlos syndrome. These valvular abnormalities include multivalvular prolapse, specific types of aortic regurgitation and pulmonary artery dilation (Boudoulas, H. and Wooley, 2001; Bowen et al., 1987). The surgical repair of the congenital cardiac malformation, tetralogy of Fallot (ToF), often results in pulmonary regurgitation (Redington, 2006). Congenital pulmonary stenosis that may or may not be associated with other congenital abnormalities can be seen when the mother is exposed to an infection, particularly rubella, during foetal development of the affected infant (Emmanouilides et al., 1964).

Despite being less common in industrialised countries, rheumatic fever is still prevalent in developing countries (Carapetis et al., 2005). Mitral and aortic valvulitis are common clinical manifestations of rheumatic fever. Mitral regurgitation is the most common initial clinical presentation following rheumatic fever infection, with aortic regurgitation being less frequent (Vasan et al., 1996).

Patients with ischemic and non-ischemic cardiomyopathy commonly present with mitral and tricuspid regurgitation. This is due to consequential papillary muscle displacement as a result of left-ventricular dilation, fibrosis, and dysynchrony of left ventricular contraction (Boudoulas, K.D. et al., 2013).

Calcification of the aortic valve cusps usually occurs after the 7th decade of life and progresses to create aortic stenosis. It was believed that this occurrence was related to processes associated with ageing. However, recent evidence suggests that aortic stenosis and atherosclerosis share a relation to the same pathophysiological mechanisms that involve a genetic predisposition to metabolic processes (Boudoulas, K.D. et al., 2013; Otto, Catherine M. et al., 1999).

Valvular heart disease may persist following interventional valve therapy, such as balloon valvuloplasty, and valvular reconstructive surgery involving valve repair or replacement. Prosthetic valve replacements are more prone to post-surgery complications, such as mechanical dysfunction, thrombosis, and endocarditis which further compromises valvular function (Huang, G. and Rahimtoola, 2011).

## 1.5 Heart Valve Replacements

Prior to the development of the first valve prosthesis in 1952, Theodor Tuffier made the first attempt to treat aortic valve stenosis in 1912, where a 'closed heart' approach was adopted to open the valve through the aortic wall. In the late 1940's, Charles Hufnagel designed a methacrylate chamber that contained a methacrylate ball (Figure 1.7). The high pressure of the forward flow of blood would push the ball downstream, opening the orifice. The passive movement of the ball occludes the valve orifice, preventing the backflow of blood during relaxation. After 1953, more than 200 patients with aortic regurgitation received this implantation into their descending thoracic aorta as opposed to receiving the implant in place of the diseased aortic valve (Dasi et al., 2009). Some of these implanted Hufnagel valves functioned for up to 30 years following implantation without displaying significant deterioration (Gott et al., 2003). It was soon after this that Albert Starr and Miles Edwards collaborated to invent a valve based on the concept of a wine bottle stopper. A methacrylate cage containing a silicone elastomer rubber ball was fabricated and implanted into a patient with calcific mitral stenosis in 1960. The 10-year follow up of the patient did not reveal any adverse effects consequential of the implant (Starr et al., 1969). Nonetheless, the first decades of heart valve surgery uncovered a number of aspects that needed to be addressed to enhance the safety and efficacy of replacement heart valves. Continuous research has been and is still being conducted into materials, techniques, and technologies to replace the natural valve whilst addressing challenges presented.

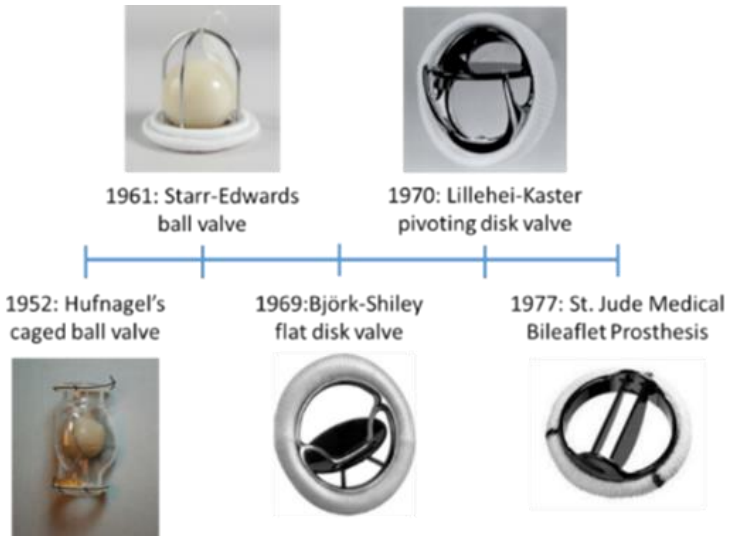


**Figure 1.7 Evolution of Mechanical Heart Valve Replacements.** Image adapted from Mahmood et al. (2018) and Blot et al. (2005).

### 1.5.1 Mechanical Heart Valves

The heart valve prosthesis should possess a haemodynamic performance that closely simulates the haemodynamic performance of the native valve, i.e. low resistance to the forward haemodynamic flow and only allowing negate regurgitation upon the closure of the occluder of the prosthesis (Gallegos et al., 2011). The detection of paravalvular leakage, most often due to a lack of sufficient sealing of the prosthesis to the cardiac tissue, was an indication for reoperation on two patients that each received a cage ball valve prosthesis. Paravalvular leakage results in the regurgitation of blood flow through an exposed channel between the implanted device and the cardiac tissue (Sampaio et al., 2009). Additionally, the methacrylate ball employed in the Hufnagel prosthesis was associated with valve noises, which was addressed by replacing the use of a methacrylate ball with silicone coated nylon ball. The risk of coagulation associated with the use of mechanical valves was highlighted in preclinical studies, and it was shown that anticoagulation therapy was required in conjunction with the mechanical valve prosthesis to avoid thromboembolic events and valve occlusion (Russo et al., 2017).

The central ball occluder prostheses, as employed by Hufnagel and Starr-Edwards, caused lateralisation of the blood flow and consequential high turbulence and enhanced thrombogenic potential. Moreover, the opening of the ball valve required

a substantial amount of energy in the form of a greater ventricular systolic pressure to drive cardiac output, which was accompanied by an increase in myocardial oxygen consumption (Chaikof, 2007). These poor haemodynamic properties of the caged ball valves inspired the fabrication of a second generation of mechanical prostheses.

The development of the tilting disk prostheses in the late 1960's provided a central flow, simulating the physiological pattern of blood flow through the valves (Russo et al., 2017). The Björk-Shiley valve was introduced to minimise the resistance to the forward flow of blood, decrease the turbulence that was observed with caged ball valves, limit stagnation regions, and to reduce shear stress. It was designed with a central disk, held in place by two metal struts; an inflow and an outflow strut (Lindblom et al., 1989). These struts essentially permitted the disk to pivot into open and closed position of the valve orifice. Aforementioned, the use of mechanical valves was associated with thromboembolic events. The adoption of the Björk-Shiley valve led to a high incidence of embolization due to leverage loading of the outflow strut. Although this issue was not eliminated, the requirements for anticoagulation therapy was reduced.

Mr Robert Kaster and Dr C. Walton Lillehei collaborated to design a tilting disk valve with a novel disk containment configuration. The Lillehei-Kaster pivoting disk valve was implanted in the aortic position of 313 patients. The results from this study demonstrated the excellent mechanical durability and resistance to thromboembolic events in patients that were receiving appropriate anticoagulation therapy. However, the Lillehei-Kaster valve was not appropriate for patients with a smaller effective orifice area due to an unfavourable effective orifice area to tissue diameter ratio (Stewart et al., 1988).

In 1977, the St. Jude Medical (SJM) bileaflet prosthesis was introduced. The design of the SJM bileaflet valve provides three areas of blood flow through the valve orifice with a more uniform and streamline flow. The enhanced haemodynamics was related to less stagnation of blood. Being the most widely used prosthetic valve globally, it is remarkable that the original design has virtually remained unchanged over the past 26 years since its introduction. However, there have been some changes introduced, such as modifications of the sewing ring, and the

incorporation of a housing design to accommodate the smaller orifice size of smaller valve prostheses (Emery et al., 2002).

Mechanical heart valve prostheses have been evolving for more than 50 years to provide an optimal treatment for diseased valves (Figure 1.7), with studies demonstrating the desired mechanical durability of the prostheses and a progressive decrease in mortality of patients receiving mechanical valve implants. However, the thrombogenic potential of the mechanical valves still poses an issue with the use of these devices. The formation of a thrombus can occlude the orifice of the valve and obscure the essential streamlined haemodynamics, or the thrombus can dislodge and emoblise to a distant organ such as the brain. Although, it could be possible for innovative anticoagulation strategies to prevent thrombus formation. Animal studies showed that dabigatran was effective in preventing valve thrombosis following mitral valve surgery (Russo et al., 2017). These findings regrettably were not verified in human studies. Eikelboom et al. (2013) designed and executed the Randomized, Phase II Study to Evaluate the Safety and Pharmacokinetics of Oral Dabigatran Etexilate in Patients after Heart Valve Replacement (RE-ALIGN). Patients that had undergone aortic or mitral valve replacement were randomly assigned to receive either dabigatran or warfarin. This study concluded that the use of dabigatran was associated with excess thromboembolic events in comparison to warfarin. In consideration of these issues presented by the use of mechanical heart valves, it is not uncommon for patients to receive biological tissue valves to avoid the use of anticoagulation therapy. This is particularly relevant to fertile female patients as lifelong anticoagulation therapy has significant foetal toxic effects, which is unsuitable for women planning pregnancy (Barbarash et al., 2016).

### 1.5.2 Biological Heart Valves

As opposed to being composed of non-biologic materials such as polymer, metal or carbon, biological heart valves are composed of biological material derived from a human or animal source. Biological heart valves hold advantages over mechanical heart valves, in the sense that tissue valve substitutes possess inherent biocompatibility and physiological haemodynamic properties. In addition to this, biological heart valves do not require the use of life-long anticoagulation therapy

(Levy et al., 1983). The number of patients undergoing a biological heart replacement instead of a mechanical heart replacement has increased from 59 % in 1999 to 86 % in 2013 (Hickey et al., 2017).

There are three types of biological heart valve substitutes; allogeneic, autologous, and bioprosthetic.

### 1.5.2.1 Allogeneic and Autologous Valves

The use of human valves present several advantages over the aforementioned replacement valve options. They have been demonstrated to possess enhanced haemodynamic properties and resistance to infection (Ciubotaru et al., 2013). The human valves could be allograft or autograft.

Allograft human heart valves are harvested from cadavers, or from live donors that are undergoing heart lung transplantation. There are a number of factors that can have an impact on the durability of the valve allograft following implantation. These factors include the method adopted to carry out the harvesting procedure, the preservation protocol that the allograft is exposed to, as well as the selection of the patient based on compatibility.

In 1962, Donald Ross performed the first successful allograft aortic valve replacement. Similarly, Barratt Boyes corroborated the results of Ross's study in 1965 by accepting allograft valve replacement as the optimal method for surgical treatment of aortic incompetence and calcific aortic stenosis in that era, based on the results of his clinical study. The work of Ross and Boyes led to the implementation of allograft valves in clinical practice (Delmo Walter et al., 2012).

At the emergence of the use of allografts in clinical practice, the valves were initially sterilised with a cocktail of antibiotics and wet-stored. This approach resulted in enhanced viability of donor cells which can induce and exacerbate an adverse immunological response of the recipient. Neves et al. (1997) provided evidence to suggest that the induction of an immunological reaction is responsible for the degradation of cryopreserved allografts. Cells found in allograft human tissue have been shown to express major histocompatibility complex (MHC) I and II which can elicit a cellular and a humoral immunological response. Smith, J.D. et al. (1995) found that patients receiving allograft replacement of the aortic valve

demonstrated a strong humoral response specific to the donor. The antibodies formed by the recipient were against the donor human lymphocyte antigens (HLA) class I. Consequently, this can have a detrimental effect on the allograft, and thus a limited durability of the valve. This method was replaced with cryopreservation of the allograft heart valve, which has the advantage of enabling longer storage period of the tissue in addition to providing enhance durability of the valve. Allografts are usually frozen in dimethyl sulfoxide and subsequently stored at -196 °C. However, it is essential that the graft is homogenously defrosted to avoid the formation of interstitial ice as this can induce degeneration of the valve (Delmo Walter et al., 2012). Another disadvantage of allograft valves is the lack of growth and remodelling capacity to accommodate the growth of the recipient, potentially requiring multiple re-operations to replace the outgrown valve (Ciubotaru et al., 2013).

In 1967, Ross used an autologous pulmonary valve to reconstruct a dysfunctional aortic or mitral valve. During the Ross procedure, the diseased valve is removed and replaced with the patient's own pulmonary valve. The patient's pulmonary valve is then replaced with a cryopreserved allograft or a glutaraldehyde fixed-xenogeneic heart valve. Ideally, valve repair should be considered instead of replacement. However, this may not always be anatomically possible (Bowdish et al., 2016).

The approach taken in the Ross procedure emanates from the idea that the use of the patients own valve to replace the diseased valves in the left side of the heart that are physiologically exposed to high haemodynamic pressures would have freedom from thromboembolism, sufficient haemodynamic function, and growth with time, evading the limitations presented by valves composed of prosthetic and xenogeneic materials (Gonzalez-Lavin et al., 1970). The implantation of these materials into the position of the patient's pulmonary position would result in a slower degeneration due to a lower shear-stress environment. The dysfunction of these materials is tolerated better and for a longer duration of time when situated in the right side of the heart as opposed to the left side of the heart. Andreas et al. (2014) performed a non-matched analysis to compare the 15-year survival rate of young adults that underwent the Ross procedure against young adults receiving a mechanical aortic valve replacement. This study reported that the 15-year survival

of the Ross patients was 93 %, in comparison to 75 % of the patients receiving a mechanical aortic valve replacement. This suggests the potential benefits of the Ross procedure being conducted in young adult patients with aortic valve disease.

However, there are limitations associated with the Ross procedure. Two valves are addressed to resolve the issue posed by a single diseased valve, and this can potentially lead to two failing valves if the autograft was to fail, in addition to the deterioration of the cryopreserved allograft or glutaraldehyde fixed xenograft used to replace the pulmonary valve.

In order to avoid the use of allografts or xenografts to replace the pulmonary root during the Ross procedure and to address the potential issue of introducing valvular dysfunction in two valves, Ionescu and Ross (1969) fabricated an artificial valve using autologous fascia lata mounted on a Dacron covered titanium frame welded into a tri-leaflet valve shape. This was clinically implanted into the left side of the heart. However, long term exposure of this implantation to the high pressure environment of the left side of the heart resulted in a decline in the function of the replacement valve, and was subsequently abandoned as a clinical procedure. Nonetheless, autologous pericardium is routinely used in valve reconstruction or partial cusp replacement (Acar et al., 2004).

#### 1.5.2.2 Bioprosthetic Heart Valves

Bioprosthetic heart valves tend to be composed of tissue sourced from an animal origin, most often porcine or bovine. The sourced tissue is either the animal heart valves, or animal pericardial tissue (Ciubotaru et al., 2013). Bioprosthetic heart valve tissues are fixed with glutaraldehyde prior to being available for clinical use. The very first successful aortic valve replacement using a xenogeneic heart valve in a human was performed by Carpentier and his colleagues in 1965 (Binet et al., 1965). Finding that the anatomy of the porcine valves resembled that of the native human valve, Carpentier's group had proceeded to implant 61 porcine valves in 53 patients, albeit with a high failure rate. The porcine valves implanted were aortic or mitral valves that were sterilised with a mercurial solution or freeze dried prior to being directly sutured into the patient, as well as frame mounted grafts sterilised with mercurial solution or formalin. At 6 months following the implant of

the porcine valves, only around 60 % were functioning sufficiently. By 1 year following the procedure, the functionality of the heart valves further decreased to approximately 45 % (Carpentier et al., 1969). This was indicated to be due to an adverse host immune response to the animal tissue, initiating investigation studies into decreasing the adverse immune response to the xenogeneic heart valves (Manji et al., 2015).

A protocol was produced to;

1. Eliminate soluble proteins via washing or electrolysis

2. Denaturise mucopolysaccharides and structural glycoproteins via oxidation using sodium periodate

3. Neutralise with ethylene glycol

4. Place the valves in a glutaraldehyde-buffered solution which crosslinked with amino acids

These processes significantly reduced the antigenicity of the xenogeneic heart valves, improved the stability of the material, and preserved the resistance to thromboembolic events. By 5 years following the implantation of the xenogeneic valves that had been exposed to this procedure, the percentage of functional valves in patients was 77 %, 89 % and 96 % in the mitral, aortic and pulmonary positions, respectively (Carpentier et al., 1974).

Ionescu developed glutaraldehyde-stabilised pericardial xenografts designed using bovine pericardium mounted on a Dacron covered titanium frame, which is a synthetic material. In 1971, Ionescu implanted these xenogeneic valves in human patients after the demonstration of exceptional hydrodynamic performance and durability in *in vivo* studies (Ionescu et al., 1977). The encouraging results generated by Ionescu's xenogenic valves led to the production and global distribution of the valves in 1976 in collaboration with the Shiley laboratory in California. Years from the introduction and implementation of the Ionescu-Shiley pericardial xenograft, the desired haemodynamic performance and reduced susceptibility to thrombotic events inspired other companies to adopt a similar approach in manufacturing and distributing pericardial valves (Ciubotaru et al., 2013; Liao et al., 1992).

However, a major disadvantage of xenogenic heart valves is the imminent deterioration and limited durability, regardless of whether the valve is porcine or bovine derived. There are numerous factors that are directly responsible for this structural deterioration, including the chemical fixation process, the method of preservation, the medical history and the age of the patient, immunological interactions between the donor and recipient tissue, and an increase in haemodynamic shear stress following implantation (Schoen, F. J., 2008). Although fixation in glutaraldehyde is believed to reduce immunogenicity by cross-linking collagen to mask tissue antigens, it can also lead to basement membrane damage. This can cause a calcium influx as calcium combines with membrane phospholipids. When *in vivo*, the exposure of tissue to mechanical stress can initiate calcium phosphate crystal nucleation, the growth of crystals which then cause tears and stenosis leading to valve failure (Cunanan et al., 2001).

Some studies have attempted anti-calcification treatments of glutaraldehyde fixed bioprosthetic heart valves by masking free aldehyde groups. Flameng et al. (2015) investigated the impact of stable functional group capping and gylcerolisation of bovine pericardium bioprosthetic heart valves on function and durability using an *in vivo* sheep model. Following 8 months of implantation into the mitral position of juvenile sheep, the haemodynamic (cardiac output, mean transvalvular pressure gradient and flow turbulence) and anti-calcification properties of the treated bioprosthetic heart valves were significantly improved in comparison to the standard glutaraldehyde fixed bioprosthetic heart valve. Capping was used to reduce functional groups such as aldehydes which was believed to prevent tissue oxidation and diminish tissue calcification. The valves were also treated with a glycerol and ethanol mix which resulted in the glycerolisation of the bovine pericardium tissue (water present in the pericardium was replaced with glycerol). This technology allows the packaging and storage of the valves in a dry state without the requirement for liquid-based storage solutions such as glutaraldehyde.

### 1.5.3 Transcatheter Valve Implantation

The replacement of heart valves can be an invasive procedure, with the death rate following operative replacement of the aortic valve being as high as 10 % in patients with an impaired left ventricular function. The emergence of transcatheter

valve implantation provides a minimally invasive option that is deemed the most suitable option for patients considered to be poor candidates for surgery. The evolution and adaptation of transcatheter valve implantation arises from the desire of cardiologists to treat stenotic valves percutaneously, reducing the risks associated with open-heart valve surgery (Inoue et al., 1984; Sharony et al., 2003).

There are two types of transcatheter valves that are currently approved by the U.S Food and Drug Administration (FDA); (i) the CoreValve® Revalving system (Medtronic, Inc.; Minneapolis, Minn), (ii) the Edwards Sapien system (Edwards Lifesciences Corporation; Irvine, Calif).

The CoreValve® Revalving system is composed of a nitinol frame that is self-expanding, encasing a porcine pericardial tissue prosthesis. The delivery of this system is via a catheter that is retrogradely guided through the femoral, axillary, or subclavian artery to the intended destination; the aortic annulus. The CoreValve US Pivotal trial provided evidence for the clinical effectiveness of these valves. This trial compared the use of transcatheter aortic valve replacement (TAVR) using the CoreValve® Revalving system against surgical aortic valve replacement (SAVR). The inclusion criteria of participants was New York Heart Association (NYHA) functional class II and above, with severe aortic stenosis. The primary endpoint was all-cause death at 1-year following the procedure. The all-cause mortality rate at 1-year from the TAVR group was approximately 14 % in comparison to the SAVR group, which had an all-cause mortality rate of approximately 19 %. The haemodynamic performance was also superior in the TAVR group in comparison to the SAVR group (Arora et al., 2017).

The Edwards Sapien aortic valve is composed of a stainless-steel frame encasing a trileaflet equine pericardial valve. This system is balloon-expandable as opposed to self-expandable. The clinical feasibility of this valve was demonstrated via the PARTNER trial, which was a randomised prospective trial. The design of this trial involved dividing patients into two cohorts; PARTNER A and PARTNER B. Within the PARTNER A cohort, TAVR was compared against SAVR in patients that are poor candidates for surgery. This was defined as the patient having a predicted risk of operative death of ≥ 15 % (Smith, C.R. et al., 2011). Within the PARTNER B cohort, TAVR was compared against conventional medical therapy. Patients were allocated into the PARTNER B cohort based on their death risk and risk of

irreversible comorbidities of more than 50 %. From the PARTNER A cohort, the 1-year mortality rate was 24 % and 26 % for the TAVR and the SAVR groups, respectively (Mack et al., 2015). The results from the PARTNER B cohort significantly favoured TAVR in comparison to the group receiving conventional medical therapy, with a 1-year mortality rate of 30 % and 50 %, respectively (Kapadia et al., 2015).

### 1.5.4 The Unmet Clinical Need for Paediatric Patients

The current gold standard for heart valve replacement in paediatric patients is the cryopreserved allograft (Schlein et al., 2021). However, it is widely recognised that cryopreserved allograft valves demonstrate rapid degeneration particularly in young paediatric patients. In a study conducted by Hawkins, J.A. et al. (1992), it was found that paediatric patients greater than 1 years of age (mean age was 4.5 years) had a 94 % freedom from death or valve explantation following 3 years of aortic or pulmonary cryopreserved allograft valve implantation in comparison to 50 % in children younger than 1 years of age. There are a number of non-immunologic and immunologic factors that can contribute to the accelerated degradation of the allografts. Mechanical factors, anatomical distortion, and allograft size mismatch play a significant role in allograft dysfunction and degradation (Tweddell et al., 2000). Cryopreservation of the valves may also result in the persistence of donor derived viable cells which can produce an immunostimulatory response in the host (Cochran and Kunzelman, 1989). This can lead to immune injury as a mechanism of valve dysfunction and degeneration. Vogt et al. (1999) reported that cryopreserved pulmonary heart valve allografts were explanted from eleven paediatric patients aged 2 – 16 years due to regurgitation, aneurysm and calcifying allograft stenosis at the distal anastomosis. Immunohistochemical analysis of the explanted allografts showed an active T lymphocyte mediated cellular rejection, limiting the durability of the tissue. In addition to this, current options lack the ability to encourage and support somatic growth following implantation. These factors necessitate multiple reoperations in children due technical and clinical implications, despite multiple reoperations further increasing morbidity and worsening the clinical outcome. Therefore, there

is a substantial requirement to address the clinical need for a successful heart valve replacement option, particularly for paediatric patients.

### 1.5.5 Tissue Engineered Heart Valves

Tissue engineering is a pioneering avenue being explored for tissue regeneration and restoration, with great therapeutic potential. The approach taken to fabricate tissue emerges from the idea that the use of three dimensional scaffolds, composed of biologic or synthetic material, provides a hospitable environment that resembles our native extracellular matrix (ECM) for cells to adhere to and proliferate. This ultimately forms viable tissue with the ability to remodel (Haraguchi et al., 2012).

There are requirements that need to be met when designing a feasible tissue engineered heart valve. The size of the heart valve must be tailored to a size that is compatible with the patient, with the leaflets offering minimal resistance to the flow of blood whilst coapting appropriately and efficiently. Additionally, the most appropriate materials selected for engineering a heart valve should not introduce the potential of thromboembolic events when *in vivo*. Furthermore, the components of the valve should be able to endure stress introduced by the cardiac cycle with minimal changes in the geometric features (Ghanbari et al., 2009; Mercer et al., 1973). The material that the scaffold is composed of and the methodology adopted in producing the scaffold can have a significant influence in the success of the fabricated heart valve in meeting these requirements.

#### 1.5.5.1 Synthetic Scaffolds

Synthetic biodegradable polymers such as polyglycolic acid (PGA) and polylactic acid (PLA) have attracted attention for the application of heart valve engineering. The manipulatable properties of polymeric materials can synthetically enhance their mechanical properties (Chetta and Lloyd, 1980).

An advantage of using biodegradable synthetic materials is the controlled degradation rate. It is important for the material to degrade at a rate that is equivalent to the formation of ECM. This factor is particularly important for leaving

behind newly formed tissue that is fully integrated with the patient's anatomical configuration. If the biodegradation rate of the synthetic material is faster than the rate of ECM production, this may result incompetent tissue that may not possess the essential structural and functional integrity. It has been attempted to create heart valve leaflets using synthetic biodegradable materials such as PGA. Hoerstrup et al. (2000) fabricated trileaflet valve scaffolds using PGA mesh coated with bioabsorbable poly-4-hydroxybutyrate prior to seeding with myofibroblasts and endothelial cells, harvested from lambs, for up to 28 days. The seeded trileaflet heart valve constructs were then implanted into the same lambs from which the cells were harvested. Functional leaflets without stenosis, thrombosis or aneurysm was demonstrated up to 20 weeks post-implantation. The collagen, elastin and GAG ECM components and mechanical properties such as Young's modulus and suture retention strength were comparable to native pulmonary artery leaflet tissue. Polymers such as PGA and PLA are able to degrade via cleavage of the polymer chains followed by hydrolysis of the ester bonds. A downside to the *in vivo* degradation of biodegradable synthetic materials is that an adverse immune reaction may be induced by the breakdown products. However, in the case of PGA and PLA, the resultant monomer is usually excreted within urine or enters the tricarboxylic acid (TCA) cycle.

Jana, Soumen et al. (2019) developed electrospun microfibrous scaffolds using polycaprolactone (PCL) in concentrations of 14 %, 16 % and 18 % (w/v) which all had pore sizes that supported the *in vitro* viability, proliferation and infiltration of porcine VICs for 14 days. Although mechanical strength was found to be lowest in the 14 % PCL scaffolds, the tensile strength may be more suitable for heart valve tissue engineering applications as opposed to higher mechanical properties. This is because higher than necessary mechanical properties can negatively influence developing heart valve tissue functionality by causing cells to produce fibrous collagen which can harden the tissue structure (Jana, S. and Lerman, 2019). Following implantation of the 14 %, 16 % and 18 % PCL scaffold materials into the dorsal region of rats for 2 months, the 14 % PCL scaffold was shown to support higher numbers of cell infiltration with macrophages expressing the anti-inflammatory M2 phenotype. This study highlights the low immunogenicity and mechanical compliance of some biodegradable synthetic scaffolds that may be suitable for heart valve tissue engineering.

Coyan et al. (2019) examined the microstructural integrity, haemodynamic function and biocompatibility of a degradable polymeric scaffold implanted into the pulmonary position of 5 porcine models for 12 hours. The polymeric scaffold was generated as a functional tri-leaflet heart valve using electrospun polycarbonate urethane urea mounted onto magnesium stents. All animals showed normal leaflet function and no regurgitation following the cardiopulmonary bypass. The microstructural architecture was also retained with no thrombosis. However, a fibrin sheath formed on 2 out of 5 of the magnesium stents. The acute nature of the work done by Coyan et al. (2019) did not allow investigations into cellularisation potential and long-term durability of the synthetic valves. The translation of *in situ* heart valves engineered from synthetic biodegradable materials into a clinical setting represents a challenge. Tissue development is required to replace the synthetic graft material with self-generated ECM whilst stimulating and maintaining cellular populations. Biological cues should be incorporated into the grafts to promote cellular adhesion as well as orchestration of tissue development (Stassen et al., 2017).

Prodan et al. (2022) investigated the *in vivo* function of bioabsorbable Xeltis pulmonary valve conduits (composed of poly-caprolactone-based and poly-carbonate-based supramolecular 2-ureido-4[1H]-pyrimidone) in the right ventricular outflow tract of twelve children over a 24 month period. Although there were no deaths, no evidence of aneurysm or degeneration, and clinical improvement of all of the patients, six patients had developed severe pulmonary insufficiency, one patient had developed moderate pulmonary insufficiency and six had developed mild pulmonary insufficiency. The development of pulmonary insufficiency was related to anatomical factors such as significant residual gradients distal to the conduit, kinking of the conduit and most prolapse of one of the valve leaflets.

As discussed in section 1.3.2.1, the layers of the valve leaflets are instrumental for the mechanisms involved in the opening and closing of the leaflets. The mechanical compliance of the intricate and complex multiscale fibrous structures as well as the shock-absorbing properties of the spongiosa layers can be difficult to recapitulate using synthetic materials collectively with the ideal morphological, mechanical, and physical properties of the construct (Xue et al., 2017).

### 1.5.5.2 Hydrogel Scaffolds

Hydrogels are materials composed of hydrophilic polymers that are able to conform to three-dimensional (3D) macromolecular network structures. Hydrogels possess physiochemical properties similar to the microenvironment of ECM in addition to allowing the permeability of nutrients and gasses. This is essential to enhance cell viability as cells are normally found within a range of 100-200 μm from a source of oxygen and nutrients *in vivo* (Carmeliet and Jain, 2000). Valvular cells can be entrapped within hydrogels or cultured on the surface of a 3D structure composed of hydrogels, making this model ideal for investigating the interaction between cellular behaviour and the ECM environment provided by the hydrogel.

Hydrogels can be divided into natural and synthetic hydrogels. Natural hydrogels are composed of materials that are found in native ECM, such as collagen, fibrin, and hyaluronan. This is advantageous because these materials would possess an inherent biocompatibility and bioactivity. Duan et al. (2013) fabricated living heterogenous aortic valve conduits composed of natural alginate/gelatin hydrogel formulations with human aortic smooth muscle cells and porcine VICs encapsulated. The ultimate tensile strength of resultant the hydrogels encapsulated with cells was significantly less than the ultimate tensile strength of cell-free hydrogels. The tensile properties of the fabricated conduits in comparison to native or decellularised tissue was not assessed. However, there was good cell viability and phenotypic retention after 7 days of culture.

Synthetic hydrogels are composed of synthetic material such as polyethylene glycol (PEG). Synthetic hydrogels hold advantages over natural hydrogels, in that the properties are manipulatable to allow the adjustment of the biomechanical properties of the polymers as well as the fidelity of the polymer structures. Additionally, synthetic hydrogels can be modified by the addition of biological composites to enhance the biological functions of the polymer structures (Nicodemus and Bryant, 2008). Guo et al. (2021) developed a polyhedral oligomeric silsesquioxane-PEG hybrid hydrogel and assessed platelet adhesion in comparison to porcine aortic valve leaflets. Using a platelet adhesion assay, platelet adhesion was shown to be significantly less on the hybrid hydrogel scaffolds in comparison to the decellularised heart valve leaflet control. However,

the biomechanical properties such as tensile strength of the hydrogels in comparison to the decellularised tissue was not assessed.

Hydrogels are in general mechanically weaker than native heart valve ECM which is not ideal for the fabrication of heart valve constructs that must have mechanical integrity that mimics native conduit performance until remodelling of the conduit is complete *in vivo* (Ciolacu et al., 2022).

## 1.6 Decellularised Heart Valves

Natural scaffolds are comprised of pure ECM components, such as collagen and fibrin. In the context of a natural heart valve, this refers to decellularised intact allografts or xenograft tissue. The removal of cellular components found within the allograft or xenograft tissue would remove the antigenic components of the graft, and thus would eradicate the possibility of an adverse immune reaction being induced within the recipient in addition to reducing the risk of calcification. Additionally, the removal of the donor cells may encourage the proliferation of endogenous cells that are capable of repair and remodelling *in vivo*. This addresses the limitations presented by current options by overcoming the issue of valve structural and functional deterioration overtime, as well as potentially removing the requirement of multiple reoperations by the graft being able to grow with the recipient.

The SynerGraft™ process was developed by CryoLife Inc as a process aimed to reduce antigens within donated human heart valves. This process induces lysis of resident cells by incubation within water and nuclease digestion, followed by isotonic wash out phase (O'Brien et al., 1999). Applying this SynerGraft™ process to pulmonary allografts, subsequent *in vitro* analysis demonstrated the almost complete removal of cellular components, which was confirmed by using histological and immunocytochemical analysis (Elkins et al., 2001). Additionally, there was no significant changes to the biomechanical properties *in vitro* . Simon et al. (2003) implanted SynerGraft porcine pulmonary heart valves into the right ventricular outflow tract of four children aged 2.5 – 9 years. This study was the first to report the rapid failure of the Synergraft processed grafts. Three of the four children died, two with severely degenerated SynerGraft valves at 6 weeks and 1

year following implantation, and the third after 7 days post-implantation due to spontaneous rupture of the SynerGraft valve commissures. The fourth graft was explanted from the patient 2 days following implantation, as a precaution. Macroscopic evaluation of the SynerGraft valves used in this study demonstrated severe inflammation of the valve following implantation, leading to the fatal structural failure of the grafts. Calcific deposits were detected in the SynerGraft valves, most likely due to incomplete decellularisation (Simon et al., 2003). The severe inflammatory response in the recipients of these implants may have been due to residual immunogenicity of the ECM, or the incomplete removal of xenoantigens. Consequentially, the implantation of the SynerGraft (porcine) valves were aborted.

The rapid failure of the SynerGraft valve highlighted the requirement for a more robust decellularisation process that can effectively deceullularise valve grafts without compromise of the structural and functional properties of the grafts. Within the literature, various methods of tissue decellularisation have been explored. This includes physical, chemical, and enzymatic methods (**Table 1.1**).

**Table 1.1 Methods of Decellularisation.**

| Method | Mode of Action | Effect on ECM | References |
|---|---|---|---|
| **Physical** | | | |
| Snap Freezing | Ice crystals disrupt the cellular membrane | Fracture or disruption of ECM during rapid freezing | (Keane et al., 2015) |
| High hydrostatic pressure | Induces necrosis | Reduces biomechanical properties | (Watanabe, N. et al., 2019) |
| Supercritical Fluid | Facilitate chemical agent infiltration to achieve enhanced cell lysis | Can dehydrate ECM | (Sawada et al., 2008; White, A. et al., 2006) |
| **Chemical** | | | |
| Acid; Alkaline | Disrupt nucleic acids, solubilise cytoplasmic components of cells | Removes GAGs | (Keane et al., 2015) |
| **Non-Ionic Detergents** | | | |
| Triton X-100 | Disrupts the interactions between lipids and lipids/proteins, whilst leaving protein-protein interactions undisturbed | Removes GAGs | (Mendoza-Novelo et al., 2011) |
| **Ionic Detergents** | | | |
| Sodium Dodecyl Sulphate (SDS) | Solubilise cytoplasmic and nuclear cellular membranes | Disrupts native tissue structure, damages collagen, removes GAGs | (Uygun et al., 2010) |
| Sodium Deoxycholate | | Less disruptive to tissue structure than SDS | (Faulk et al., 2014b) |
| Triton X-200 | | Greater cell removal when used in conjunction with each other | (Gilbert et al., 2006) |
| Zwitterionic Detergents | | | |
| Hypotonic and Hypertonic Solutions | Induces cell lysis by osmotic shock | Does not effectively remove cellular debris | (Moffat et al., 2022) |
| **Enzymatic** | | | |
| Trypsin | Cleaves peptide bonds on the C-side of Arg and Lys | ECM structure can be disrupted when exposed for too long, removes laminin, fibronectin, elastin, and GAGs | (Zou and Zhang, 2012) |
| Nucleases | Catalyse the hydrolysis of the interior bonds of ribonucleotide and deoxyribonucleotide chains | Could invoke immune response | (Moffat et al., 2022) |

There have been some clinical studies that reported on the success of decellularised heart valves that were exposed to different decellularisation protocols. Bechtel et al. (2008) reported on the fifty-two months' mean follow up of decellularised human pulmonary allografts (CryoValve SG; CryoLife inc). The decellularised allografts investigated within the clinical study were prepared using a cellular lysis step with hypotonic sterile water followed by treatment with a combined solution of ribonuclease and deoxyribonuclease. Tissue was then exposed to a washout period with isotonic neutral buffer solution. The time and temperature conditions used for the tissue decellularisation were unspecified (O'Brien et al., 1999). No reoperations were required after a mean follow up of 52 months post-implantation into the right ventricular outflow tract of 23 adult patients. However, the mean transvalvular pressure gradient increased at 52 months in comparison to conventional allografts. Boethig et al. (2019) also reported on the clinical success of decellularised human pulmonary valve allografts (Corlife oHG). The decellularised allografts were prepared using 0.5% sodium deoxycholate and 0.5% sodium-dodecylsulphate for 36 hours at room temperature with agitation. The allografts were then washed with NaCl 0.9% solution and stored at 4°C for up to 3 weeks until implantation. Following 2.2 ± 0.6 years post-implantation into 121 patients aged 21.3 ± 14.4 years, the decellularised heart valves functioned with excellent short-term haemodynamics. da Costa, F. et al. (2007) evaluated the medium-term performance of decellularised human pulmonary allografts implanted into the right ventricular outflow tract of 68 patients aged 9 to 56 years during Ross procedure. The allografts were first cryopreserved with 10% dimethyl sulphoxide and 10% fetal bovine serum which protects the tissue from damage induced by ice crystal formation (Park et al., 2018). The grafts were then thawed 15 to 30 days before undergoing the decellularisation process that included 24 h of agitation with 1% sodium deoxycholic acid and 80% ethanol or 0.1% sodium dodecylsulphate. Although decellularisation of allografts using deoxycholic acid previously demonstrated a reduced immune response and better haemodynamic performance in comparison to cryopreserved allografts up to 18 months post-implantation into patients, the medium term study demonstrated that some allografts decellularised using deoxycholic acid had some pressure gradient rises which was most likely due to incomplete decellularisation (da Costa, F. et al., 2007; da Costa, F.D. et al., 2005).

The decellularisation method was then changed to use SDS instead of deoxycholic acid due to evidenced complete and reliable graft decellularisation (Korossis, S.A. et al., 2005). Subsequently, medium term (up to 6-years) follow-up on the SDS-decellularised grafts has demonstrated an equivalent or superior rate of reoperation compared to standard cryopreserved pulmonary valve allografts (da Costa, F.D. et al., 2014; da Costa, F.D.A. et al., 2018). Clinical studies performed by the same group to assess decellularised aortic valves demonstrated the low rate of calcification and sufficient haemodynamic performance (da Costa, F.D. et al., 2010).

## 1.7 The Importance of Sterilisation of Decellularised Heart Valves

Despite there being an extensive amount of research into replacement heart valves, a terminal sterilisation process is not yet included within the decellularisation procedure. Decellularised allograft heart valves currently in clinical use rely on aseptic conditions during procurement and production and antibiotic or chemical disinfection to assume sterility (da Costa, F.D. et al., 2006; Waqanivavalagi et al., 2020). However, an effective and robust sterilisation process is essential to eliminate pathogenic microorganisms from xenogeneic heart valves without adversely affecting the inherent biomechanical and biocompatible properties of the valve. Sterilisation can essentially enhance the safety and clinical efficacy of these heart valve replacements by providing a superior sterility assurance level (SAL) and supplement the production efficiency of these valves. Sterility of an object is defined as the absence of living microorganisms that could otherwise introduce adverse effects when administered. This includes spore forming bacteria, non-spore forming bacteria, fungi, protozoa and viruses. A SAL of at least $10^{-6}$ is the requirement for a sterilisation method to obtain when applied to healthcare products, in accordance to international standard ISO 14937 (ISO, 2009). This refers to the probability that no more than one viable microorganism will be detected out of a million sterilised healthcare products (von Woedtke and Kramer, 2008).

### 1.7.1 Pathogenic Microorganisms Associated With Tissue Grafts

Various pathogenic microorganisms such as bacteria and viruses may contaminate tissue grafts making them unfit for clinical use. The pathogenic microorganisms may be resident within the tissue graft or may be acquired from the environment during processing and production of the implant. The resident microorganisms may cause failure of the tissue graft when implanted into the recipient, as well as potentially inducing life threatening consequences. Therefore, a suitable sterilisation method needs to exert biocidal effects against a wide range of pathogens (Figure 1.8).

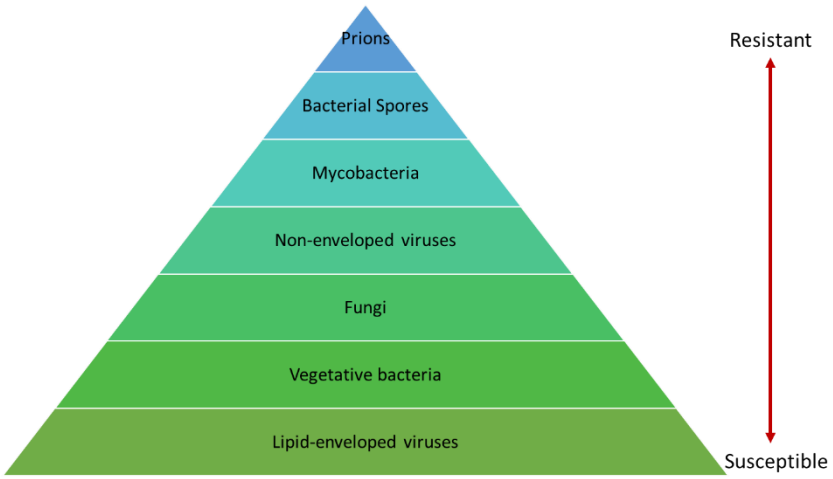


**Figure 1.8 Order of microorganisms resistance to sterilisation.** Adapted from Mohapatra (2017).

#### 1.7.1.1 Bacteria

Bacteria are unicellular prokaryotic organisms which can be separated into two classes; Gram-negative bacteria and Gram-positive bacteria, based on the composition of the distinctive peptidoglycan cell wall. Gram-positive bacteria possess a thick peptidoglycan cell wall along with teichoic acid, whereas Gram-negative bacteria possess a thin peptidoglycan cell wall with no teichoic acid, but with porins and hydrophilic channels present in the outer membrane.

The use of antibiotic treatment for allograft aortic valves was introduced in 1977, and has since been used for banking valve allografts in combination with cryopreservation (Farrington et al., 2002). Antibiotics are effective in terminating bacteria by interfering with essential cellular processes such as cell wall synthesis and protein synthesis (Dai et al., 2016). However, there are a number of limitations associated with the application of antibiotics as a decontaminant procedure for

healthcare products. The activity of antibiotics does not consistently decontaminate tissue as they may be specific to cellular processes specific to one type of bacteria. A cocktail of antibiotics may resolve this issue by including antibiotics that target different cellular processes that are specific to the bacteria. However, antibiotic resistance is an alarming issue on a global scale. The use of antibiotics to eradicate bacteria may become ineffective, or may even contribute toward the antibiotic resistance crisis. Furthermore, bacteria adopt evasion strategies for immunity against bactericidal exposures.

#### 1.7.1.2 Biofilms

Bacteria exist in two different forms; the planktonic state refers to bacteria that are free floating, and the sessile state refers to bacteria that are adhered to a surface. The attachment of bacteria to a surface results in the alteration of gene expressions that are responsible for the production and maturation of exopolysaccharide (EPS). This produces a protective barrier of EPS matrix surrounding a community of bacteria adhered to a surface. The biofilm provides protection against the organism's endogenous defence system as well as external agents such as antibiotics.

Gram-positive and gram-negative bacteria both have the ability to form biofilms on medical devices. The most common forms are *Enterococcus faecalis*, *Staphylococcus aureus*, *Staphylococcus epidermidis*, *Streptococcus viridans*, *E. coli*, *Klebsiella pneumoniae*, *Proteus mirabilis* and *Pseudomonas aeruginosa*, with *S. aureus* and *S. epidermidis* estimated to cause about 40–50 % of prosthetic heart valve infections (Khatoon et al., 2018).

#### 1.7.1.3 Bacterial Endospores

Some bacteria, such as such as *Bacillus subtilis*, *Bacillus anthracis* and *Clostridioides difficile* can form endospores which are dormant structures produced in response to harsh environmental conditions, such as lack of nutrients. Sporulation facilitates the survival of the population, as spores can germinate and outgrow into vegetative bacteria capable of reproduction under suitable environmental conditions. The endospores possess novel architectural and molecular properties endowing them with the tools required to resist extreme environmental stresses.

This includes the structure of the spore, the presence of protective components, and the ability of the spore to retain water.

A protective multi-layered coat composed of proteins, lipids and polysaccharides, and a cortex layer surrounds the membrane bound core which contains the genetic material and the spore enzymes. These external layers provide a protective barrier to the spore by preventing the penetration of chemical agents that can induce reactive oxidative species formation. The core itself possesses unique survival features, such as a low water content which decreases hydroxyl radical formation, and spore-specific proteins aiding DNA stabilisation. The core is able to immobilise water, affecting the movement of peroxide and radical species, enabling resistance against a number of sterilisation methods that depend on free radical formation as the assault (Laue et al., 2018). Therefore, the ability of bacterial endospores to survive extreme conditions needs to be considered when choosing a suitable sterilisation method and appropriate dosage.

#### 1.7.1.4 Viruses

Viruses are non-cellular microorganisms that are composed of a central nucleoplasmid made from single or double stranded RNA or DNA, which is contained by a protein capsid. Viruses lack the molecular components to orchestrate and execute viral replication. Because of this, viruses are dependent on host cells to replicate nucleic acids, synthesise viral proteins to replicate itself, and ensure the release of viral particles.

Antibiotic ineffectiveness against viruses is problematic, especially when applying xenogenic sources of tissue for *in vivo* use as there is a chance of zoonotic transmission of diseases from the animal tissue into the human host. Pigs have significantly attributed towards zoonotic infections in humans, such as the 'swine flu' epidemic that also resulted in fatal cases (Wells et al., 1991). Additionally, the encephalitis epidemic in Singapore and Malaysia caused by the porcine derived Nipah virus demonstrates the catastrophic consequences of porcine derived zoonotic infections. Porcine endogenous retrovirus (PERV) is another threat as it is able to infect human cells *in vitro* (Boneva et al., 2001). In 2022, a human patient that received a genetically modified porcine heart transplant died two months

following implantation, with no obvious cause initially identified. It was later learned that the porcine heart was affected by porcine cytomegalovirus, which potentially contributed towards the patient's death (Mueller, 2022). Therefore, the development of an effective terminal sterilisation procedure following decellularisation of porcine heart valves is essential to enhance safety when clinically translated.

#### 1.7.1.5 Fungi

Fungi are eukaryotic microorganisms that are composed of complex structures, such as hyphae adapted to allow growth on solid surfaces and tissues. There has been increasing evidence to suggest that fungal species, such as *Cryptococcus*, *Trichosporon*, *Saccharomyces*, and in particular *Candida*, contribute largely to medical device infections. Fungi are responsible for 2-10 % of all prosthetic valve endocarditis, with *Candida* accounting for 90 % of these fungal infections.

Fungal species are also able to form fungal biofilms on medical devices, either by themselves or in conjunction with bacteria, complicating the extermination of these pathogens. Fungal cells arrive at the medical device surface and adhere, initiating IC communication triggering a phenotypic switch that results in the production of ECM and biofilm. The growth and maturation of the fungal biofilm leads to the release of planktonic cells that are able to disperse into systemic circulation. Consequentially, the fungal infection can interfere with the healing phase post-implant of a medical device, as well as cause a potentially lethal bloodstream infection (Giles et al., 2018).

Fungi are susceptible to elimination via free radical damage to DNA molecules. A potent sterilisation method that utilises this mode of biocidal action and suitable dose must be selected in order to achieve a SAL of $10^{-6}$.

#### 1.7.1.6 Prions

A prion is referred to as a mysterious proteinaceous infectious agent that was found to be responsible for several neurodegenerative diseases in humans, such as Creutzfeldt-Jakob disease. In contrast to bacteria, virus, and fungi, prions have no

nucleic acids. Prions form aggregates of proteins called amyloids which accumulate in infected tissue, leading to tissue damage and death.

Investigators have found that a combination of sodium hydroxide with steam sterilisation at 121 °C for 1 h results in complete inactivation of infectivity of prions. However, these conditions will be deleterious to tissue grafts. Based on the literature, the complete removal of animal-derived serum from the implant would be a suitable precaution to take to minimise potential of risk of contamination (CDC, 2018).

### 1.7.2 Sterilisation Techniques of Soft Tissue

Sterilisation techniques can be divided into chemical and physical sterilisation methods. These methods have different modes of action in deactivating microorganisms. Chemical sterilisation methods includes the use of nitrogen dioxide, ozone, peracetic acid, hydrogen peroxide, and most commonly ethylene oxide. Physical sterilisation methods includes the use of heat in the form of steam, dry heat and tyndallisation. Non-thermal options of physical sterilisation methods are also available, such as gamma or e-beam irradiation, and plasma sterilisation. Supercritical carbon dioxide ($ScCO_2$) is a sterilisation technique that combines both chemical and physical methods. The selection of the sterilisation method is determined by the intended application. For the purpose of sterilising decellularised heart valves, it is important to devise a sterilisation method that does not have negative implications when applied to soft tissues, whilst executing its purpose; inactivation and removal of microorganisms.

#### 1.7.2.1 Chemical Sterilisation Methods

**Ethylene Oxide**

Ethylene oxide (EtO) is most commonly used to sterilise rubber and plastic products in a healthcare setting. It is effective at low temperatures and active against a wide spectrum of microorganisms, including gram-positive bacteria, fungal, spores and viruses. EtO exerts its sterilisation effects by permanently suppressing cellular metabolism and division due to the irreversible alkylation of

cellular molecules. The effectiveness of EtO as a successful sterilant is dependent on parameters such as temperature, pressure, concentration and contact time (Hsiao et al., 2012).

It has been observed that the use of EtO is associated with a lower rate of collagen degradation within ECM structures in comparison to other sterilisation methods (Delgado et al., 2014). Although tissue banks would commonly use EtO treatment as a sterilisation process of tissue, the cytotoxic effect of residual EtO has been reported widely. Butterworth and Chapman (2007) demonstrated the genotoxic risk of residual biologically active EtO in driving donor cell leukaemia. The *in vivo* cytotoxicity of a bone material that was treated with EtO was also investigated by Hastings et al. (1990), with degassing being unable to remove the cytotoxic residual EtO.

**Peracetic Acid**

Peracetic acid (PAA) is a sterilising technique that is effective at low temperatures and has a high penetration potential. PAA is active against a wide spectrum of microorganisms, including bacteria, spores, viruses and fungi. The mechanistic actions of PAA involves the production of hydroxyl radicals (Clapp et al., 1994) and activity as an oxidising agent, inactivating enzymes essential for microorganism survival. The antimicrobial activity of PAA is dependent upon parameters such as concentration, temperature, pH and humidity, with a higher concentration and temperature of PAA demonstrating greater antimicrobial activity. It has also been reported that when PAA is used in conjunction with hydrogen peroxide, a synergistic effect is exerted with an enhanced sterilisation ability. The by-products generated by PAA, such as carbon dioxide, water and oxygen have a low toxicity (Huang, Q. et al., 2004). Chemical modifications of the collagenous tissue surface by PAA has also been show to enhance cell adhesion (Matuska and McFetridge, 2015).

The acidity and strong oxidation capacity of PAA can impact the biological and biomechanical properties of some materials. Fidalgo et al. (2018) reported on the effects of 0.05 % and 1 % PAA sterilisation treatment decellularised porcine pericardium. The structural integrity and biocompatibility of the tissue scaffolds was retained following PAA sterilisation. However, the distinct cobblestone-like morphology of the pericardium surface structures appeared uncharacteristically

smooth and unwrinkled following PAA sterilisation. There was evidence to suggest that PAA sterilisation under both concentrations also impaired cell adhesion as the adhesion of human bone marrow mesenchymal stem cells appeared distorted after 7 days of culture with PAA treated decellularised porcine pericardium (Fidalgo et al., 2018). Rosario et al. (2008) found that the Young's modulus of decellularised porcine bladder significantly decreased following sterilisation with 0.1 % PAA for 3 hours. The use of PAA on collagenous tissue can be detrimental, particularly to type IV collagen, as found within the basement membrane of blood vessels in decellularised human dermis (Hogg et al., 2015), and surface of decellularised porcine pericardium (Fidalgo et al., 2018) . Despite this, immersion of porcine aortic roots in PAA is included within the decellularisation protocol devised by Paniagua Gutierrez et al. (2015). The inclusion of this step did not negatively impact the biomechanical function of the valves used within the study, and excellent biocompatibility was demonstrated *in vivo* in a sheep model.

**Hydrogen Peroxide**

Hydrogen peroxide ($H_2O_2$) exerts bactericidal, virucidal, sporicidal and fungicidal effects by producing hydroxyl free radicals that are detrimental to membrane lipids, DNA, and proteins essential for cellular metabolism. Wardle and Renninger (1975) demonstrated that a 10 % concentration of $H_2O_2$ resulted in a complete elimination of $10^6$ *Bacillus* spores with a 60-minute exposure time. A 1:16 dilution of 7 % $H_2O_2$ was also proven to exert bactericidal, virucidal, sporicidal, and fungicidal effects at different lengths of exposure for each type of microorganism (Sattar et al., 1998). $H_2O_2$ is commonly applied as a wound antiseptic, dental disinfectant, contact lens treatment and food disinfection post-harvesting (Linley et al., 2012).

Gardner et al. (2013) reported that 5 mins of treatment with 3 % (v/v) $H_2O_2$ does not alter the ultimate tensile strength of human allograft tendons. The selected treatment time and concentration conditions were selected to reduce tendon allograft bacterial contamination. However, the sterilisation potential of the treatment (i.e. the effect on microbial load) was not investigated during the study. Leow-Dyke et al. (2016) tested a range of concentrations and pH values of $H_2O_2$ to determine the impact of this sterilisation technique on decellularised human

dermis, alone and in conjunction with copper chloride ($CuCl_2$) at varying pH. The use of $CuCl_2$ alongside $H_2O_2$ was inspired by the sterilisation potential of copper-based formulations. Copper impregnated surfaces have been shown to significantly reduce the bacterial bioburden and hospital-acquired infections. Leow-Dyke et al. (2016) demonstrated that $CuCl_2$ in a concentration range within 0.1 mg/L-1 g/L and $H_2O_2$ within a concentration range of 0.01-7.5 % had no detrimental impact on the morphology, biocompatibility, and biomechanical properties of the decellularised human dermis. Additionally, the bactericidal and sporicidal activity of the investigated concentrations against *Staphylococcus epidermidis* (*S.epidermidis)*, *Escherichia coli* (*E.coli)* and *Bacillus subtilis* (*B.subtilis)* spores was demonstrated (Leow-Dyke et al., 2017). $CuCl_2$ and $H_2O_2$ as a potential tissue sterilising agent has not yet been applied to decellularised porcine pulmonary heart valves as this treatment is relatively unexplored within the literature.

**Ethanol**

Ethanol is a low cost treatment and a potent bactericidal agent at different concentrations and exposure times that can operate at ambient temperatures. Ethanol inactivates microorganisms by causing the denaturation of proteins, dehydration of cells, and disruption of lipids present within cell membranes. Ten seconds of ethanol exposure at concentrations ranging from 30-40 % was effective for eliminating *Pseudomonas aeruginosa*, *Serratia marcescens*, *E. coli* and *Salmonella typhosa* (Coulthard and Sykes, 1936). At concentrations of 60-80 % ethanol is also a potent virucidal agent (Mbithi et al., 1990).

Although the immersion of collagen scaffolds within ethanol has been used in laboratories as a disinfection step (Ma et al., 2003), the use of ethanol for the sterilisation of medical and surgical materials is not recommended. This is due to ethanol lacking sporicidal activity, and the penetration of protein-rich material is poor. There is evidence to suggest that the immersion of a medical device into ethanol may alter the structural properties of the material, which can subsequently impact the biomechanical properties (Shearer et al., 2006).

**Electrolysed Water**

Electrolysed water is an emerging novel technology that is used in a wide range of fields, such as agriculture, food sanitisation and medical sterilisation. Electrolysed water is active against a wide range of microorganisms, including bacteria, viruses, fungi and spores, in a relatively short time frame of 5 to 20 seconds (Quan et al., 2010; Rahman et al., 2016). The production of electrolysed water involves an electrolysis chamber that contains sodium chloride ($NaCl_2$) solution with a diaphragm separating the cathode and anode. A current is passed through the electrolysis chamber, forming alkaline electrolysed water at the cathode, and acidic electrolysed water at the anode. The oxidation-reduction potential, chlorine concentration and pH of the electrolysed water influences the antimicrobial efficacy. Chlorine infiltrates the membrane of microorganisms and produces hydroxyl radicals which exert antimicrobial activity via oxidation disrupting essential metabolic components (Rahman et al., 2016).

In a study conducted by Yanik et al. (2015) it was found that a 1:10 dilution of 100 % electrolysed water was sufficient in reducing bacteria that are responsible for certain types of hospital acquired infections. Hussein et al. (2013) reported the sterilisation efficacy of electrolysed water on decellularised porcine liver without adverse impact on collagen and GAG content, cytocompatibility and cell attachment. However, the efficacy of electrolysed water as a sterilisation technique for porcine decellularised aortic heart valves was investigated by Hennessy et al. (2017). This research group found that electrolysed water did not have a significant impact on the sterility of the decellularised heart valves.

### 1.7.2.2 Physical Sterilisation Methods

**Gamma Irradiation**

Gamma irradiation is a common sterilisation method used by tissue banks to terminally sterilise skin or bone allografts and medical equipment. The ionising gamma irradiation is sourced from radionuclide elements such as cobalt-60 which emit gamma rays that are able to readily pass through the materials and lyse DNA and RNA strands (Brinston and Wilson, 1993; Eagle et al., 2005; Rooney et al.,

2008). Gamma rays generate reactive oxygen species (ROS) which have a deleterious effect on DNA molecules, and cause the dysfunction of enzymes (Rendic and Guengerich, 2012). Gamma irradiation has been proven to inactivate bacteria, moulds, yeasts, viruses, and spores, making it a potent option for reducing bioburden of medical devices (Dai et al., 2016).

Despite being effective at terminating a broad range of microorganisms, there is a growing amount of evidence to suggest that the application of gamma irradiation for the sterilisation of tissue allografts results in detrimental morphological and functional alterations. In a study conducted by Helder et al. (2016), decellularised porcine aortic heart valves were exposed to gamma irradiation in doses of 1,000 Gy, 3,000 Gy, or 10,000 Gy to assess both sterility and ECM integrity. *In vitro* mechanical testing showed a decrease in the stiffness and ultimate tensile strength of cusps of the gamma irradiated tissue in comparison to control valves that received no gamma irradiation. Despite this *in vitro* finding, decellularised porcine aortic heart valves gamma irradiated with 1,500 Gy and 3,000 Gy were implanted into 3 sheep models. Valve malfunction was apparent at 1 week post-implantation with signs of stenosis. The proposed mechanism for these findings is that irradiation of collagen fibres may fraction the α-polypeptide chains or induce cross-linking via the presence of free radicals altering biomechanical behaviour(Cheung et al., 1990).

Somers et al. (2009) also demonstrated that the exposure of decellularised porcine heart valve matrices to 1, 10, 50 and 100 Gy gamma irradiation exerted detrimental effects on the microenvironment of the scaffolds which negatively impacted the elasticity and tensile strength properties. Gamma irradiation of wet tissues causes radiolysis of water molecules that releases free radicals that can cross-link collagen molecules. As well as detrimentally impacting the mechanical properties in a dose dependent manner, cross-linking of collagen fibres can also make the tissue more susceptible to calcification which can also impact the biomechanical function and long-term durability of the valves (Nguyen et al., 2007; Somers et al., 2009).

**E-beam Radiation**

E-beam radiation is considered to be an alternative to gamma irradiation, with a similar mode of action. The highly charged e-beam is generated by the acceleration of electrons, with energy levels within the beam controlled by altering the concentration and acceleration rate. The exposure time to e-beam radiation is relatively short and causes less deleterious effects of materials than gamma irradiation (Silindir Gunay and Ozer, 2009). Although, the penetration potential of e-beam is determined by the kinetic energy of electrons and the density of the biomaterial intended for sterilisation, e-beam radiation is typically characterised by a low permeability potential (Dai et al., 2016).

Elenes and Hunter (2014) compared the biomechanical properties of tendon allograft to aseptic, non-sterilised controls and gamma-irradiated grafts. Allografts were exposed to either a high (17.1 to 21.0 KGy), or a low dose of e-beam (9.2 to 12.2 KGy). Exposure of the tendon allografts to a high dose of e-beam radiation did not significantly alter the biomechanical properties in comparison to the controls, suggesting that e-beam radiation is less damaging to the architectural composure of collagenous tissue in comparison to gamma radiation. However, the effectiveness of e-beam radiation in reducing bioburden was not explored within the study.

**Electroporation**

Electroporation, or pulsed electric field, refers to the application of an electric field to cells resulting in the increase in the permeability of the cellular outer membrane. This causes the loss of the membrane barrier function, disrupting the intracellular homeostasis and subsequently resulting in the termination of the targeted microorganism. Effectiveness of electroporation is determined by the strength of the electric field, and the length of time that the field is applied (Yarmush et al., 2014). Electroporation is an innovative tool because it does not depend on the use of thermal energy or chemical reactions to exert its effects. The use of electroporation in the food and liquid decontamination industries is extensively explored because it provides a low energy alternative to current decontamination methods such as pasteurisation, which causes a reduction in the nutritional value of foods in addition to altering taste (Kishore et al., 2007). The

potential of electroporation as a terminal sterilisation method for tissue grafts is, however, relatively unexplored within the literature.

**Supercritical Carbon Dioxide**

Supercritical carbon dioxide ($ScCO_2$) is a novel sterilisation technique that has gathered attention due to possessing properties that are ideal for the sterilisation of tissues and biomaterials.

$ScCO_2$ is recognised as an environmentally benign solvent that has a diverse range of applications across food, biomaterials and pharmaceutical industries (Zhang, X. et al., 2014). $ScCO_2$ has been investigated and used for the extraction of valuable compounds for the past three decades (Ali Mansoori et al., 1988). The critical point of carbon dioxide is achieved at temperatures of 31 °C and pressures of 1099 psi. At conditions above the critical point, carbon dioxide becomes a supercritical fluid with properties of both gaseous and liquid states (Cooper, 2000). As the critical point of $ScCO_2$ is achieved at mild temperature and pressure conditions, $ScCO_2$ treatment ideal for the application of tissues and materials that are sensitive to heat degradation. In the food industry, $ScCO_2$ technology has been used for fruit and vegetable preservation without adversely impacting food quality (Damar and Balaban, 2006). $ScCO_2$ is non-toxic and does not leave toxic residuals following its application. The structural and functional properties of biological tissue scaffolds exposed to $ScCO_2$ would not be compromised as $CO_2$ is non-reactive (Nichols et al., 2009). Furthermore, $ScCO_2$ has a low viscosity and surface tension, making it an ideal choice for the penetration of tissues and materials.

The penetration potential of $ScCO_2$ allows $ScCO_2$ accumulation within cells which results in acidic intracellular pH levels, disrupting the metabolic processes and ultimately resulting in microbial death (White, A. et al., 2006). $ScCO_2$ is effective against bacterial, viral, and fungal bioburden (Spilimbergo and Bertucco, 2003). When combined with additives such as hydrogen peroxide and PAA, the biocidal activity of $ScCO_2$ is enhanced which is likely due to the acidic or oxidative properties of these reagents. The acidification of the cytoplasm and extracellular medium by the formation of carbonic acid from $CO_2$ causes damage to the cell membrane, increasing the penetration of $CO_2$ by increasing membrane permeability. Using $ScCO_2$ and 0.1 % $H_2O_2$ at moderate temperature and pressure

conditions of 50 °C and 1176 psi, within 30 minutes Checinska et al. (2011) were able to obtain a 6-log reduction of *Bacillus pumilus* SAFR-032 endospores that have been shown to be resistant to UV irradiation and 5 % $H_2O_2$ when compared to other *Bacillus* species. Other mechanisms of $ScCO_2$ treatment can also contribute towards sterilisation efficacy, such as extraction. $CO_2$ is lipophilic and therefore has the ability to extract phospholipids from the cell membrane and intracellular structures (Lin et al., 1992; Ribeiro, N. et al., 2020).

The sterility and mechanical properties of $ScCO_2$ treated decellularised porcine aortic valves were investigated by Hennessy et al. (2017). The decellularised valves were sterilised in Tyvek pouches using the NovaProcess™, which is a patented $ScCO_2$ sterilisation protocol commercially available by NovaSterilis (NovaSterilis, NY). The sterilisation protocol relies on the Nova2200™ supercritical vessel and a reagent containing PAA and $H_2O_2$ to supplement the $ScCO_2$ treatment. The findings from this study demonstrated that the use of $ScCO_2$ with the enhancing reagents did not adversely affect the tensile mechanical properties in comparison to controls, but functional studies were not carried out. However, $ScCO_2$ sterilisation of decellularised porcine pulmonary heart valves has not yet been investigated within the literature. Additionally, there is no published work investigating $ScCO_2$ processing of decellularised tissue grafts whilst submerged in PBS during processing. The impact of $ScCO_2$ sterilisation on decellularised peripheral nerve grafts whilst submerged in PBS was investigated at University of Leeds Institute of Medical and Biological Engineering (Holland, 2019). There was found to be a superior retention and distribution of collagen IV, laminin and fibronectin in comparison to $ScCO_2$ sterilisation treatment of the decellularised peripheral nerve grafts processed in Tyvek pouches (Holland, 2019). It was proposed that PBS solution during processing had a protective effect by diluting the local concentration of oxidising agents (Holland, 2019). Thus, it is also relevant to investigate if these protective effects are also translated to $ScCO_2$ sterilisation of decellularised porcine pulmonary heart valves.

## 1.8 Rationale, Aims and Objectives

### 1.8.1 Rationale

The rationale for this research is that decellularised pulmonary heart valves pose a promising alternative to current heart valve replacement options for the reconstruction of the right ventricular outflow tract during the Ross procedure. With an increasing awareness and requirement for sterility assurance of medical devices, the inclusion of a robust sterilisation method is essential to make this option fit for clinical use. Although many sterilisation methods may be detrimental when applied to decellularised heart valves, there are still a number of unexplored avenues for sterilisation. Exploration of such novel methods would provide an initial appraisal of the most suitable sterilisation method for decellularised heart valves. This would ultimately facilitate the translation of decellularised heart valves to commercial production whilst assuring patient safety to promote the clinical utilisation of decellularised heart valves.

$CuCl_2$ and $H_2O_2$ is a novel sterilisation method that is relatively unexplored within the literature for tissue sterilisation applications. Preliminary studies (unpublished) conducted within University of Leeds Institute of Medical and Biological Engineering demonstrated the potential of $CuCl_2$ and $H_2O_2$ treatment for decellularised porcine pulmonary heart valve sterilisation. However, optimisation of $CuCl_2$ and $H_2O_2$ treatment conditions prior to investigation of the impact on decellularised porcine pulmonary heart valves would be beneficial.

$ScCO_2$ is a novel sterilisation method that has been demonstrated to be ideal for tissue sterilisation. However, the impact of $ScCO_2$ on the biological and biomechanical properties of decellularised porcine pulmonary heart valves that have been decellularised using a specifically designed method that incorporates 0.1 % SDS, nuclease and protease inhibitors has not yet been reported (Luo et al., 2014).

### 1.8.2 Aim

The aim of this research was to assess the impact of the novel sterilisation methods ($CuCl_2$ and $H_2O_2$ and $ScCO_2$) on the biological and biomechanical properties of decellularised porcine pulmonary heart valves.

### 1.8.3 Objectives

i. To validate a decellularisation protocol modified from Luo et al. (2014) (with the absence of peracetic acid decontamination step) for porcine pulmonary heart valves.

ii. To identify and optimise $CuCl_2$ & $H_2O_2$ formulations for decellularised porcine PHV (dPHV) sterilisation;

iii. To characterise the effects of $CuCl_2$ & $H_2O_2$ sterilisation on the biological and biomechanical properties of dPHVs.

iv. To characterise the effects of a commercially available $ScCO_2$ sterilisation protocol, The NovaProcess™, on the biological and biomechanical properties of dPHVs;

v. To further characterise the effects of a commercially available $ScCO_2$ sterilisation protocol, The NovaProcess™, on the functional biomechanical performance of dPHVs.

# Chapter 2 : Materials and Methods

This chapter details the general materials and methods used throughout this study. Specific methods are described in the pertinent chapters.

## 2.1 Materials

### 2.1.1 Chemicals and Reagents

The chemicals and reagents and the suppliers used are listed in Appendix A, supplementary table 1.

### 2.1.2 Equipment

The equipment and the suppliers used are listed in Appendix A, supplementary table 2.

### 2.1.3 Labware and Consumables

The labware and consumables and the suppliers used are listed in Appendix A, supplementary table 3.

### 2.1.4 Glassware

All glassware (duran bottles, beakers and measuring cylinders at 100 mL, 1,000 mL and 2,000mL volumes) were cleaned using 1 % (v/v) Neutracon ® detergent solution (Decon Laboratories Ltd., UK). Glassware were rinsed in tap water, followed by distilled water to remove residual detergent. Items were then dried in a drying oven and sterilised as described in Section 2.2.1.3.

### 2.1.5 Cell Lines

The cell lines and suppliers used in this study are listed in Table 2.1.

**Table 2.1 Cell Lines Used Throughout This Study.**

| Cells | Type | Species | Supplier |
|---|---|---|---|
| **L929** | Immortalised Fibroblast | Murine | Health Protection Agency |

## 2.1.6 General Chemical Stock Solutions

### 2.1.6.1 Phosphate Buffered Saline

Ten phosphate buffered saline (PBS) tablets were dissolved in 1 L of distilled water. The pH was then adjusted to 7.2-7.4, as described in Section 2.2.1.1 . The solution was autoclaved, as described in Section 2.2.1.3, and stored at room temperature for up to one month.

### 2.1.6.2 Sodium Hydroxide Solution, 6 M

Sodium hydroxide (NaOH) pellets (120 g) were dissolved into 500 mL distilled water and stored at room temperature for up to six months.

### 2.1.6.3 Ethanol (70 %; v/v)

Distilled water (300 mL) was added to 100 % (v/v) ethanol (700 mL), making 1 L of 70 % (v/v) ethanol.

## 2.1.7 Decellularisation Solutions

### 2.1.7.1 Antibiotic Disinfection Solution (100 U.mL-1 penicillin, 100 µg.mL-1 streptomycin, 100 µg.mL-1 gentamicin)

Prior to use, 2 mL of sterile penicillin – streptomycin solution (5,000 U.ml-1 penicillin, 5 mg.ml-1 streptomycin) and 1 mL of sterile gentamicin solution (10 $mg.ml^{-1}$) was added to 97 mL of autoclaved PBS (Section 2.1.7.1), and mixed by gentle agitation. This was carried out inside a class II biological safety cabinet. For every PHV root, 100 mL of antibiotic disinfection solution was prepared.

### 2.1.7.2 Agarose Solution (1 %; w/v)

Low temperature melting point agarose (1 g) was dissolved in distilled water (100 mL). The solution was then autoclaved, as described in Section 2.2.1.3. Prior to use, the agarose was melted in a water bath held at 70 °C, and was then left to equilibrate to 40 °C.

### 2.1.7.3 Trypsin Solution (2.25 x 104 $U.mL^{-1}$ in PBS)

The quantity of trypsin powder required was calculated in accordance to the volume of trypsin solution required (1 mL per PHV root), and the units of activity

specific to the batch of trypsin. The calculated amount was dissolved into the appropriate volume of PBS (prepared as described in Section 2.1.7.1). The solution was filter sterilised, as described in section 2.2.1.3. The solution was prepared immediately before use.

#### 2.1.7.4 Trypsin Treatment Paste (1.125 x 104 U.mL$^{-1}$ trypsin, 0.5 % (w/v) agarose)

The molten agarose solution (Section 2.1.8.2) and the trypsin solution (Section 2.1.8.3) was mixed in a 1:1 ratio to achieve a volume of 2 mL per PHV root. This was carried out inside a class II biological safety cabinet. The mixture was placed into the fridge (4 °C) until solidified.

#### 2.1.7.5 PBS Wash Buffer-A (PBS-A; contains 10 KIU.mL$^{-1}$ aprotinin)

Prior to use, 1 mL aprotinin (10000 KIU.mL$^{-1}$) to 999 mL of PBS (Section 2.1.7.1) using a sterile syringe. This was carried out inside a class II biological safety cabinet.

#### 2.1.7.6 PBS Wash Buffer-E (PBS-E; contains 2.7 mM EDTA)

Ten PBS tablets and 1.005 g of EDTA was dissolved in 800 mL of distilled water. The pH was adjusted to 7.2-7.4 (Section 2.2.1.1) and the volume was made up to 1 L using distilled water. The solution was autoclaved as described in Section 2.2.1.3. The solution was stored up to one month at room temperature.

#### 2.1.7.7 Trypsin Inhibitor Solution (2.7 mM EDTA, 10 KIU.mL$^{-1}$ aprotinin, and 67.5 mg trypsin inhibitor)

In accordance to the certificate of analysis (CoA) of trypsin inhibitor stating that one mg of trypsin inhibitor (TI) will inhibit a minimum of 1.0 mg or a minimum of 1.5 mg Trypsin (T) of activity, 67.5 mg of trypsin was added to 50 mL of PBS-E (Section 2.1.8.6) that was aseptically transferred into a 60 mL sterile pot. The 50 mL volume was filter sterilised into the remaining PBS-E. Into to 999 mL of the sterile trypsin inhibitor solution, 1 mL aprotinin (10000 KIU.mL-1) was added using a sterile syringe.

### 2.1.7.8 Hypertonic Solution (50 mM Tris, 1.5 M sodium chloride)

Sodium Chloride (87.66 g) and trizma base (6.06 g) were dissolved into 900 mL of distilled water. The pH of the solution was adjusted as described in Section 2.2.1.1, and the volume was made up to 1 L using distilled water. The solution was autoclaved as described in Section 2.2.1.3, and stored at room temperature for up to a month.

### 2.1.7.9 Hypotonic Buffer (10 mM Tris, 2.7 mM EDTA, 10 KIU.mL$^{-1}$ aprotinin)

Trizma base (1.21 g) and EDTA (1.005 g) were dissolved in 900 mL of distilled water. The pH of the solution was adjusted to 8.0-8.2 (Section 2.2.1.1). The solution was made up to 1 L and autoclaved, as described in Section 2.2.1.3 . The solution was stored for up to one month at room temperature. Prior to use, 1 mL of aprotinin solution (10,000 KIU/mL stock) was aseptically added to 999 mL hypotonic buffer.

### 2.1.7.10 Sodium dodecyl sulphate Solution (10% w/v)

Sodium dodecyl sulphate (SDS) powder (10 g) was dissolved in distilled water (100 mL). The SDS solution was filter sterilised, as described in section 2.2.1.3. The solution was aliquoted into 10 mL volumes and stored aseptically for up to six months at room temperature.

### 2.1.7.11 SDS Hypotonic Buffer (0.1 % [w/v] SDS, 10 mM Tris, 2.7 mM EDTA, 10 KIU.mL$^{-1}$ aprotinin)

To 989 mL of hypotonic buffer (Section 2.1.8.9), 10 mL of 10% (w/v) SDS solution (section 2.1.8.10) was added aseptically in a class II biological safety cabinet prior to use. Following this, 1 mL of aprotinin (10,000 KIU.mL$^{-1}$) also aseptically added in a class II biological safety cabinet.

### 2.1.7.12 Nuclease Solution (50 mM Tris, 1 mM $MgCl_2$, 10 U.mL$^{-1}$ Benzonase)

Trizma base (6.1 g) and magnesium chloride ($MgCl_2$; 0.203 g) was dissolved in distilled water (900 mL). The pH was adjusted to 7.5-7.7 (Section 2.2.1.1). The volume of the solution was made up to 1 L with distilled water and autoclaved as described in Section 2.2.1.3. The autoclaved solution was stored for up to one month at room temperature. In a class II biological safety cabinet, an appropriate

volume of bezonase was aseptically added to achieve a stock concentration of 250 $U.mL^{-1}$ prior to use. The solution was used within ten minutes of preparation.

#### 2.1.7.13 Peracetic Acid Solution (0.1 %; v/v)

Peracetic acid (PAA) was diluted in accordance to the starting concentration and required volume, to achieve 0.1 % PAA, 200 mL per PHV root. The pH of the PAA solution was adjusted to 7.2-7.5 (Section 2.2.1.1), and used within one hour of production.

## 2.2 Methods

### 2.2.1 General Methods

#### 2.2.1.1 pH Measurement and Adjustment

The pH of solutions was measured using a Jenway 3020 pH meter. The pH meter was calibrated using pH standard solutions at pH 4, pH 7, and pH 10 prior to use. To account for the temperature dependency of pH readings, a temperature probe was used for each measurement. To adjust the pH of solutions, 1-6 M hydrochloric acid (HCl) or 1-6 M NaOH was used.

#### 2.2.1.2 Microscopy

***Bright Field Microscopy***

Bright field (Köhler) microscopy was performed using an upright microscope for imaging histology slides (AXIO Imager.M2, Zeiss). Prior to use, the microscope was calibrated and optimised to enhance the quality and clarity of images. Images were captured using the digital camera associated with the microscope, as well as Zen Pro software (Zeiss blue edition version 2.3) .

***Fluorescent Microscopy***

Fluorescent microscopy was carried out using the upright microscope (AXIO Imager.M2, Zeiss), but with a fluorescent illuminator in conjunction with the appropriate filters.

***Polarised Light Microscopy***

Polarised light microscopy was performed using the upright microscope (AXIO Imager.M2, Zeiss) in conjunction with the associated polarised filters. This displayed birefringence of the histological structures.

***Scanning Electron Microscopy***

Scanning electron microscopy (SEM) was performed using Carl Zeiss EVO MA15 (Leeds Electron Microscopy and Spectroscopy Centre). Prior to imaging, samples were fixed using the schedule described in Table 2.2 and critical point dried using Polaron E3000 critical point drying apparatus with $CO_2$ as the transition fluid. Samples were then mounted onto 13 mm pin stubs using carbon tape tabs and then coated in iridium to a thickness of 22 nm using an Agar high resolution sputter coater. A voltage of 20 KV and a working distance of 13 mm was used to capture images. The following five magnifications were used to capture images: 50 X, 200 X, 400 X, 600 X, 1000 X. The fields of view captured were kept as consistent as possible amongst the different samples from different groups.

**Table 2.2 Tissue Fixation Protocol.**

| Step | Solution | Duration |
|---|---|---|
| 1 | 2.5 % (v/v) glutaraldehyde in 0.1 M phosphate buffer | 2 h |
| 2 | 0.1 M (w/v) phosphate buffer | 30 mins x 2 |
| 3 | 1.0% (v/v) osmium tetroxide in 0.1 M phosphate buffer | 16 – 18 h |
| 4 | 20 %, 40 %, 60 %, 80 %, 2 x 100 % acetone | 30 mins for each ascending concentration |

### 2.2.1.3 Sterilisation

Equipment and solutions were sterilised using dry heat, moist heat, or filter sterilisation.

Items that were free from moisture, such as equipment, were placed into a hot air oven for four hours at 180 °C.

Solutions were sterilised by autoclaving for 20 minutes at 121 °C, with a pressure of 15 pounds per square inch (psi).

Solutions that were unsuitable for heat sterilisation were filtered using 0.2 µm pore sized filters with disposable syringes. The solutions were filtered into sterile containers in a Class II biological safety cabinet.

## 2.2.2 Acquisition of Porcine Pulmonary Heart Valves

### 2.2.2.1 Porcine Heart and Lung Procurement

Fresh porcine hearts with the lungs attached from Large White Yorkshire pigs (26 to 28 weeks of age) were obtained from two local abattoirs (J. Penny, Leeds, United Kingdom; M&C Meats, Leeds, United Kingdom). The hearts and attached lungs were delivered within four hours of slaughter.

### 2.2.2.2 Porcine Pulmonary Heart Valve Dissection

The pulmonary artery and aorta were located and used as a guide for removal of the lungs. The apex of the heart was then removed via transverse incision to create a stable flat surface for further dissection of the pulmonary heart valve root which consists of the pulmonary artery, pulmonary heart valve, and inferior myocardium skirt. The pericardium was removed to expose the pulmonary artery and aorta. The aorta and pulmonary artery were carefully separated using a scalpel blade, dissecting scissors and forceps. Using a scalpel blade, the pulmonary artery, pulmonary valve and the inferior myocardium skirt was separated from the heart (Figure 2.1). The pulmonary artery was trimmed to an appropriate length of ≥ 6 cm. The dissected pulmonary heart valve roots were washed with PBS to wash away blood and to prevent drying of the tissue. The pulmonary roots were sealed inside 60 mL pots that contained PBS soaked filter paper. These were then stored at -20 °C for later use.

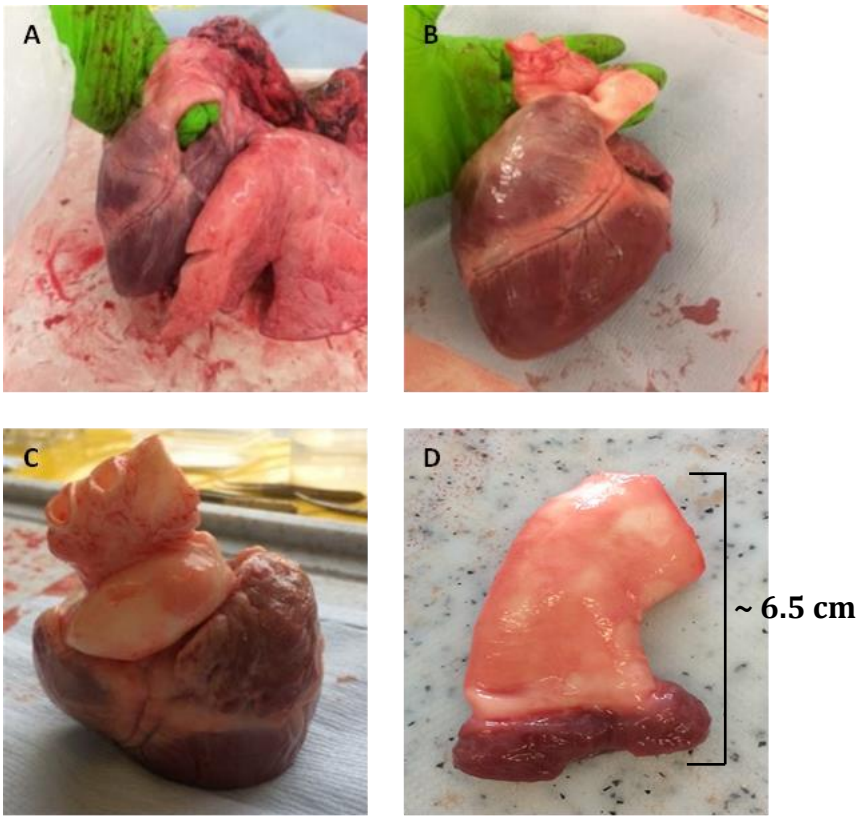


**Figure 2.1 Porcine PHV Root Dissection.** Location of the pulmonary artery and aorta (A). Removal of lungs leaving the heart (B). The removal of the apex from the heart (C). PHV root (D).

#### 2.2.2.3 Fine Dissection of Porcine Pulmonary Heart Valve Roots

Before commencing porcine pulmonary heart valve root decellularisation, the PHV roots were thawed at 37 °C for 30 minutes prior to further fine dissection. Excess fat and connective tissue was carefully removed from the pulmonary heart valve root. The myocardium skirt was trimmed to 5 mm length below the pulmonary valve leaflets and 3 mm width. The pulmonary heart valve roots were scraped, whereby a scalpel blade was ran along the length of the adventitial layer of the pulmonary artery.

### 2.2.3 Decellularisation of Porcine Pulmonary Heart Valves

Native porcine PHV roots were exposed to a decellularisation protocol modified from Luo et al. (2014) (Table 2.3). Dissected porcine PHV roots were thawed for approximately 30 minutes at 37 °C. All steps following thawing of the PHVs were carried out using aseptic technique inside a class II safety cabinet, using sterile equipment. All washes were carried out using 200 mL of solution, except for

antibiotic disinfection (100 mL). All washes were carried out horizontally with agitation at 110 RPM, except for the nuclease wash step which was carried out at 80 RPM. Following decellularisation, the decellularised PHVs were immersed in 100 mL of fresh sterile PBS in fresh sterile 150 mL containers and stored upright at 4 °C in the dark until use.

**Table 2.3 Decellularisation protocol for porcine pulmonary heart valves**

| Step | Solution/Action | Temperature (°C) | Incubation Period |
|---|---|---|---|
| **1** | Thaw pulmonary valve roots | 37 | Until thawed (~30 minutes) |
| **2** | Disinfection solution (100U.ml$^{-1}$ penicillin, 100µg.ml$^{-1}$ streptomycin,100 µg.ml$^{-1}$ gentamicin) | 4 | Overnight (16-17 hours) |
| **3** | Melt agarose | 70 | Until melted (~4 hours) |
| **4** | Equilibrate agarose | 40 | Overnight (16-17 hours) |
| **5** | Insert cotton wool soaked with 50% (v/v) FBS in PBS into leaflets and artery lumen. Prepare trypsin agarose paste and allow to set | Room temp | 1-2 hours |
| **6** | Apply trypsin agarose paste to adventitial layer of pulmonary wall and myocardium skirt | 37 | 2 hours |

| | | | |
|---|---|---|---|
| **7** | Trypsin inhibitor (PBS EDTA, trypsin inhibitor, aprotinin) | 42 | 30 Minutes x 3 |
| **8** | Hypotonic buffer with aprotinin | 42 | 24 hours |
| **9** | Hypotonic buffer with aprotinin and SDS | 42 | 24 hours |
| **10** | PBS with aprotinin added | 42 | 30 minutes x 3 |
| **11** | PBS with aprotinin added | 42 | Weekend (~66 hours) |
| **12** | Nuclease solution with benzonase | 37 | 3 hours x 2 |
| **13** | PBS | 42 | 30 minutes x 3 |
| **14** | Hypertonic solution | 42 | 24 hours |
| **15** | PBS | 42 | 30 minutes x 2 |
| **16** | PBS #3 | 42 | 24 hours |
| **17** | PBS #4 | 42 | 24 hours |
| **18** | PBS #5 | 42 | Overnight (16-17 hours) |
| **19** | PBS | 42 | 30 minutes x 3 |
| **20** | PBS | 4 | Weekend (~66 hours) |
| **21** | Transfer decell PHVs into fresh PBS for storage | 4 | |

## 2.2.4 Basic Histological Techniques

### 2.2.4.1 Fixation, Processing, and Paraffin Wax Embedding of Tissue

A segment of the valve consisting of the right pulmonary leaflet was dissected from the remainder of the pulmonary root. This was then vertically cut in half, leaving two PHV tissue samples consisting of the pulmonary artery, the right leaflet, and myocardium skirt (15 mm length, 5 mm width). The tissue samples were placed into labelled plastic histology cassettes. One portion of the tissue sample was fixed in neutral buffered formalin (NBF), and the other was fixed in zinc fixative for 24 hours at room temperature (22-24 °C). The tissue containing plastic cassettes were then transferred to the automated tissue processor (Leica TP1020), where they were exposed to a predetermined programme (Table 2.3).

**Table 2.4 Automated Tissue Processing Programme Protocol.**

| Step | Solution | Duration |
|---|---|---|
| 1 | 70% (v/v) ethanol | 1 h |
| 2 | 90% (v/v) ethanol | 1 h |
| 3 | 100% (v/v) ethanol | 2 h 20 mins |
| 4 | 100% (v/v) ethanol | 3 h 20 mins |
| 5 | 100% (v/v) ethanol | 4 h 20 mins |
| 6 | 100% (v/v) ethanol | 1 h |
| 7 | Xylene | 1 h 30 mins |
| 8 | Xylene | 2 h |
| 9 | Xylene | 1 h 30 mins |
| 10 | Molten wax | 2 h |
| 11 | Molten wax | 2 h |

Upon completion of the tissue processor programme, the cassettes were transferred into fresh molten wax inside a wax oven at 60 °C. The tissue samples were then removed from the cassettes and orientated into metal wax block moulds using hot forceps, covered in molten paraffin wax, and were left to set at room temperature (22-24 °C) overnight (16-18 hours).

#### 2.2.4.2 Sectioning of Paraffin Wax Embedded Tissue Blocks

The wax embedded tissue samples were sectioned at a thickness of 7 μm using a microtome (Leica RM2255). The tissue sections were delicately transferred from the microtome to a water bath set at 50 °C using forceps. These floating sections were collected from the water bath onto Superfrost Plus slides. The slides were then placed onto hotplate rails set at 60 °C for up to 1 hour before being placed into a 37 °C incubator overnight (16-18 hours).

#### 2.2.4.3 Dewaxing and rehydration

The paraffin wax embedded tissue sections were dewaxed and rehydrated by submerging the paraffin wax embedded tissue samples on glass slides into xylene for 10 minutes, twice, followed by immersion into fresh jars of absolute ethanol for 3, 2, and 2 minutes. The slides were then placed into 70 % ethanol for 2 minutes followed by immersion into running tap water for 3 minutes.

#### 2.2.4.4 Dehydration and Mounting

Stained sections were dehydrated by immersion into 70 % ethanol for 5 seconds, followed by immersion for 1, 2 and 3 minutes into fresh jars of absolute ethanol. The slides were then placed into xylene twice, 10 minutes at each time. Each section was mounted using DPX mountant and a glass coverslip. Slides were left to air-dry in the fume cupboard for a minimum of 4 hours prior to imaging.

### 2.2.5 Histological Staining

#### 2.2.5.1 Haematoxylin and Eosin

Haematoxylin and eosin (H&E) staining was used for visualisation of cellular morphology and histoarchitecture. Tissue sections were first dewaxed and rehydrated (Section 2.2.4.3). Following dewaxing and rehydration, the tissue sections were immersed into Mayer's haematoxylin for 1 minute, rinsed in running tap water until clear, and immersed into Scott's tap water substitute for 3 minutes. Sections were rinsed again in running tap water for 3 minutes and then immersed into eosin for 3 minutes. Sections were then dehydrated and mounted (Section 2.2.4.4). Stained slides were visualised using Köhler illumination (Section 2.2.1.2).

### 2.2.5.2 Picrosirius Red & Miller's Elastin

Reagents:

| | |
|---|---|
| • Potassium Permanganate (5 %; w/v) | Potassium permanganate- 15 g<br>Distilled water- 300 mL |
| • Oxalic Acid (1 %; w/v) | Oxalic Acid – 3 g<br>Distilled water – 300 mL |
| • Weigert's Haematoxylin | One part solution A<br>One part solution B |
| • Acid Alcohol (1 %; v/v) | Concentrated hydrochloric acid- 5 mL<br>Ethanol (70 %) - 495 mL |
| • Picrosirius Red (0.1 %; w/v) | Picrosirius red - 0.3 g<br>Aqueous saturated picric acid solution- 300 mL |

Method:

Picrosirius red staining was used to visualise collagen fibres, and Miller's elastin staining was used to visualise elastin fibres. Under polarised light, the birefringence of the collagen fibres is associated with the fibre diameter, with an increase in diameter being related to the transition in observed colour from green to yellow to orange to red (Junqueira et al., 1979). It is believed that the alignment of the fibres and the packing density also influences the observed colour.

Tissue sections (Section 2.2.4.2) were first dewaxed and rehydrated, as described in section 2.2.4.3. Sections were then immersed into potassium permanganate (5 %; w/v) for 5 minutes, and subsequently rinsed using distilled water. Sections were immersed into 1 % (w/v) oxalic acid for 2 minutes, followed by distilled water for 1 then 4 minutes. Sections were then immersed into 70 % (v/v) ethanol for 1 minute, followed by 95 % (v/v) ethanol for 1 minute. Sections were then stained using Miller's stain for 1 hour. Following this, sections were rinsed using 95 % (v/v) ethanol for 1 minute, 70 % (v/v) ethanol for 1 minute, and tap water

for 2 minutes. Sections were then stained using Weigert's haematoxylin for 10 minutes, followed by differentiation in 1 % acid alcohol for one minute. Sections were then rinsed using distilled water for 30 seconds and stained using Picrosirius red (0.1 %; w/v) for 1 hour. Sections were then rinsed in distilled water for 30 seconds and blot dry prior to dehydration and mounting (Section 2.2.4.4). Slides were viewed and imaged under both Köhler illumination and polarised light (Section 2.2.1.2).

### 2.2.5.3 Movat's Pentachrome

Movat Pentachrome Stain Kit (ab245884) proprietary reagents were used:

| | |
|---|---|
| • Working Elastic Stain Solution | Haematoxylin Solution (5 %) – two parts<br><br>Ferric Chloride Solution (10 %) – one part<br><br>Lugol's Iodine Solution – one part |
| • Ferric Chloride Differentiating Solution (2 %)<br>• Sodium Thiosulfate Solution (5 %)<br>• Acetic Acid Solution (1 %)<br>• Alcian Blue Solution, pH 2.5<br>• Biebrich Scarlet – Acid Fuchsin Solution<br>• Phosphotungstic Acid Solution (5 %)<br>• Yellow Stain Solution | As supplied |

Method:

Movat's pentachrome staining was used to visualise collagen, elastin, muscle, mucin, and fibrin in tissue sections. Tissue sections (Section 2.2.4.2) were first dewaxed and rehydrated, as described in Section 2.2.4.3. Sections were then immersed in Working Elastic Stain Solution for 20 minutes, rinsed in running tap water until no excess stain remained, then dipped into Ferric Chloride Differentiating Solution (2 %) 15 times. Sections were then rinsed in tap water followed by distilled water twice prior to immersion in Sodium Thiosulfate

Solution (5 %) for 1 minute. Sections were again rinsed in tap water followed by distilled water twice prior to immersion in Acetic Acid Solution (1 %) for 2 minutes, and then Alcian Blue Solution, pH 2.5, for 25 minutes. Again, sections were rinsed in tap water followed by distilled water twice. Sections were immersed in Biebrish Scarlet – Acid Fuchsin Solution for 2 minutes, rinsed in distilled water twice, immersed in Acetic Acid Solution (1 %) for 10 seconds and then rinsed in distilled water. Sections were differentiated in 2 changes of Phosphotungstic Acid Solution (5 %) for 7 minutes each, rinsed in distilled water, and then incubated in Acetic Acid Solution (1 %) for 1 minute. Sections were then stained with Yellow Stain Solution for 25 minutes, rinsed in 100 % (v/v) ethanol for 1, 2 and 3 minutes, prior to mounting (Section 2.2.4.4). Sections were viewed and imaged under Köhler illumination (Section 2.2.1.2).

### 2.2.6 Immunohistochemistry

Immunohistochemistry was used to visualise the presence of specific ECM components in the pulmonary artery, leaflet and myocardium. The primary antibodies and isotype controls used for antibody labelling are listed in Table 2.4.

**Table 2.5. Primary Antibodies and Isotype Controls Used for Collagen IV and Fibronectin Labelling**

| Antigen | Primary Antibody | Isotype Antibody |
|---|---|---|
| Collagen IV | Monoclonal Mouse Anti-collagen IV, IgG1(50 mg.mL$^{-1}$)<br>Dako M0785<br>1:50 dilution | Mouse IgG1<br>Dako X0931 |
| Fibronectin | Polyclonal Rabbit Anti-Fibronectin, IgG (4.9 mg.mL$^{-1}$)<br>Dako A0245<br>1:200 dilution | Rabbit Polyclonal IgG<br>Dako X0936 |

Reagents:

| | |
|---|---|
| • Sodium Chloride (NaCl) Solution (3 M) | NaCl – 175.32 g<br>Distilled water – 1 L |
| • Tris Solution (2M, pH 7.6) | Trizma base – 242.26 g<br>Made up to 1 L with distilled water |
| • Tris-Buffered Saline (TBS) (20 mM tris, 150 mM NaCl, pH 7.6) | NaCl Solution (3 M) – 50 mL<br>Tris Solution (2 M) – 25 mL<br>Made up to 1 L with distilled water |
| • Milk in TBS (2 %; w/v milk, 20 mM tris, 150 mM NaCl, pH 7.6) | Milk Powder – 200 mg<br>TBS – 10 mL |
| • Bovine serum albumin (BSA) Solution (5 %; w/v) | BSA – 2.5 g<br>PBS – 50 mL |
| • Antibody Diluent (TBS, 0.1 % (w/v) BSA, 0.1 % (w/v) sodium azide, pH 6) | BSA Solution – 300 µL<br>Sodium Azide Solution (1 %; w/v) – 6mL<br>Made up to 60 mL with TBS |
| • DAKO Dual Endogenous Enzyme Block (S2003) | As supplied |
| • DAKO Anti-Mouse HRP (K4001) | As supplied |
| • DAB+ Substrate Chromogen (K3468) | Liquid DAB+ Chromogen – 20 µL<br>Substrate Buffer – 1 mL |

Method:

Tissue was first zinc fixed and processed, as described in Section 2.2.4.1. The tissue was then sectioned (Section 2.2.4.2), dewaxed and rehydrated (Section 2.2.4.3). All steps were carried out at room temperature. Each section was drawn around using

a hydrophobic marker pen (ImmEdge barrier pen) prior to being washed in TBS with gentle agitation. Sections were then incubated with DAKO Dual Endogenous Enzyme Block for 10 minutes, followed by milk in TBS for 30 minutes. Sections were washed in TBS for 5 minutes with gentle agitation, thrice. Primary antibodies and isotype control antibodies diluted to appropriate concentrations in antibody diluent were added to test and isotype control sections, respectively. Antibody diluent was also added to negative control sections. The sections were incubated in a humidified chamber for 45 minutes. Sections were then washed in TBS for 5 minutes with gentle agitation, thrice. DAKO Anti-Mouse Horseradish Peroxidase (HRP) was added to the sections and incubated for 30 minutes prior to three 5 minute washes in TBS with gentle agitation. DAB+ Substrate Chromogen was added to the sections and incubated for 5 minutes, followed by four washes in distilled water, immersion in haematoxylin for 5 seconds, and then running tap water for 3 minutes. Sections were immersed in Scott's Tap Water Substitute for 1 minute and running tap water for 1 minute, before dehydration and mounting (Section 2.2.4.4). Sections were viewed and imaged under Köhler illumination (Section 2.2.1.2).

### 2.2.7 Differential scanning calorimetry

Differential scanning calorimetry (DSC) is a thermo-analytical technique used to assess the denaturation temperature of materials, which is related to the three-dimensional structure of the material. Therefore, this technique was used to assess structural changes introduced to PHV root tissue in response to different sterilisation treatment. Thermal stability of the PHV pulmonary artery wall and leaflet tissue was assessed using DSC. Approximately 20 mg PHV pulmonary artery wall samples and 5 mg PHV leaflet samples (wet weight) were analysed on a Q2000 DSC Instrument (TA Instruments). Samples were heated from 15 to 130 °C at a rate of 4 °C.min$^{-1}$ in hermetically sealed aluminium pans. Heat flow through the samples was measured and normalised against the mass of the sample, giving a value of Watts per gram (W/g).The denaturation temperature was taken as the peak heat flow through the sample.

## 2.2.8 Biochemical Analysis

### 2.2.8.1 Lyophilisation

PHV root pulmonary wall and leaflet samples (approximately 50 mg wet weight) were finely macerated. The tissue samples were then placed into sterile bijous, with the weight of each tissue sample recorded. Samples were placed in a freeze dryer (Thermo, Savant ModulyoD) at -50 °C, 0.15 – 0.2 mbar. The sample weights were measured every 48 hours until constant (48 – 96 hours).

### 2.2.8.2 Acid Hydrolysis of Tissue Samples

Tissue samples were lyophilised, as described in section 2.2.8.1. The lyophilised tissue was then placed into a polypropylene universal, along with 5 mL of 6 M HCl. Samples were then placed into a block heater set at 120 °C and incubated overnight (≥ 8 hours). Following the overnight incubation, the samples were allowed to cool at room temperature and were then neutralised to pH 6.8-7.2 using NaOH (6M). The final volume of the sample was recorded. The samples were assayed immediately or stored at -20 °C for up to 3 months for later use.

### 2.2.8.3 Quantification of Hydroxyproline Content

Hydroxyproline is an amino acid that forms a major constituent of collagen. Therefore, quantification of hydroxyproline content can be used to estimate total collagen content. A colourimetric assay was used to quantify hydroxyproline conent. The oxidation of hydroxyproline results in the formation of pyrroles, which reacts with p-dimethylaminobenzaldehyde, forming a red chromophore. This allows quantification of hydroxyproline via spectrophotometric analysis.

Reagents:

| | |
|---|---|
| • Hydroxyproline Buffer | Citric acid- 13.3 g<br>Sodium acetate (trihydrate)- 32 g<br>NaOH- 9.1 g<br>Propan-1-ol (n-propanol)- 80 mL<br>Glacial acetic acid- 3.2 mL<br>pH adjusted to 6.0-6.5 (Section 2.2.1.1) |

| | |
|---|---|
| | Made up to 400 mL using distilled water |
| • Chloramine T Solution | Chloramine T- 1.41 g<br>Distilled water- 100 mL |
| • Ehrlich's Reagent | p-dimethylaminobenzaldehyde- 7.5 g<br>Perchloric acid (62 %; v/v)- 13 mL<br>Propan-1-ol (n-propanol)- 30 mL<br>Made up to 50 mL using distilled water |

Method:

Tissue samples were lyophilised and acid hydrolysed (section 2.2.8.1 and 2.2.8.2). A range of standards of known hydroxyproline concentrations were made by diluting trans-4-hydroxy-L-proline (0, 2, 4, 6, 8, 10, 15, 20, 25, and 30μg.mL$^{-1}$). Test samples were diluted 1:20 using hydroxyproline buffer. Test samples and standards (50 μL) were added to a clear flat-bottomed 96 well plate in triplicate. Chloramine T solution (100 μL) was added to each well, and the plate was incubated at room temperature with gentle agitation. Ehrlich's reagent (100 μL) was then added to each well, and the plate was incubated at 60 °C for 45 minutes. The optical density of each well was then measured using a microplate spectrophotometer at 570 nm. A hydroxyproline standard curve was created, showing absorbance vs concentration. The unknown test values were interpolated, and tissue sample hydroxyproline content (μg.mg$^{-1}$) was normalised for dilution volume and dry tissue weight.

### 2.2.8.4 Quantification of Glycosaminoglycan Content

The sulphated glycosaminoglycan (GAG) content of tissue samples was determined using a colourimetric assay. Sulphated GAGs react with 1,9-dimethylene blue (DMB) dye solution under acidic conditions, allowing spectrophotometric quantification.

Reagents:

| | |
|---|---|
| • Papain Digestion Buffer | L-cysteine hydrochloride - 0.788 g<br>Disodium ethylenediaminetetraacetic acid - 1.8612 g<br>PBS (Section 2.1.7.1) - 1 L<br>pH adjusted to 7.9 - 6.1 (Section 2.2.1.1) |
| • Papain digestion solution | Papain - 4000 kUnits<br>Papain digestion buffer- 5 mL<br>Per sample, 5 mL was prepared |
| • Sodium di-hydrogen orthophosphate monohydrate (0.1 M) | Sodium di-hydrogen orthophosphate monohydrate – 3.45 g<br>Distilled water - 250 mL |
| • Di-sodium hydrogen orthophosphate (0.1 M) | Di-sodium hydrogen orthophosphate – 3.55 g<br>Distilled water – 250 mL |
| • GAG Assay Buffer | Di-sodium hydrogen orthophosphate (0.1 M) - 137 mL<br>Di-sodium hydrogen orthophosphate (0.1 M) – 63 mL<br>pH adjusted to 6.8 (Section 2.2.1.1) |
| • DMB Dye Solution | 1,9 dimethylene blue – 16 mg<br>Absolute ethanol – 5 mL<br>Formic acid – 2 mL<br>Sodium Formate – 2 g<br>Volume adjusted to 1 L using distilled water |

Method:

Tissue samples were first lyophilised to a constant weight, as described in section 2.2.8.1. Papain digestion solution (5 mL) was added to each sample, and were then incubated at 60 °C for 36 - 48 hours. A series of chondroitin sulphate B dilutions

were made to produce chondroitin sulphate B standard concentrations of 0, 3.125, 6.25, 12.5, 25, 50, 100, 150 and 200 $\mu g.mL^{-1}$. Test samples and standards (40 µL) were added into a clear flat-bottomed 96 well plate in triplicate. DMB dye solution (250 µL) was added into each well. The well plate was incubated at room temperature for two minutes with gentle agitation. The optical densities of each well was then measured using a microplate spectrophotometer at 525 nm. A standard curve of chondroitin sulphate B concentration vs absorbance was plotted, and the unknown values were interpolated. The unknown test values were interpolated, and tissue sample GAG content ($\mu g.mg^{-1}$) was normalised for dilution volume and dry tissue weight.

## 2.2.9 Cell Culture

All cell culture was performed aseptically in a class II biological safety cabinet. Cells were cultured in cell culture medium specific to the cell type (Section 2.2.9.1). Cells were incubated at 37 °C in 5 % $CO_2$ (v/v) in air. All cell culture medium and appropriate reagents added were allowed to equilibrate to 37 °C before use.

### 2.2.9.1 L929 Cell Culture Media

***Tryptone Phosphate Broth Stock Solution (29.5 $g.L^{-1}$)***

Tryptone phosphate broth (TPB) stock (7.98 g) was added to distilled water (250 mL). The solution was filter sterilised (Section 2.2.1.3), and stored at -25 °C for up to six months.

***L929 cell culture medium (10 % (v/v) FBS, 2 mM L-glutamine, penicillin/ streptomycin 100 U / 100 $\mu g.mL^{-1}$)***

L929 cell culture medium was made by adding 10 mL FBS, 1 mL L-glutamine (200 mM) and 2 mL penicillin/ streptomycin (penicillin 5000 $U.mL^{-1}$; streptomycin 5 $mg.mL^{-1}$) to 87 mL Dulbecco's minimal essential medium (DMEM). The medium was stored at 4 °C for up to one week.

### 2.2.9.2 Resurrection and Maintenance of Cells

L929 cells were stored in appropriate culture medium containing dimethyl sulfoxide (DMSO; 10 %; v/v) in the vapour phase of liquid nitrogen. Following

removal from the liquid nitrogen, the cells were thawed rapidly in a water bath at 37 °C. Appropriate cell culture medium (10 mL) was added to the cells dropwise. The cell suspension was then centrifuged at 150 g for ten minutes to remove the DMSO. The supernatant was aspirated, and the cells were re-suspended in 10 mL of fresh appropriate cell culture medium. The cell suspension was then transferred to a T75 tissue culture flask, and placed for incubation (Section 2.2.9). Cell culture medium was replaced every 48 hours until cells had reached approximately 80 % confluency, at which cells were passaged.

#### 2.2.9.3 Cell Passaging

Cell culture medium was aspirated from the T75 flask, and the cell monolayer was briefly rinsed with 10 mL PBS (without $Ca^{2+}$ or $Mg^{2+}$), which was then aspirated. Trypsin/EDTA solution (2.5 mL) was added to the flask and incubated for five minutes to detach adherent cells from the flask surface. The appropriate cell culture medium (10 mL) was then added to the flask to inactivate the trypsin. The cell suspension was centrifuged at 150 g for ten minutes. The supernatant was then aspirated discarded, and the remaining cell pellet was resuspended in 1 mL of the appropriate cell culture medium. A cell count was then performed, as described in section 2.2.9.4. A suitable dilution of the cell suspension was achieved by inserting the appropriate volume into a T75 flask containing fresh appropriate cell culture medium (12 mL). The cell culture medium was changed every 48 hours until the cells reached approximately 80 % confluency, at which cells were passaged again.

#### 2.2.9.4 Cell Counting and Cell Viability Determination

In order to determine cell viability, trypan blue was added to cell suspensions. Dead cells have a loss of membrane potential, allowing trypan blue to cross the cell membrane and enter the cell. Therefore, dead cells appear blue and live cells appear transparent. This is detected by the Invitrogen Countess II Automated Cell Counter (Thermo Fisher Scientific). To perform the cell count, 20 µL cell suspension was added to 20 µL trypan blue (0.4 %; w/v) and mixed well. This was then added to a disposable Countess ™ Cell Counting Chamber Slide (Invitrogen,

Thermo Fisher Scientific), which was then inserted into the automated cell counter instrument. The total number of cells.mL$^{-1}$ and cell viability percentage was generated.

#### 2.2.9.5 Cell cryopreservation

Cells were harvested from flasks (Section 2.2.9.3) and counted (Section 2.2.9.4). Cells were resuspended to achieve a density of 1 x 10$^{6}$.mL$^{-1}$ using cryopreservation medium (appropriate cell culture medium containing 10 % (v/v) DMSO). DMSO was used to prevent the formation of ice crystals during the cell cryopreservation process. Cell aliquots (1 mL) were transferred to cryovials which were placed into cryofreezing chambers containing isopropanol, and frozen at -80 °C overnight. Cell cryovials were then transferred to liquid nitrogen for long term storage.

### 2.2.10 Biocompatibility Assessments

Cytotoxicity assessments were used to assess the *in vitro* tissue biocompatibility in accordance to ISO standard 10993-5 (2009).

#### 2.2.10.1 Contact Cytotoxicity Testing

Tissue samples (5 mm$^2$) were aseptically dissected and attached to the centre of three wells of a six well-plate using wound closure strips (SteriStrips). Cyanoacrylate contact adhesive and SteriStrips were used as positive and negative control wells respectively. Each well was washed three times with PBS (without $Ca^{2+}$ or $Mg^{2+}$) for ten minutes without agitation. L929 cells were adjusted to a concentration of 250,000 cells.mL$^{-1}$ (Section 2.2.9.3), and 2 mL of cell suspension was added to each well. The plates were then incubated at 37 °C in 5 % (v/v) in air until confluent (approximately 48 hours). Phase contrast microscopy was used to examine the cell-sample interface. Cell culture medium was then aspirated from each well, and the cell monolayer was gently washed with PBS (without $Ca^{2+}$ or $Mg^{2+}$) without agitation. Cells were then fixed by adding 2 mL NBF (10 %; v/v) to each well, and incubating for 10 minutes at room temperature. NBF was then aspirated from each well, and Giemsa stain was added to each well (enough to ensure coverage of the cell monolayer). The plates were incubated for five minutes

at room temperature. The Giemsa stain was then washed from each well with running tap water, until it ran clear. Plates were then left to air-dry before examining and capturing images of the cells using an inverted Olympus IX71 microscope and Olympus XC50 digital colour camera, under normal Köhler illumination. Images were used to examine cell confluency and morphology.

### 2.2.10.2 Extract Cytotoxicity Assay

Reagents:

| | |
|---|---|
| • Double Strength L929 Cell Culture Medium | DMEM - 14.8 mL<br>FBS - 4 mL |
| | L-glutamine - 0.4 mL<br>Penicillin/streptomycin solution - 0.8 mL |
| • Positive Control | DMEM – 12 mL<br>DMSO – 8 mL<br>Solution was filter sterilised (Section 2.2.1.3) |
| • Negative Control | Single strength fully supplemented DMEM |

Method:

Tissue samples were aseptically dissected and macerated before being placed into a sterile bijou. The weight of each tissue sample was recorded, so that DMEM was added at a ratio of 100 mg of tissue per 1 mL of DMEM. The bijous containing the tissue samples and DMEM were then incubated at 37 °C with agitation (240 rpm) for 72 hours. The tissue was then aseptically removed from the bijous for sterility assessments (Section 2.2.11) . The remaining extract containing bijous were stored at -20 °C until sterility was assured. L929 cells were harvested to obtain a cell concentration of 25,000 cells/200 µL of cell culture medium. Cells were seeded into a 96-well plate in triplicates (200 µL of cell suspension per well), and incubated for 24 hours at 37 °C with 5 % (v/v) $CO_2$ in air. The extract was thawed and warmed to 37 °C on the day of the assay. The cell culture was aspirated from

the wells of the 96-well plate, and replaced with 100 µL of the appropriate double strength cell culture medium. Test extract and controls were added to the appropriate wells in triplicate. Positive controls consisted of DMEM containing 40% DMSO. The negative controls consisted of appropriate cell culture medium alone. The 96-well plates were then incubated at 37 °C with 5 % $CO_2$ in air for 48 hours. The cell viability was then determined using the ATPLite-M® assay.

***ATPLite-M® Assay for Cell Viability Assessment***

Reagents:

| | |
|---|---|
| • Mammalian Cell Lysis Solution | Perkin-Elmer |
| • Substrate Solution | Perkin-Elmer; One vial of lyophilised substrate solution with 25 mL substrate buffer. Substrate solution was aliquoted (5 mL) and stored in the dark at -20 °C. |

Method:

The ATPLite-M® assay was used to assess cell viability by quantifying the ATP content. The ATPLite-M reagents were allowed to equilibrate to room temperature. The original cell culture medium was aspirated from each well in the 96-well plate, and 50 µL of fresh cell culture medium was added into each well. Mammalian cell lysis solution was added into each well (50 µL). The well plate was then incubated at room temperature with agitation of 500 rpm for five minutes. The solution from each well (100 µL total) was transferred into a white 96 well optiplate. Substrate solution was added into each well (50 µL), and the well plate was agitated at 500 rpm for 5 minutes. The ATP luminescence of each well was then determined using the Chameleon Plate reader.

### 2.2.11 Sterility Testing

Tissue samples were assessed for sterility. This was done using thioglycolate broth, which is a multipurpose medium used for the cultivation of both aerobic and

anaerobic organisms, along with tryptone soya broth (TSB), which is an enriched medium used for the cultivation of aerobic microorganisms.

#### 2.2.11.1 Thioglycolate Broth

Thioglycolate broth was made by dissolving thioglycolate medium USP (2.97 g) into distilled water (100 mL). The solution was aliquoted into narrow neck glass bottles (45ml per bottle), which were then autoclaved (Section 2.2.1.3). The media was then stored at room temperature in the dark, ready for sterility testing of the tissue samples within 3 days.

#### 2.2.11.2 Tryptone Soya Broth

TSB was dissolved into distilled water to achieve a concentration of 30 g/L. The solution was aliquoted into 30 mL glass universals (15 mL per bottle), which were then autoclaved (section 2.2.1.3). The media was then stored at room temperature in the dark, ready for sterility testing of the tissue samples within 3 days.

#### 2.2.11.3 Tissue Sterility Testing Method

Inside a class II safety biological cabinet, tissue samples (Section 2.2.10.2) were aseptically placed into the broth bottles using sterile inoculating loops. The bottles were then sealed and incubated at 37 °C, and were observed over 2, 7, and 14 days for growth. Positive and negative controls were also incubated and observed. The positive control was broth that was contaminated by inserting an inoculating loop that was spread on unwashed surfaces. The negative control was blank broth.

### 2.2.12 Uniaxial Tensile Testing

Uniaxial tensile testing was used to assess the structural biomechanical properties of the different groups of treated PHVs.

The uniaxial tensile testing was performed using an Instron 3365 materials testing machine. The BioPlus bath was mounted to the Instron 3365 materials testing apparatus. This was filled with PBS to keep the tissue hydrated, and set to maintain

a physiological temperature of 37 °C throughout the uniaxial tensile testing session. The Instron was mounted with a load cell of 50 Newtons (N) rating which had a greater sensitivity and accuracy for the resulting load measured in the tissue samples.

#### 2.2.12.1 Tissue Preparation and Mounting

The tissue specimens were dissected consistently and appropriately for mounting into the Instron BioPlus apparatus. A custom made tissue cutter (Figure 2.2) was used to prepare strips of wall or leaflet to be mounted in the machine. The width between the two blades of the custom made tissue cutter defined the width of the resultant dissected tissue specimen. From the PHV wall, circumferential and axial tissue samples that conformed to the dimensions of 5 mm width and greater than 10 mm length were prepared. From the PHV leaflets, circumferential samples that conformed to 5 mm width and greater than 10 mm length were prepared, in addition to radial leaflet samples that conformed to 3 mm width and greater than 6 mm length due to restrictions in tissue size (Figure 2.2). The gauge length was 10 mm for wall tissue specimens in axial and circumferential orientations and leaflet tissue specimens in circumferential orientation. The gauge length for leaflet radial tissue specimens was 6 mm.

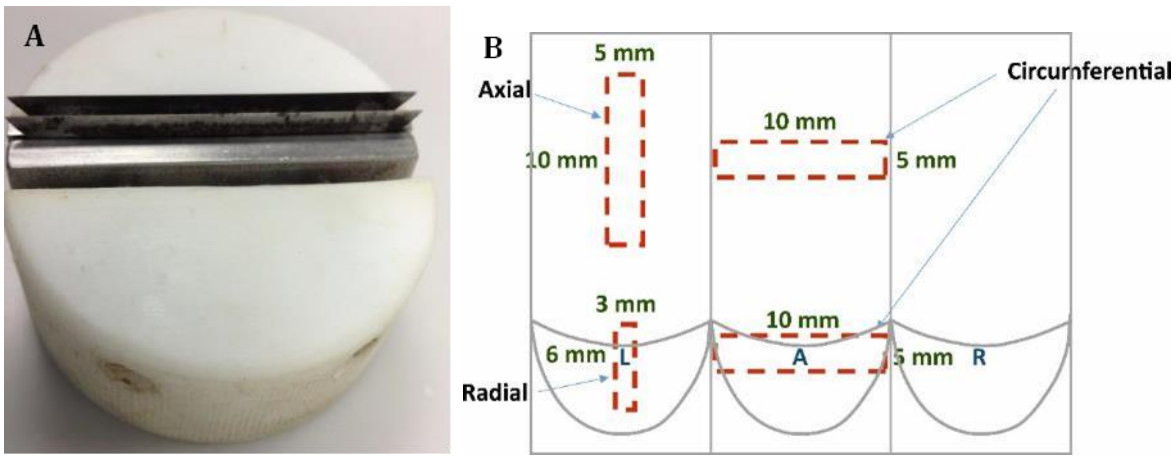


**Figure 2.2 Cutting Tissue Samples for Uniaxial Tensile Testing.** Custom made tissue cutter (A) used to cut tissue samples. Representation of the dimensions of the tissue specimens (B).

The thickness of the tissue was measured at six places along the length of the sample using a thickness gauge (James H. Heal and Company Limited) (Figure 2.3 Thickness Gauge and Custom Made Grips for Uniaxial Tensile Testing.). The tissue

specimen was placed onto the middle of the fixed bottom anvil and the top anvil was gently dropped until it made contact with an area of the specimen. Between each measurement, the tissue was kept hydrated by applying PBS. Prior to noting the tissue thickness readings, three seconds were allowed to pass for stabilisation of the readings. The mean was recorded as the thickness of the tissue specimen (mm). Custom made tissue holder grips were used to secure the strips in the machine (Figure 2.3). These were composed of two holder parts which were used to attach the tissue holder into the cell and base of the BioPlus Instron apparatus. These holders were aligned within removable bracket. A stainless steel block secured in the centre of the removable bracket determined the gauge length of the specimen. A 10 mm wide separating block was used for the samples that required a 10 mm gauge length, and a 6 mm wide separating block was used for the samples that required a 6 mm gauge length. The clamping arrangement was then mounted into the tensile testing rig, and the bracket was removed before the tissue specimen was submerged into the PBS set at 37 °C.

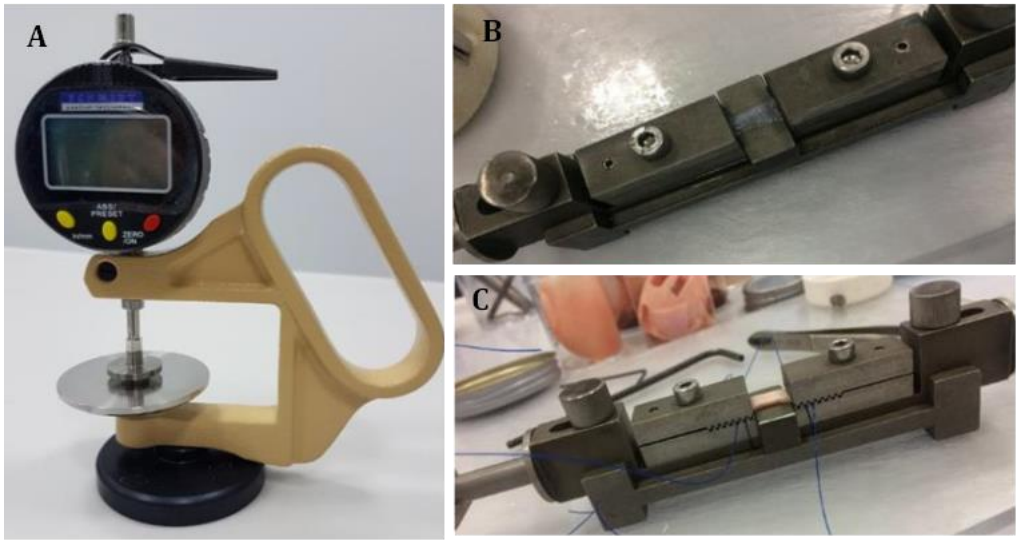


**Figure 2.3 Thickness Gauge and Custom Made Grips for Uniaxial Tensile Testing.** Thickness gauge used to assess the thickness of specimens (A). PHV leaflet (B) and PHV artery wall (C) mounted to custom made tissue holder grips.

#### 2.2.12.2 Test Procedure

The tensile testing was performed using an Instron 3365 materials testing apparatus fitted with a 50 N load cell. Similar to the majority of heart valve mechanical property investigations, a non-physiological strain rate of 10 mm/min

was used. The tissue was then exposed to uniaxial tensile loading. No sample pre-conditioning or pre-load was used. The resulting load and extension of the tissue was recorded. This continued until failure of the tissue, whereby the specimen fractured (Figure 2.4). The output load-extension data of the specimens was saved for further data processing.

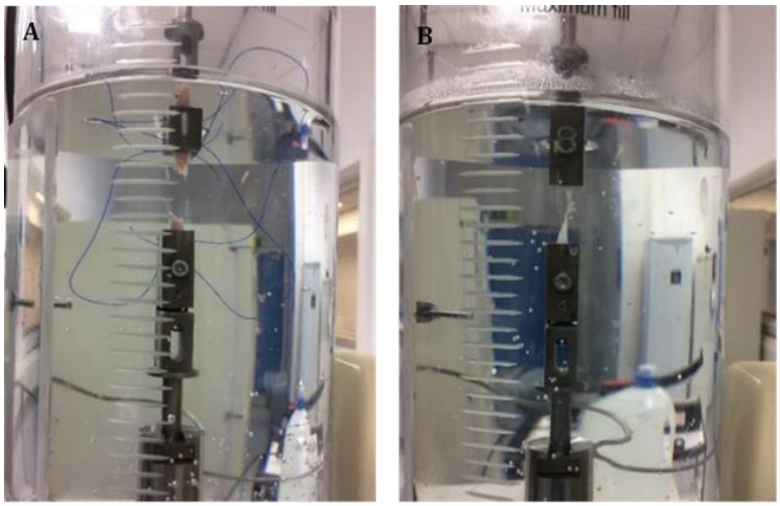


**Figure 2.4 Uniaxial Tensile Loading Until Failure.** Failure of PHV artery wall specimen (A) and PHV leaflet specimen (B).

### 2.2.12.3 Data Processing

The output load-extension data was converted into stress-strain data (Equation 1), and then plotted as shown in Figure 2.5. This was done manually in Excel by importing the output load-extension data from the operating programme of the materials testing machine.

*F = Load (Newtons)*

*Ao = Cross-sectional area (mm²)*

*L = Extension from original gauge length (mm)*

*Lo = Original gauge length (mm)*

$$Stress = \frac{F}{Ao}$$

$$Strain = \frac{L}{Lo}$$

**Equation 1. Equations used to calculate mechanical properties of heart valve tissues.**

Using the stress-strain curve on Microsoft Excel, elastin and collagen phase slopes were created through linear regression of the approximated respective linear regions, with $R^2$ values > 0.90 (Figure 2.5), as described previously by Desai (2019). The maximum failure stress was regarded to be the ultimate tensile strength (UTS). The analysis of these parameters was calculated per treatment

group (n=6 per group). The results of these parameters were averaged over the number of specimens in each group. Statistical analysis was conducted as described in Section 2.2.13.

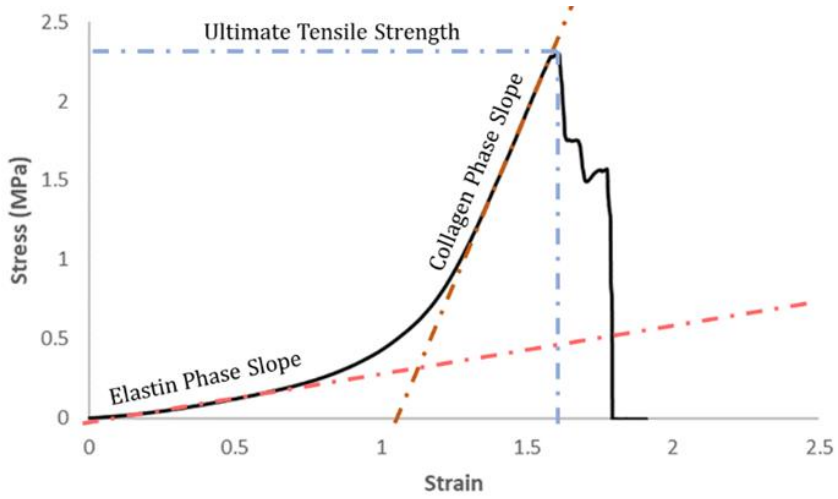


**Figure 2.5 Representative Stress-Strain Curve.** The stress strain curve obtained from the tensile load to failure assessments were used to determine the elastin phase slope (Young's modulus), collagen phase slope and the ultimate tensile strength of the samples, using Microsoft Excel.

### 2.2.13 Statistical Analysis

GraphPad Prism 7 software (GraphPad Software, San Diego, CA, USA) was used to statistically analyse data within this study. All numerical values are presented as mean ± 95 % confidence limits (C.l). Shapiro-Wilk test was used to determine the distribution of data. If the data was normally distributed, the difference between two means was determined using unpaired t-test, or one-way ANOVA to compare the means of multiple groups. The location of the significant differences was identified using Tukey's post hoc testing, unless otherwise stated in specific sections.

If the data was not normally distributed, the difference between two means was determined using a Mann-U Whitney test, or Kruskal-Wallis test to compare the means of multiple groups. The location of the significant differences was identified using Dunn's multiple comparison test, unless otherwise stated in specific sections

The difference between the means of the groups was considered significant if the p value was less than 0.05.

# Chapter 3 : Production and Characterisation of Decellularised Porcine Pulmonary Heart Valves

## 3.1 Introduction

As discussed in Chapter 1, there is an unmet clinical need for a heart valve replacement option that has native cardiac valve properties, with the absence of inherent or acquired antigens that can trigger an adverse immune response when implanted into patients. Decellularised tissues can meet these requirements and pose a great potential for tissue engineering and regeneration applications. Decellularisation removes cells and cellular materials from tissue grafts, leaving behind a three-dimensional ECM scaffold. The retention of native ECM properties such as the biochemical configuration, microarchitecture, biological cues for cell signalling, and biomechanical properties can provide the optimal microenvironment essential for cellular infiltration and tissue regeneration whilst supporting the physiological function of the tissue graft *in vivo* (Badylak et al., 2009). It is hypothesised that the removal of all foreign antigens from tissue grafts prior to implantation can facilitate successful fusion of the graft with the recipient's own anatomical structures. This will allow somatic growth of the implantation, eliminating the requirement for multiple reoperations in patients (Hopkins, R., 2006).

*In vitro* cytocompatibility issues and *in vivo* adverse host responses may be triggered by residual cellular material within the ECM. Despite gaining FDA approval for clinical use, the concerns for the safety and efficacy of porcine derived Restore™ small intestine submucosa (SIS) membrane for rotator cuff repair were raised by Zheng et al. (2005). It was found that SIS membrane contained porcine DNA material which most likely elicited an inflammatory reaction characterised by mass lymphocyte infiltration following subcutaneous implantation into mice and rabbits for 21 days. The presence of cellular components within scaffolds is indicated to shift the macrophage polarisation to the proinflammatory M1 phenotype. This was demonstrated using an *in vivo* study that used acellular allogeneic rat body wall ECM, xenogeneic pig urinary bladder tissue, or acellular xenogeneic pig urinary bladder to repair abdominal wall musculature of rats. Following 28 days, the host tissue response demonstrated that the decellularised tissue elicited the M2 anti-inflammatory macrophage response, with tissue

remodelling evidenced by angiogenesis and organised collagenous and adipose tissue deposition at the wound site. The cellular material on the other hand elicited a predominantly M1 pro-inflammatory macrophage response with the undesirable deposition of dense connective tissue and scarring at the wound site (Brown, B.N. et al., 2009).

A set of quantifiable criteria was established by Crapo et al. (2011) to define tissue decellularisation. This includes; less than 50 ng of double stranded DNA per mg of tissue (dry weight), DNA fragments less than 200 base pairs in length, and no visible nuclei when tissue sections are stained with 4′,6-diamidino-2-phenylindole (DAPI) or haematoxylin and eosin (H&E) (Crapo et al., 2011). Some studies have used a reduction of greater than 90 % (w/w) reduction in DNA content to determine sufficient DNA removal. A study determining human saphenous vein decellularisation using 0.1 % SDS detailed a > 96 % cellular reduction (Schaner et al., 2004). It may also be appropriate to demonstrate the removal of tissue specific cellular materials, such as the xeno-antigen, α 1,3-galactose, which is essential to prevent immune rejection of grafts derived from xenogeneic tissues (Xu et al., 2008).

Decellularisation methods can incorporate a combination of chemical and enzymatic agents, and physical mechanisms to achieve cell lysis and removal of cellular debris, with the objective of preserving ECM composition, structure and therefore function (Crapo et al., 2011).

Detergents are the most prominently used chemical methods for tissue decellularisation. This includes ionic, non-ionic, and zwitterionic detergents. Ionic detergents use the ability to solubilise cell and nucleic membranes as the mode of action for decellularisation (Ahyayauch et al., 2010). The anionic detergents sodium dodecyl sulphate (SDS) and sodium deoxycholate (SDC) are commonly used for heart valve decellularisation by disrupting the phospholipid bilayer of cell membranes and removing phospholipid and cellular protein residues from the ECM. As mentioned in Chapter 1, SDC is reported to be less disruptive to biological tissue in comparison to SDS. White, L. J. et al. (2017) found that treatment of porcine urinary bladder matrix with 4 % SDC for 24 hours retained the intricate collagen fibre network, whereas treatment with 1 % SDS altered collagen fibre organisation. Prolonged chemical exposure to SDS detergents is associated with

disruption to the integrity of the tissue ECM collagenous network as well as the elimination of growth factors (Kasimir et al., 2003; Reing et al., 2010). Kasimir et al. (2003) found a matrix fibre disintegration after exposing porcine aortic and pulmonary heart valve roots to 0.1 %, 0.03 % and 0.01 % SDS with RNase and DNase with agitation for 24 and 48 hours at 37 °C. Reing et al. (2010) reported that porcine dermis decellularised 0.1 % SDS for 6 hours then overnight at room temperature with agitation resulted in a significant decrease in VEGF, bFGF and TGF-β1 growth factors and an 81 % decreased ability to support cell growth in comparison to untreated dermis. Additionally, SDS can penetrate thick tissues which threatens the possibility of cytotoxicity if not sufficiently flushed from the tissue scaffold. It has been demonstrated that pulmonary heart valves decellularised using concentrations of SDS ranging from 0.5 and 1 % require adequate washing steps with agitation for detergent removal, necessary for cytocompatibility (Cebotari et al., 2010; Luo et al., 2014).

Non-ionic detergents such as Triton X-100 have been shown to effectively remove cell and DNA residues from valve conduits. The mode of action employed by non-ionic detergents is the disruption of DNA-protein, lipid-protein, and lipid-lipid interactions (Seddon et al., 2004). However, decellularisation using Triton X-100 has been shown to reduce GAG content of heart valve leaflet which can have a consequential impact on the biomechanical behaviour (Converse et al., 2012; VeDepo et al., 2017). VeDepo et al. (2017) have shown that following decellularisation with Triton X-100, there was a significant reduction in valve leaflet stress-relaxation. Studies have also shown that Triton X-100 is less effective for DNA and nuclei removal in rat aortic valves in comparison to treatment with SDS (Grauss et al., 2003).

Zwitterionic detergents such as 3-[(3-Cholamidopropyl)dimethylammonio]-1-propanesulfonate (CHAPS) demonstrate properties of both ionic and non-ionic detergents. CHAPS has been used to decellularise thin tissues such as lung (Petersen, T. H. et al., 2010). However, evidence suggests that CHAPS may be ineffective for the decellularisation of thicker tissues and has been shown to fail in achieving complete decellularisation of a whole porcine heart (Ferng et al., 2017).

Hypotonic and hypertonic buffer solutions are also commonly used in decellularisation protocols to introduce an osmotic gradient. This induces cell lysis

by osmotic shock. Hypertonic buffer solutions also have the ability to dissociate DNA-protein complexes within the ECM (Cox and Emili, 2006). Both hypotonic and hypertonic buffer solutions are also effective for rinsing cellular debris products of cell lysis from within the tissue ECM. The use of buffers is often combined with other decellularisation agents such as detergents which can reduce the required detergent concentration and time exposure, possibly preventing extensive disruption to the ECM ultrastructure and composition (Crapo et al., 2011).

Chelating agents such as ethylenediaminetetraacetic acid (EDTA) aid in decellularisation by sequestering metallic ions required for cell adhesion, disrupting cell adhesion to the ECM (Crapo et al., 2011; Klebe, 1974).

Intracellular serine proteases such as members of the plasminogen cascade may be released during cell lysis which can have undesirable degradative effects on the ECM components including collagen, elastin and fibronectin as reported by Weiss (1989). These effects can be prevented by adding aprotinin to solutions, which is a small polypeptide that can competitively inhibit proteases (Booth et al., 2002; Waxler and Rabito, 2003)

Enzymatic agents such as nucleases and proteases can provide targeted removal of cell residues and other ECM components. Nucleases facilitate the removal of nucleotides that often remain following cell lysis by cleaving nucleic acid sequences. Endonucleases such as benzonase are effective for this function as they can cleave nucleotides mid-sequence, creating multiple fragments of DNA ready for removal (Petersen, Thomas H. et al., 2010). Trypsin is a serine protease that can be used to disrupt the tissue ultrastructure by cleaving peptide bonds on the C-side of Arg and Lys. It is recommended to include exposure of tissue to trypsin as an initial step in the decellularisation protocol as the tissue ultrastructure disruption aids in the penetration of subsequent decellularisation agents (Yang et al., 2010).

It is common for tissues to be immersed in decellularisation agents whilst being agitated to facilitate the removal of cellular material. This approach has been applied for the decellularisation of a range of tissue types such as heart valves, dermis, tendon, cartilage, and meniscus (Kheir et al., 2011; Luo et al., 2014; Stapleton et al., 2008; Ventura et al., 2019).

A robust low concentration detergent based process for heart valve decellularisation has previously been described (Booth et al., 2002; Desai et al.,

2018; Luo et al., 2014; Vafaee et al., 2018; Wilcox et al., 2005). Initially, a protocol incorporating hypotonic buffer, 0.1% (w/v) SDS, nuclease digestion was developed for porcine aortic heart valve decellularisation which demonstrated successful tissue decellularisation and histoarchitectural retention (Wilcox et al., 2005; Booth et al., 2002). The decellularisation process described by Wilcox et al. (2005) was modified to include a PAA sterilisation step by Luo et al. (2014) for the decellularisation and decontamination of porcine pulmonary heart valve roots. The impact of the process on the biological and biomechanical properties and regenerative potential of the valves was assessed *in vitro*. This decellularisation protocol was subsequently modified to be applicable to human pulmonary and aortic conduits. Vafaee et al. (2018) presented a comprehensive description of the biological characteristics of human valve conduits exposed to a specific decellularisation protocol that did not include a PAA sterilisation step due to the degradative effects on the ECM basement membrane (Luo et al., 2014; Vafaee et al., 2018). Human cryopreserved pulmonary and aortic valve allografts were decellularised using hypotonic buffer, 0.1% (w/v) SDS, and nuclease digestion. Histological examination and quantification of DNA provided evidence for the removal of cells and cellular remnants whilst retaining components of the ECM, such as collagen. The decellularised tissue demonstrated good biocompatibility which was verified by the *in vivo* implantation into a mouse subcutaneous implant model.

A modified decellularisation process specific for porcine pulmonary heart valve roots as described by Luo et al. (2014) was used throughout this study.

## 3.2 Aims and Objectives

### 3.2.1 Aim

The aim of the work described in this chapter was to characterise the properties of native and decellularised porcine pulmonary heart valves using a modification of a previously developed decellularisation method with the absence of the PAA sterilisation step. The work described within this chapter was therefore essential to provide a baseline for subsequent studies.

### 3.2.2 Objectives

i. To determine the efficacy of decellularisation through staining with H & E.

ii. To determine the effect of decellularisation on the tissue histoarchitecture through staining with H & E and antibody labelling of collagen IV.

iii. To confirm the decellularisation process has sufficiently reduced the DNA content of porcine pulmonary heart valves through DNA quantification.

iv. To validate the sufficient removal of decellularisation agents and the biocompatibility of decellularised porcine pulmonary heart valves using contact and extract cytotoxicity assays.

v. To determine the impact of the decellularisation process on the biomechanical properties of porcine pulmonary heart valves using uniaxial tensile testing.

## 3.3 Study Experimental Approach

A decellularisation protocol has previously been optimised for the successful decellularisation of porcine pulmonary heart valves (Luo et al., 2014). The replicability of this process with the absence of PAA sterilisation step was assessed during this work package, to demonstrate the ability to successfully decellularise porcine pulmonary heart valves (Figure 3.1). This was essential for subsequent studies to investigate the impact of sterilisation methods on decellularised porcine pulmonary heart valves.

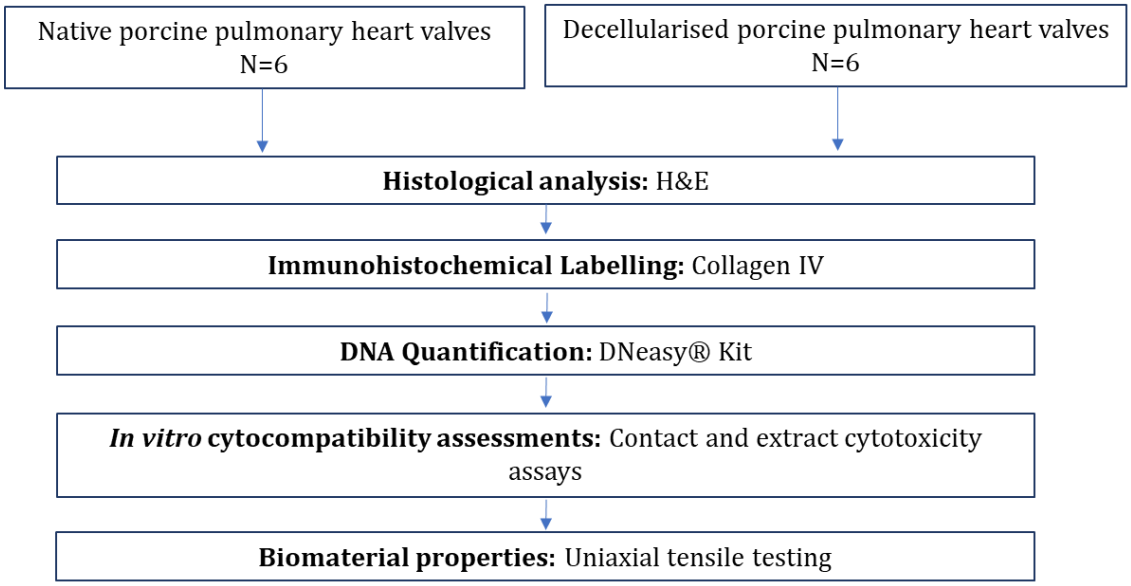


**Figure 3.1 Schematic of the Experimental Approach Adopted to Characterise Decellularisation Efficacy and the Impact of Decellularisation on the Biological and Biomechanical Properties of Porcine Pulmonary Heart Valves.**

## 3.4 Methods

### 3.4.1 Production of Decellularised Porcine Pulmonary Heart Valves

As described in section 2.2.2, porcine pulmonary heart valves were acquired and exposed to the decellularisation process described in section 2.2.3.

### 3.4.2 Histological Analysis

To assess the efficacy of the decellularisation process, H & E staining was used to observe the presence of nuclei (Section 2.2.5.1). The impact of the decellularisation process on the histoarchitecture of native porcine pulmonary heart valves was also assessed using H & E staining of native and decellularised PHV tissue sections.

### 3.4.3 Immunohistochemical Labelling of Collagen IV

To assess the impact of decellularisation on the preservation of collagen IV in PHV tissue, native and decellularised PHV roots were dissected longitudinally, incorporating half a leaflet, pulmonary artery wall and myocardium skirt (N=3 each). Processing and sectioning of tissue was conducted as described in section 2.2.4.1. Labelling of sections with specific antibodies against collagen IV was conducted as described in section 2.2.6.

### 3.4.4 DNA Purification and Quantification DNA of Native and Decellularised Porcine Pulmonary Heart Valves

The DNA levels in native and decellularised porcine PHVs were quantified and compared to determine potential residual DNA in the tissue following the decellularisation process.

#### 3.4.4.1 DNA Purification

DNA was extracted from native and decellularised porcine PHVs using a commercially available DNeasy® blood and tissue kit from QIAgen. Pulmonary

artery wall tissue was taken from native PHV roots (25-50mg wet weight, N=3) and decellularised PHV roots (100-250mg, N=3). A segment that equated to roughly 1/3rd of the left valve leaflet was also taken from each PHV root for analysis. The tissue was macerated and placed in a sterile 2ml micro centrifuge tube. The tissue was lyophilised to a constant weight using a freeze dryer. Buffer ATL (180µl for native pulmonary artery wall and native and decellularised leaflet; 360µl for decellularised pulmonary wall) and proteinase K (20µl for native pulmonary artery wall and native and decellularised leaflet; 40µl for decellularised pulmonary wall) from the QIAgen kit were added to the samples, and mixed thoroughly by pulse vortexing (10 seconds). The samples containing the buffer ATL and proteinase K were then incubated at 56°C for three hours, or until the tissue completely lysed. During this incubation period, the samples were pulse vortexed (10 seconds) every 30 minutes to disperse the sample. Following the incubation period, the samples were pulse vortexed (15 seconds) before buffer AL from the QIAgen kit and absolute ethanol was added (200µl of each buffer AL and ethanol for native pulmonary artery wall and native and decellularised leaflet; 400µl for decellularised pulmonary wall). The samples were mixed thoroughly by vortexing (10 seconds). Each sample was transferred to a separate DNeasy Mini spin column placed in a 2 ml collection tube, and centrifuged at 6000 x g for 1 minute. The flow-through was discarded together with the collection tube. The DNeasy Mini spin column was placed in a new 2ml collection tube. 500µl of buffer AW1 from the QIAgen kit was added to the column. This was centrifuged at 6000 x g for 1 minute. The flow through was discarded. 500µl of buffer AW2 from the QIAgen kit was then added to the column. This was centrifuged at 20,000 x g for 3 minutes to dry the membrane of the DNeasy spin column as residual ethanol could interfere with subsequent reactions. The flow-through was discarded along with the collection tube. The DNeasy mini spin column was placed in a clean 2ml microcentrifuge tube, and 200µl of buffer AE from the QIAgen kit was pipetted directly onto the DNeasy membrane. This was incubated at room temperature for 1 minute and then centrifuged for 1 minute at 6000 x g to elute. The extracted DNA in buffer AE was quantified immediately or stored at -20 °C until quantification.

#### 3.4.4.2 DNA Quantification

The NanoDrop spectrophotometer was used to quantify the concentration of purified DNA from the samples. Buffer AE from the QIAgen kit was used as a test sample blank. 2µl from the tissue samples were loaded onto the NanoDrop and the absorbance was recorded at 260nm. Triplicate measurements were made per sample, and the mean was considered the absorbance of the sample. The DNA concentration (ng.µl-1) in the sample was displayed in the nanodrop software. However, the values given for the DNA concentration in the samples were interpolated into a DNA standards curve. Standard DNA concentrations of 0, 5, 10, 15, 20, 25, 30, 35, 40, 45 and 50 $\mu g.ml^{-1}$ were prepared. Measurements of DNA standards were blanked against DNA stock buffer. The DNA concentration in the samples were normalised for volume and initial tissue mass to determine DNA concentration in $ng.mg^{-1}$.

### 3.4.5 *In Vitro* Cytocompatibility Assessments

The *in vitro* cytocompatibility of decellularised pulmonary artery wall and leaflet samples was assessed using contact cytotoxicity (N=3) as described in section 2.2.10.1 and extract cytotoxicity assays (N=6), as described in section 2.2.10.2.

### 3.4.6 Uniaxial Tensile Testing

Native and decellularised pulmonary artery wall and leaflet samples were subject to uniaxial tensile testing, as described in section 2.2.12.

## 3.5 Results

### 3.5.1 Histological Analysis

H & E staining was used to evaluate the efficacy of the decellularisation process. Staining of native PHV tissue revealed a dense population of cells within the artery, leaflet and myocardium. Staining of decellularised PHVs revealed the absence of cells and cell residues (Figure 3.2).

The impact of the decellularisation process on the histoarchitecture of PHV tissue was also assessed using H & E staining. H & E staining showed that there was no major damage introduced to the PHV tissue following decellularisation. The luminal side of the pulmonary artery displayed highly organised ECM fibres that appeared slightly looser in comparison to the native artery. Both native and decellularised artery adventitia displayed loosely organised structures. The well-defined *arterialis*, *fibrosa*, *spongiosa*, and *ventricularis* layers of the leaflet were observed in the tissue sections following decellularisation. The fibres in the *spongiosa* appeared more loosely organised in comparison to the fibres in the *fibrosa* and *ventricularis* layers, and the *fibrosa* layer appeared thicker than then *ventricularis* layer in both native and decellularised specimens. The myocardium bundles were arranged in a similar manner to native untreated PHV sections.

### 3.5.2 Immunohistochemical Labelling of Collagen IV

As shown in Figure 3.3, the intensity of collagen IV positive staining on decellularised PHVs was similar to native PHVs. The lumen surface of the artery displayed brown staining of the organised crimpled fibres. The connective tissue layer outside of the adventitial artery surface displayed positive staining in the blood vessels. A prominent brown lining of collagen IV positive staining was observed at the *ventricularis* and *arterialis* surfaces of the leaflet, with less intense staining of interstitial fibres of both native and decellularised PHV leaflets. The myocardium displayed a network of defined positive labelling, with greatest intensity in the lining of blood vessels.

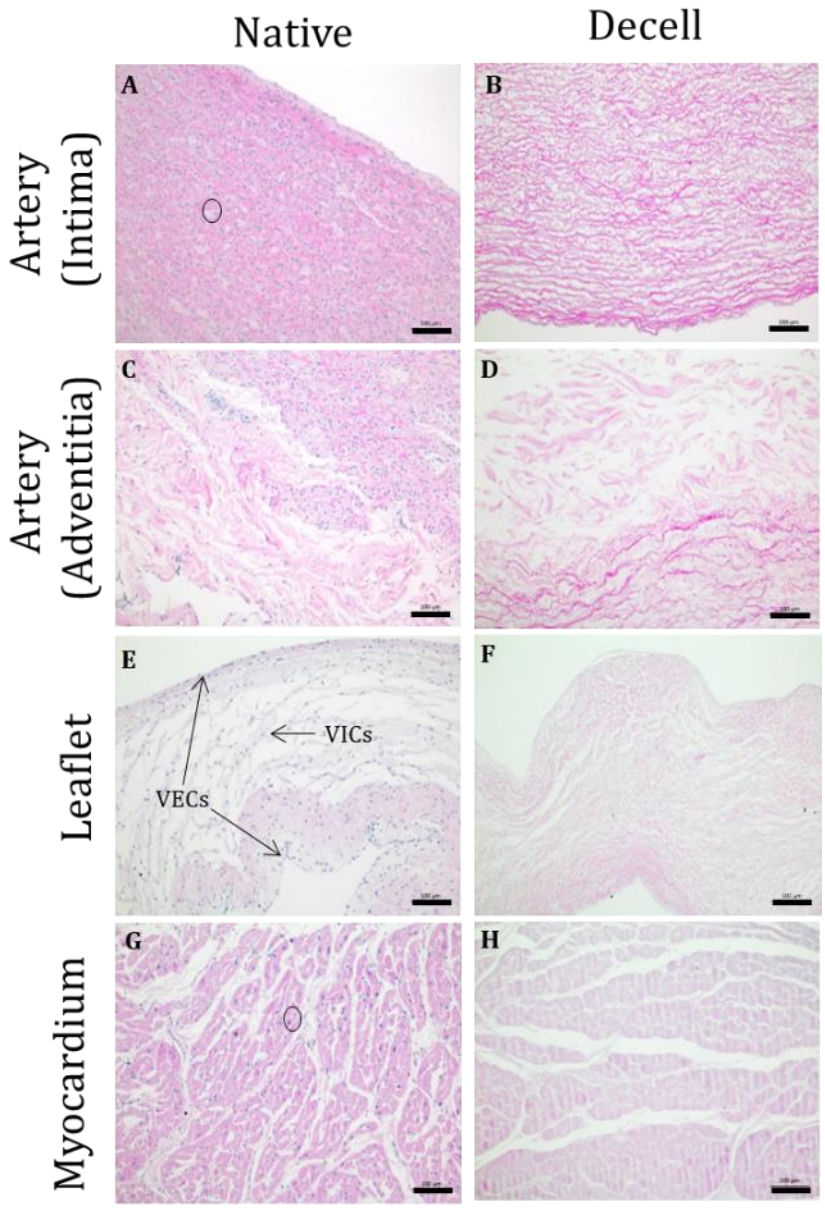


**Figure 3.2 Representative Images of H & E Stained Native and Decellularised PHVs.** Images show native PHV wall intima (A), adventitia (C), leaflet (E), and myocardium (G); and decellularised PHV wall intima (B), adventitia (D), leaflet (F) and myocardium (H). Images were taken using Köhler illumination and a x 10 objective. Representative images shown, Scale bars 100 μm.

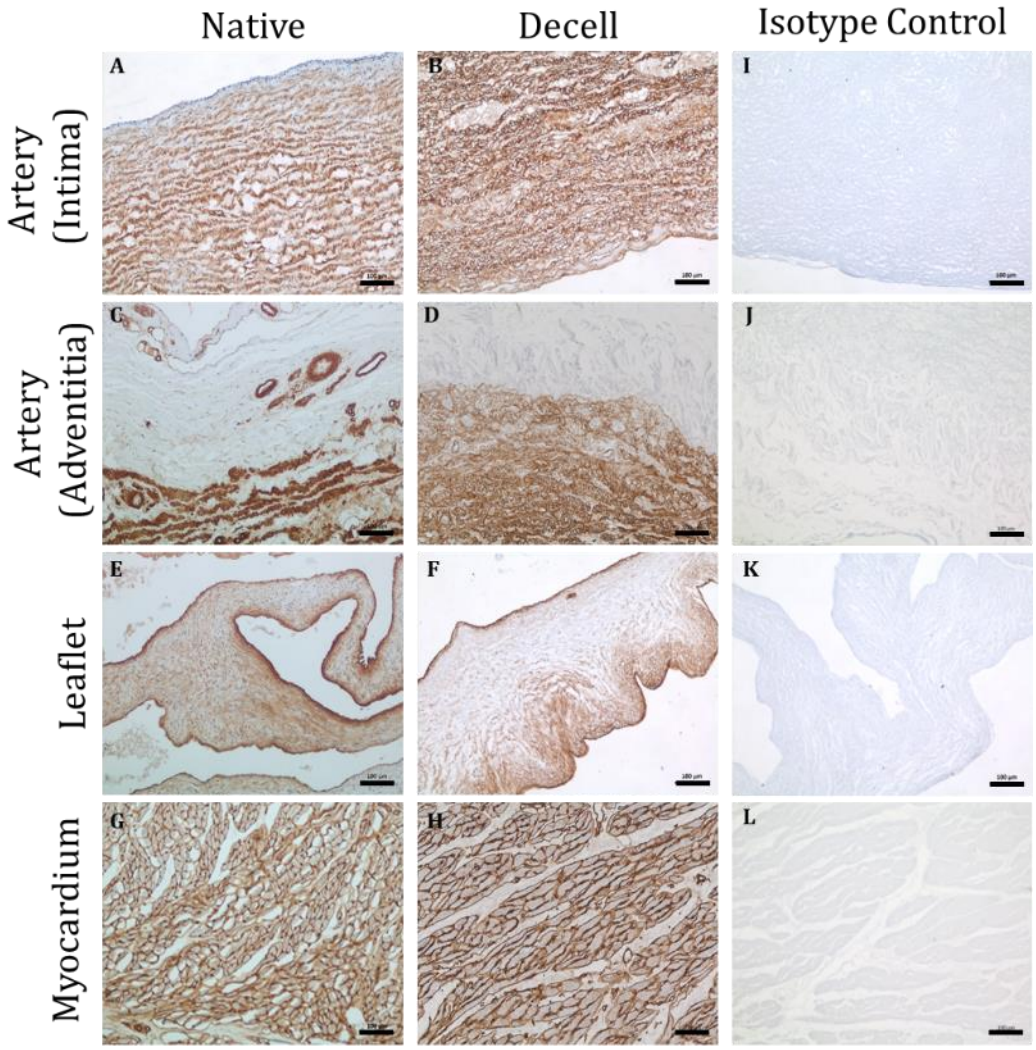


**Figure 3.3 Representative Images of Native and Decellularised PHVs Labelled with Monoclonal Antibodies Against Collagen IV.** Images show native wall intima (A), adventitia (D), leaflet (G), and myocardium (J); Decellularised wall intima (B), adventitia (E), leaflet (H) and myocardium (K); Isotype controls for dPHV wall intima (C), adventitia (F), leaflet (I) and myocardium (L). Images were taken using Köhler illumination and a x 10 objective. Representative images shown, Scale bars 100 μm.

### 3.5.3 DNA Content of Native and Decellularised Porcine Pulmonary Heart Valves

DNA was extracted and quantified from native and decellularised porcine pulmonary heart valve artery wall and leaflet specimens. There was a significant reduction in DNA content of decellularised porcine pulmonary artery and PHV leaflet specimens in comparison to native specimens (Figure 3.4)

A percentage DNA removal greater than 95 % from porcine pulmonary heart valves was achieved following decellularisation. DNA content of native PHV wall specimens was found to be 928.70 ± 225.79 $ng.mg^{-1}$, whereas the DNA content of decellularised PHV wall specimens was found to be 43.08 ± 25.24 $ng.mg^{-1}$. The DNA content of decellularised PHV leaflet specimens was found to be 47.75 ± 51.84 $ng.mg^{-1}$, which was significantly lower than the DNA content of native PHV leaflet specimens (1079.10 ±232.16 $ng.mg^{-1}$).

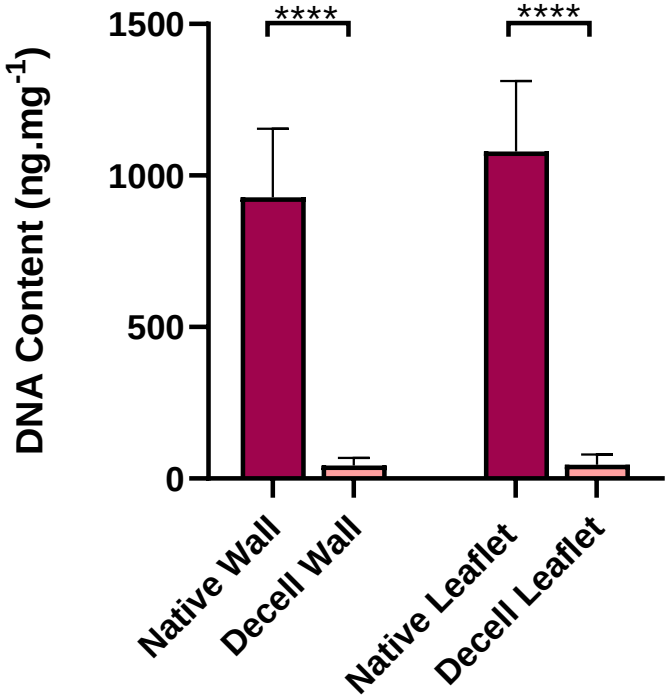


**Figure 3.4 DNA Content of Native and Decellularised Porcine Pulmonary Heart Valves. Data presented as mean (n=3) ± 95% C.I. Data was analysed using unpaired t-test between the two groups in each specimen type.** **** ($p<0.001$) denotes significant difference between the groups.

### 3.5.4 *In Vitro* Cytocompatibility Assessments

Contact culture of L929 cells with decellularised porcine PHV wall and leaflet samples was used to determine cytocompatibility of decellularised tissues. The extract cytotoxicity assay was also used to determine if toxins were leached from decellularised PHV wall and leaflet samples.

The contact cytotoxicity assay showed no evidence of decellularised tissue cytotoxicity (Figure 3.5 A-D). L929 cells grew up to and in contact with decellularised artery wall and leaflet tissue specimens with no change in the cellular morphology in comparison to the negative steri-strip control. L929 cells were also incubated with cyanoacrylate adhesive as a positive cytotoxic control, which resulted in rounded dead cells that were non-adherent. The rounded appearance of non-adherent dead cells was absent in cells cultured with decellularised artery wall and leaflet tissue specimens.

The results from the extract cytotoxicity assay showed no evidence of cytotoxicity (Figure 3.5 E). ATP levels of cells cultured with decellularised porcine PHV artery wall and leaflet extracts were significantly greater than cells cultured with the positive DMSO control only, and not the negative DMEM control.

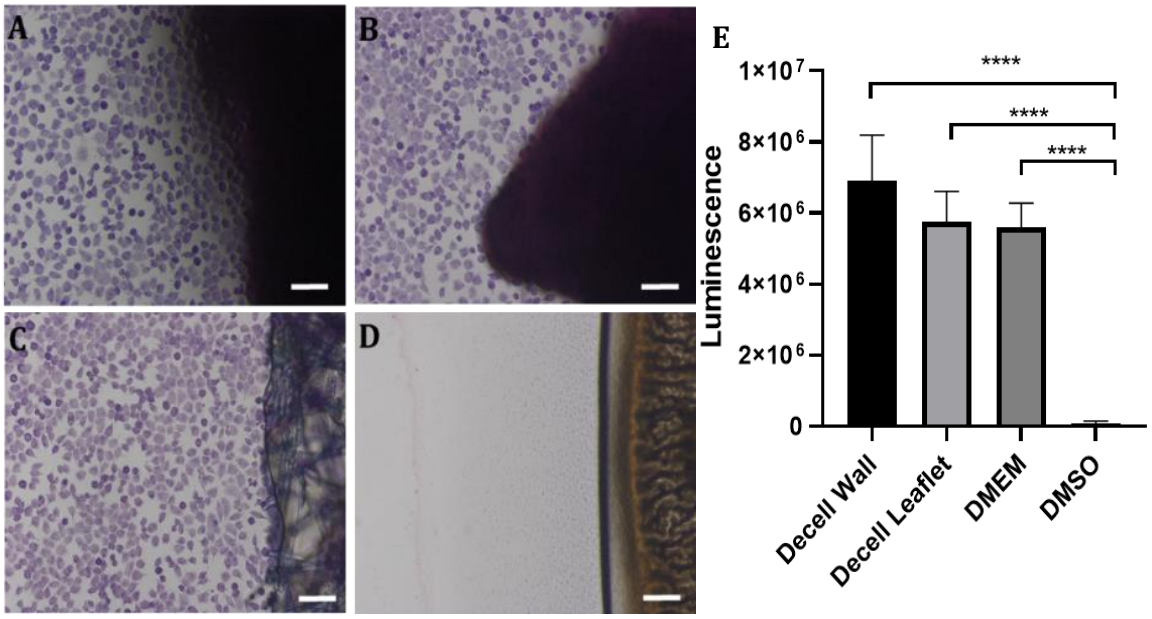


**Figure 3.5 Giemsa Stained Cell Cultures From Contact Cytotoxicity of dPHV Wall and Leaflet Specimens, and Cell Viability of L929 Cells Following Incubation with dPHV Wall and Leaflet Tissue Extracts.** Images show a representative dPHV wall specimen (A), leaflet specimen (B), negative control (C), and positive control (D). Scale bars are 100µm. (E) Data presented as mean (n=6) ± 95% C.I. Data was analysed using one way ANOVA with Tukey's post-hoc test. **** ($p<0.0001$) denotes significant difference between the groups.

### 3.5.5 Uniaxial Tensile Testing

Native and decellularised PHV wall and leaflet tissue specimens were subjected to uniaxial tensile testing.

The stress-strain graphs for native and decellularised wall and leaflet tissue specimens are shown in Figure 3.6. All graphs demonstrate the typical tri-phasic characteristics. There are no clear differences shown in the stress-strain graphs of decellularised axial and circumferential wall specimens, and radial and circumferential leaflet specimens, in comparison to the native specimens.

Graphs displaying the tensile parameters decellularised PHV artery wall specimens in comparison to native specimens are shown in Figure 3.7**.** There was a significant increase in the elastin phase slopes of decellularised circumferential wall (0.08 ± 0.02 MPa) and axial wall (0.12 ±0.05 MPa) specimens in comparison to the native circumferential wall (0.04 ± 0.03 MPa) and axial wall (0.04 ± 0.01 MPa) specimens. There were no significant differences in the collagen phase slopes of decellularised PHV artery wall specimens in comparison to the native specimens. The ultimate tensile strength of circumferential decellularised PHV artery wall specimens was not significantly different to circumferential native PHV artery wall specimens. However, there was a significant increase in the ultimate tensile strength of axial decellularised PHV artery wall specimens (1.21 ± 0.20 MPa) in comparison to axial native PHV artery wall specimens (0.91 ± 0.24 MPa).

There was no significant difference in the elastin phase slope, collagen phase slope, and ultimate tensile strength of decellularised PHV leaflets in comparison to native PHV leaflets.

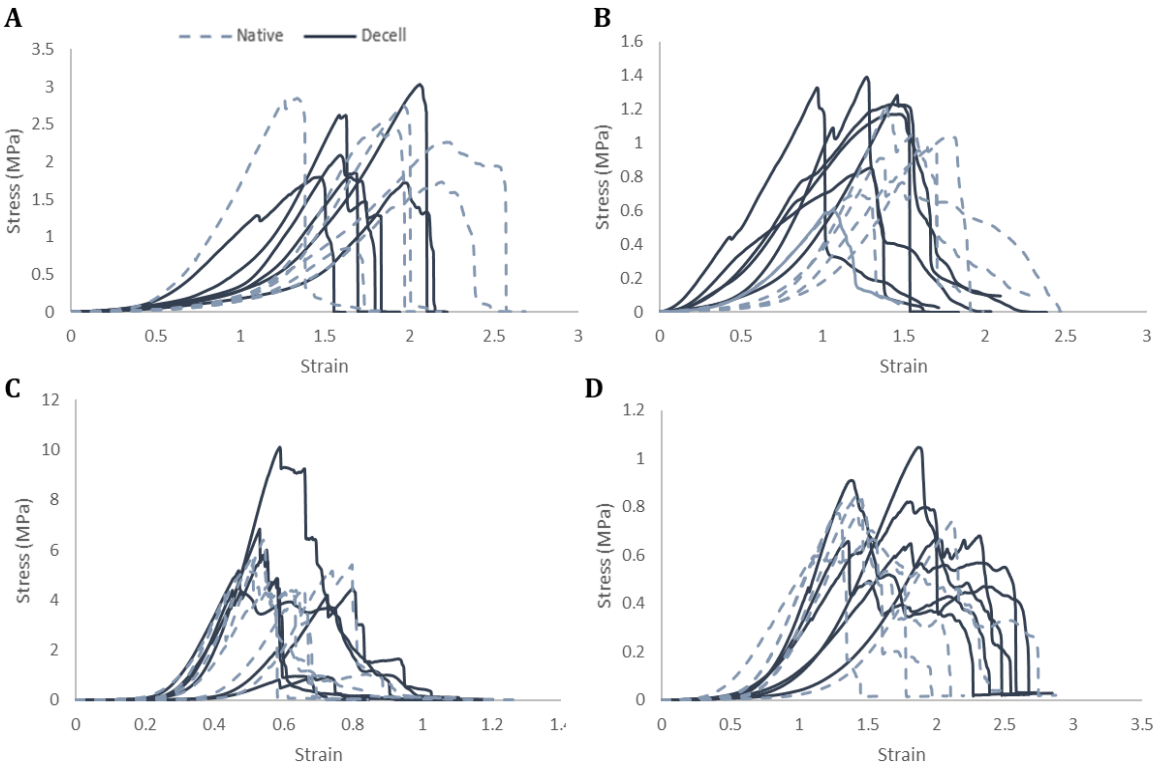


**Figure 3.6 Stress-Strain Graphs of Native and Decellularised PHV Wall and Leaflet Specimens.** Stress-strain graphs shown for native and decellularised axial wall (A); native and decellularised circumferential wall (B); native and decellularised radial leaflet (C); native and decellularised radial leaflet (D). N=6 for all specimens.

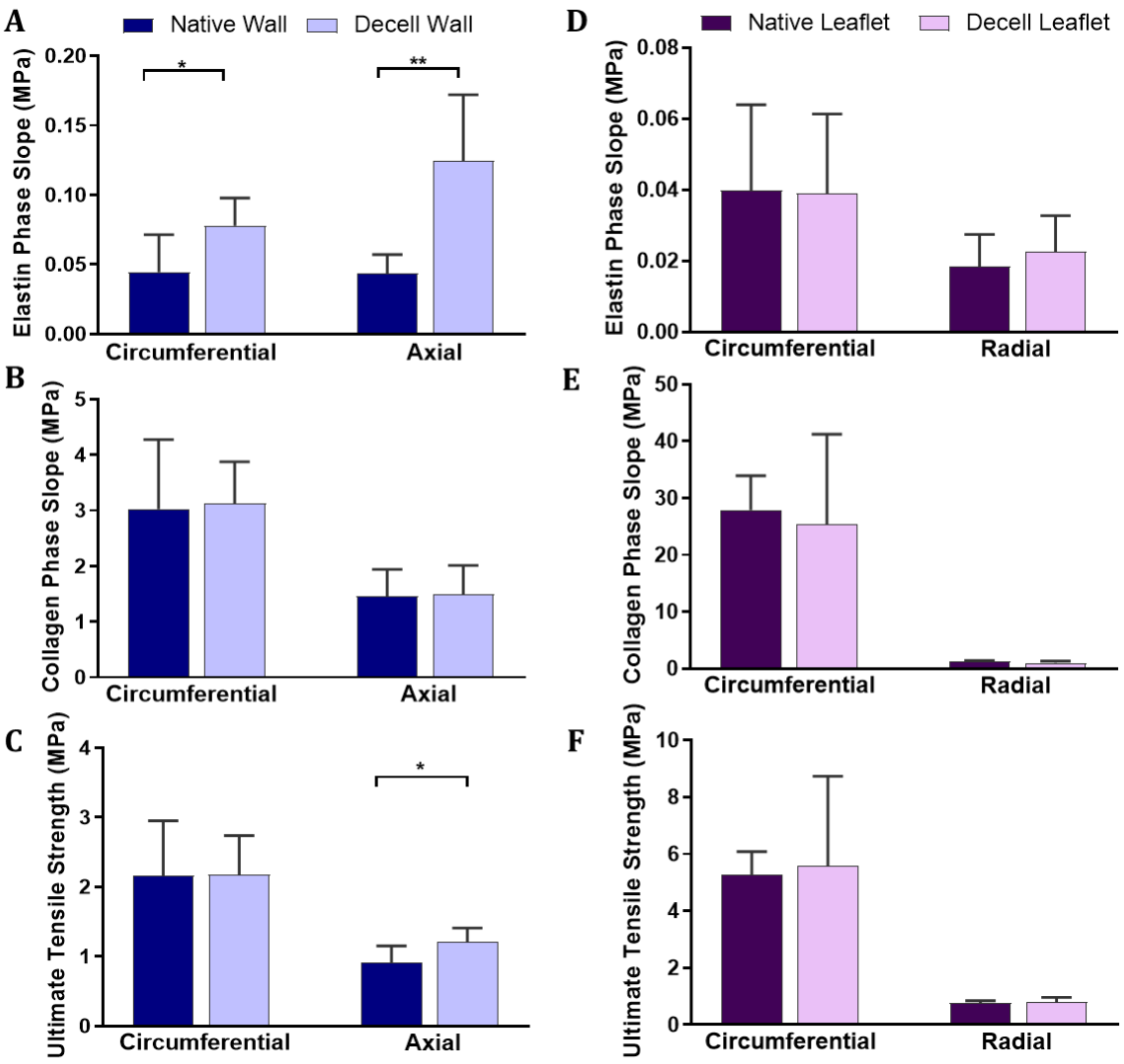


**Figure 3.7 Tensile Parameters of Decellularised PHV Artery Wall and Leaflet Specimens in Comparison to Native PHVs**. Elastin phase slopes (A, D), collagen phase slopes (B, E) and ultimate tensile strengths (C, F) of decellularised and native wall and leaflet specimens. Data presented as mean (n=6) ± 95% C.I. Data was analysed using unpaired t-test between the two groups in each specimen type. Significant differences between groups are represented with * ($p<0.05$) and ** ($p<0.01$).

## 3.6 Discussion

Within the present study, a modification of an established decellularisation method incorporating low concentration SDS, hypotonic and hypertonic buffers, and nuclease enzymes was applied to porcine pulmonary heart valves (Luo et al., 2014). The established decellularisation protocol described by Luo et al. (2014) previously included a PAA incubation step for sterilisation. However, it was suggested that PAA treatment abrogated collagen IV staining in the decellularised porcine PHVs as demonstrated by the devoid of collagen IV staining. The PAA treatment potentially removed collagen IV from the tissue or altered the collagen IV epitope. In the current study, PAA treatment was eliminated from the protocol used within this study (Table 2.3, section 2.2.3) to prevent adverse effects to the tissue prior to applying a novel sterilisation method, which was the overarching aim of this research.

SDS is a commonly used decellularisation agent that effectively removes nuclear remnants and cytoplasmic proteins from tissues. However, it is known that high SDS concentrations or prolonged SDS exposure of tissues can denature proteins, and therefore adversely impact the native tissue microenvironment (Mendibil et al., 2020). This was demonstrated by Faulk et al. (2014a), who exposed the basement membrane complex (BMC) of porcine urinary bladder to 1 % SDS for 24 hours with physical agitation at 37 °C. The collagen fibres within the BMC samples appeared denatured following treatment. Histological analysis with H & E staining was used to assess the effectiveness of the decellularisation protocol as well as the impact of decellularisation on the ECM histoarchitecture. There were no cells present throughout the PHV tissue following decellularisation, indicating the sufficient removal of cells in accordance to the criteria highlighted by Crapo et al. (2011).

The ECM structure was generally retained following decellularisation, although, the structure of the pulmonary artery intima appeared looser in comparison to the native tissue. This could be due to the presence of cavities that remained following the removal of cells that had occupied the tissue in the native state. Additionally, the loose structures observed could be due to the degradation of small collagen fibres during the decellularisation process without significant injury to the tissue microstructure and biomechanical properties. Similar results were presented by

Cai et al. (2021), whereby the microstructure of porcine carotid arteries became porous and loose following decellularisation with 0.25 % and 0.5 % SDS combined with 1 % Triton-X-100. It has been hypothesised that some disruption to the ECM structure may facilitate decellularisation. Cheng, J. et al. (2021) found that porcine carotid arteries that became more porous during decellularisation were more efficiently decellularised in comparison to porcine carotid arteries that became less porous. It was believed that the formation of larger pores facilitated tissue chemical exposure by enabling even access of the decellularisation agents within the tissue network, as well as providing routes for the exit of cellular material. However, the resultant porous tissue structure following decellularisation could be due to detrimental degradation of ECM collagen fibres which can negatively impact the tissue mechanical properties. Cai et al. (2021) found that porcine carotid arteries that were decellularised with 0.5 % Tritonx-100 solution for 24 hours and 0.25 % SDS solution for 72 hours resulted in the smallest size pores and greatest retention of native biomechanical properties in comparison to other decellularisation methods investigated. Therefore, a fine balance should be obtained between obtaining sufficient tissue porosity that can aid decellularisation without significantly impacting the tissue microstructure and biomechanical performance. Despite the alterations in the structure of the pulmonary artery intima following decellularisation, the biomechanical properties of the tissue were largely retained.

Minor disruption to tissue ECM may also facilitate the infiltration of cells during autologous recellularisation of decellularised grafts (Zhang, Y. et al., 2005). Sheridan et al. (2012) removed varying amounts of collagen from decellularised porcine carotid arteries to promote porosity prior to seeding with aortic smooth muscle cells. It was found that the highest porosity scaffolds retained the largest number of cells following direct injection of 1 x $10^6$ human aortic smooth muscle cells/ml media and culture for 24 hours. The slight structural alteration in the pulmonary artery intima observed in the present study may therefore be beneficial in decellularised PHVs.

Collagen IV also plays a role in graft remodelling as it is believed to be important for tissue endothelialisation. Collagen IV was retained throughout the PHV tissue following decellularisation within this study. These results were comparative to

Vafaee et al. (2018) who followed a similar decellularisation protocol for human pulmonary heart valves. Tissue integration and recolonisation of decellularised human pulmonary leaflets by host cells was observed in *in vivo* biocompatibility assessments using a mouse subcutaneous implant model (Vafaee et al., 2018).

The sufficient removal of DNA from tissue grafts is also essential for the appropriate integration of the graft *in vivo*, and to avoid calcification of the graft as a result of host immune response. In a study conducted by Paniagua Gutierrez et al. (2015), native and low-concentration SDS decellularised porcine aortic roots were implanted into the descending aorta of pigs for biocompatibility assessments. The decellularised roots did not display any signs of calcification, with regeneration evidenced by cellular infiltration within the neointima and luminal artery surfaces. Whereas, the native roots demonstrated an intense immune response with T cell infiltration and severe calcification triggered by the presence of allogeneic donor cells. Decellularised porcine aortic roots were also implanted into the right ventricular outflow tract of juvenile sheep. After 6 months, some grafts showed evidence of recellularisation by the presence of proliferative SMC phenotypic cells in the medial area of the aortic wall. Two grafts showed some degree of calcification, most likely due to the presence of residual cellular material within the aortic wall at the time of implantation (Paniagua Gutierrez et al., 2015). Gilbert et al. (2009) quantified the DNA content of several commercially available ECM scaffolds. This included Oasis™ (Cook Biotech, Inc.) porcine small intestinal submucosa matrix which is indicated for wound management, . Mostow et al. (2005) investigated the effectiveness of The Oasis™ (Cook Biotech, Inc.) porcine small intestinal submucosa matrix in healing chronic leg ulcers. Patients were assigned to receive a weekly topical treatment of the matrix with compression therapy (n=62) or compression therapy alone (n=58). After 12 weeks, it was found that the matrix significantly improved the healing of chronic leg ulcers (55 % of patients) in comparison to the compression therapy alone (34 % of patients). Although small amounts of DNA were detected in Oasis™ samples, and most of the other ECM devices, the clinical efficacy has generally been found to be positive, indicating that the presence of residual DNA within biological scaffold materials may not trigger an adverse immune response (Gilbert et al., 2006; Gilbert et al., 2009). It was therefore appropriate that an upper limit of 50 ng of double stranded DNA per mg of tissue was accepted as the gold standard measurement by

many research groups to determine successful decellularisation (Crapo et al., 2011). The decellularised porcine PHVs within this study met this criterion as the DNA content was quantified to be less than 50 ng per mg of tissue and no visible nuclei were present.

Inadequate removal of the decellularisation reagents from PHVs can result in cytotoxicity, which could lead to calcification and rejection of the implant in clinical use. Rieder, E. et al. (2004) reported a toxic influence of porcine heart valve conduits decellularised with 0.1 % SDS on seeded human saphenous vein endothelial cells and myofibroblasts after 5 and 10 days incubation, respectively. The most likely cause for the reported cytotoxicity was insufficient washing of residual SDS from the decellularised tissue. Cebotari et al. (2010) found that washing 1 % SDS from decellularised PHVs after 8 wash cycles decreased the residual reagent concentration to less than 50 mg/L. This resulted in no significant toxicity on cell cultures and the decellualrised scaffolds were able to support growth of surface seeded human endothelial cell growth following culture for 72 hours. SDS detergent, EDTA, aprotinin, and PAA can have cytotoxic effects, and it is essential that these are completely removed from the tissue along with products of cell lysis. *In vitro* cytocompatibility assessments indicated that decellularised PHVs were not cytotoxic, suggesting that potentially cytotoxic decellularisation agents were sufficiently removed during the decellularisation process. Similar findings were also reported by Luo et al. (2014) and Vafaee et al. (2018).

Biomechanical properties of the decellularised PHV tissue was not significantly different to native tissue, except for a significant increase in the elastin phase slope of axial and circumferential pulmonary wall and a significant increase in the UTS of axial pulmonary wall. Similar alterations were described by Luo et al. (2014) for porcine pulmonary arteries. Theodoridis et al. (2016) also reported an increase in UTS of decellularised porcine pulmonary artery which was proposed to be due to a reduction in wall thickness following decellularisation. The loosening of fibres following the removal of cells may also be a contributing factor for this change. The recellularisation of the PHV graft *in vivo* is expected to aid in the biomechanical function restoration (Desai et al., 2018).

Several allogeneic decellularised heart valve products are currently commercially available for clinical applications. This includes CryoValve Synergraft® family

(Aortic valves and SG pulmonary valves; CryoLife, Kennesaw, GA), and Espoir PV® (Corlife, Germany) derived from human aortic and pulmonary valves (Badria et al., 2020). Synergraft valves demonstrated good clinical performance as there was no difference found in early or late insufficiency at a follow-up time of 46 ± 14 months following implantation into 41 patients in comparison to matched standard allograft controls (Konuma et al., 2009). Tudorache et al. (2016) reported on the clinical efficacy of pulmonary heart valves decellularised in an equivalent manner to Espoir PV and found that haemodynamic performance of the decellularised grafts were exceptional up to 7.6 years of patient follow-up, with stable valvular gradients and no significant valvular regurgitation. However, a shortage of allogeneic cardiac valves for transplantation has shifted the focus onto xenogeneic cardiac valves as a valuable and unlimited source for tissue. Xenogeneic tissue is available in a range of shapes and sizes, making it a suitable option to align with patient unique anatomical configurations.

Decellularised xenogeneic tissues need to be safe and clinically viable before being implanted into patients. The decellularisation method used within this study was designed to produce biocompatible decellularised porcine pulmonary roots with minimal detrimental impact to the ECM and biomechanical properties of the valves. Previous studies have validated the effectiveness of the decellularisation protocol with and without PAA on porcine and human heart valves, respectively (Desai et al., 2018; Luo et al., 2014; Vafaee et al., 2018). It was shown that DNA levels of porcine PHVs were reduced by more than 96%, with a retention of total collagen levels and minimal distinction between the biomechanical properties of native and decellularised PHVs. These findings were reflected within the current study, as the histoarchitecture of PHV tissue was largely retained, DNA was sufficiently removed, adequate removal of decellularisation agents was demonstrated by good cytocompatibility, and biomechanical properties were not detrimentally impacted following decellularisation.

# Chapter 4 : The Impact of Copper Chloride & Hydrogen Peroxide Sterilisation on the Biological and Biomechanical Properties of Decellularised Heart Valves

## 4.1 Introduction

The use of chemical sterilisation methods for the sterilisation of tissue grafts has been widely explored. Chemical sterilisation methods incorporate the use of chemicals such as oxides and peroxides, alcohols and heavy metals during sterilisation treatment.

Commercially available ethylene oxide treatment has been used to sterilise surgical equipment and tissue grafts, particularly bone matrices, by tissue banks (Kearney et al., 1993). In a study conducted by Kearney et al. (1989), the penetrative potential of ethylene oxide was investigated by exposing *Bacillus subtilis* var *niger* (NCTC 10073) spore strips, sandwiched between dermal tissue sheets, to ethylene oxide for varying time periods. Sterilisation was achieved following 100 minutes of ethylene oxide exposure. The potent microbicidal activity of ethylene oxide is believed to be the result of protein, DNA and RNA alkylation. Alkylation of alkyl groups found within cells prevents the normal cellular metabolism and replication, leading to microbial death. However, there is controversy surrounding the use of ethylene oxide as a sterilisation method for tissue grafts. Following implantation of tissue grafts sterilised with ethylene oxide, an adverse host immune response can be triggered. This was demonstrated in a study conducted by Jackson et al. (1990), where 7 patients that received bone-tendon-bone anterior cruciate ligament replacement sterilised with ethylene oxide developed chronic intraarticular inflammatory reaction. As a result, the impacted patients required explant of the graft. Ethylene chlorohydrin is the breakdown product of ethylene oxide, and it was concluded that the presence of this breakdown product was the trigger of the adverse immune response (Jackson et al., 1990). In addition to inducing an adverse immune response, many studies have shown the potential carcinogenic implications of residual ethylene oxide once the sterilised tissue graft is implanted (Butterworth and Chapman, 2007). Due to this, the use of ethylene oxide amongst tissue banks as a sterilisation agent has become less common.

PAA sterilisation has been used as an alternative across a range of tissue types, including bone and dermis (Huang, Q. et al., 2004; Rauh et al., 2014). In solution, PAA exists in equilibrium with acetic acid and $H_2O_2$. Because of this, PAA has a high oxidative potential which triggers the denaturation of intracellular and membrane-associated proteins, critically disrupting the cell's metabolic activity (Matuska and McFetridge, 2015). Sterilisation with PAA is effective at low temperatures and has a high penetration potential. *In vitro* testing showed that PAA sterilisation of patellar tendon allografts did not induce cytotoxic or inflammatory responses (Lomas et al., 2004). However, the use of PAA on collagenous tissue can result in the loss of type IV collagen found within the basement membrane (Holland, J. D. R. et al., 2021). Additionally, the oxidative function of PAA may be damaging to other ECM components such as GAGs. Hussein et al. (2013) reported a 44 % reduction in GAG content of PAA treated decellularised liver in comparison to untreated decellularised liver.

Hydrogen peroxide ($H_2O_2$) is a potent oxidising agent active against a broad spectrum of microbes. In either liquid or gaseous state, $H_2O_2$ sterilisation is believed to be achieved as a result of oxidative damage to nucleic acids as well as cell membrane components which can cause microbial cell lysis (King and Gould, 1969; Shin et al., 1994). $H_2O_2$ sterilisation is therefore used in a wide range of industries such as medical, food and environment (Leow-Dyke et al., 2016). Gardner et al. (2013) demonstrated that sterilisation of tendon allografts with 3 % $H_2O_2$ did not impact the biomechanical strength of the tissue. During bone allograft processing, some tissue banks incorporate 3 % $H_2O_2$ into the graft wash solutions for 10 minutes with sonication at room temperature to reduce pathogen contamination without adversely impacting the bone mechanical strength and demineralised bone matrix osteoinductivity (Eagle et al., 2015).

The United States Environmental Protection Agency (US EPA) recognised copper as the first solid antimicrobial metal in 2008. This was due to various studies demonstrating the elimination of pathogens following contact with solid copper surfaces. Noyce et al. (2006) demonstrated the antimicrobial effect of copper alloys ranging from 61 – 95 % Cu concentration, on *E.coli* O157 at 22 °C and 4 ° C, with 95 % Cu completely eliminating *E.coli*. It was also demonstrated that copper alloy surfaces ranging from 65 – 100 % Cu concentration significantly reduced the

survival of Clostridium difficile (*C.difficile*) vegetative cells and spores, with a complete elimination after 24 – 48 hours of contact (Weaver et al., 2008). Copper surfaces also have the ability to eliminate viral contamination, and can destroy viruses such as influenza viruses, noroviruses, or human immunodeficiency virus (Vincent et al., 2018). The antimicrobial activity of copper is linked to the solubility of copper oxides along with the oxidative behaviour (Hans et al., 2016; Vincent et al., 2016). Copper ions are believed to cause oxidative damage of membrane phospholipids, which disrupts the membrane integrity. The intracellular accumulation of copper ions resulting from the loss of membrane integrity is believed to cause DNA degradation. The increase in the intrinsic amount of copper can cause oxidative stress which is demonstrated by redox cycling between native Cu, Cu (I) and Cu (II) (Espírito Santo et al., 2008). Under aerobic conditions, copper itself can produce hydroxyl radicals through Haber-Weiss and Fenton chemical reactions (Liochev and Fridovich, 2002). The production and release of reactive oxygen species (ROS) can damage lipids, proteins and nucleic acids, essentially destroying the components, structures and all genetic material required for the survival and expansion of the pathogenic microorganisms (Dalecki et al., 2017). As such, copper has been recognised as a self-sanitising coating, and has been used for high-touch surfaces such as bed rails, overbed tables and IV poles in the hospital environment to tackle healthcare-associated infections (Montero et al., 2019).

To prevent damage to tissue grafts by exposure to the high $H_2O_2$ concentration required for effective sterilisation, $H_2O_2$ can often be supplemented with a metal based formulation. Transition metals such as copper and iron can catalyse the formation of free radicals essential for microbicidal activity (McEvoy and Rowan, 2019). Sagripanti and Kraemer (1989) found that a mixture of low concentration Cu (II) and $H_2O_2$ produced *in vitro* DNA strand breakages, which was inhibited by metal chelators, catalase and free radical scavengers. These results implied that Cu (II), $H_2O_2$ and hydroxyl free radicals were involved in the reaction. The antimicrobial and virucidal activity of cupric and ferric ions have been documented within many experimental studies. Sagripanti et al. (1993) found that cupric and ferric ions inactivated five virus strands from an array of biochemical and structural compositions. The addition of peroxide synergistically enhanced this virucidal activity of cupric ions to a greater extent than ferric ions.

Within the tissue banking and tissue engineering fields, a chemical formulation of copper (II) chloride ($CuCl_2$) and $H_2O_2$ has not yet been routinely included as a tissue sterilising agent. Recent work published by Leow-Dyke et al. explored the suitability of $CuCl_2$ and $H_2O_2$ treatment for the sterilisation of decellularised (dCELL®) human dermal allografts (Leow-Dyke et al., 2016; Leow-Dyke et al., 2017). The dCELL dermis allografts were exposed to concentrations of 0.1 and 1 mg/L $CuCl_2$ combined with 0.01, 0.1, 0.5 and 1 % (v/v) $H_2O_2$. All concentration combinations displayed bactericidal and sporicidal activity against *Staphylococcus epidermidis* (*S.epidermidis)*, *Escherichia coli* (*E.coli)* and *Bacillus subtilis* (*B.subtilis)* spores, with the exception of 0.1 mg/L $CuCl_2$ combined with 0.01 and 0.1 % $H_2O_2$. The composition of the $CuCl_2$ & $H_2O_2$ solutions that exhibited effective biocidal and sporicidal properties used in the study conducted by Leow-Dyke et al. (2016) had no effect on the biocompatibility, biological and biomechanical properties of decellularised human dermis. However, in the study, the pH of the sterilant solutions were not altered to pH 7, and the highest temperature used to sterilise decellularised human dermis with the $CuCl_2$ & $H_2O_2$ solutions was 25 °C. This is because $H_2O_2$ is stable at lower pH levels such as pH 3-5 which were used within their study. Additionally, temperatures above 30 °C may impact the stability of $H_2O_2$, and temperature increase by 10 °C may cause approximately 2.2-fold increase in the rate of degradation (Yazici and Deveci, 2010). Furthermore, the presence of free copper ions particularly at higher $CuCl_2$ concentrations can also induce the degradation of $H_2O_2$, reducing the amount of measurable $H_2O_2$ which was demonstrated within their study (Leow-Dyke et al., 2016).

$CuCl_2$ and $H_2O_2$ as a potential tissue sterilising agent has not yet been applied to decellularised porcine pulmonary heart valves as this treatment is relatively unexplored within the literature. Preliminary studies (unpublished) conducted within University of Leeds Institute of Medical and Biological Engineering demonstrated that acidic solutions of $CuCl_2$ and $H_2O_2$ detrimentally impacted dPHV leaflet histoarchitecture. Dermis is composed of two layers; the papillary dermis and the reticular dermis. Although the papillary dermis is composed of highly vascular loose connective tissue, the reticular layer is composed of thick and dense connective tissue that was able to withstand the acidic conditions used by Leow-Dyke et al. (2016). Adjusting the pH of the solution may produce a less harsh condition for the complex and intricate multilayer fibrous structures within heart

valve leaflets. Leow-Dyke et al. (2017) found that bactericidal activity of $CuCl_2$ and $H_2O_2$ sterilants on inoculated dCELL dermis was temperature dependent, whereby the bactericidal activity was accelerated at 37 °C in comparison to 25 °C. Using 37 °C as the tissue-sterilant exposure temperature may therefore aid sterilisation. An optimised $CuCl_2$ and $H_2O_2$ formulation that exerts microbicidal effects on bioburden without adversely impacting decellularised porcine pulmonary heart valves tissue histoarchitecture is not yet known. Additionally, the stability and sporicidal activity of the $CuCl_2$ and $H_2O_2$ solutions when adjusted to pH 7 at 37 °C has not yet been elucidated.

## 4.2 Aims and Objectives

### 4.2.1 Aim

The aim of the study described in this chapter was to characterise the effects of a $CuCl_2$ & $H_2O_2$ formulation on the biological and biomechanical properties of decellularised porcine pulmonary heart valves (Luo et al., 2014)

### 4.2.2 Objectives

i. To determine an optimised $CuCl_2$ and $H_2O_2$ formulation using the following preliminary experiments:

   - Solution stability analysis of the formulations selected based on the study conducted by Leow-Dyke et al. (2016)
   - Sporicidal activity assessment of the selected formulations using *B.subtilis* spores
   - Sporicidal activity assessment of the selected formulations on *B.subtilis* spiked dPHV segments
   - Impact of $CuCl_2$ & $H_2O_2$ formulations on the histoarchitecture of dPHV segments using histological staining

ii. To produce decellularised porcine pulmonary heart valves and expose them to the selected $CuCl_2$ & $H_2O_2$ formulation under the optimal time conditions

iii. To determine the impact of $CuCl_2$ & $H_2O_2$ treatment on the structure of collagen, elastin and specific basement membrane proteins (collagen IV and fibronectin) within decellularised porcine pulmonary heart valves, using histological staining and immunohistochemistry antibody labelling

iv. To determine the impact of $CuCl_2$ & $H_2O_2$ treatment on the surface structure of decellularised porcine pulmonary heart valve leaflets and pulmonary artery using scanning electron microscopy

v. To determine the impact of $CuCl_2$ & $H_2O_2$ treatment on the biochemical composition of decellularised porcine pulmonary heart valves, through quantification of collagen and glycosaminoglycans

vi. To determine the impact of $CuCl_2$ & $H_2O_2$ treatment on the denaturation temperature of the collagen within decellularised porcine pulmonary heart valve ECM, using differential scanning calorimetry

vii. To determine the *in vitro* biocompatibility of $CuCl_2$ & $H_2O_2$ treated decellularised porcine pulmonary heart valves using contact and extract cytotoxicity assays

viii. To determine the impact of $CuCl_2$ & $H_2O_2$ treatment on the mechanical properties of decellularised porcine pulmonary heart valves, using uniaxial tensile testing

## 4.3 Study Experimental Approach

Based on the results reported by Leow-Dyke et al. (2016), four $CuCl_2$ & $H_2O_2$ formulations were chosen for investigation within this study, as shown in the schematic within Figure 4.1. Preliminary experiments were performed to select an optimised formulation of $CuCl_2$ & $H_2O_2$ and to determine a sufficient exposure time for dPHV sterilisation (Figure 4.1). Once a $CuCl_2$ and $H_2O_2$ formulation had been selected and the exposure time for effective sterilisation had been determined, dPHVs were exposed to $CuCl_2$ & $H_2O_2$ sterilisation before biological and biomechanical characterisation, as described in Figure 4.2.

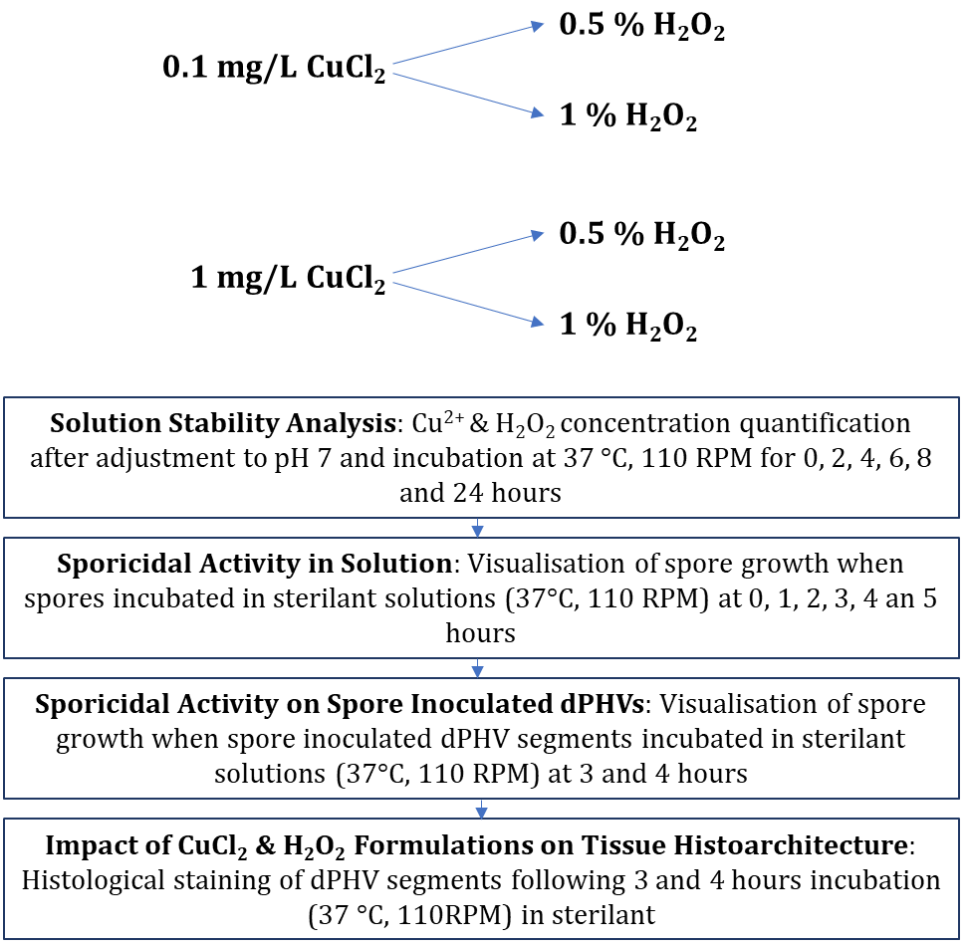


**Figure 4.1 Schematic of the Preliminary Experiments Used to Select an Optimised $CuCl_2$ & $H_2O_2$ Formulation and Sterilisation Time Conditions.**

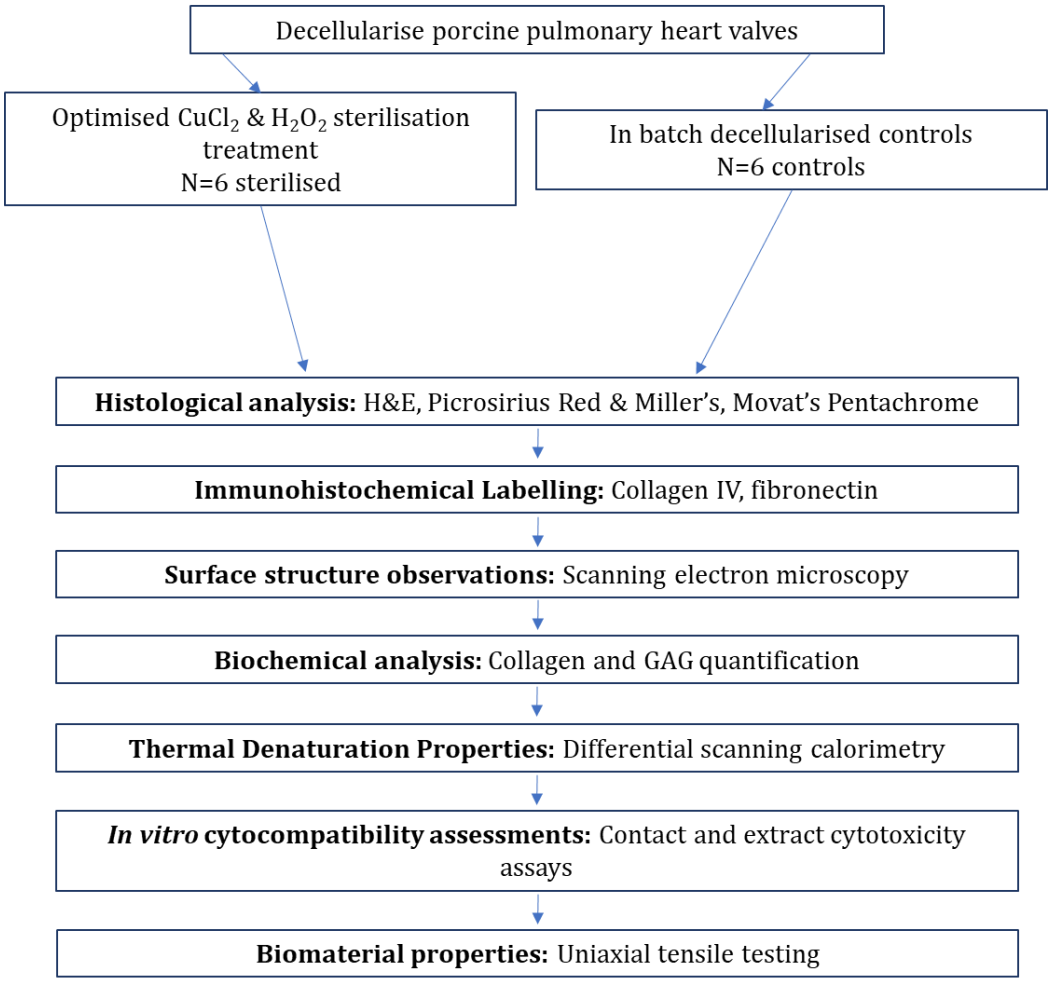


**Figure 4.2 Schematic of the Experimental Approach Adopted to Characterise the Impact of $CuCl_2$ & $H_2O_2$ Sterilisation on the Biological and Biomechanical Properties of Decellularised Porcine Pulmonary Heart Valves.**

## 4.4 Methods

### 4.4.1 Preliminary Experiments

Preliminary experiments were performed to determine the optimal $CuCl_2$ and $H_2O_2$ concentration combination for the effective sterilisation of dPHVs without adversely affecting the tissue histoarchitecture, prior to exposing a full batch of dPHVs to the chosen $CuCl_2$ and $H_2O_2$ concentration sterilisation for biological and biomechanical analysis. Based on a study conducted by Leow-Dyke et al. (2016), four concentration combinations that demonstrated good bactericidal and sporicidal activity, and minimal impact on dCELL human dermis biological and biomechanical properties, were chosen for analysis. The concentration combinations were; 0.1 mg/L $CuCl_2$ combined with 0.5 % $H_2O_2$, 0.1 mg/L $CuCl_2$ combined with 1 % $H_2O_2$, 1 mg/L $CuCl_2$ combined with 0.5 % $H_2O_2$, and 1 mg/L $CuCl_2$ combined with 1 % $H_2O_2$.

#### 4.4.1.1 Copper Chloride and Hydrogen Peroxide Solution Preparation

Solutions containing a combination of 0.1 and 1 mg/L $CuCl_2$ with 0.5 and 1 % $H_2O_2$ were made using 100 mg/L (w/v) stock of $CuCl_2$ and 30 % (v/v) stock $H_2O_2$ diluted to appropriate concentrations in distilled water. The pH of all solutions was adjusted to pH 7 ± 0.1 (section 2.2.1.1).

#### 4.4.1.2 Stability of Copper Chloride and Hydrogen Peroxide Solutions

Stability testing of copper chloride and hydrogen peroxide combination solutions was performed to establish if pH and temperature adjustment impacts degradation over 24 hours.

Solutions were prepared (N=6 per concentration combination) as described in 4.4.1.1, and the pH was noted immediately (0 hours). Promptly after all the solutions were made, the concentrations of $Cu^{2+}$ ions and $H_2O_2$ were determined (0 hours). The solutions were then placed into a 37 °C incubator and agitated at 110 RPM, (the intended conditions for dPHV sterilisation). At 2, 4, 6, 8 and 24 hours following this incubation of the solutions, $Cu^{2+}$ ions and $H_2O_2$ concentrations were

determined using their respective assay methods. The pH of all solutions was also measured at each timepoint.

#### 4.4.1.2.1 Quantification of $Cu^{2+}$ Concentration

$Cu^{2+}$ Concentration was quantified using Spectroquant® Copper Reagent Test (Merk Millipore), a photometric assay that quantifies $Cu^{2+}$ ions based on the reaction with cuprizone to form a blue complex. The assay was performed according to the manufacturer's instructions. Briefly, a range of standards of known $CuCl_2$ concentrations (0, 0.2, 0.4, 0.6, 0.8, 1, 2, 3, 4 mg/L) were made by diluting 100 mg/L (w/v) $CuCl_2$ in distilled water. Test samples (diluted as appropriate in distilled water) and standards (5 mL) were first placed into universal tubes in triplicate. Two scoops of solid reagent Cu-1 was added to the test samples and standards using a dosing spoon provided with the kit. The universal tubes were then mixed vigorously until the reagent Cu-1 had dissolved. Following this, 10 drops of liquid reagent Cu-2 was added to the universal tubes which were then vigorously mixed. The test samples and standard solutions were then left to stand for 5 minutes, before 4 mL of the solution was inserted into a 10 mm cuvette. The absorbance of the sample was measured at 605 nm using a spectrophotometer. A $CuCl_2$ standard curve was created showing absorbance vs concentration. The unknown test values were interpolated and normalised for dilution volumes if appropriate to determine the test sample solution $Cu^{2+}$ concentration.

Shapiro-Wilk test was used to determine the distribution of data. If the data was normally distributed, One-way ANOVA with Dunnett's post-hoc testing was used to compare the means at each timepoint against 0h. If the data was not normally distributed, Kruskal-Wallis and Dunn's multiple comparison test was used to compare the means at each timepoint against 0h.

#### 4.4.1.2.2 Quantification of $H_2O_2$ Concentration

$H_2O_2$ concentrations were measured photometrically using the Pierce™ Quantitative Peroxide Assay Kit (Thermo Fisher). Peroxides oxidise ferrous ions to

ferric ions in the presence of xylenol orange dye, producing a purple product with an absorbance at 595 nm.

Method:

A range of standards of known $H_2O_2$ concentrations (0, 10, 20, 30, 40, 50, 60, 70, 80, 90, 100 µmol/L) were made by diluting 30 % (v/v) $H_2O_2$ in distilled water. In a 96-well plate, 20 µl of test samples and standards were added to each well in triplicate, followed by 200 µl of working reagent (Pierce™ Quantitative Peroxide Assay Kit, Thermo Fisher) per sample and standard. The plate was gently agitated to mix the contents of the wells, and then incubated for 15-20 minutes at room temperature. The optical densities of each well were then measured using a microplate spectrophotometer at a wavelength of 595 nm. A $H_2O_2$ standard curve was created showing absorbance vs concentration. The unknown test values were interpolated and normalised for dilution volume if appropriate to determine the test sample solution $H_2O_2$ concentration.

Shapiro-Wilk test was used to determine the distribution of data. If the data was normally distributed, One-way ANOVA with Dunnett's post-hoc testing was used to compare the means at each timepoint against 0h. If the data was not normally distributed, Kruskal-Wallis and Dunn's multiple comparison test was used to compare the means at each timepoint against 0h.

#### 4.4.1.3 Impact of $CuCl_2$ & $H_2O_2$ Solutions on Spore Viability

The sporicidal activity of the $CuCl_2$ & $H_2O_2$ combination solutions at 37 °C was determined.

$CuCl_2$ & $H_2O_2$ solutions (0.1 and 1 mg/L (w/v) $CuCl_2$ combined with 0.5 % and 1 % (v/v) $H_2O_2$) were prepared in distilled water in triplicates and passed through a 0.22 µm filter into 10 mL vials. Under aseptic conditions using a Bunsen flame, *Bacillus subtilis* spores were added to the 10 mL solution vials to achieve an approximate spore concentration of $10^7$/mL. Immediately after vortexing (timepoint 0 hours), 1 mL neat samples from each of the four $CuCl_2$ and $H_2O_2$ combination solutions was added to 9 mL nutrient broth vials before being placed into a 37 °C incubator with agitation at 110 RPM. The nutrient broth containing the sterilant and spores was then vortexed, and 200 µL was taken and spread onto a

nutrient agar plate. To ensure there was no carry over of $CuCl_2$ and $H_2O_2$ onto the plates, more *B.subtilis* spores (approximately $10^7$/mL) were added to the nutrient broth containing the sterilant and spores, which was then spread onto a nutrient agar plate as a positive control. This was repeated at timepoints 1, 2, 3, 4, and 5 hours of sterilant and spore incubation and agitation (37 °C, 110 RPM). All plates were incubated at 37 °C for 48 hours prior to capturing images of the plates using UV Products BioSpectrum 810 with Mega Cam 810 for observatory analysis.

#### 4.4.1.4 Impact of $CuCl_2$ & $H_2O_2$ Solutions on Spore Viability of Spore Inoculated Tissue

The sporicidal activity of $CuCl_2$ & $H_2O_2$ solutions on spore inoculated dPHV tissue segments was determined to ensure $CuCl_2$ & $H_2O_2$ functions on tissue substrates. First, whole dPHV roots were prepared (N=6) as described in section 2.2.3. The dPHVs were divided into three segments (Figure 4.3). *B. subtilis* spores (approximately $10^6$/mL) were deposited into the pulmonary sinus of each dPHV tissue segment (approximately 1 $cm^2$). The tissue segments were then incubated at room temperature for 1 hour. Based on the results from section 4.4.1.3, each inoculated tissue segment was then added to 67 mL of 0.22 µm filter sterilised 0.1 mg/L $CuCl_2$ & 1 % $H_2O_2$, 1 mg/L $CuCl_2$ & 1 % $H_2O_2$, or distilled water (control), in a sterile 150 mL pot (N=6 per treatment). The 67 mL volume for each dPHV segment represented one-third of the volume that a whole dPHV would be exposed to. Inoculated dPHV segments were incubated at 37 °C with agitation of 110 RPM for 3 and 4 hours (N=3 per treatment at each timepoint). At the 3 and 4 hour timepoints, the dPHV tissue segments were removed from the $CuCl_2$ & $H_2O_2$ sterilants or sterile distilled water, macerated and incubated in 10 mL of nutrient broth at 37 °C with agitation of 220 RPM for 1 hour. Following incubation, 200 µL of the nutrient broth was spread onto nutrient agar plates and incubated at 37 °C for 48 hours prior to capturing images of the plates using UV Products BioSpectrum 810 with Mega Cam 810 for colony count analysis.

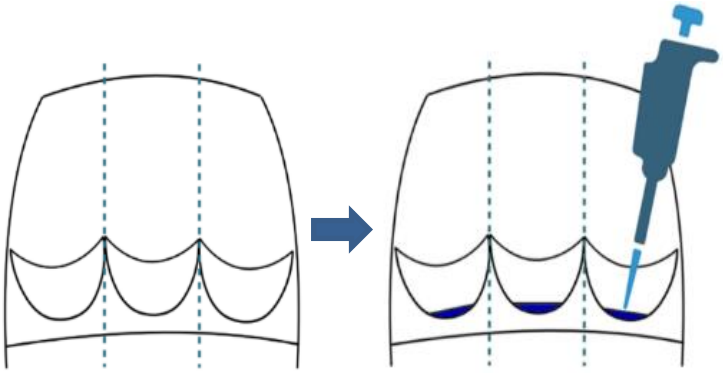

**Figure 4.3 Schematic of dPHV Inoculation with Spores.** Blue region demonstrates the position of spores inside the leaflet at the pulmonary sinus.

#### 4.4.1.5 Impact of $CuCl_2$ & $H_2O_2$ Solutions on dPHV Tissue Histoarchitecture

Based on the results from sections 4.4.1.3 and 4.4.1.4, the impact of 0.1 and 1 mg/L $CuCl_2$ combined with 1 % $H_2O_2$ over 3 and 4 hours on the histoarchitecture of dPHV tissue was determined.

dPHVs were prepared, as described in section 2.2.3. The dPHVs were divided into three segments (Figure 4.3). The segments from each dPHV were exposed to either 0.1 mg/L $CuCl_2$ & 1 % $H_2O_2$ or 1 mg/L $CuCl_2$ & 1 % $H_2O_2$ for 3 or 4 hours, or sterile distilled water (negative control) (N=3 per treatment at each timepoint). Each segment was placed into a sterile 150 mL pot along with the sterilant solution or sterile distilled water. Samples were then incubated at 37 °C whilst agitated horizontally at 110 RPM. At 3 and 4 hours, samples were removed from the sterilant or sterile distilled water and rinsed with PBS at 42 °C, 110 RPM, for 3 x 30 minutes. Sections were then processed, sectioned and stained with H & E and Picrosirius Red & Miller's Elastin stain, as described in sections 2.2.5.1 and 2.2.5.2.

### 4.4.2 Production of Decellularised Porcine Pulmonary Heart Valves

As described in section 2.2.3, porcine pulmonary heart valves were acquired and exposed to a decellularisation process modified from Luo et al. (2014) (Table 2.3, section 2.2.3).

### 4.4.3 $CuCl_2$ & $H_2O_2$ Sterilisation

Immediately following exposure to the last wash step of the decellularisation protocol (section 3.4.1), 200 mL of 1mg/L $CuCl_2$ & 1 % $H_2O_2$ (section 4.4.1.1) was added into each sterile 250 mL pot containing the dPHV root (N=6) prior to incubating horizontally at 37 °C, 110 RPM for 3 hours. The dPHVs were then rinsed with 200 mL PBS at 37 °C, 110 RPM for 3 x 30 minutes. The dPHVs were transferred into fresh sterile 150 mL pots with 100 mL PBS and stored at 4 °C up to 2 weeks prior to biological and biomechanical analysis. Controls used in the experiments were dPHV roots (N=6) that were exposed to all the wash steps, but with PBS used instead of 1mg/L $CuCl_2$ & 1 % $H_2O_2$ during the $CuCl_2$ & $H_2O_2$ sterilisation step.

### 4.4.4 Histological Analysis

To assess the impact of 1 mg/L $CuCl_2$ & 1 % $H_2O_2$ sterilisation on the histoarchitecture of dPHVs, Control dPHV roots, 1 mg/L $CuCl_2$ & 1 % $H_2O_2$ roots were dissected longitudinally, incorporating half a leaflet, pulmonary artery wall and myocardium skirt (N=3 each). These tissue samples were then processed and sectioned as described in section 2.2.4. Staining of sections with H & E, Picrosirius Red & Miller's Elastin, and Movat's Pentachrome was conducted as described in sections 2.2.5.1, 2.2.5.2, and 2.2.5.3.

### 4.4.5 Immunohistochemical Labelling of Collagen IV and Fibronectin

To assess the impact of 1 mg/L $CuCl_2$ & 1 % $H_2O_2$ sterilisation on the preservation of collagen IV and fibronectin in dPHVs, Control dPHV roots and 1 mg/L $CuCl_2$ & 1 % $H_2O_2$ roots were dissected longitudinally, incorporating half a leaflet, pulmonary artery wall and myocardium skirt (N=3 each). Processing and sectioning of tissue was conducted as described in section 2.2.4. Labelling of sections with specific antibodies against collagen IV and fibronectin was conducted as described in section 2.2.6.

### 4.4.6 Visualisation of Tissue Surface Microscopic Structure

Scanning electron Microscopy (SEM) was used to visualise the impact of 1 mg/L $CuCl_2$ & 1 % $H_2O_2$ sterilisation on dPHV pulmonary artery wall and leaflet surface microscopic structures (N=3 each), as described in section 2.2.1.2.4.

### 4.4.7 Quantification of Collagen Content

Pulmonary artery wall (N=6 per group) and leaflet (N=6 per group) collagen content for dPHV control and 1 mg/L $CuCl_2$ & 1 % $H_2O_2$ dPHVs was quantified as described in section 2.2.8.3.

### 4.4.8 Quantification of GAG Content

Pulmonary artery wall (N=6 per group) and leaflet (N=6 per group) GAG content for dPHV control, and 1 mg/L $CuCl_2$ & 1 % $H_2O_2$ dPHVs was quantified as described in section 2.2.8.4.

### 4.4.9 DSC Analysis

The collagen denaturation temperature of dPHV control and 1 mg/L $CuCl_2$ & 1 % $H_2O_2$ pulmonary artery wall (N=6 per group) and leaflet (N=6 per group) samples was determined using DSC, as described in section 2.2.7.

### 4.4.10 *In Vitro* Cytocompatibility Assessments

The *in vitro* cytocompatibility of 1 mg/L $CuCl_2$ & 1 % $H_2O_2$ pulmonary artery wall and leaflet samples was assessed using contact cytotoxicity (N=3) as described in Section 2.2.10.1 and extract cytotoxicity assays (N=6), as described in Section 2.2.10.2.

### 4.4.11 Uniaxial Tensile Testing

The DPHV control and 1 mg/L $CuCl_2$ & 1 % $H_2O_2$ pulmonary artery wall and leaflet samples were subject to uniaxial tensile testing, as described in Section 2.2.12.

## 4.5 Results

### 4.5.1 Preliminary Experiments

#### 4.5.1.1 Stability of Copper Chloride and Hydrogen Peroxide Solutions

Solutions of 0.1 mg/L $CuCl_2$ were below the lower sensitivity threshold of the $Cu^{2+}$ quantification assay (section 4.4.1.2.1), so the copper ion concentration stability in 0.1 mg/L $CuCl_2$ & 0.5 % $H_2O_2$ and 0.1 mg/L $CuCl_2$ & 1 % $H_2O_2$ was not tested.

Fluctuations in the $Cu^{2+}$ concentration of solutions containing 1 mg/L $CuCl_2$ were observed over the timepoints when combined with both 0.5 % $H_2O_2$ and 1 % $H_2O_2$ (Figure 4.4 A) . However, the fluctuations observed were not statistically significant from 0 hours, apart from a significant decrease in $CuCl_2$ concentration at 2 and 8 hours in solutions containing 1 mg/L $CuCl_2$ and 1 % $H_2O_2$. Fluctuations in the pH of 1 mg/L $CuCl_2$ solutions combined with 0.5 % and 1 % $H_2O_2$ were also observed. The pH of solutions containing 1 mg/L $CuCl_2$ solutions combined with 0.5 % $H_2O_2$ demonstrated an upward trend in pH, with a significant increase in the pH being observed at 24 hours in comparison to 0 hours. The pH of solutions containing 1 mg/L $CuCl_2$ solutions combined with 1 % $H_2O_2$ generally displayed a downward trend in pH with increasing time, however there were no significant differences from the pH at timepoint 0 hours (Figure 4.4 B).

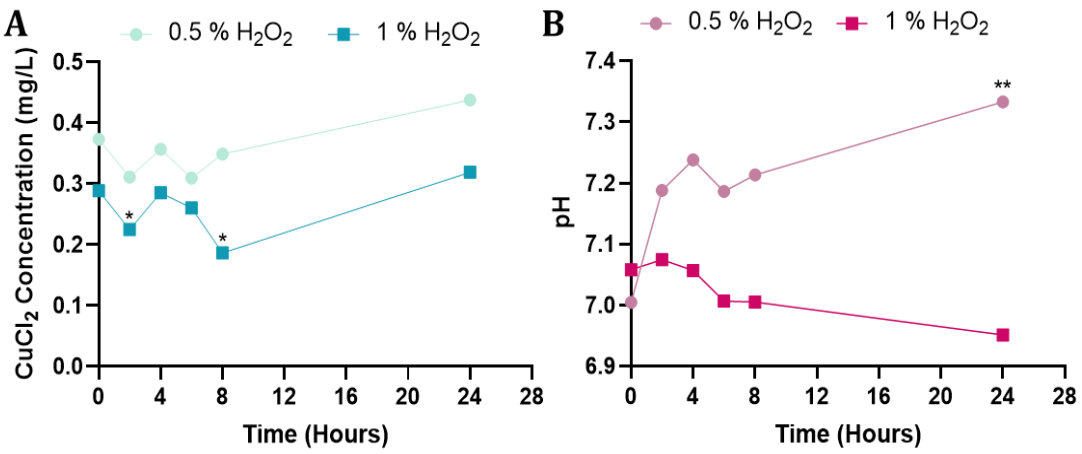


**Figure 4.4 $CuCl_2$ Concentration (A) and pH (B) of 1 mg/L $CuCl_2$ Solutions When Combined with 0.5 % and 1 % $H_2O_2$ Over 24 Hours.** Statistical analysis for all was by One-way ANOVA with Dunnett's post hoc-test against 0h. Data presented as mean, N=6. *($p<0.05$) and ** ($p<0.01$) denotes significant difference between the groups.

Over all timepoints, 0.5 % and 1 % $H_2O_2$ concentrations displayed a downward trend when combined with 0.1 mg/L $CuCl_2$ and 1 mg/L $CuCl_2$ (Figure 4.5 A, B). The $H_2O_2$ concentration of solutions containing 0.5 % $H_2O_2$ and 0.1 mg/L $CuCl_2$ was significantly lower at 6, 8, and 24 hours in comparison to 0 hours (Figure 4.5 A). The reduction in $H_2O_2$ concentration in solutions containing 0.5 % $H_2O_2$ and 1 mg/L $CuCl_2$ was only significant at 24 hours in comparison to 0 hours. Although solutions containing 1 % $H_2O_2$ combined with 0.1 mg/L $CuCl_2$ displayed a trend in the reduction of $H_2O_2$ concentration, this was not significant at any in comparison to 0 hours (Figure 4.5 B). Solutions containing 1 % $H_2O_2$ and 1 mg/L $CuCl_2$ had a significant reduction in $H_2O_2$ concentration at 8 and 24 hours in comparison to 0 hours (Figure 4.5 B).

The pH of the solutions displayed fluctuations with no obvious trends (Figure 4.5 C, D). There were no significant differences in the pH of solutions containing 0.5 % $H_2O_2$ and 0.1 mg/L $CuCl_2$ in comparison to 0 hours. Solutions containing 0.5 % $H_2O_2$ and 1 mg/L $CuCl_2$ demonstrated a significant increase in the pH at 2, 4, 6, 8, and 24 hours in comparison to 0 hours (Figure 4.5 C). There was a significant increase in the pH of solutions containing 1 % $H_2O_2$ and 0.1 mg/L $CuCl_2$ at 2, 4, 8 and 24 hours in comparison to 0 hours (Figure 4.5 D). There was a significant reduction in the pH of solutions containing 1 % $H_2O_2$ and 1 mg/L $CuCl_2$ at 2 hours, and then a significant increase in the pH at 24 hours in comparison to 0 hours (Figure 4.5 D).

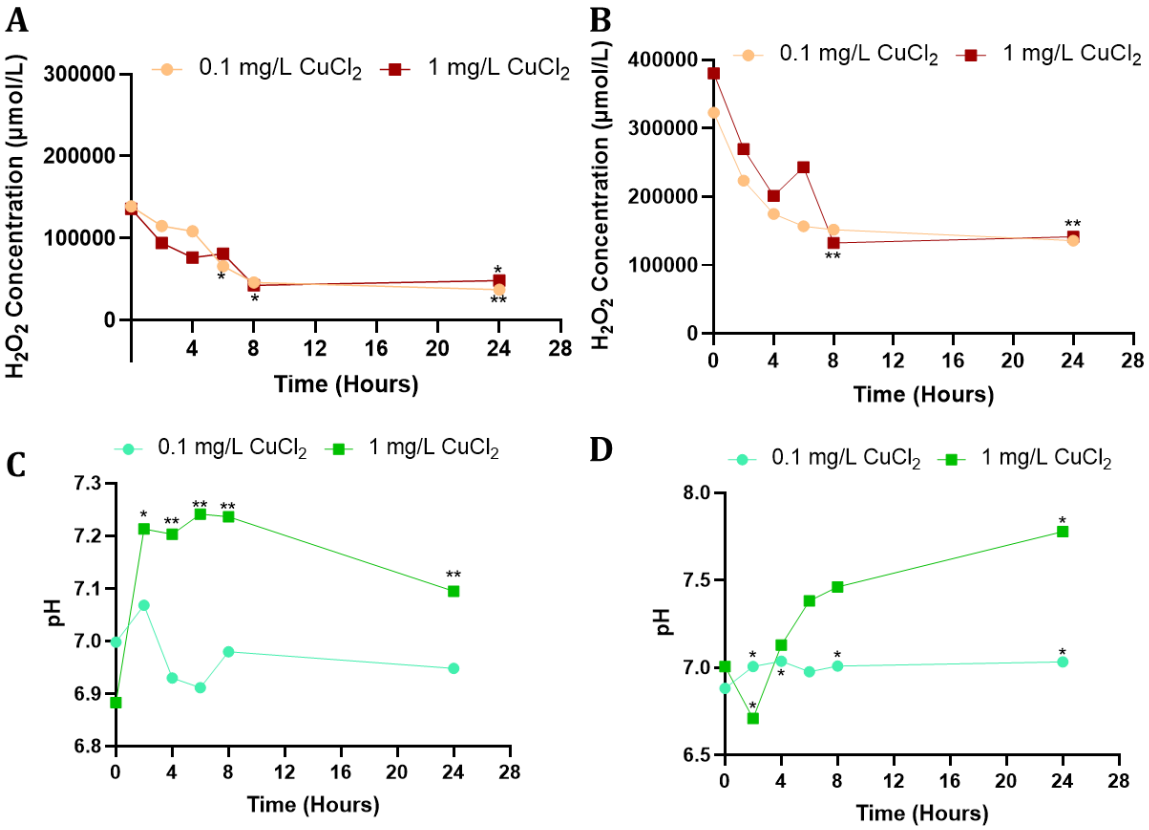


**Figure 4.5 $H_2O_2$ Concentration and pH of 0.5 % (A, C) and 1 % (B, D) $H_2O_2$ Solutions When Combined with 0.1 and 1 mg/L $CuCl_2$ Over 24 Hours.** Statistical analysis for all was by One-way ANOVA with Dunnett's post hoc-test against 0h, except for the comparison of 0.5 % $H_2O_2$ concentration with 1mg/L $CuCl_2$ (A) which used Kruskal-Wallis test with Dunn's multiple comparison test against 0h. Data presented as mean, N=6. *($p<0.05$) and ** ($p<0.01$) denotes significant difference between the groups.

### 4.5.1.2 Impact of $CuCl_2$ & $H_2O_2$ Solutions on Spore Viability

The susceptibility of *Bacillus subtilis* spores to 0.1 and 1 mg/L (w/v) $CuCl_2$ combined with 0.5 % and 1 % (v/v) $H_2O_2$ at 37 °C, 110 RPM was determined up to 5 hours (Figure 4.6). This timeframe was selected based on findings by Leow-Dyke et al. (2017) who found that 4 hours of treatment at 37 °C with 0.1 mg/L (w/v) $CuCl_2$ combined with 1 % (v/v) $H_2O_2$ was sufficient for inactivation of spores inoculated on to dCELL dermis samples.

At 0 hours, lawns of *B. subtilis* spores were observed for all sterilants where individual spores could not be distinguished. Following incubation with spores at 1 hour, 0.1 mg/L $CuCl_2$ & 0.5 % $H_2O_2$ still displayed a lawn of spores with the plating streaks becoming visible. When incubated with 0.1 mg/L $CuCl_2$ & 1 % $H_2O_2$,

individual spores were distinguished. However, the spores did still grow abundantly.

After 1 hour of incubation with 1 mg/L $CuCl_2$ & 0.5 % $H_2O_2$, similar results were displayed to those demonstrated with 0.1 mg/L $CuCl_2$ & 0.5 % $H_2O_2$ where individual spores could not be distinguished. The appearance of spore growth following 1 hour of incubation with 1 mg/L $CuCl_2$ & 1 % $H_2O_2$ appeared less in comparison to the other sterilants investigated, with sparse areas of spore colonies being observed in some areas.

Following 2 hours of incubation, 0.1 mg/L $CuCl_2$ and 1 mg/L $CuCl_2$ combined with 1 % $H_2O_2$ displayed the most efficient sporicidal activity, with no spores being observed following incubation with 1 mg/L $CuCl_2$ & 1 % $H_2O_2$ and few colonies being observed when incubated with 0.1 mg/L $CuCl_2$ & 1 % $H_2O_2$. A lawn of spores still appeared after incubation with 0.1 mg/L $CuCl_2$ % 0.5 % $H_2O_2$, although colonies did start to become distinguishable. The growth of spores remained abundant following incubation with 0.1 mg/L $CuCl_2$ & 5 % $H_2O_2$ for 2 hours.

Following 3 hours of incubation, 0.1 mg/L $CuCl_2$ and 1 mg/L $CuCl_2$ combined with 1 % $H_2O_2$ eliminated all spores, demonstrated by the lack of spore growth. Spores were still present following incubation with 0.1 mg/L $CuCl_2$ and 1 mg/L $CuCl_2$ combined with 0.5 % $H_2O_2$, with spore growth being less abundant after incubation with 1 mg/L $CuCl_2$ & 0.5 % $H_2O_2$ in comparison to 0.1 mg/L $CuCl_2$ & 0.5 % $H_2O_2$.

At 4 hours of incubation, 0.1 mg/L $CuCl_2$ & 1 % $H_2O_2$, 1mg/L $CuCl_2$ & 0.5 % $H_2O_2$, 1mg/L $CuCl_2$ & 1 % $H_2O_2$ eliminated the presence of spores. Spores were still sparsely present following incubation with 0.1 mg/L $CuCl_2$ & 0.5 % $H_2O_2$. No spore growth was observed after 5 hours incubation with all four sterilants.

Positive control plates of all four sterilants that were inoculated with more *B.subtilis* spores demonstrated a lawn of spore growth at each timepoint.

Based on these results, 0.1 mg/L $CuCl_2$ & 0.5 % $H_2O_2$ and 1mg/L $CuCl_2$ & 0.5 % $H_2O_2$ sterilants were eliminated from further investigation. Sterilants of 0.1 mg/L $CuCl_2$ & 1 % $H_2O_2$ and 1 mg/L $CuCl_2$ & 1 % $H_2O_2$ were further investigated at timepoints 3 and 4 hours for time exposure optimisation of inoculated dPHV tissue.

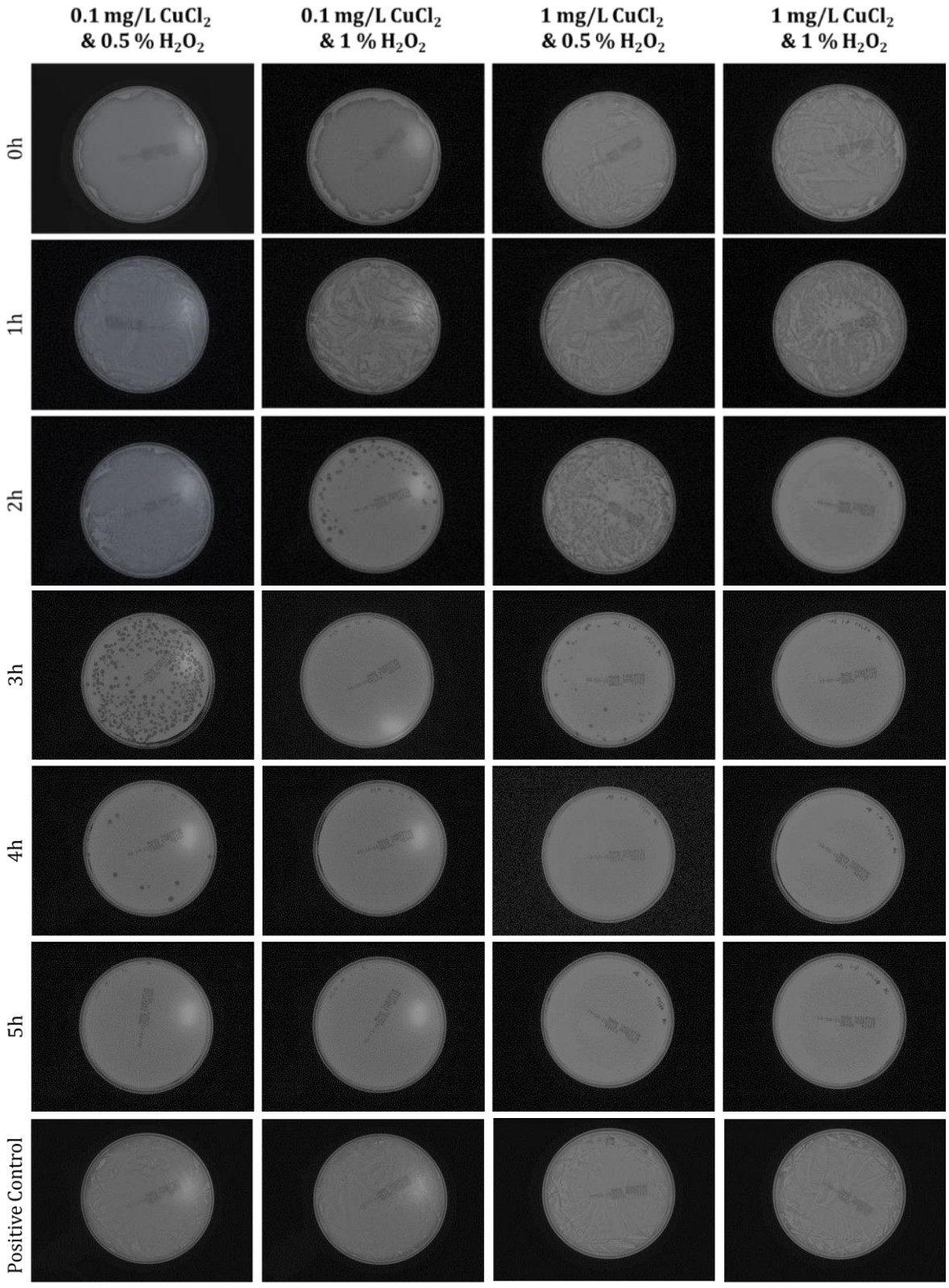


**Figure 4.6 Growth of *B.subtilis* Spores Exposed to 0.1 mg/L $CuCl_2$ & 0.5 % $H_2O_2$, 0.1 mg/L $CuCl_2$ & 1 % $H_2O_2$, 1 mg/L $CuCl_2$ & 0.5 % $H_2O_2$, and 1 mg/L $CuCl_2$ & 1 % $H_2O_2$ Over 5 hours.** Representative images from n=3 shown.

#### 4.5.1.3 Impact of $CuCl_2$ & $H_2O_2$ Solutions on Spore Viability of Spore Inoculated Tissue

The susceptibility of *Bacillus subtilis* spores, inoculated onto dPHV tissue, to 0.1 and 1 mg/L (w/v) $CuCl_2$ combined with 1 % (v/v) $H_2O_2$ at 37 °C, 110 RPM was determined over 3 and 4 hours.

As shown in Figure 4.7, both 1 mg/L (w/v) $CuCl_2$ combined with 1 % (v/v) $H_2O_2$ decontaminated the spore inoculated dPHV tissue segments 37 °C, 110 RPM at both 3 and 4 hours. This was demonstrated by the absence of spore growth. In contrast, inoculated tissue segments that were incubated in sterile distilled water displayed spore growth.

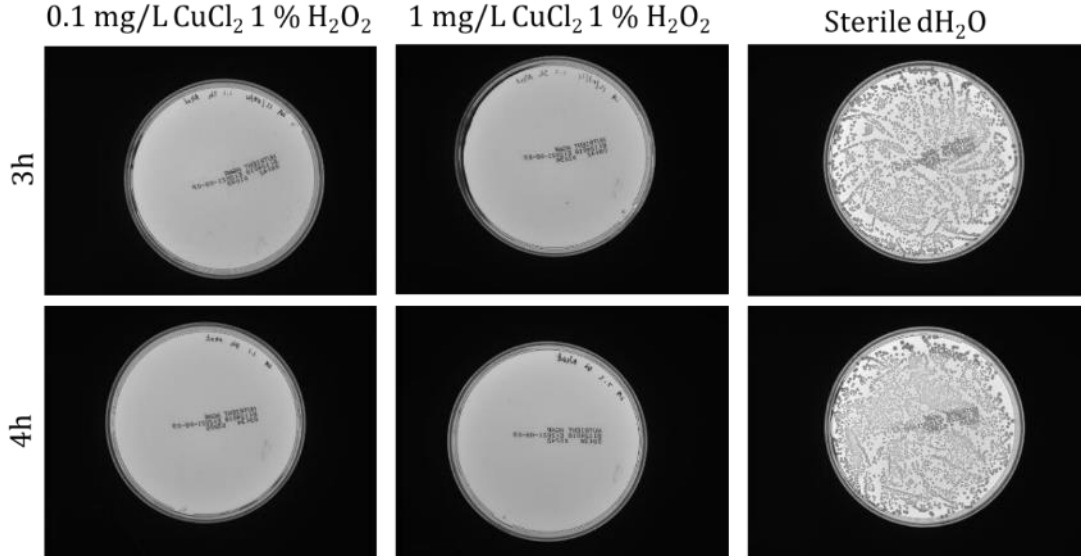


**Figure 4.7 Growth of *B.subtilis* Spores on Inoculated dPHV Segments Exposed to 0.1 mg/L $CuCl_2$ & 1 % $H_2O_2$, 1 mg/L $CuCl_2$ & 1 % $H_2O_2$ and Sterile $dH_2O$ Over 3 and 4 hours**. Representative images from n=3 shown.

#### 4.5.1.4 Impact of $CuCl_2$ & $H_2O_2$ Solutions on dPHV Tissue Histoarchitecture

Based on the results from sections 4.5.1.2 and 4.5.1.3, the impact of 0.1 and 1 mg/L $CuCl_2$ combined with 1 % $H_2O_2$ over 3 and 4 hours on the histoarchitecture of dPHV tissue was determined. This step was used to select suitable sterilisation time conditions that do not adversely impact tissue histoarchitecture.

H & E staining was used to observe the gross histoarchitecture of the tissue sections. In comparison to dPHV untreated controls, 0.1 mg/L $CuCl_2$ & 1 % $H_2O_2$ (Figure 4.8), and 1mg/L $CuCl_2$ & 1 % $H_2O_2$ (Figure 4.9) did not induce any obvious detrimental impact to the dPHV artery tissue after 3 and 4 hours exposure. The

tightly crimped ECM fibres of the treated dPHV artery intima sections appeared well preserved after 3 and 4 hours of exposure in comparison to dPHV controls. The loose ECM structure characteristic of the artery adventitia was also preserved. The *arterialis*, *fibrosa*, *spongiosa*, and *ventricularis* layers of the leaflet remained well defined after 3 hours of sterilant exposure. However, the staining of the 0.1 mg/L $CuCl_2$ & 1 % $H_2O_2$ treated *arterialis, fibrosa and ventricularis* layers appeared less intense following 4 hours of exposure. Treatment with 0.1 mg/L $CuCl_2$ & 1 % $H_2O_2$ also resulted in the appearance of loose fibres at the leaflet *arterialis* following 4 hours of exposure (Shown by black arrow on Figure 4.8 I). The regularly arranged myocardium bundles remained unaltered between the dPHV controls and dPHV tissue exposed to 0.1 mg/L $CuCl_2$ & 1 % $H_2O_2$ and 1 mg/L $CuCl_2$ & 1 % $H_2O_2$ for 3 and 4 hours.

Picrosirius Red & Miller's Elastin staining was used to investigate the impact of the sterilants and exposure times on the composition of collagen and elastin fibres of the dPHV tissue sections. Similar results were observed to those found from H & E staining. There were no obvious changes to the collagen and elastin fibre composition of the artery intima, artery adventitia, and myocardium of dPHV segments treated with 0.1 mg/L $CuCl_2$ & 1 % $H_2O_2$ (Figure 4.10, Figure 4.12) and 1 mg/L $CuCl_2$ & 1 % $H_2O_2$ (Figure 4.11, Figure 4.13) for 3 and 4 hours in comparison to the untreated dPHV controls. Leaflets treated with 0.1 mg/L $CuCl_2$ & 1 % $H_2O_2$ and 1 mg/L $CuCl_2$ & 1 % $H_2O_2$ for 3 hours also resembled the dPHV control leaflets. However, both of the sterilants induced alterations to the leaflet structure following 4 hours of exposure. The *arterialis* layer of leaflets treated with 0.1 mg/L $CuCl_2$ & 1 % $H_2O_2$ for 4 hours displayed loose elastin fibres which was shown with bright field imaging (Shown by black arrow on Figure 4.10 I). Although, imaging under polarised light did not reveal any obvious differences, suggesting that the collagen content remained largely unaltered (Figure 4.12 I). The *ventricularis* layer of leaflets exposed to 1 mg/L $CuCl_2$ & 1 % $H_2O_2$ for 4 hours was not as well defined, and the intensity of the collagen staining and colour was less prominent in comparison to 3 hours of exposure (Figure 4.11 I and Figure 4.13 I).

Based on the collective results presented within section 4.5.1, 1 mg/L $CuCl_2$ & 1 % $H_2O_2$ was the chosen concentration for the sterilisation of dPHVs with 3 hours of exposure at 37 °C, 110 RPM.

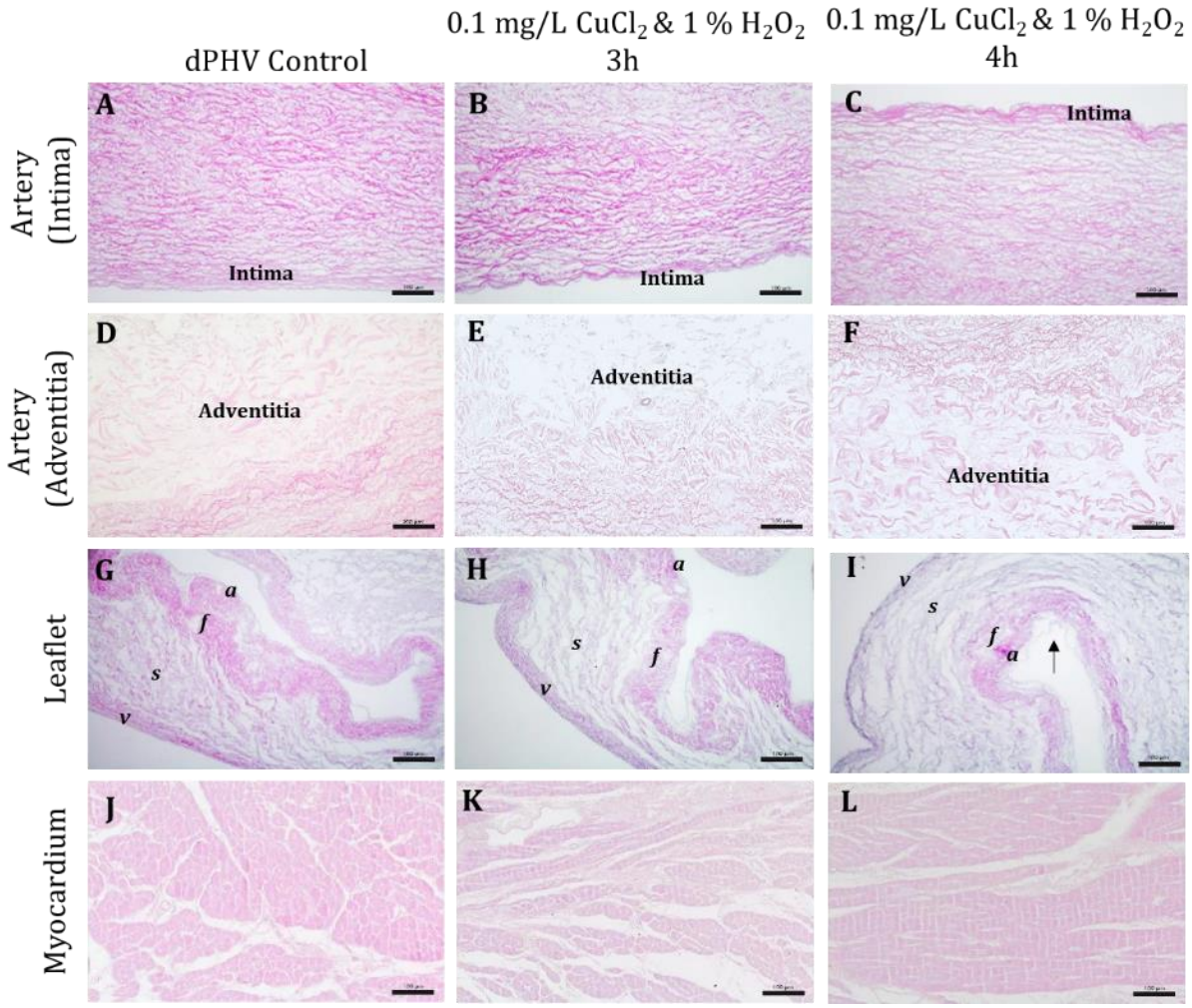


**Figure 4.8 Representative Images of H & E Stained dPHV Control, dPHVs Incubated with 0.1 mg/L $CuCl_2$ & 1 % $H_2O_2$ for 3 hours, and dPHVs Incubated with 0.1 mg/L $CuCl_2$ & 1 % $H_2O_2$ for 4 hours.** Images show control dPHV wall intima (A), adventitia (D), leaflet (G), and myocardium (J); 0.1 mg/L $CuCl_2$ & 1 % $H_2O_2$ at 3 hours incubation dPHV wall intima (B), adventitia (E), leaflet (H) and myocardium (K); 0.1 mg/L $CuCl_2$ & 1 % $H_2O_2$ at 4 hours incubation dPHV wall intima (C), adventitia (F), leaflet (I) and myocardium (L). Images were taken using Köhler illumination and a x 10 objective. *v: ventricularis; s: spongiosa; f: fibrosa; a: arterialis.* Black arrow shows loose fibres. Representative images shown, Scale bars 100 µm.

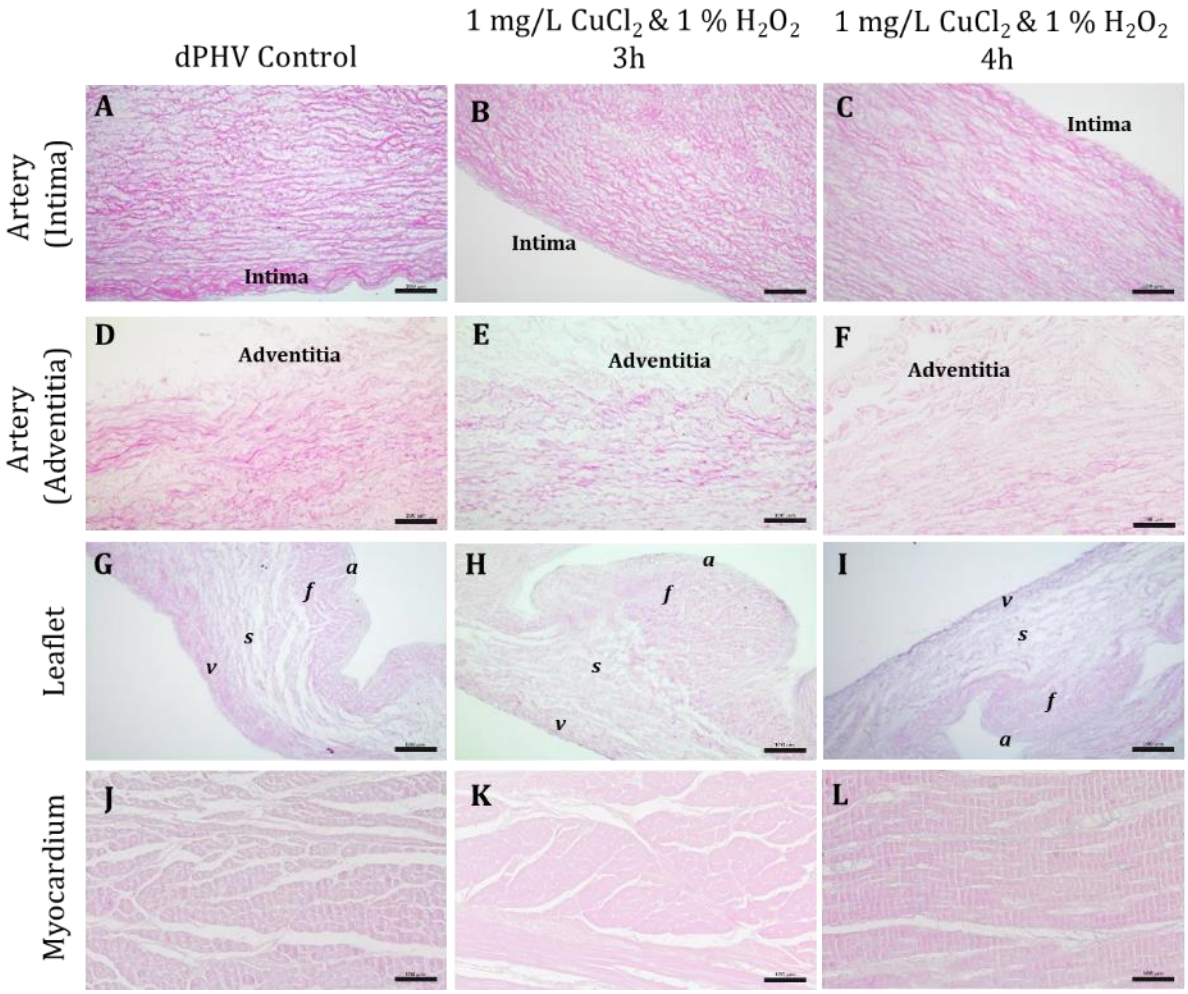


**Figure 4.9 Representative Images of H & E Stained dPHV Control, dPHVs Incubated with 1 mg/L $CuCl_2$ & 1 % $H_2O_2$ for 3 hours, and dPHVs Incubated with 1 mg/L $CuCl_2$ & 1 % $H_2O_2$ for 4 hours.** Images show control dPHV wall intima (A), adventitia (D), leaflet (G), and myocardium (J); 1 mg/L $CuCl_2$ & 1 % $H_2O_2$ at 3 hours incubation dPHV wall intima (B), adventitia (E), leaflet (H) and myocardium (K); 1 mg/L $CuCl_2$ & 1 % $H_2O_2$ at 4 hours incubation dPHV wall intima (C), adventitia (F), leaflet (I) and myocardium (L). Images were taken using Köhler illumination and a x 10 objective. *v: ventricularis; s: spongiosa; f: fibrosa; a: arterialis.* Representative images shown, Scale bars 100 µm.

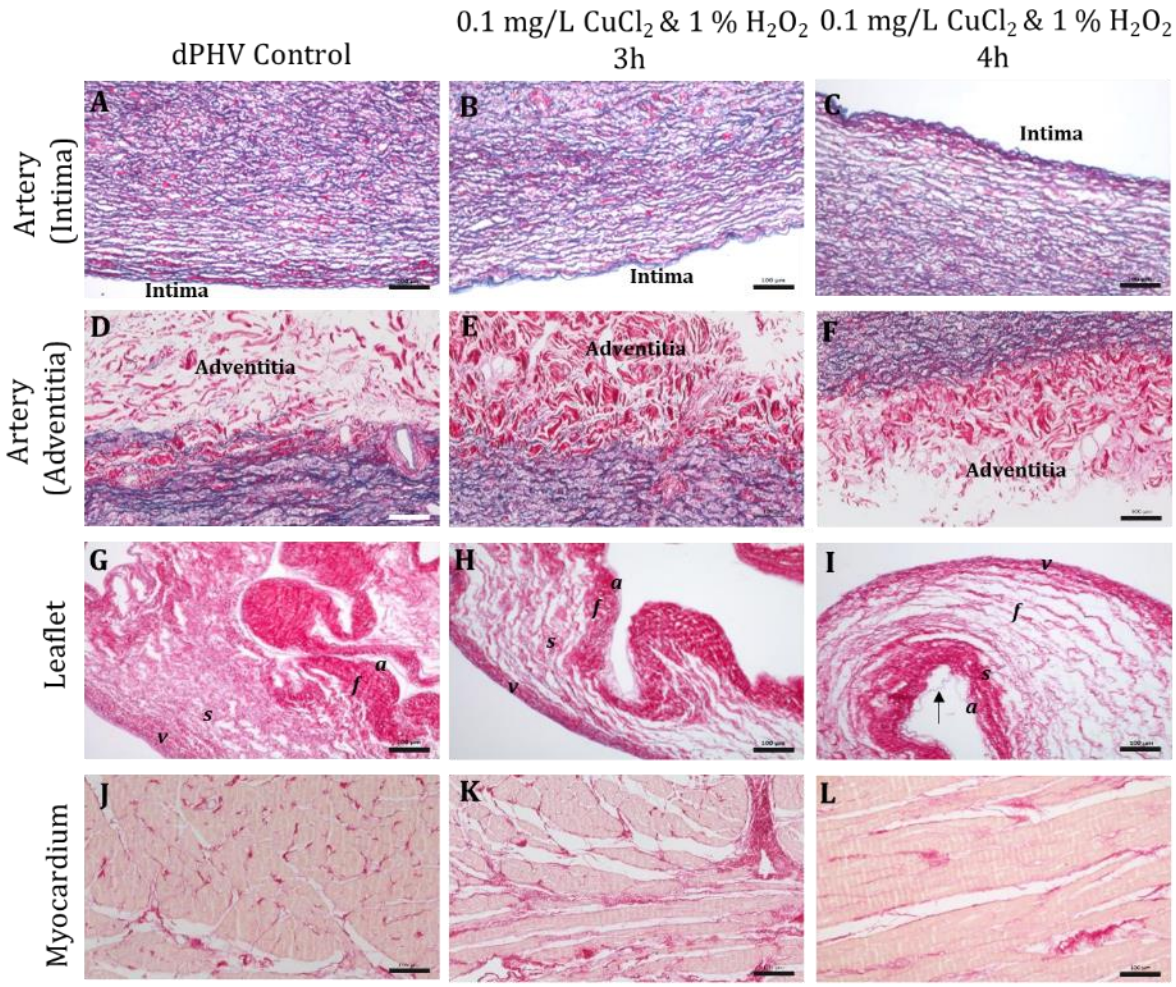


**Figure 4.10 Representative Bright Field Images of Picrosirius Red & Miller's Elastin Stained dPHV Control, dPHVs Incubated with 0.1 mg/L $CuCl_2$ & 1 % $H_2O_2$ for 3 hours, and dPHVs Incubated with 0.1 mg/L $CuCl_2$ & 1 % $H_2O_2$ for 4 hours.** Images show control dPHV wall intima (A), adventitia (D), leaflet (G), and myocardium (J); 0.1 mg/L $CuCl_2$ & 1 % $H_2O_2$ at 3 hours incubation dPHV wall intima (B), adventitia (E), leaflet (H) and myocardium (K); 0.1 mg/L $CuCl_2$ & 1 % $H_2O_2$ at 4 hours incubation dPHV wall intima (C), adventitia (F), leaflet (I) and myocardium (L). Images were taken using Köhler illumination and a x 10 objective. *v: ventricularis; s: spongiosa; f: fibrosa; a: arterialis*. Black arrow shows loose fibres. Representative images shown, Scale bars 100 µm.

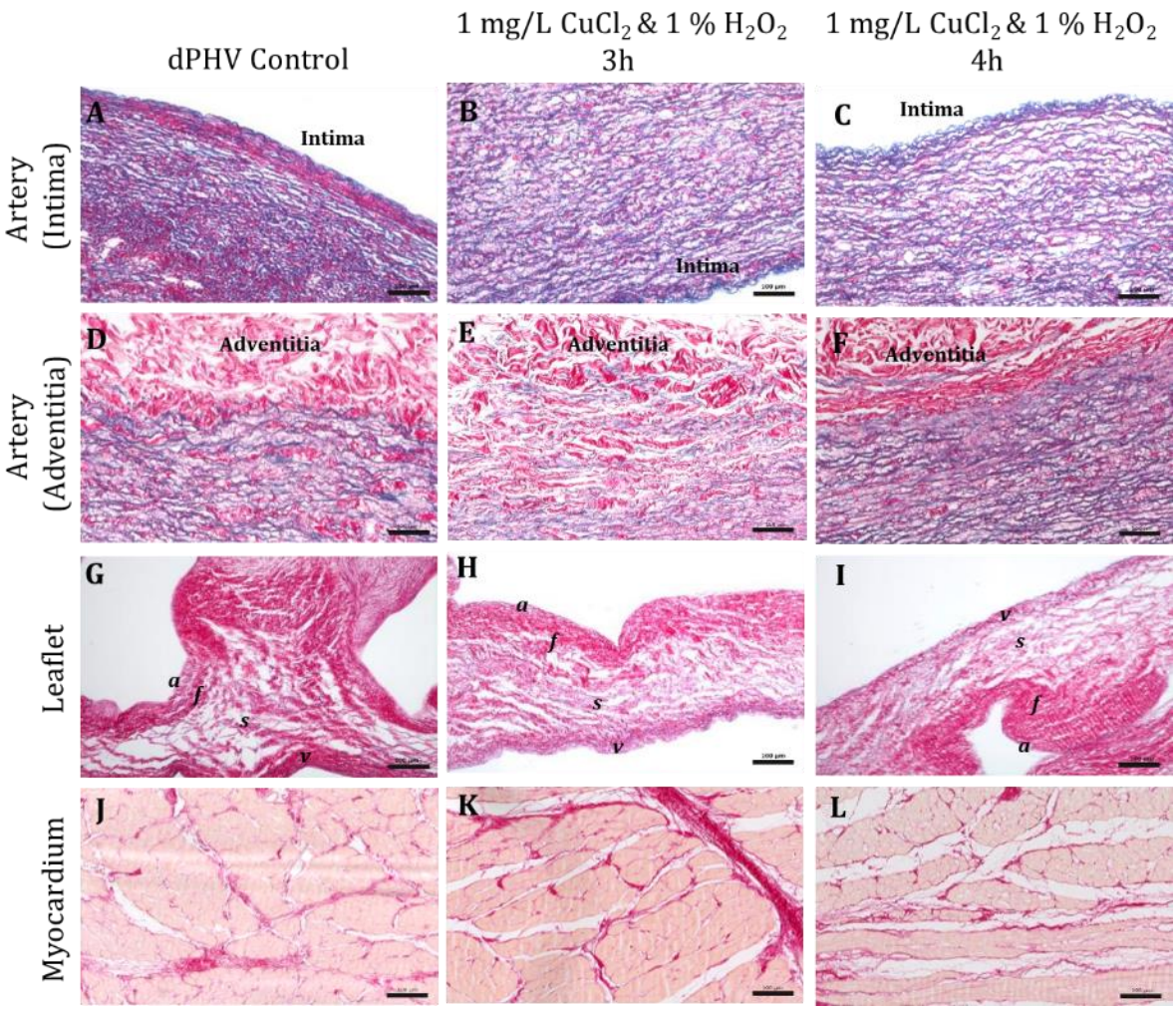


**Figure 4.11 Representative Bright Field Images of Picrosirius Red & Miller's Elastin Stained dPHV Control, dPHVs Incubated with 1 mg/L $CuCl_2$ & 1 % $H_2O_2$ for 3 hours, and dPHVs Incubated with 1 mg/L $CuCl_2$ & 1 % $H_2O_2$ for 4 hours.** Images show control dPHV wall intima (A), adventitia (D), leaflet (G), and myocardium (J); 1 mg/L $CuCl_2$ & 1 % $H_2O_2$ at 3 hours incubation dPHV wall intima (B), adventitia (E), leaflet (H) and myocardium (K); 1 mg/L $CuCl_2$ & 1 % $H_2O_2$ at 4 hours incubation dPHV wall intima (C), adventitia (F), leaflet (I) and myocardium (L). Images were taken using Köhler illumination and a x 10 objective. *v: ventricularis; s: spongiosa; f: fibrosa; a: arterialis.* Representative images shown, Scale bars 100 µm.

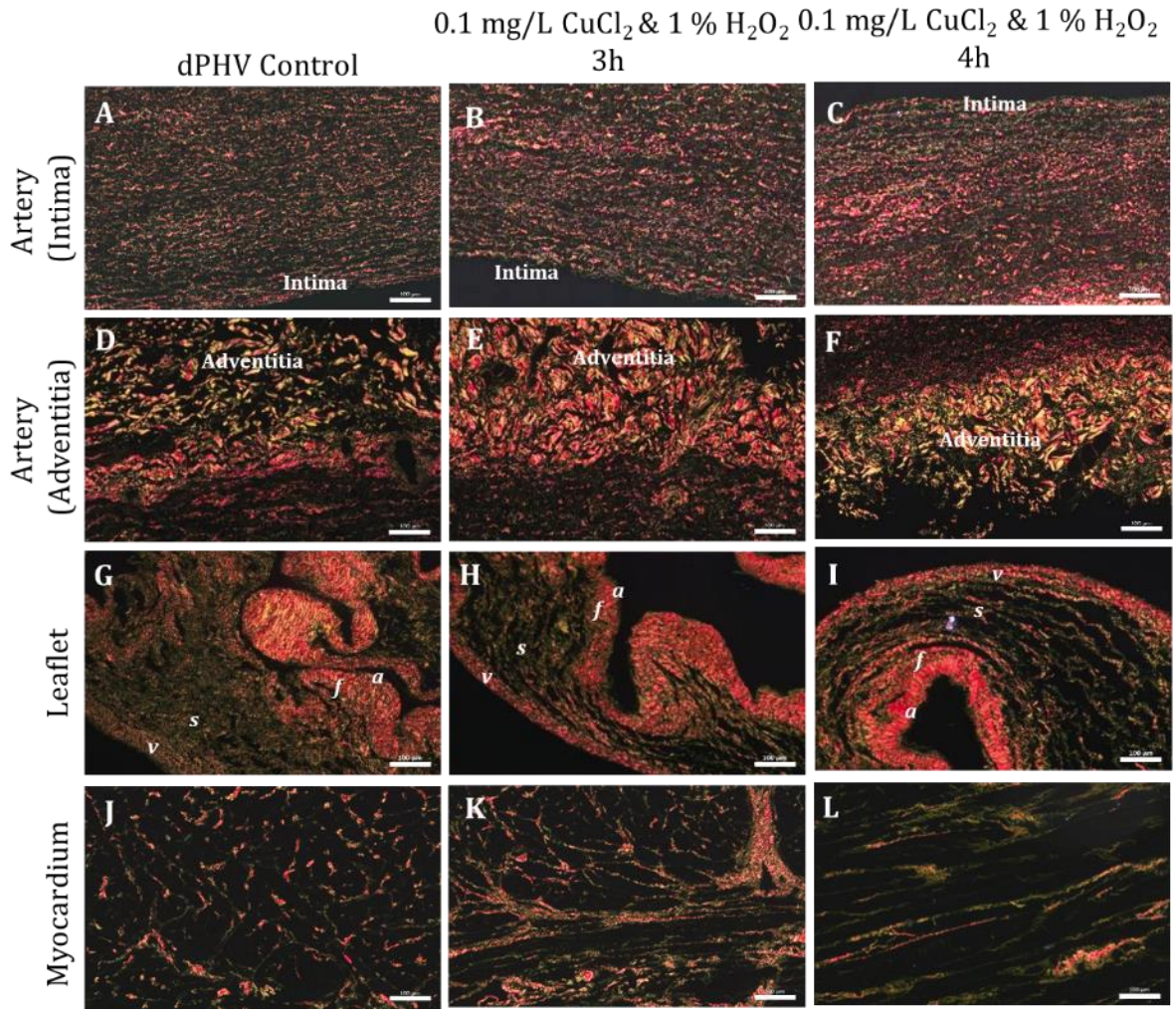


**Figure 4.12 Representative Polarised Light Images of Picrosirius Red & Miller's Elastin Stained dPHV Control, dPHVs Incubated with 0.1 mg/L $CuCl_2$ & 1 % $H_2O_2$ for 3 hours, and dPHVs Incubated with 0.1 mg/L $CuCl_2$ & 1 % $H_2O_2$ for 4 hours.** Images show control dPHV wall intima (A), adventitia (D), leaflet (G), and myocardium (J); 0.1 mg/L $CuCl_2$ & 1 % $H_2O_2$ at 3 hours incubation dPHV wall intima (B), adventitia (E), leaflet (H) and myocardium (K); 0.1 mg/L $CuCl_2$ & 1 % $H_2O_2$ at 4 hours incubation dPHV wall intima (C), adventitia (F), leaflet (I) and myocardium (L). Images were taken using polarised light and a x 10 objective. *v: ventricularis; s: spongiosa; f: fibrosa; a: arterialis.* Representative images shown, Scale bars 100 µm.

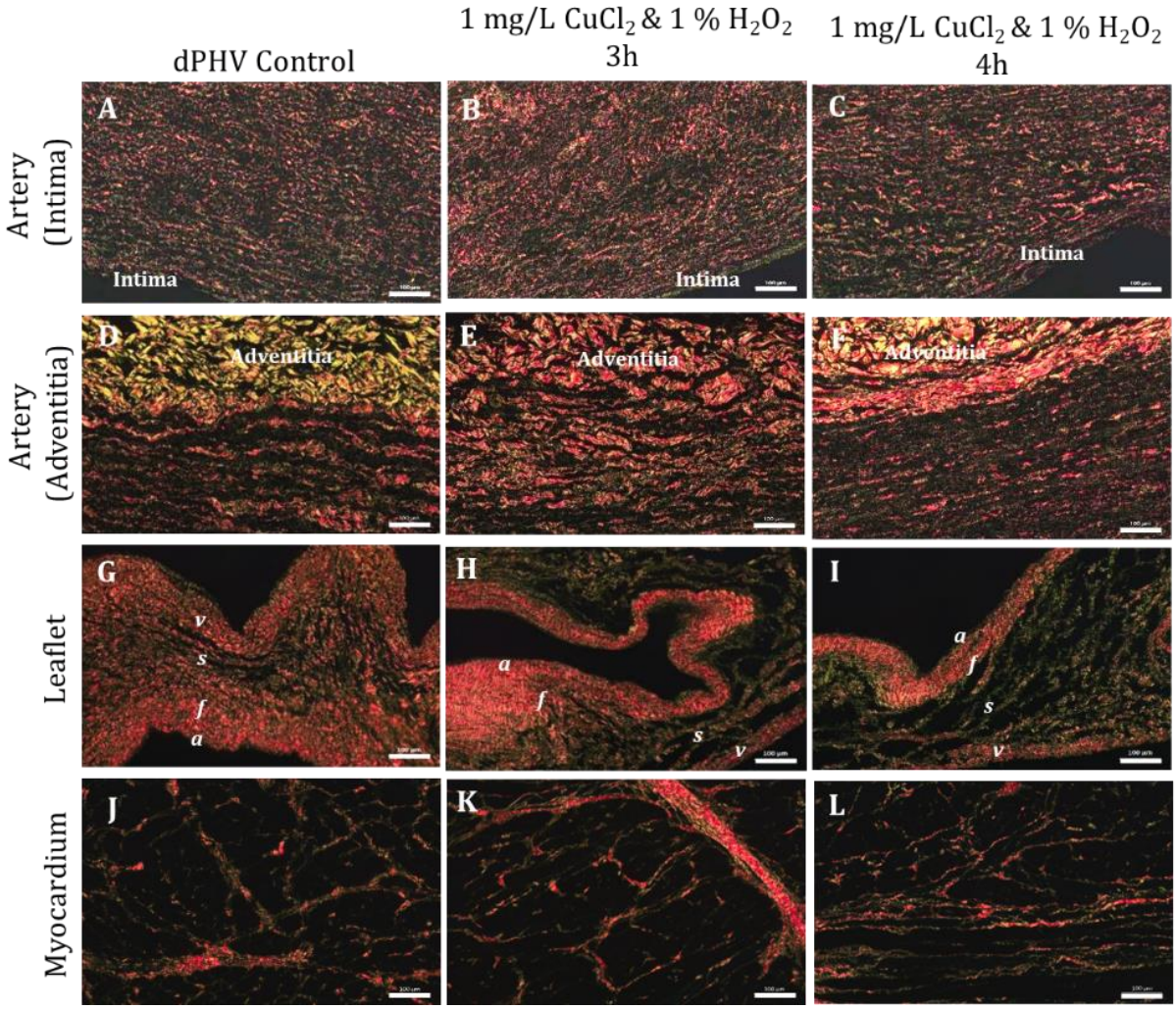


**Figure 4.13 Representative Polarised Light Images of Picrosirius Red & Miller's Elastin Stained dPHV Control, dPHVs Incubated with 0.1 mg/L $CuCl_2$ & 1 % $H_2O_2$ for 3 hours, and dPHVs Incubated with 0.1 mg/L $CuCl_2$ & 1 % $H_2O_2$ for 4 hours.** Images show control dPHV wall intima (A), adventitia (D), leaflet (G), and myocardium (J); 0.1 mg/L $CuCl_2$ & 1 % $H_2O_2$ at 3 hours incubation dPHV wall intima (B), adventitia (E), leaflet (H) and myocardium (K); 0.1 mg/L $CuCl_2$ & 1 % $H_2O_2$ at 4 hours incubation dPHV wall intima (C), adventitia (F), leaflet (I) and myocardium (L). Images were taken using polarised light and a x 10 objective. *v: ventricularis; s: spongiosa; f: fibrosa; a: arterialis.* Representative images shown, Scale bars 100 µm.

### 4.5.2 Histological Analysis

Following treatment of whole dPHV roots with 1mg/L $CuCl_2$ & 1 % $H_2O_2$ for 3 hours, the structure of collagen, elastin and specific membrane proteins within the dPHVs were characterised using H & E, Picrosirius Red & Miller's Elastin, and Movat's Pentachrome staining.

H & E staining defined the gross ECM histoarchitecture of the tissue sections (Figure 4.14). There were no apparent differences between 1mg/L $CuCl_2$ & 1 % $H_2O_2$ and dPHV control artery intima sections, with the tightly crimped collagen and elastin fibres appearing to be well preserved. The loosely arranged adventitial surface of 1mg/L $CuCl_2$ & 1 % $H_2O_2$ ECM treated tissue also resembled the dPHV control. Although the *arterialis*, *fibrosa*, *spongiosa*, and *ventricularis* layers of the 1mg/L $CuCl_2$ & 1 % $H_2O_2$ treated leaflet are well-defined, the *ventricularis* shows loose disconnected fibres that are not as tightly organised as shown in the dPHV control (Figure 4.14 F). The myocardium bundles appear regularly arranged between the two groups.

Picrosirius Red & Miller's elastin staining was used to stain collagen and elastin fibres within the ECM of the tissue sections (Figure 4.15). Visualisation under normal Köhler illumination revealed collagen and elastin fibres. Visualisation under polarised light conditions revealed the configuration and distribution of collagen fibres, with the birefringence of the collagen fibres being associated with the fibre diameter. The tightly crimped elastin structure of the artery intima was disrupted following 1mg/L $CuCl_2$ & 1 % $H_2O_2$ treatment, with porous arrangements being visible (Figure 4.15 B). However, the intensity of the collagen stain of the artery intima was similar between both groups, and structural alterations were not apparent. The loose ECM arrangement found at the artery adventitia was also undisrupted between both groups. The elastin network present in the *ventricularis* layer of the leaflet treated with 1mg/L $CuCl_2$ & 1 % $H_2O_2$ appeared disorganised in comparison to the dPHV control (Figure 4.15 F). However, this disorganisation was not present under polarised light conditions. A network of interspersed collagen fibres was present between the myocardium bundles in both groups.

Movat's Pentachrome staining was used to visualise collagen, elastin, muscle, GAGs and fibrin. As demonstrated by Picrosirius Red & Miller's elastin staining, 1mg/L $CuCl_2$ & 1 % $H_2O_2$ treated artery intima displayed a loose arrangement of elastin

fibres in comparison to the compact arrangement of the elastin fibres shown in the dPHV control artery intima. Collagen and elastin fibres appeared similarly arranged in the artery adventitia sections of both groups, although the elastin fibres were not as compact in 1mg/L $CuCl_2$ & 1 % $H_2O_2$ treated samples. An abundance of GAGs were present in the *spongiosa* layer of both 1mg/L $CuCl_2$ & 1 % $H_2O_2$ treated and dPHV control leaflets. This was sandwiched between the *fibrosa* layer which was populated with collagen fibres and the *ventricularis* composed of collagen fibres intertwined with elastin fibres. The *arterialis* layer of 1mg/L $CuCl_2$ & 1 % $H_2O_2$ treated leaflets also displayed loose elastin fibres in comparison to the tight elastin fibre organisation demonstrated in the dPHV control.

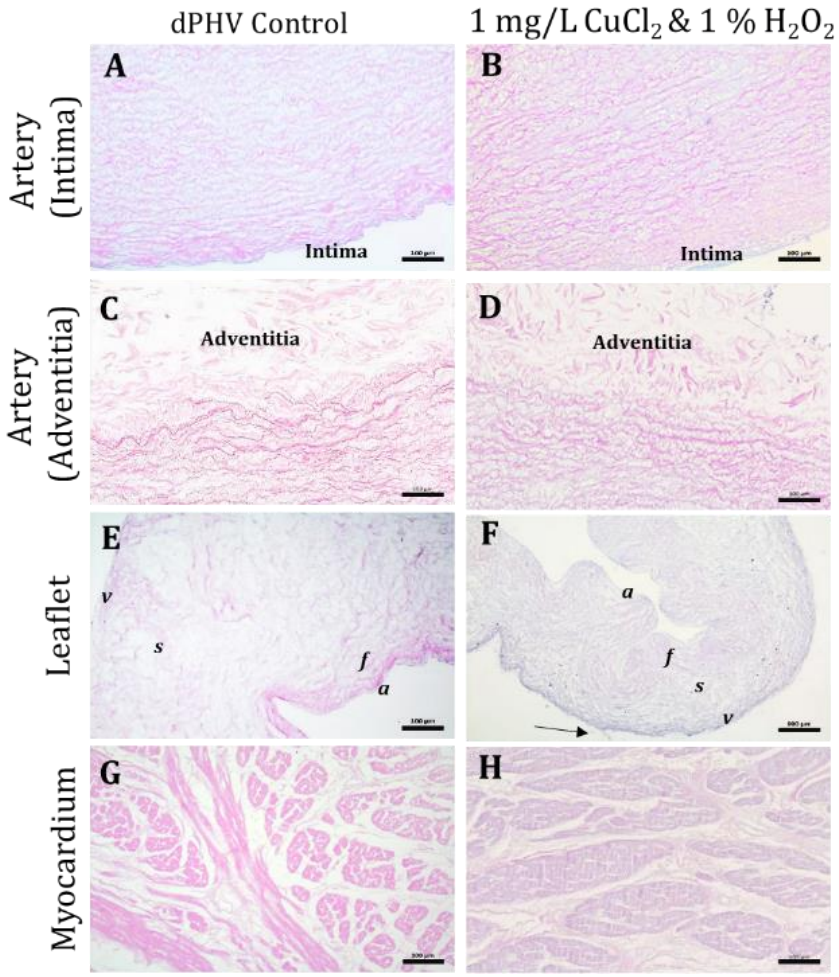


**Figure 4.14 Representative H & E Stained Control and 1 mg/L CuCl2 & 1 % H2O2 Sterilised dPHVs**. Images show control dPHV wall intima (A), adventitia (C), leaflet (E), and myocardium (G); and 1 mg/L CuCl2 & 1 % H2O2 wall intima (B), adventitia (D), leaflet (F) and myocardium (H). Images were taken using Köhler illumination and a x 10 objective. *v: ventricularis; s: spongiosa; f: fibrosa; a: arterialis.* Black arrow shows loose fibres. Representative images shown, Scale bars 100 µm.

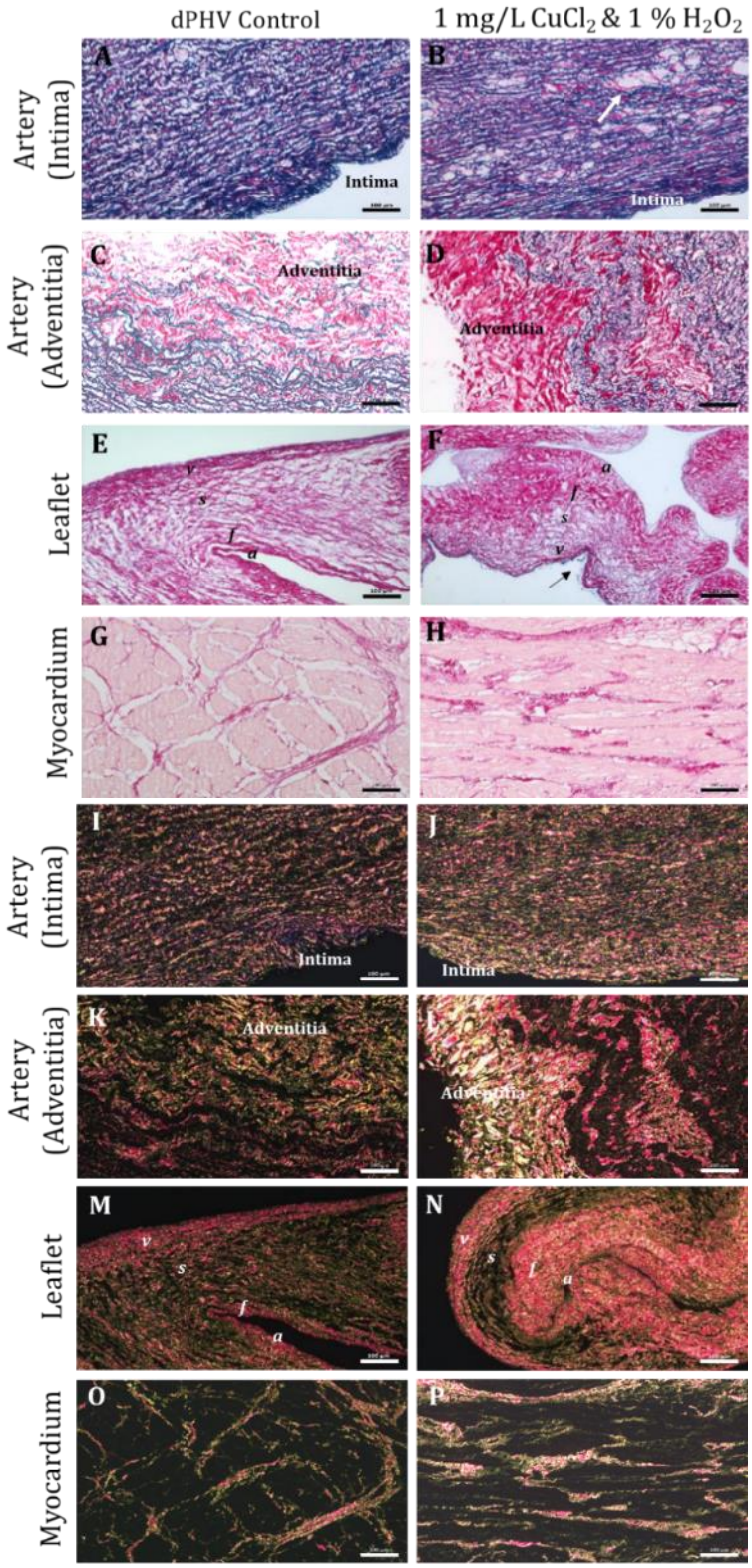


**Figure 4.15 Representative Images of Picrosirius Red & Miller's Elastin Stained Control and 1mg/L $CuCl_2$ & 1 % $H_2O_2$ Sterilised dPHV Artery Wall Intima, Adventitia, Leaflet, and Myocardium Sections.** Images show control dPHV wall intima (A, I), adventitia (C, K), leaflet (E, M), and myocardium (G, O); 1 mg/L $CuCl_2$ & 1 % $H_2O_2$ dPHV wall intima (B, J), adventitia (D, L), leaflet (F, N) and myocardium (H, P). Images were taken using Köhler illumination (A-H) and polarised light conditions (I-P), using a x 10 objective. *v: ventricularis; s: spongiosa; f: fibrosa; a: arterialis*. White arrow shows pores. Black arrow shows loose fibres. Representative images shown, Scale bars 100 µm.

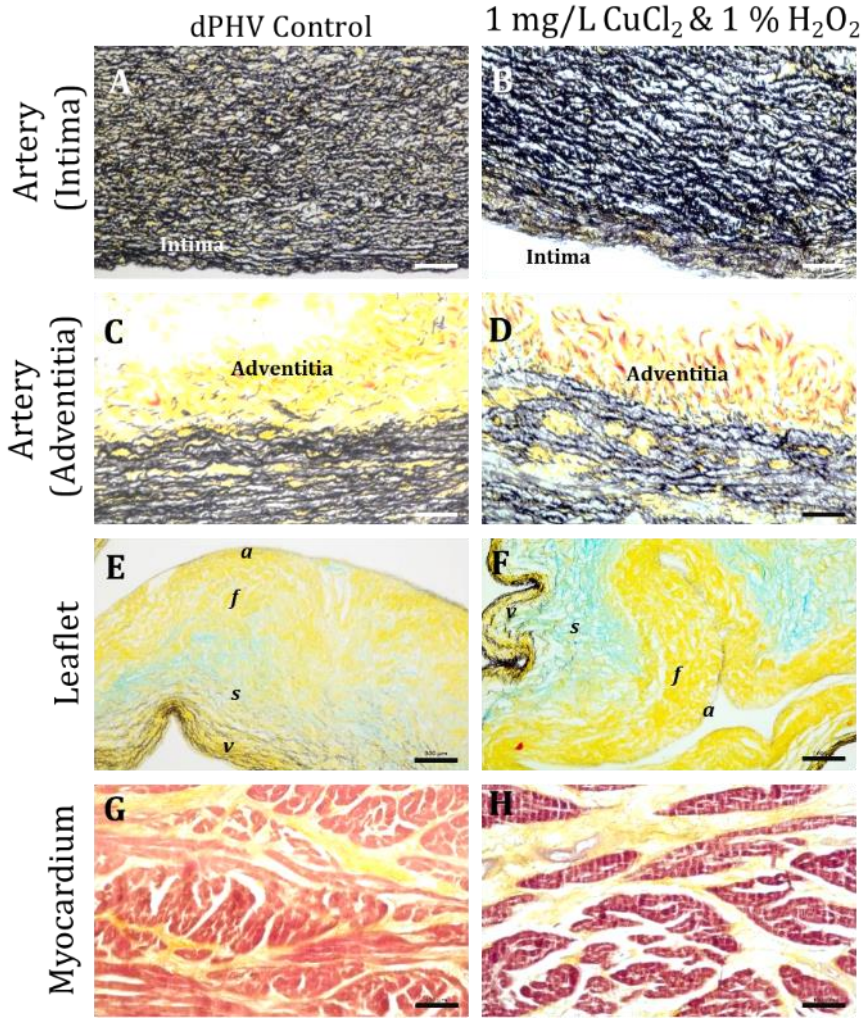


**Figure 4.16 Representative Images of Movat's Pentachrome Stained Control and 1 mg/L $CuCl_2$ & 1 % $H_2O_2$ Sterilised dPHVs.** Images show control dPHV wall intima (A), adventitia (C), leaflet (E), and myocardium (G); and 1 mg/L $CuCl_2$ & 1 % $H_2O_2$ wall intima (B), adventitia (D), leaflet (F) and myocardium (H). Images were taken using Köhler illumination and a x 10 objective. *v: ventricularis; s: spongiosa; f: fibrosa; a: arterialis*. Representative images shown, Scale bars 100 µm.

### 4.5.3 Immunohistochemical Labelling of Collagen IV and Fibronectin

DPHV control and 1 mg/L $CuCl_2$ & 1 % $H_2O_2$ dPHVs were labelled with monoclonal antibodies against collagen IV and fibronectin.

The intensity of the collagen IV staining was less on the surface of the 1 mg/L CuCl2 & 1 % H2O2 artery intima in comparison to the dPHV control (Figure 4.17). Both dPHV control and 1 mg/L CuCl2 & 1 % H2O2 artery adventitia displayed a similar intensity of positive staining in the artery adventitia. The leaflets of both groups also displayed a similar level of positive staining, with the most intensity being displayed in the arterialis layer. A well-defined layer of positive staining was also observed in the leaflet ventricularis layer of both groups. The myocardium displayed a network of defined positive labelling in both groups with greatest intensity in the lining of blood vessels. There was no staining observed in sections stained with the isotype control.

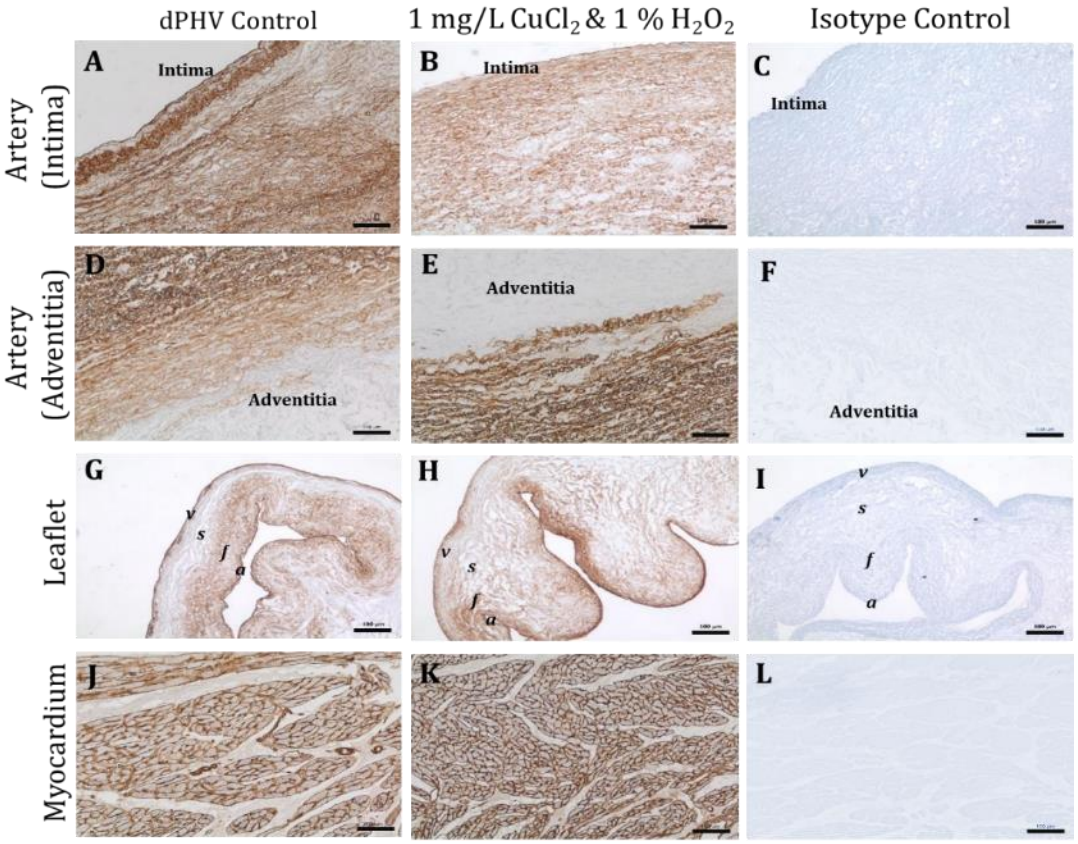


**Figure 4.17 Representative Images of Control and 1 mg/L $CuCl_2$ & 1 % $H_2O_2$ Sterilised dPHV Sections Labelled with Monoclonal Antibodies Against Collagen IV.** Images show control dPHV wall intima (A), adventitia (D), leaflet (G), and myocardium (J); 1 mg/L $CuCl_2$ & 1 % $H_2O_2$ wall intima (B), adventitia (E), leaflet (H) and myocardium (K); Isotype controls for dPHV wall intima (C), adventitia (F), leaflet (I) and myocardium (L). Images were taken using Köhler illumination and a x 10 objective. *v: ventricularis; s: spongiosa; f: fibrosa; a: arterialis*. Representative images shown, Scale bars 100 µm.

The results from fibronectin labelling indicate that the dPHV control and 1 mg/L $CuCl_2$ & 1 % $H_2O_2$ dPHV tissues were both stained positive (Figure 4.18). The artery intima and adventitia tissues displayed similar fibronectin labelling intensities in both groups, as did the leaflets with the greatest intensities being observed at the *arterialis* and *ventricularis* surfaces. Fibronectin labelling of the myocardium of both groups revealed a well-defined network of positive staining. Minimal brown staining was observed in undefined areas of sections stained with the isotype control.

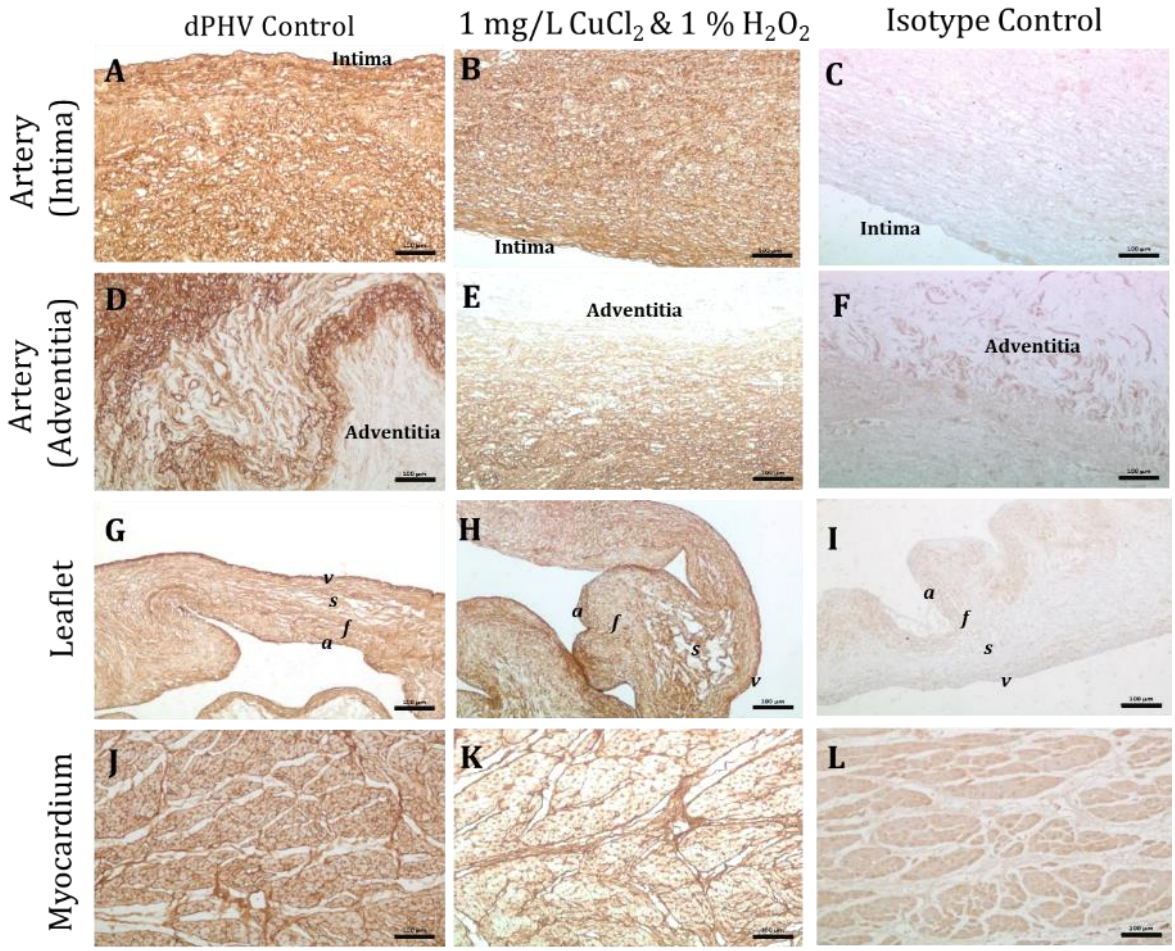


**Figure 4.18 Representative Images of Control and 1 mg/L $CuCl_2$ & 1 % $H_2O_2$ Sterilised dPHV Sections Labelled with Monoclonal Antibodies Against Fibronectin.** Images show control dPHV wall intima (A), adventitia (D), leaflet (G), and myocardium (J); 1 mg/L $CuCl_2$ & 1 % $H_2O_2$ wall intima (B), adventitia (E), leaflet (H) and myocardium (K); Isotype controls for dPHV wall intima (C), adventitia (F), leaflet (I) and myocardium (L). Images were taken using Köhler illumination and a x 10 objective. *v: ventricularis; s: spongiosa; f: fibrosa; a: arterialis.* Representative images shown, Scale bars 100 µm.

### 4.5.4 Visualisation of Tissue Surface Microscopic Structure

Scanning electron Microscopy (SEM) was used to visualise the impact of 1 mg/L $CuCl_2$ & 1 % $H_2O_2$ sterilisation on dPHV pulmonary artery wall and leaflet surface microscopic structures (Figure 4.19).

The artery intima of both dPHV control and 1 mg/L $CuCl_2$ & 1 % $H_2O_2$ displayed a slight cobblestone structure, although the dPHV control artery intima appeared smoother than the 1 mg/L $CuCl_2$ & 1 % $H_2O_2$ sterilised artery intima which showed loose and disorganised fibres. The adventitia of both groups also displayed loose fibres which appeared more crimped after 1 mg/L $CuCl_2$ & 1 % $H_2O_2$ sterilisation. The leaflet *ventricularis* tissues displayed undisrupted, slightly cobbled layers of reticular fibres. The leaflet *arterialis* surface displayed small tears within the reticular fibre layers, revealing bundles of arranged collagenous fibres.

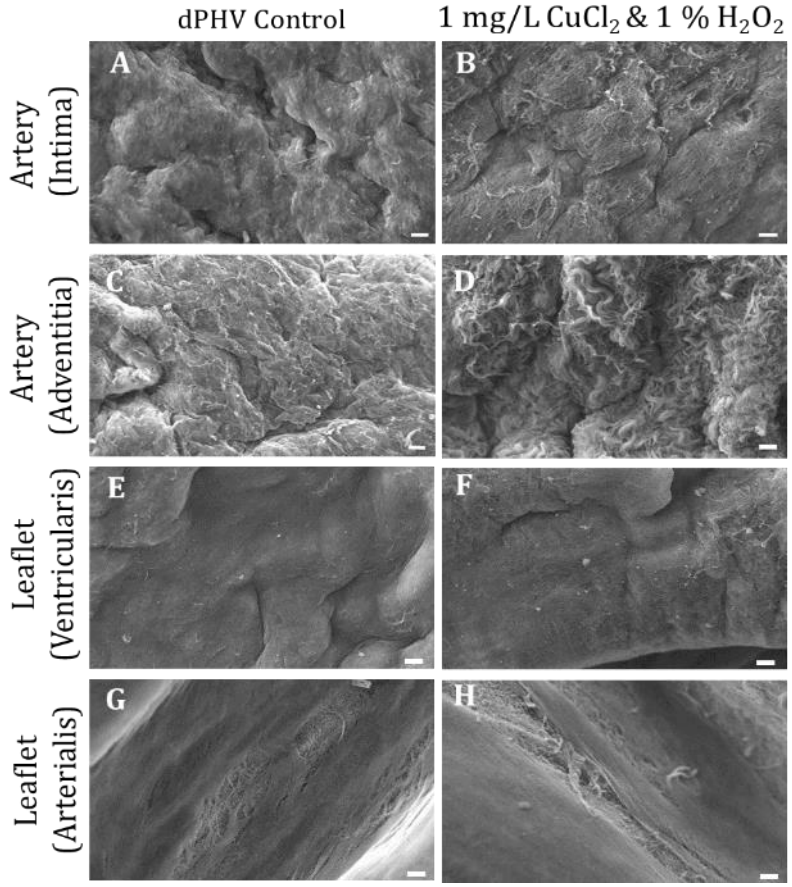


**Figure 4.19 Microscopic Structure of Control and 1 mg/L $CuCl_2$ & 1 % $H_2O_2$ dPHV Artery Wall Intima, Adventitia, Leaflet Ventricularis, and Leaflet Arterialis Surfaces.** Images show control dPHV wall intima surface (A), adventitia surface (C), leaflet ventricularis surface (E), and leaflet arterialis surface (G); 1 mg/L $CuCl_2$ & 1 % $H_2O_2$ dPHV wall intima surface (B), adventitia surface (D), leaflet ventricularis surface (F) and leaflet arterialis surface (H). SEM images were taken using Carl Zeiss EVO MA15. Scale bars show 20 µm.

### 4.5.5 Quantification of Collagen Content

To determine the impact of 1 mg/L $CuCl_2$ & 1 % $H_2O_2$ sterilisation on dPHV collagen content, pulmonary artery wall and leaflet samples were assayed for hydroxyproline content (Figure 4.20).

The collagen content of 1 mg/L $CuCl_2$ & 1 % $H_2O_2$ artery wall samples was 308.71 ± 47.19 $\mu g.mg^{-1}$ which was not significantly different to the control dPHV artery wall collagen content (282.28 ± 54.11 $\mu g.mg^{-1}$).

There was also no significant difference in the collagen content of 1 mg/L $CuCl_2$ & 1 % $H_2O_2$ artery leaflet samples (887.33 ± 110.05 $\mu g.mg^{-1}$) in comparison to the dPHV controls (799.06 ± 212.36 $\mu g.mg^{-1}$).

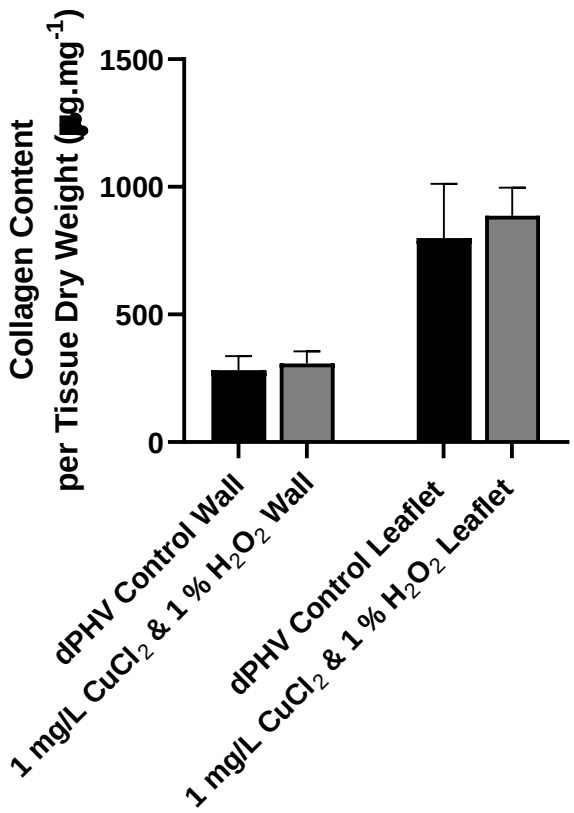


**Figure 4.20 Collagen Content of 1 mg/L $CuCl_2$ & 1 % $H_2O_2$ dPHV Artery Wall and Leaflet Specimens in Comparison to dPHV Controls.** Data presented as mean (n=6) ± 95% C.I. Data was analysed using unpaired t-test between the two groups in each specimen type.

### 4.5.6 Quantification of GAG Content

The dPHV control and 1 mg/L $CuCl_2$ & 1 % $H_2O_2$ artery wall and leaflet samples were digested with papain prior to GAG quantification using the dimethylene blue (DMMB) assay.

The dPHV control and 1 mg/L $CuCl_2$ & 1 % $H_2O_2$ artery wall samples were found to have a GAG content of 2.81 ± 1.82 $\mu g.mg^{-1}$ and 4.41 ± 1.65 $\mu g.mg^{-1}$, respectively. The dPHV control and 1 mg/L $CuCl_2$ & 1 % $H_2O_2$ leaflet samples were found to have a GAG content of 4.34 ± 1.28 $\mu g.mg^{-1}$ and 4.27 ± 0.83 $\mu g.mg^{-1}$, respectively. There were no significant differences in GAG content found (Figure 4.21).

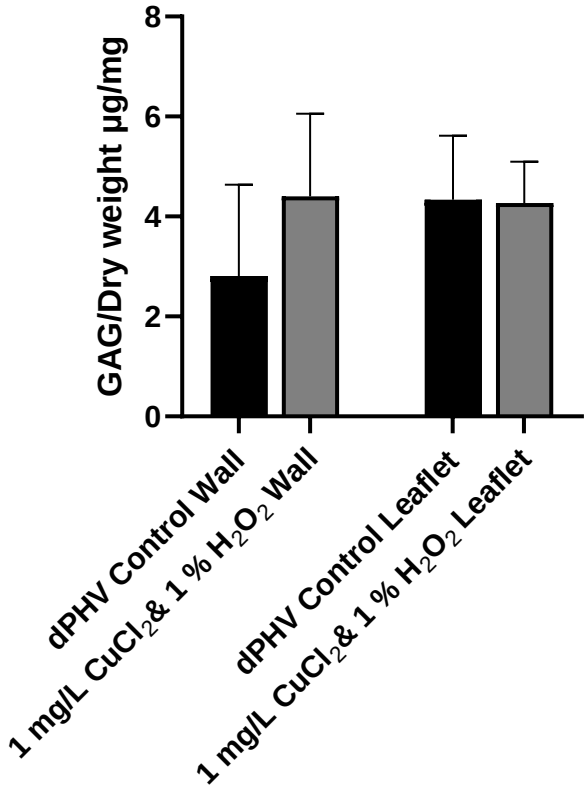


**Figure 4.21 GAG Content of 1 mg/L $CuCl_2$ & 1 % $H_2O_2$ dPHV Artery Wall and Leaflet Specimens in Comparison to dPHV Controls.** Data presented as mean (n=6) ± 95% C.I. Data was analysed using unpaired t-test between the two groups in each specimen type.

### 4.5.7 DSC Analysis

The collagen denaturation temperatures of dPHV control and 1 mg/L $CuCl_2$ & 1 % $H_2O_2$ wall and leaflet samples were quantified by measuring heat flow (W/g) in a differential scanning calorimeter.

As displayed in Figure 4.22, the collagen denaturation temperature of 1 mg/L $CuCl_2$ & 1 % $H_2O_2$ wall samples was 62.56 ± 0.78 °C, which was significantly less than the collagen denaturation temperature of dPHV control wall samples (65.57 ± 0.81 °C). The collagen denaturation temperature of 1 mg/L $CuCl_2$ & 1 % $H_2O_2$ leaflet samples was also significantly lower than the collagen denaturation temperature of dPHV control leaflet samples, at 61.88 ± 0.90 °C and 65.45 ± 0.78 °C, respectively.

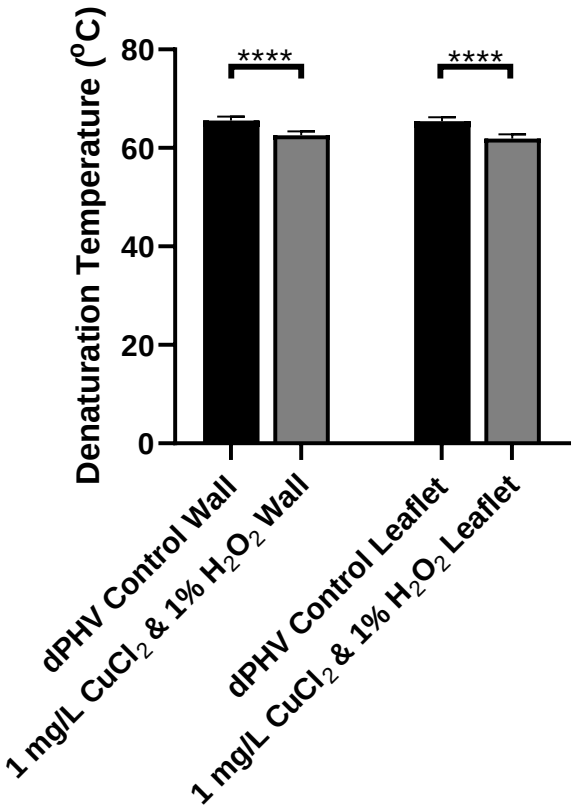


**Figure 4.22 Collagen Thermal Stability of 1 mg/L $CuCl_2$ & 1 % $H_2O_2$ dPHV Artery Wall and Leaflet Specimens in Comparison to dPHV Controls.** Data presented as mean (n=6) ± 95% C.I. Data was analysed using unpaired t-test between the two groups in each specimen type. ****($p<0.001$) denotes significant difference between the groups.

### 4.5.8 *In Vitro* Cytocompatibility Assessments

Contact culture of L929 cells with 1 mg/L $CuCl_2$ & 1 % $H_2O_2$ wall and leaflet samples was used to determine cytocompatibility of the sterilised tissues. The extract cytotoxicity assay was also used to determine if toxins were leached from 1 mg/L $CuCl_2$ & 1 % $H_2O_2$ wall and leaflet samples.

Prior to conducting contact culture and extract cytotoxicity assays with 1 mg/L $CuCl_2$ & 1 % $H_2O_2$ wall and leaflet samples, sterility was determined by incubating the tissues in thioglycollate broth (section 2.2.11.3). The broth remained clear for all samples (N=6 for each specimen type) and negative controls, and only the positive control showed microbial growth (Figure 4.23). Therefore, 1 mg/L $CuCl_2$ & 1 % $H_2O_2$ wall and leaflet samples were not contaminated.


**Figure 4.23 Images of 1 mg/L $CuCl_2$ & 1 % $H_2O_2$ dPHV Artery Wall (W) and Leaflet (L) Specimen Sterility Tests 48 hours Post Inoculation.** 1 mg/L $CuCl_2$ & 1 % $H_2O_2$ dPHV Artery Wall (A) and Leaflet (B) specimens were incubated in Thioglycolate broth. N=6 of wall and leaflet samples were used. Positive controls (+VE) of dermal commensal organisms and negative controls (-VE) of sterile thioglycolate broth were incubated alongside samples.

The contact cytotoxicity assays showed no evidence of 1 mg/L $CuCl_2$ & 1 % $H_2O_2$ treated tissue cytotoxicity. L929 cells grew up to and in contact with 1 mg/L $CuCl_2$ & 1 % $H_2O_2$ dPHV artery wall and leaflet tissue specimens, with no change in the cellular morphology in comparison to the negative steri-strip control. The rounded appearance of dead cells cultured in wells with the positive cyanoacrylate adhesive was absent in cells cultured with 1 mg/L $CuCl_2$ & 1 % $H_2O_2$ dPHV artery wall and leaflet tissue specimens (Figure 4.24).

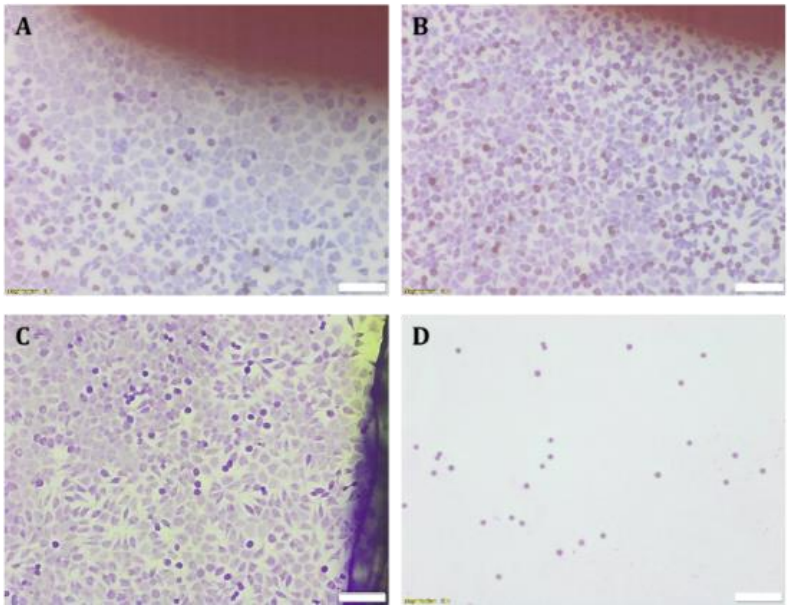


**Figure 4.24 Giemsa Stained Cell Cultures From Contact Cytotoxicity of 1 mg/L $CuCl_2$ & 1 % $H_2O_2$ dPHV Wall and Leaflet Specimens.** Images show a representative 1 mg/L $CuCl_2$ & 1 % $H_2O_2$ dPHV wall specimen (A), leaflet specimen (B), negative control (C), and positive control (D). Scale bars are 100 µm.

The results from the extract cytotoxicity assay showed no evidence of cytotoxicity. ATP levels of cells cultured with 1 mg/L $CuCl_2$ & 1 % $H_2O_2$ dPHV wall and leaflet control extracts were significantly greater than cells cultured with the positive DMSO control only, and not the negative DMEM control (Figure 4.25).

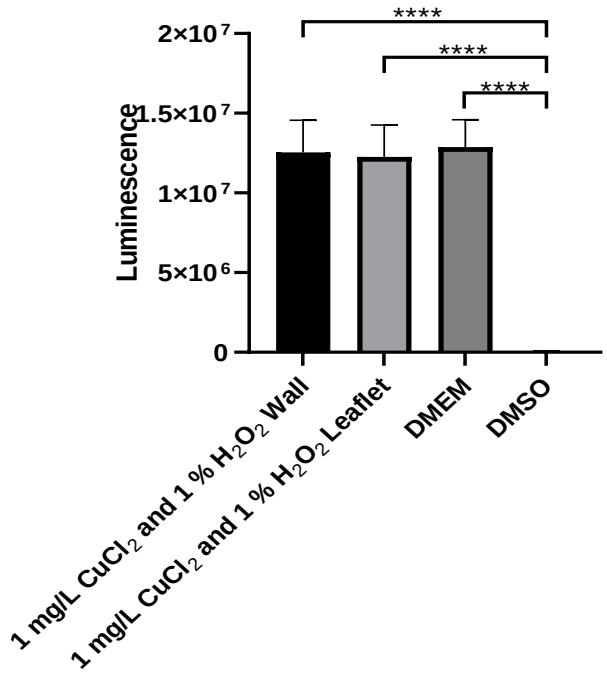


**Figure 4.25 Cell Viability of L929 Cells Cultured With 1 mg/L $CuCl_2$ & 1 % $H_2O_2$ Wall and Leaflet Tissue Extracts.** Data presented as mean (n=6) ± 95% C.I. Data was analysed using one way ANOVA with Tukey's post-hoc test. **** ($p<0.0001$) denotes significant difference between the groups.

### 4.5.9 Uniaxial Tensile Testing

Uniaxial tensile testing on 1 mg/L $CuCl_2$ & 1 % $H_2O_2$ dPHV artery wall and leaflet tissue specimens was performed to determine the effects of 1 mg/L $CuCl_2$ & 1 % $H_2O_2$ sterilisation on dPHV tensile properties.

The stress-strain graphs for all dPHV controls and 1 mg/L $CuCl_2$ & 1 % $H_2O_2$ dPHV artery wall and leaflet tissue specimens are displayed in Figure 4.26. All artery wall and leaflet tissue specimens demonstrate the typical tri-phasic characteristics. The circumferential wall stress-strain graphs generally showed a decrease in the 1 mg/L $CuCl_2$ & 1 % $H_2O_2$ ultimate tensile strength in comparison to the dPHV controls (Figure 4.26 A). The axial wall specimens stress-strain graph did not show any obvious differences between the two groups (Figure 4.26 B). The circumferential and radial 1 mg/L $CuCl_2$ & 1 % $H_2O_2$ leaflet specimens also showed a trend for decreasing ultimate tensile strengths in comparison to dPHV controls (Figure 4.26 C, D).

As shown in Figure 4.27 A, there was no significant difference in the elastin phase slope of 1 mg/L $CuCl_2$ & 1 % $H_2O_2$ circumferential wall (0.11 ± 0.03 MPa) and axial wall (0.10 ± 0.03 MPa) in comparison to the dPHV controls (0.11 ± 0.03 MPa and 0.10 ± 0.03 MPa, respectively). As shown in Figure 4.27 C, there was also no significant difference in the collagen phase slope of 1 mg/L $CuCl_2$ & 1 % $H_2O_2$ circumferential wall (1.52 ± 0.46 MPa) and axial wall (0.68 ± 0.18 MPa) in comparison to the dPHV controls (2.24 ± 1.04 MPa and 0.84 ± 0.36 MPa, respectively). Despite the trend for a decrease in UTS for the 1 mg/L $CuCl_2$ & 1 % $H_2O_2$ circumferential wall (Figure 4.26 A), the ultimate tensile strength of circumferential and axial 1 mg/L $CuCl_2$ & 1 % $H_2O_2$ wall was 1.04 ± 0.27 MPa and 1.39 ± 0.20 MPa respectively, which was not significantly different to the dPHV control wall specimens (0.71 ± 0.33 MPa and 0.81 ± 0.27 MPa, respectively), shown in Figure 4.27 E.

Shown in Figure 4.27 B, the elastin phase slopes of 1 mg/L $CuCl_2$ & 1 % $H_2O_2$ circumferential (0.04 ± 0.01 MPa) and radial (0.02 ± 0.01 MPa) leaflet specimens were not significantly different to the elastin phase slopes of dPHV control circumferential (0.03 ± 0.01 MPa) and radial (0.02 ± 0.01 MPa) leaflet specimens. The collagen phase slope of 1 mg/L $CuCl_2$ & 1 % $H_2O_2$ circumferential leaflet specimens was 17.04 ± 5.15 MPa, which was significantly lower than the collagen

phase slope of dPHV control circumferential leaflet specimens (25.63 ± 7.29 MPa), There was no significant difference in the collagen phase slopes of 1 mg/L $CuCl_2$ & 1 % $H_2O_2$ radial (0.61 ± 0.30 MPa) and dPHV control radial leaflet specimens (0.88 ± 0.31 MPa) shown in Figure 4.27 D. In line with the trend for a decrease in ultimate tensile strength (Figure 4.26 C), there was a significant decrease in the ultimate tensile strength of 1 mg/L $CuCl_2$ & 1 % $H_2O_2$ circumferential leaflet specimens (4.74 ± 1.49 MPa) in comparison to the dPHV controls (6.29 ± 0.99 MPa). However, there was no significant difference in the ultimate tensile strength of 1 mg/L $CuCl_2$ & 1 % $H_2O_2$ radial specimens (0.52 ± 0.17 MPa) in comparison to the dPHV controls (0.75 ± 0.27 MPa), shown in Figure 4.27 F.

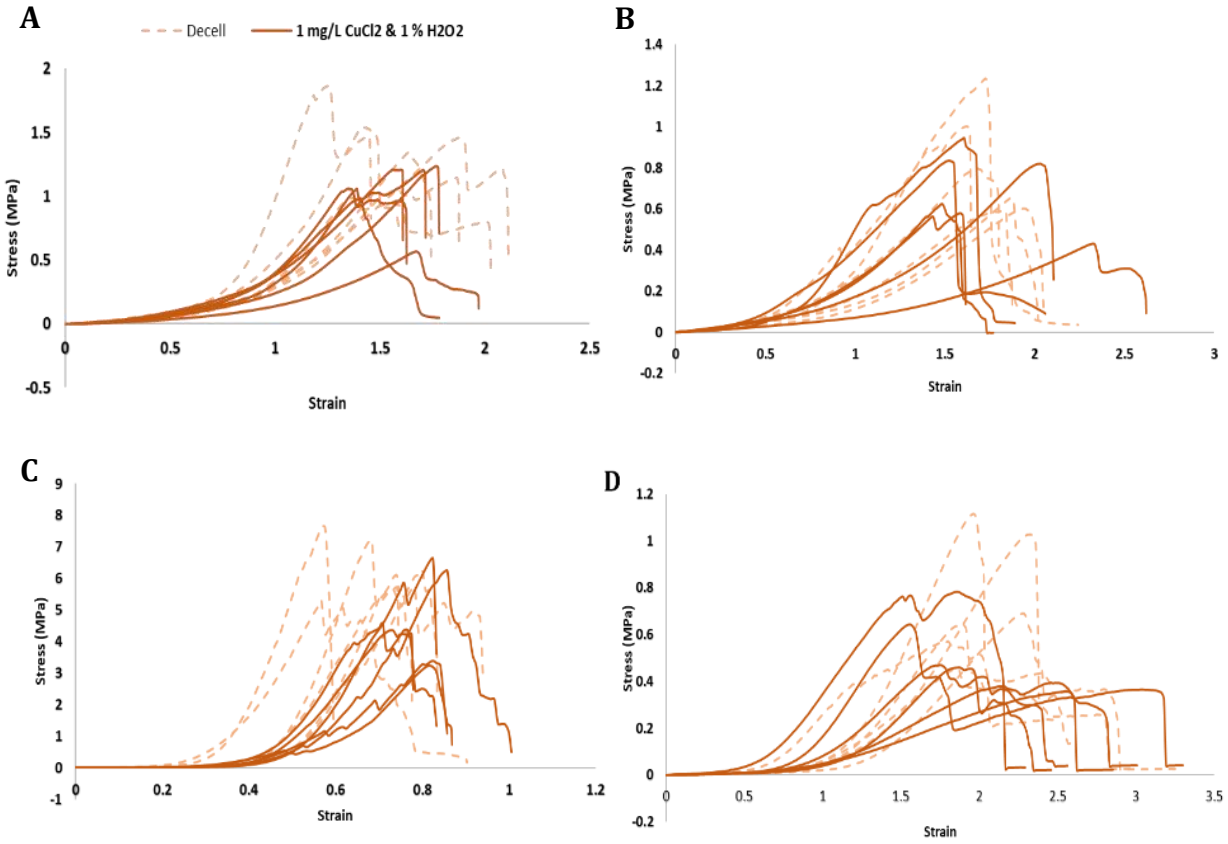


**Figure 4.26 Stress-Strain Graphs of Control and 1 mg/L $CuCl_2$ & 1 % $H_2O_2$ dPHV Wall and Leaflet Specimens.** Stress-strain graphs shown for (A) dPHV control and 1 mg/L $CuCl_2$ & 1 % $H_2O_2$ circumferential wall; (B) dPHV control and 1 mg/L $CuCl_2$ & 1 % $H_2O_2$ axial wall; (C) dPHV control and 1 mg/L $CuCl_2$ & 1 % $H_2O_2$ circumferential leaflet; (D) dPHV control and 1 mg/L $CuCl_2$ & 1 % $H_2O_2$ radial leaflet. N=6 for all specimens.

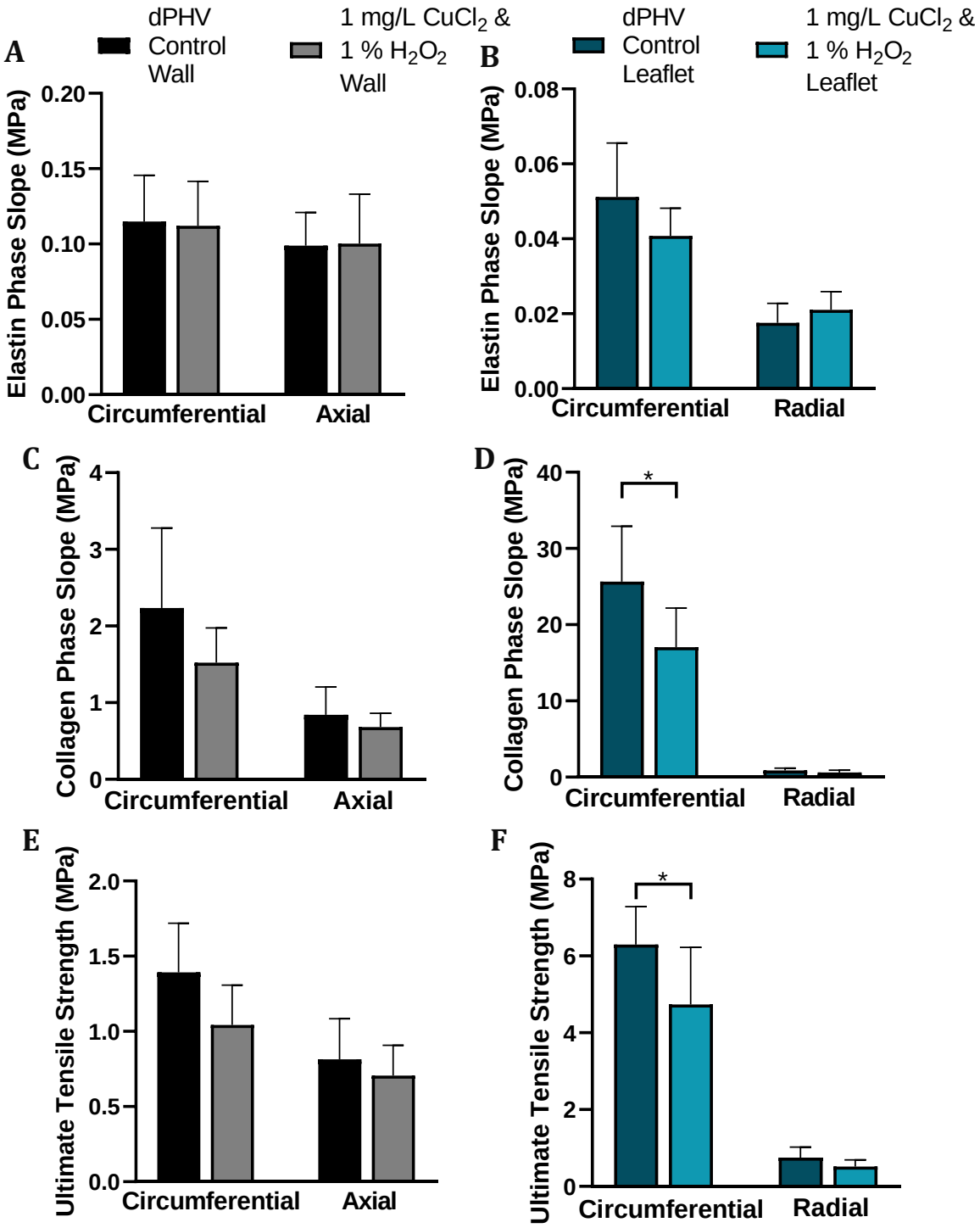


**Figure 4.27 Tensile Parameters of 1 mg/L $CuCl_2$ & 1 % $H_2O_2$ dPHV Artery Wall and Leaflet Specimens in Comparison to dPHV Controls. Elastin phase slopes (A,B), collagen phase slopes (C, D) and ultimate tensile strengths (E,F) of dPHV control and 1 mg/L $CuCl_2$ & 1 % $H_2O_2$ wall and leaflet specimens, respectively.** Data presented as mean (n=6) ± 95% C.I. Data was analysed using unpaired t-test between the two groups in each specimen type. * ($p<0.05$) denotes significant difference between the groups.

## 4.6 Discussion

The first aim of this study was to determine the appropriate concentration and time exposure of $CuCl_2$ in combination with $H_2O_2$ for the effective sterilisation of dPHVs without inducing major changes to the histoarchitecture of the tissue, prior to conducting further biological and biomechanical analysis.

The stability of $H_2O_2$ is affected by pH, temperature and the presence of metal ions. $H_2O_2$ is stable at a low pH (Leow-Dyke et al., 2016). Leow-Dyke et al. (2016) did not alter the pH of the $CuCl_2$ and $H_2O_2$ sterilants investigated within their study, and there were no alterations introduced to the morphological architecture of dCELL human dermis following exposure to $CuCl_2$ and $H_2O_2$ solutions with pH ranging between 3.1-4.9. However, preliminary data from a study conducted at University of Leeds Institute of Medical and Biological Engineering (unpublished) demonstrated that the microarchitecture of dPHV leaflet specimens was disrupted following exposure to acidic $CuCl_2$ & $H_2O_2$ solutions with pH ranging from 3-5. Within this current study an attempt was made to prevent potential damage to the delicate dPHV leaflet ECM as a result of exposure to acidic pH by adjusting the pH of sterilants investigated to pH 7 (± 1).

An increase in temperature to 40 °C can also accelerate the decomposition of $H_2O_2$ by approximately 2.2 fold. Leow-Dyke et al. (2016) carried out dCELL human dermis sterilisation treatment at 25 °C, despite it being identified that the biocidal activity of $CuCl_2$ and $H_2O_2$ sterilants on *S. epidermis*, *E.coli* and *B.subtilis* spores was enhanced at 37 °C in comparison to 25 °C. Oxidising agents can exert sporicidal activity by damaging the spore inner membrane which subsequently ruptures following spore germination (Setlow, 2006). The oxidative potential of the $CuCl_2$ and $H_2O_2$ elements increase with an increase in temperature. This is because the increase in temperature could increase the reaction rate between Cu (II) and $H_2O_2$, thus increasing the generation of ·OH radicals (Zazo et al., 2010).

Within the present study, solution stability analysis was conducted to assess the impact of the sterilisation conditions (temperature at 37 °C, pH alteration to 7 ± 1, agitation at 110 RPM) on $CuCl_2$ and $H_2O_2$ concentration over time. The pH alterations to pH 7 (± 1) and temperature increase to 37 °C did not detrimentally impact $CuCl_2$ concentration in solutions, with fluctuations in the $CuCl_2$ concentrations being measured over 24 hours. However, the concentration of $H_2O_2$

in solutions containing 0.5 % and 1 % $H_2O_2$ combined with 0.1 mg/L and 1 mg/L $CuCl_2$ did decrease over 24 hours. Leow-Dyke et al. (2016) conducted solution stability analysis for the intended purpose of investigating storage conditions on solution stability. It was found that solutions of 0.1 mg/L $CuCl_2$ and 0.5 % $H_2O_2$, and 1 mg/L $CuCl_2$ and 0.5 % $H_2O_2$, exhibited steady $H_2O_2$ concentration readings over a period of 44 days at 4 °C, with a slight downward trend. Solutions containing of 0.1 mg/L $CuCl_2$ and 1 % $H_2O_2$ also displayed steady $H_2O_2$ concentration readings over a period of 44 days with no downward trend, and solutions containing 1 mg/L $CuCl_2$ and 1 % $H_2O_2$ demonstrated a rapid downward trend in $H_2O_2$ concentration, particularly in the period between 21 and 44 days. Free copper ions can induce the breakdown of $H_2O_2$ which can explain these observations. However, in the case of the present study the alterations in the $H_2O_2$ are most likely explained by the alterations in pH and temperature causing $H_2O_2$ to become unstable.

Concentrations of 0.1 mg/L and 1 mg/L $CuCl_2$, which are below the toxic levels for humans (Garba et al., 2006), in combination with 0.5 % and 1 % $H_2O_2$ were chosen for investigation within this study as these concentrations have been identified to exert biocidal and sporicidal effects against *S.epidermidis*, *E.coli* and *B.subtilis* spores (Leow-Dyke et al., 2017). The ability of a microbial inactivation process to eliminate bacterial spores determines whether the process can be considered a sterilisation method as opposed to a disinfection method (Leow-Dyke et al., 2017). As such, the microbial inactivation effects of the chosen $CuCl_2$ and $H_2O_2$ concentrations against *B.subtilis* spores was utilised within this study to optimise the concentrations and conditions for effective sterilisation. *B.subtilis* spores were selected within the present study because bacterial spores are the most resistant microorganisms against sterilisation methods, and *B.subtilis* spores have been demonstrated to be resistant to killing by heat, radiation, UV and gamma irradiation (Dai et al., 2016; Setlow, 2006). All four solutions were inoculated with $10^6$ spores and incubated at 37 °C, 110 RPM. It was shown that after 2 hours incubation, only 1 mg/L $CuCl_2$ and 1 % $H_2O_2$ killed all *B.subtilis* spores that were present. After 3 hours of exposure, 0.1 mg/L $CuCl_2$ and 1 % $H_2O_2$ also killed all *B.subtilis* spores, followed by 1 mg/L $CuCl_2$ and 0.5 % $H_2O_2$ after 4 hours exposure and finally 0.1 mg/L $CuCl_2$ and 0.5 %$H_2O_2$ after 5 hours of exposure. These findings indicated that concentration increases in $CuCl_2$ and $H_2O_2$ are associated with

enhanced sporicidal activity. Similar results were demonstrated by Leow-Dyke et al. (2017), whereby concentrations of 0.1 mg/L $CuCl_2$ and 1 % $H_2O_2$ had the shortest D-value for *S.epidermidis*, *E.coli* and *B.subtilis* spores. Although the D-values could not be determined at this stage in the current study, solutions containing 0.5 % $H_2O_2$ were eliminated from the study due to gradual sporicidal effects observed in comparison to the rapid sporicidal effects observed with 0.1 mg/L $CuCl_2$ and 1 % $H_2O_2$, and 1 mg/L $CuCl_2$ and 1 % $H_2O_2$.

Whether the sporicidal effects of inoculated sterilant solutions was translated to inoculated dPHV tissue was also determined. *B.subtilis* spores were deposited as deeply as possible within the pulmonary sinuses of each cusp forming the dPHV segments. This was considered to be a difficult area of the dPHV segment for the solutions to reach and effectively sterilise. Commonly in practice, sterilant exposure time is extended to achieve a 12 log reduction to obtain overkill sterilisation (von Woedtke and Kramer, 2008). Although the D-values could not be determined within this study, the decision was made to expose the inoculated tissue segments to 0.1 mg/L $CuCl_2$ and 1 % $H_2O_2$, and 1 mg/L $CuCl_2$ and 1 % $H_2O_2$ for 3 and 4 hours even though 1 mg/L $CuCl_2$ and 1 % $H_2O_2$ killed all *B.subtilis* spores present after 2 hours. No spore growth was observed for either 0.1 mg/L $CuCl_2$ and 1 % $H_2O_2$, and 1 mg/L $CuCl_2$ after 3 and 4 hours of exposure.

Tissue segments were exposed to 0.1 mg/L $CuCl_2$ and 1 % $H_2O_2$, and 1 mg/L $CuCl_2$ and 1 % $H_2O_2$ for 3 and 4 hours prior to conducting histological analysis. Leow-Dyke et al. (2016) showed that the histoarchitecture of dCELL dermis treated with a combination of $CuCl_2$ and $H_2O_2$ (pH 3 – 5) at concentration ranges of 0.1–10 mg/L and 0.01–1%, respectively, for 3 hours was not detrimentally impacted. Similar results were observed within this study whereby dPHV tissue segments treated with both 0.1 mg/L $CuCl_2$ and 1 % $H_2O_2$, and 1 mg/L $CuCl_2$ and 1 % $H_2O_2$ at pH 7 ± 1 for 3 hours did not impact the architectural structure of the tissue. Staining with H & E revealed the preservation of the tightly crimped ECM fibres at the pulmonary artery intima, the loose arrangement of the fibres at the adventitia, the clear definition of the valve leaflet layers, and the regularly arranged myocardium bundles. These findings were supported by Picrosirius Red and Miller's elastin staining which also demonstrated the uniform ECM arrangement of the treated dPHV segments, comparable to the untreated dPHV controls. However, histological

analysis revealed the detrimental impact to the dPHV artery intima and leaflet after 4 hours exposure to both sterilants. The intima of the artery treated with both 0.1 mg/L $CuCl_2$ and 1 % $H_2O_2$, and 1 mg/L $CuCl_2$ and 1 % $H_2O_2$ for 4 hours displayed a loose and unorganised arrangement of ECM fibres. Picrosirius Red and Miller's elastin staining determined these fibres to be elastin. H & E stain retention was less on the leaflet *ventricularis* and loose fibres were observed at both the leaflet *ventricularis* and *arterialis* layers of dPHV segments treated with both concentrations for 4 hours. Although the oxidative function of $H_2O_2$ is essential to achieve effective sterilisation of tissues and biomaterials, the potential implications to tissue integrity is not unknown. However, the disruption to the collagen integrity appeared less severe in dPHV segments treated with 1 mg/L $CuCl_2$ and 1 % $H_2O_2$ in comparison to 0.1 mg/L $CuCl_2$ and 1 % $H_2O_2$. Copper is known to play a role in the synthesis and stabilisation of elastin matrices present in ECM. Thus, it is plausible that the higher concentration of $CuCl_2$ used within this study protected the dPHV elastin stability.

Based on these results, 1mg/L $CuCl_2$ combined with 1 % $H_2O_2$ was the chosen solution to apply to whole dPHV roots for 3 hours at 34 °C, 110 RPM for effective sterilisation prior to conducting further biological and biomechanical analysis.

Histological visualisation of these samples revealed that the tightly packed and crimpled elastin fibres of the artery intima became porous, and there was damage to the leaflet elastin fibres following sterilisation. SEM analysis also demonstrated damage to the tissue surface microscopic structure. Whole dPHV roots were used as opposed to segments, and it is possible that residual $CuCl_2$ and $H_2O_2$ may have induced oxidative damage to the leaflets. The upscaling of tissue sterilisation may have also impacted the length of time that tissue was exposed to the sterilant by up to 30 minutes. Unpredictable fluctuations in $Cu^{2+}$ concentrations were also observed within the preliminary experiments and it is possible that the formation of hydroxyl radicals was not consistent leading to the observed ECM damage. It is possible that the oxidative effects of hydroxyl radicals may have altered the surface chemistry and therefore structure of the dPHV tissue (Finnegan et al., 2010). Furthermore, the dPHVs used for further biological and biomechanical analysis were not prepared alongside the dPHVs used for preliminary experiments. Segments of dPHVs were exposed to $CuCl_2$ and $H_2O_2$ for preliminary analysis,

whereas whole dPHV roots were exposed to $CuCl_2$ and $H_2O_2$ for further biological and biomechanical analysis, highlighting a discrepancy within this work. It is also possible that natural variation of the tissue also influenced the impact of 1mg/L $CuCl_2$ combined with 1 % $H_2O_2$ on dPHVs. These aspects would need to be further refined if this sterilisation method is commercially translated.

Antibody labelling of collagen IV and fibronectin revealed the retention of both proteins in artery and leaflet sections, comparable to the dPHV controls. Collagen IV and fibronectin are key ECM proteins with important roles in tissue recellularisation. Collagen IV is a dominant component of the basement membrane and is responsible for mediating tissue regeneration. Cellular responses can be influenced by collagen IV using the innate biologically active domains present, as well as providing anchor points for the affinity of molecules such as fibronectin which can facilitate cell migration and cell adhesion (Wiltz et al., 2013; Yurchenco, 2011). This suggests that dPHVs sterilised with 1 mg/L $CuCl_2$ and 1 % $H_2O_2$ do have the tools required for constructive recellularisation *in vivo*. It has been demonstrated that low levels of $H_2O_2$ (5-50 μM) are present in healing wounds, and the removal of $H_2O_2$ hinders wound healing. The mechanism underpinning this is that ROS may serve as messengers and regulators for cell signalling transduction and gene expression systems (Edwards et al., 2018; Roy et al., 2006). Copper has been proven to stimulate endothelial cell proliferation required for wound healing by upregulating the gene expression for vascular endothelial growth factor (VEGF), promoting the differentiation of mesenchymal stem cells (MSC) as well as the established antimicrobial properties used to avoid infections (Ali et al., 2018; Shi et al., 2016). Copper can augment the generation of hydrogen peroxide. Therefore potential trace quantities of $CuCl_2$ and $H_2O_2$ in addition to the retention of collagen IV and fibronectin may synergistically facilitate the regeneration of dPHVs *in vivo*. However, this has not yet been investigated within the literature.

In this study, there was no alteration found in the collagen content of 1 mg/L $CuCl_2$ and 1 % $H_2O_2$ wall and leaflet specimens in comparison to the dPHV controls. The quantification of collagen content can be determined using the hydroxyproline assay, as hydroxyproline is a major collagen constituent and plays a role in the stabilisation of the triple helical collagen structure (Leow-Dyke et al., 2016; Ramachandran et al., 1973).Within this current study, a significant decrease in the

thermal stability of the collagen within the treated tissue was found, in comparison to the dPHV controls. However, this reduction in the collagen thermal stability still falls within reported denaturation temperatures of collagen present in natural tissues at 62 °C to 68 °C (Goissis et al., 2000). It is documented that metal ions such as cuprous and cupric ions in combination with $H_2O_2$ can mediate damage to collagen by binding to certain proteins to form protein-Cu(II) complexes, resulting in site-specific cross-linking, carboxylation and fragmentation of collagen (Hawkins, C.L. and Davies, 1997). These alterations may have occurred to the dPHVs treated with $CuCl_2$ and $H_2O_2$, and it is possible that the tertiary structure of the collagen was altered as a result. Although, Leow-Dyke et al. (2016) found no evidence of collagen tertiary structure alterations of $CuCl_2$ and $H_2O_2$ treated dCELL dermis as the susceptibility of the tissue to enzyme digestion did not increase in comparison to the non-treated dCELL dermis. The $CuCl_2$ and $H_2O_2$ treatment was carried out at 25 °C by Leow-Dyke et al. as an attempt to prevent the accelerated decomposition of $H_2O_2$. Leikina et al. (2002) reported that collagen is unstable at human physiological temperatures and found that human lung type I collagen monomers unfold and form random coils at 37 °C within 2 days. Collagen triple helices reform at temperatures below 30 °C. Within this study, $CuCl_2$ and $H_2O_2$ treatment was carried out at 37 °C to enhance sporicidal activity. It is possible that the natural collagen conformational changes that occur at 37 °C may have made collagen more susceptible to $H_2O_2$ and cuprous and cupric ion mediated damage.

It is reported that elevated levels of ROS can disturb GAG expression and GAG synthesis. This has been described to occur as a result of the fragmentation of link proteins and the inhibition of proteoglycan monomers association with other ECM components (Roberts et al., 1989). Rieder, B. et al. (2018) found that elevated levels of $H_2O_2$ reduced GAG content and GAG formation in chondrogenic mesenchymal stem cell pellet cultures. However, within this study there was no alteration of GAG content found in dPHVs following exposure to $CuCl_2$ & $H_2O_2$ sterilisation. Despite there being consensus that ROS can disrupt the presence of GAGs in tissue, there are many findings that evidence the antioxidant properties of GAGs. It is proposed that the carboxylic groups found in GAGs may interact with transition metal ions such as $Cu^{2+}$ which initiates Fenton's reaction. This in turn exerts a chelating mechanism which scavenges ROS (Campo et al., 2004).

Cao, B. et al. (2012) have reported the cytotoxic effects of copper ions released from commercially available copper-containing intrauterine device contraceptives on L929 fibroblasts. Within this study, $CuCl_2$ & $H_2O_2$ sterilisation treatment of dPHVs did not negatively impact the growth and morphology of L929 fibroblasts in contact with the $CuCl_2$ & $H_2O_2$ sterilised tissue. There was no evidence of toxins leaching from the $CuCl_2$ & $H_2O_2$ sterilised tissue as L929 cell proliferation and viability was not impaired following incubation with $CuCl_2$ & $H_2O_2$ tissue extracts. This suggests that dPHVs were adequately rinsed following sterilisation with $CuCl_2$ & $H_2O_2$ to remove any potential cytotoxic residues. Additionally, $H_2O_2$ has non-toxic breakdown products of water and oxygen, and the $CuCl_2$ concentrations used within this study (0.1 mg/L and 1 mg/L $CuCl_2$) are below the toxic levels for humans (Garba et al., 2006). Similar results were reported by Leow-Dyke et al. (2017), whereby all combination sterilants investigated did not induce a cytotoxic effect on human skin fibroblasts, with the exception of 10 mg/L $CuCl_2$ combined with 1 % $H_2O_2$ which displayed a slight cytotoxic effect.

Within this study, there was found to be a significant reduction in the collagen phase slope and ultimate tensile strength of circumferentially orientated $CuCl_2$ & $H_2O_2$ treated leaflet specimens. The load-bearing collagen fibres in PHV leaflets are circumferentially aligned which may be the reason for the significant reductions to the mechanical parameters only for the circumferentially orientated leaflet specimens. Damage to the collagen fibres as a consequence of oxidative degradation of ECM components is the most likely cause for this, and this result correlates with the tissue surface microstructure observations and reduction in thermal stability of tissue treated with $CuCl_2$ & $H_2O_2$. Similar results were reported by Hennessy et al. (2017), whereby leaflets sterilised with 6 % liquid hydrogen peroxide demonstrated a reduction in the stiffness and ultimate tensile strength of decellularised leaflets.

Based on the findings presented within this study, 1mg/L $CuCl_2$ combined with 1 % $H_2O_2$ sterilisation treatment requires further optimisation to be compatible with dPHV tissue, as well as further validation.

# Chapter 5 : The Impact of Supercritical Carbon Dioxide Sterilisation on the Biological and Biomechanical Properties of Decellularised Heart Valves

## 5.1 Introduction

Despite extensive research into decellularised heart valves, a terminal sterilisation process has not yet been included after the decellularisation procedure. The CryoValve SynerGraft pulmonary allograft is not exposed to terminal sterilisation as the human tissue is handled aseptically throughout processing (Brown, J. et al., 2011). Sterilisation is essential to eliminate microorganisms from the decellularised valves, but this needs to be effective without adversely affecting the valve's biomechanical, biocompatible, and functional properties. Terminal sterilisation (a process whereby a product is sterilised within its final container) can enhance the safety of biological heart valve replacements by providing a superior sterility assurance level (SAL). Sterility of an object is defined as the absence of viable microorganisms that could otherwise introduce adverse effects when administered. This includes spore forming bacteria, non-spore forming bacteria, fungi, protozoa and viruses. According to EN 556-1 and ISO 14937-2009 standards, a SAL of at least $10^{-6}$ is the requirement for designating a terminally sterilised product as 'sterile' (ISO, 2009; BSI, 2001b). This refers to the probability that no more than one device with a viable microorganisms will be detected out of one million sterilised devices (von Woedtke and Kramer, 2008).

$ScCO_2$ for sterilisation was first explored in the food sciences field by Kamihira et al. (1987), who found that $ScCO_2$ with ethanol and acetic acid exhibited biocidal effects against *Escherichia coli, Staphylococcus aureus* and conidia of *Aspergillus niger* in baker's yeast. The diverse potential applications for $ScCO_2$ have become apparent over the past decade, and the application of $ScCO_2$ for biomaterial processing has become common within the field. Optimal conditions required for effective $ScCO_2$ sterilisation are ideal for the sterilisation of decellularised tissues and biomaterials. The critical point of carbon dioxide ($CO_2$) is achieved at a temperature of 31.1°C and a pressure of 1099 psi (Figure 5.1), making it ideal for sterilisation of tissues and materials that are sensitive to heat and pressure degradation. $ScCO_2$ is non-toxic and does not leave toxic residuals which will

reduce the possibility of a cytotoxic response. Furthermore, $ScCO_2$ is considered to be a terminal sterilisation method as it has a low viscosity and surface tension, making it an ideal choice for the penetration of tissues and materials along with their appropriate packaging.

Many mechanisms exerted by $ScCO_2$ for microorganism inactivation have been proposed. This includes acidification as $CO_2$ reacts with water, producing carbonic acid which accumulates within cells, ultimately reducing intracellular pH (Tao et al., 2021). Another mechanism is the disruption of the lipid bilayer by the mass transfer of $CO_2$, increasing the fluidity and permeability of the microorganism's phospholipid bilayer that is left unable to reform properly following the removal of the $CO_2$. There is also the possibility of essential enzyme and intracellular component denaturation and extraction which could arise from the reduction in intracellular pH as well as the mass transfer of $CO_2$ (Ribeiro, Nilza et al., 2020; Spilimbergo and Bertucco, 2003; White, A. et al., 2006). Total microbial inactivation using $ScCO_2$ alone requires harsh conditions, such as high temperature and pressure or a prolonged incubation time, making it unsuitable for heat sensitive tissue and material applications (Watanabe, T. et al., 2003). Therefore, the inclusion of volatile additives such as peroxides and carboxylic acids supplement $ScCO_2$ microorganism inactivation by allowing sterilisation to be achieved at the ideal conditions of 31.1°C, 1099 psi. Peroxides and carboxylic acids contribute towards intracellular acidification as well as being mass transferred to exert microbicidal effects on intracellular components (Russell et al., 2015; White, A. et al., 2006).

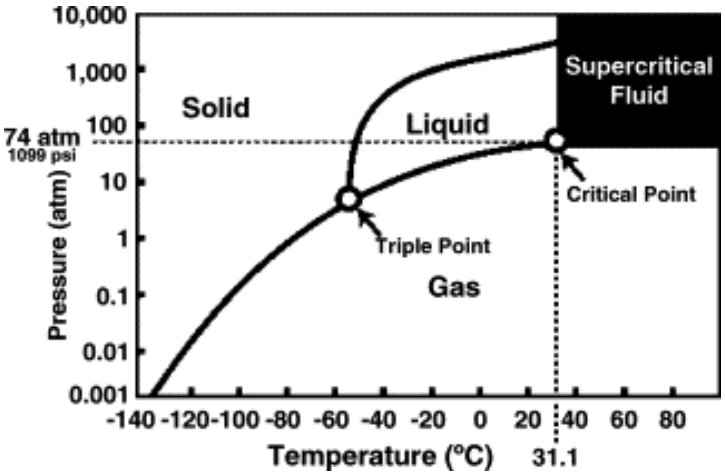


**Figure 5.1. Carbon Dioxide Phase Diagram.** Carbon dioxide transitions to supercritical state at the critical points of 31.1°C and 1099 psi. Figure taken from White, A. et al. (2006).

Specific parameters, and conditions used for $ScCO_2$ processing along with PAA and $H_2O_2$ additives for the sterilisation of tissue grafts was successfully patented and commercialised by NovaSterilis (NovaSterilis, NY), demonstrating the commercial viability of $ScCO_2$ sterilisation. The NovaProcess™ achieves the industry standard SAL $10^{-6}$ after optimisation of temperature, pressure, agitation and additive parameters for the tailored sterilisation of specific materials. As such, $ScCO_2$ has been employed by several different research groups for the tailored sterilisation of tissues such as lung matrix, aortic heart valves, bone and tendon, and dermal matrix (Balestrini et al., 2016; Hennessy et al., 2017; Nichols et al., 2009; Qiu et al., 2009).

The structural and functional properties of biological tissue scaffolds exposed to $ScCO_2$ sterilisation would not be compromised as $CO_2$ is non-reactive, and this has been analysed in several studies. Nichols et al. (2009) observed that $ScCO_2$ and PAA additive sterilisation of human tendon and cortical bone allografts did not impose any detrimental effects on the tissue biomechanical properties in comparison to gamma irradiation.

A study investigating the impact of various sterilisation techniques including $ScCO_2$ sterilisation on the material properties of decellularised porcine aortic valves was conducted by Hennessy et al. (2017). It was shown that the use of $ScCO_2$ with the enhancing reagents was the superior of the sterilisation techniques investigated, which included gamma irradiation and $H_2O_2$. $ScCO_2$ treatment did not adversely affect the decellularised porcine aortic leaflet specimen tensile stiffness in comparison to the non-sterile decellularised porcine aortic leaflet specimens which was verified using uniaxial tensile testing.

The properties of $ScCO_2$ can be further exploited to be relevant to other tissue engineering applications, one of which is decellularisation of tissue grafts. This may be because $ScCO_2$ is able to solubilise polar cellular components such as phospholipids, which are fundamental elements of cell membranes. These solubilised polar molecules are subsequently extracted whilst non-polar molecules of the ECM are preserved (Gafarova et al., 2020; Wang, C.-H. et al., 2020). The high pressure required for $CO_2$ to reach supercritical state can also cause cell lysis, and the resultant cellular fragments can be extracted upon depressurisation (Gafarova et al., 2020). In a study conducted by Gafarova et al. (2020), $ScCO_2$ assisted

decellularisation of sheep aortic heart valve roots was explored and compared to ethanol and alkaline based decellularisation protocols without the assistance of $ScCO_2$. Histological analysis using H & E, Picrosirius red and Weigert staining demonstrated preserved integrity of the ECM. There was also reduced cytotoxicity in comparison to the protocols that did not include $ScCO_2$ processing. However, there was an increase in ultimate tensile strength and Young's modulus of the aortic valve leaflets in the samples exposed to $ScCO_2$ which may have been due to dehydration of the tissue.

To my knowledge, the impact of $ScCO_2$ as a sterilisation method on porcine pulmonary heart valves is yet unexplored within the literature. Pulmonary and aortic heart valves have different material properties, with the aortic heart valve tissue typically being thicker and therefore possessing different mechanical and histological properties in comparison to pulmonary heart valve tissue (Matthews et al., 2010). Additionally, the impact of $ScCO_2$ on the biological and biomechanical properties of decellularised porcine pulmonary heart valves (dPHVs) that have been decellularised using a specifically designed method that incorporates 0.1 % SDS, nuclease and protease inhibitors has not yet been reported (Luo et al., 2014).

## 5.2 Aims and Objectives

### 5.2.1 Aim

The aim of the work described in this chapter was to characterise the effects of $ScCO_2$ on the biological and biomechanical properties of porcine pulmonary heart valves decellularised using a method incorporating 0.1 % SDS, nuclease and protease inhibitors (Luo et al., 2014).

### 5.2.2 Objectives

i. To produce decellularised porcine pulmonary heart valves and expose them to $ScCO_2$ treatment under 2 different conditions; whilst packaged in poly-Tyvek pouches (NovaPouch™) and whilst submerged in PBS

ii. To determine the impact of $ScCO_2$ treatment on the structure of collagen, elastin and specific membrane proteins within decellularised porcine pulmonary heart valves, using histological staining and immunohistochemistry antibody labelling

iii. To determine the impact of $ScCO_2$ treatment on the surface structure of decellularised porcine pulmonary heart valve leaflets and pulmonary artery using scanning electron microscopy

iv. To determine the impact of $ScCO_2$ treatment on the biochemical composition of decellularised porcine pulmonary heart valves, through quantification of collagen and glycosaminoglycans

v. To determine the impact of $ScCO_2$ treatment on the denaturation temperature of the collagen within decellularised porcine pulmonary heart valve ECM, using differential scanning calorimetry

vi. To determine the *in vitro* biocompatibility of $ScCO_2$ treated decellularised porcine pulmonary heart valves using contact and extract cytotoxicity assays

vii. To determine the impact of $ScCO_2$ treatment on the mechanical properties of decellularised porcine pulmonary heart valves, using uniaxial tensile testing of dPHV wall and leaflet specimens.

## 5.3 Study Experimental Approach

Decellularised porcine pulmonary heart valves were exposed to a $ScCO_2$ process patented and performed by NovaSterilis (NY). Samples were sterilised under two different conditions. One condition was that samples were sealed into Poly-Tyvek pouches with NovaKill™ oxidising agent propriety additive (containing PAA and $H_2O_2$) added to the reaction vessel, which is the standard ScCO2 sterilisation processing performed by NovaSterilis (NY). Initial macroscopic observations following $ScCO_2$ treatment under these standard conditions informed the decision to explore $ScCO_2$ treatment of samples whilst submerged in PBS, with NovaKill added to the PBS surrounding the samples. The biological and biomechanical properties of decellularised porcine pulmonary heart valves (dPHVs) were characterised as described by the schematic in Figure 5.2.

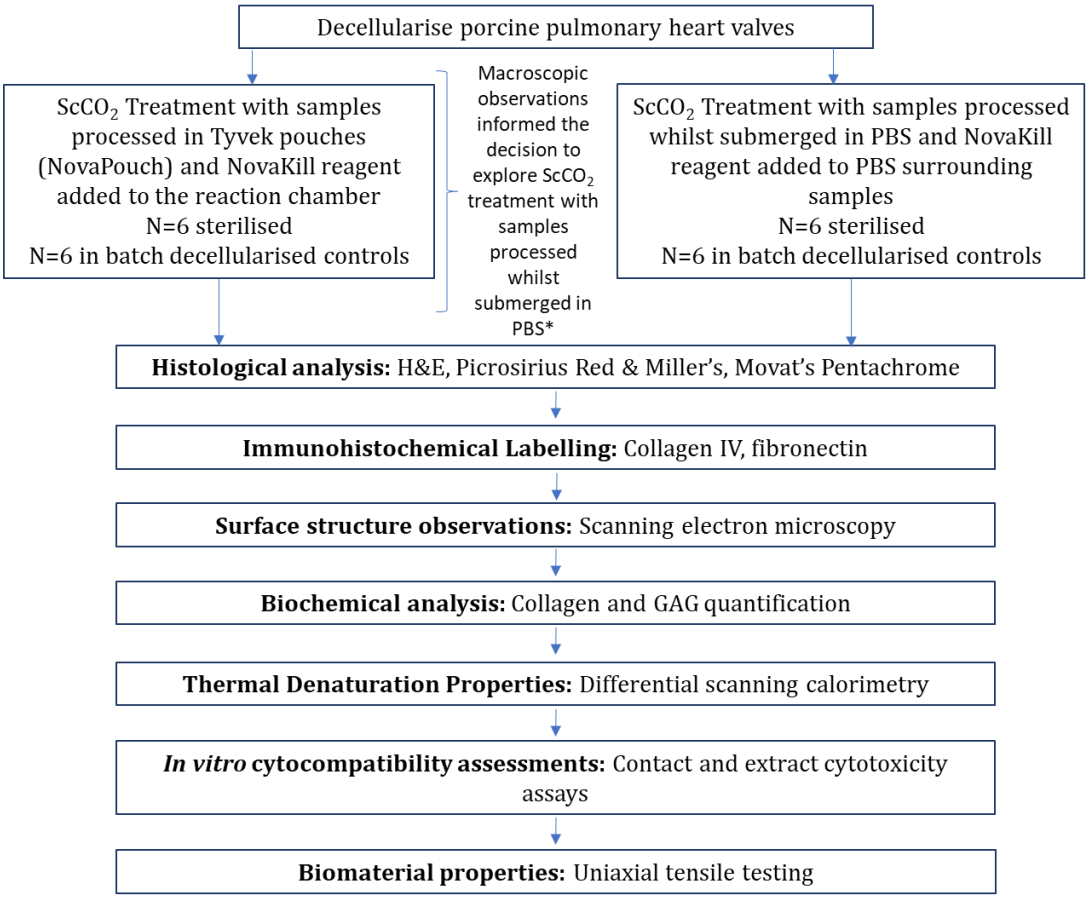


**Figure 5.2 Schematic of the Experimental Approach Adopted to Characterise the Impact of $ScCO_2$ Sterilisation on the Biological and Biomechanical Properties of Decellularised Porcine Pulmonary Heart Valves**

## 5.4 Methods

### 5.4.1 Production of Decellularised Porcine Pulmonary Heart Valves

Porcine pulmonary heart valves were acquired and decellularised as described in section 2.2.3.

### 5.4.2 $ScCO_2$ Sterilisation

A batch of dPHV roots (n=6) were placed into sterile polypropylene containers with 100 mL of PBS and shipped to NovaSterilis Inc (NY, USA) on ice packs. The valve samples were then stored at 4°C until processing. Each valve sample was removed from its container, drained of PBS, and transferred to a poly-Tyvek pouch (hereon referred to as NovaPouch. The pouches were heat sealed and then placed and sealed in individual secondary NovaPouch. The NovaPouches were then placed into Nova2200™ $ScCO_2$ reaction chamber, along with 25 mL water and NovaKill™ proprietary additive (4 mL; 13.5 - 18.5 % [v/v] PAA and 4.5 - 6 % [v/v] $H_2O_2$) on a cellulose pad. The $ScCO_2$ sterilisation equipment workflow is displayed in Figure 5.3. $CO_2$ was injected into the chamber to achieve a pressure of 1,410 psi, and the temperature was held at 35 °C for 2 hours. An extraction run was then conducted for 1 hour, under the same conditions except in the absence of NovaKill™.

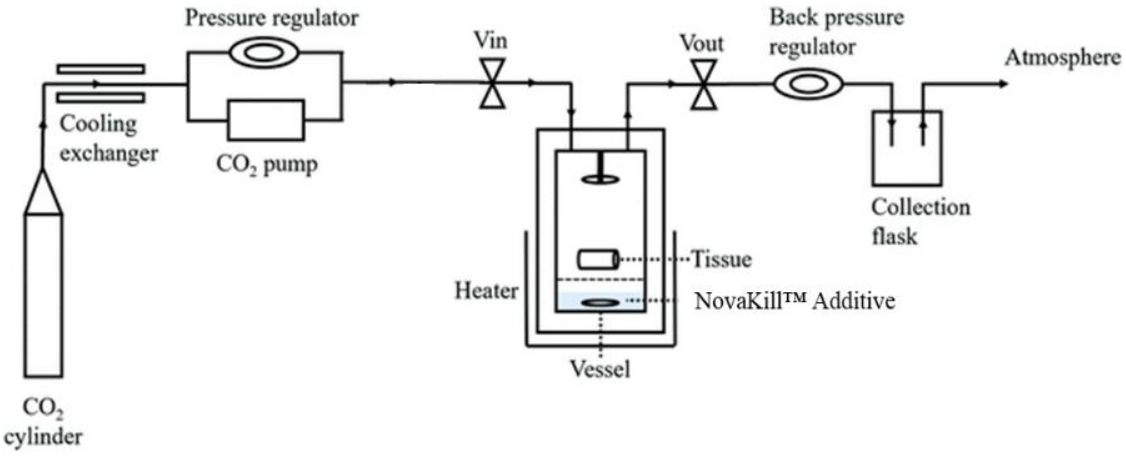


**Figure 5.3 $ScCO_2$ Equipment Workflow Schematic.** A high-pressure pump is used to insert $CO_2$ into the temperature-regulated reaction vessel until the desired pressure is reached. The back pressure regulator controls depressurisation, and extracted components are emptied into the collection flask. Figure adapted from Duarte et al. (2022).

Another set of dPHV roots (n=6) were subjected to the same $ScCO_2$ sterilisation treatment, but the individual dPHV roots were in 150 mL polypropylene containers whilst submerged in 120 mL PBS containing NovaKill (13.5 - 18.5 % [v/v] PAA and 4.5 - 6 % [v/v] $H_2O_2$) with a 3" x 3" Tyvek square placed and held over the top of the container with a perforated lid during the treatment cycle. Prior to undergoing the treatment cycle, the containers were also individually sealed into poly-Tyvek pouches.

Sterilisation was verified by *Bacillus atrophaeus* biological indicators (MesaLabs, 1-6100) that were processed in parallel with test samples. The sterilisation of samples submerged in PBS and NovaKill additive during processing was verified with the same containers containing the same PBS and NovaKill solution spiked with *B. atrophaeus* spore suspension. Unprocessed *B. atrophaeus* spores were also used as positive controls. Surviving *B. atrophaeus* spores were recovered from the biological indicators, processed and plated onto 1.5% Trypticase Soy Agar for enumeration. Samples were then shipped back to the University of Leeds on ice packs. Controls used in the experiments were dPHVs (n=6 per treatment condition) that were sent alongside test samples to NovaSterilis but were not exposed to any sterilisation treatment.

### 5.4.3 Histological Analysis

To assess the impact of $ScCO_2$ sterilisation on the histoarchitecture of dPHVs, Control dPHV roots, $ScCO_2$ (NovaPouch) roots and $ScCO_2$ (Submerged in PBS) roots were dissected longitudinally, incorporating half a leaflet, pulmonary artery wall and myocardium skirt (N=3 each). These tissue samples were then processed and sectioned as described in section 2.2.4. Staining of sections with H & E, Picrosirius Red & Miller's Elastin, and Movat's Pentachrome was conducted as described in sections 2.2.5.1, 2.2.5.2, and 2.2.5.3.

### 5.4.4 Immunohistochemical Labelling of Collagen IV and Fibronectin

To assess the impact of $ScCO_2$ sterilisation on the preservation of collagen IV and fibronectin in dPHVs, Control dPHV roots, $ScCO_2$ (NovaPouch) roots and $ScCO_2$ (Submerged in PBS) roots were dissected longitudinally, incorporating half a

leaflet, pulmonary artery wall and myocardium skirt (N=3 each). Processing and sectioning of tissue was conducted as described in section 2.2.4. Labelling of sections with specific antibodies against collagen IV and fibronectin was conducted as described in section 2.2.6.

### 5.4.5 Visualisation of Tissue Surface Microscopic Structure

Scanning electron Microscopy (SEM) was used to visualise the impact of $ScCO_2$ (NovaPouch) and $ScCO_2$ (Submerged in PBS) sterilisation on dPHV pulmonary artery wall and leaflet surface microscopic structures (N=3 each), as described in section 2.2.1.2.4.

### 5.4.6 Quantification of Collagen Content

Pulmonary artery wall (N=6 per group) and leaflet (N=6 per group) collagen content for dPHV control, $ScCO_2$ (NovaPouch) and $ScCO_2$ (Submerged in PBS) dPHVs was quantified as described in section 2.2.8.3.

### 5.4.7 Quantification of GAG Content

Pulmonary artery wall (N=6 per group) and leaflet (N=6 per group) GAG content for dPHV control, $ScCO_2$ (NovaPouch) and $ScCO_2$ (Submerged in PBS) dPHVs was quantified as described in section 2.2.8.4.

### 5.4.8 DSC Analysis

The collagen denaturation temperature of dPHV control, $ScCO_2$ (NovaPouch) and $ScCO_2$ (Submerged in PBS) pulmonary artery wall (N=6 per group) and leaflet (N=6 per group) samples was determined using DSC, as described in section 2.2.7.

### 5.4.9 *In Vitro* Cytocompatibility Assessments

The *in vitro* cytocompatibility of $ScCO_2$ (NovaPouch) and $ScCO_2$ (Submerged in PBS) pulmonary artery wall and leaflet samples was assessed using contact

cytotoxicity (N=3) as described in section 2.2.10.1 and extract cytotoxicity assays (N=6), as described in section 2.2.10.2.

### 5.4.10 Uniaxial Tensile Testing

The dPHV control, $ScCO_2$ (NovaPouch) and $ScCO_2$ (Submerged in PBS) pulmonary artery wall and leaflet samples were subject to uniaxial tensile testing, as described in section 2.2.12.

## 5.5 Results

### 5.5.1 Macroscopic Observations of $ScCO_2$ dPHVs

All dPHVs appeared compressed within the NovaPouches following $ScCO_2$ (NovaPouch) sterilisation, as shown in Figure 5.4 (n=6). The pulmonary artery lumen required manipulation to open due to the compression of the whole dPHV root. These observations informed the decision to explore $ScCO_2$ treatment of samples whilst submerged in PBS, with NovaKill added to the PBS surrounding the samples.

dPHV samples sterilised with $ScCO_2$ whilst submerged in PBS did not appear compressed. The pulmonary artery lumen was still open and the whole dPHV root appeared as it did prior to $ScCO_2$ sterilisation (Figure 5.4).

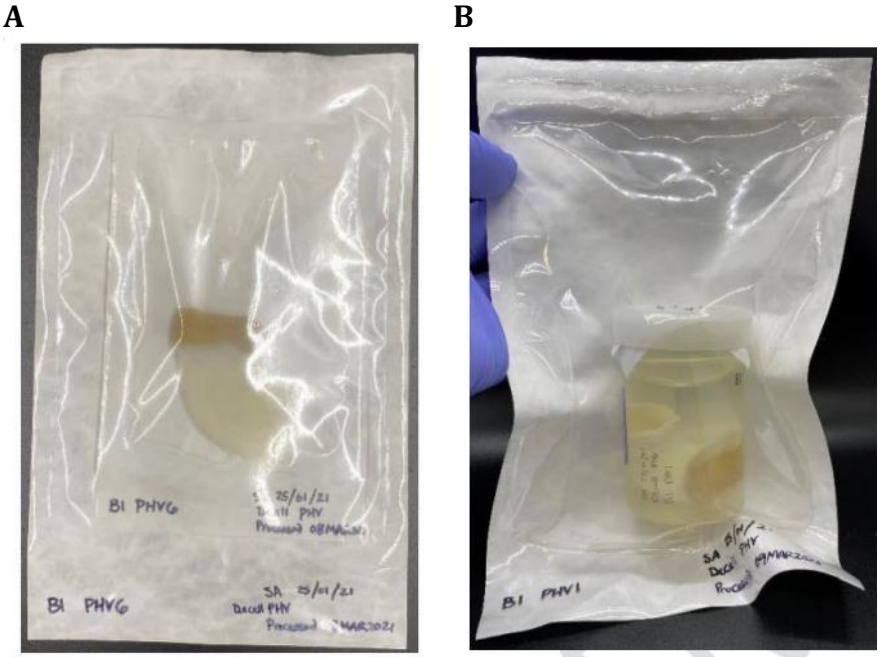


**Figure 5.4 Macroscopic Structure of dPHV Sterilised with $ScCO_2$ (A) Whilst Packaged in a NovaPouch and (B) Whilst Submerged in PBS.** Representative images shown, N=6 per group.

### 5.5.2 Histological Analysis

To characterise the impact of $ScCO_2$ treatment on the structure of collagen, elastin and specific basement membrane proteins within dPHVs, H & E, Picrosirius Red & Miller's Elastin, and Movat's Pentachrome staining was used.

H & E staining defined the gross ECM histoarchitecture of the tissue sections (Figure 5.5). The intensity of the H & E stain on the artery intima suggested the

abundant presence of collagen and elastin fibres in all groups. The tightly crimped fibres of the ECM appeared well preserved between the control and both $ScCO_2$ (NovaPouch) and $ScCO_2$ (Submerged in PBS) dPHV artery wall intima sections. The loosely organised adventitial surface ECM between control, $ScCO_2$ (NovaPouch) and $ScCO_2$ (Submerged in PBS) was also similar. The well-defined *arterialis*, *fibrosa*, *spongiosa*, and *ventricularis* layers of the leaflet are observed in the dPHV control section. These layers were also clearly displayed in $ScCO_2$ (Submerged in PBS) leaflet sections. However, these layers cannot be as easily defined in the $ScCO_2$ (NovaPouch) leaflet section (Figure 5.5 H). Although the $ScCO_2$ (NovaPouch) leaflet appears compressed, the fibres in the interstitial space are organised and connected. The myocardium bundles between all 3 groups appear regularly arranged.

Picrosirius Red & Miller's elastin staining was used to stain collagen and elastin fibres within the ECM of the tissue sections (Figure 5.6). Visualisation under normal Köhler illumination revealed collagen and elastin fibres. Visualisation under polarised light conditions revealed the configuration and distribution of collagen fibres, with the birefringence of the collagen fibres being associated with the fibre diameter. The tightly crimped structures of the collagen and elastin fibres again appeared well preserved between the control and both $ScCO_2$ (NovaPouch) and $ScCO_2$ (Submerged in PBS) dPHV artery wall intima sections. However, the intensity of the collagen stain was not as strong in $ScCO_2$ (Submerged in PBS) dPHV artery wall intima in comparison to the control and $ScCO_2$ (NovaPouch) artery wall intima. This could potentially be due to the arrangement of the tissue during preparation of the tissue for sectioning, whereby a clear cross-section displaying the collagen fibres could not be obtained. Elastin staining showed a greater intensity of elastin fibres in $ScCO_2$ (NovaPouch) and $ScCO_2$ (Submerged in PBS) artery wall intima in comparison to the dPHV control. This was also apparent in the artery wall adventitia. The artery wall adventitia of all groups displayed mainly collagen fibres, with small blood vessels lined with collagen and elastin fibres observed in the adventitial space. An elastic fibre network was present in the leaflet *ventricularis* of control, $ScCO_2$ (NovaPouch) and $ScCO_2$ (Submerged in PBS) dPHV leaflet specimens. The intensity of collagen staining was greatest in all layers of the $ScCO_2$ (NovaPouch) leaflet with little green colour being observed, and interstitial collagen fibrils appeared larger due to the tightly packed arrangement.

An interspersed network of collagen was found in between the myocardium bundles of all 3 groups.

These findings were supported by Movat's Pentachrome staining (Figure 5.7), which was used to visualise collagen (yellow), elastin (black), muscle (red), and GAGs, (blue). The pulmonary artery intima of all 3 groups maintained the tightly crimped arrangement of collagen and elastin fibres, and the adventitia displayed a loosely organised structure. $ScCO_2$ (NovaPouch) and $ScCO_2$ (Submerged in PBS) dPHV leaflets maintained similar arrangements of collagen and elastin fibres in all layers, but the presence of GAGs was sparse in comparison to dPHV control leaflet.

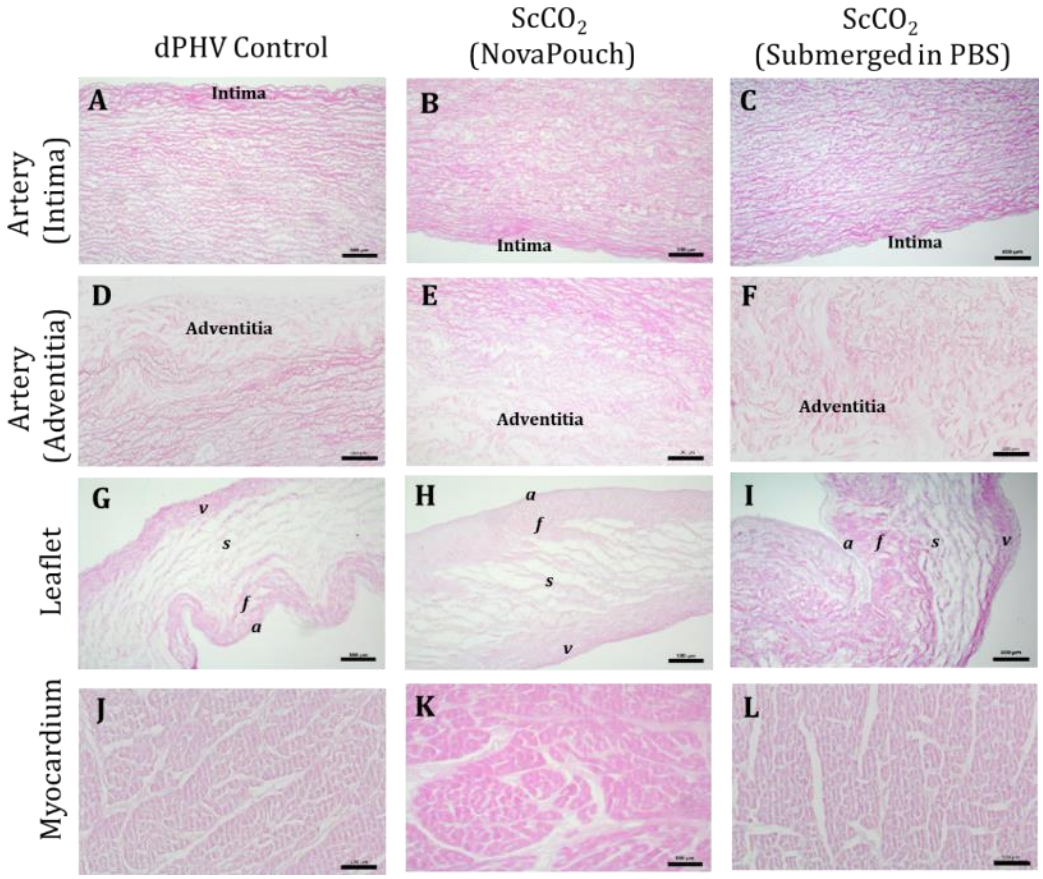


**Figure 5.5 Representative Images of Control, $ScCO_2$ (NovaPouch), and $ScCO_2$ (Submerged in PBS) dPHV Artery Wall Intima, Adventitia, Leaflet, and Myocardium Sections Stained With H & E.** Images show control dPHV wall intima (A), adventitia (D), leaflet (G), and myocardium (J); $ScCO_2$ (NovaPouch) dPHV wall intima (B), adventitia (E), leaflet (H) and myocardium (K); $ScCO_2$ (Submerged in PBS) dPHV wall intima (C), adventitia (F), leaflet (I) and myocardium (L). Images were taken using Köhler illumination and a x 10 objective. *v: ventricularis; s: spongiosa; f: fibrosa; a: arterialis.* Representative images shown, Scale bars 100 μm.

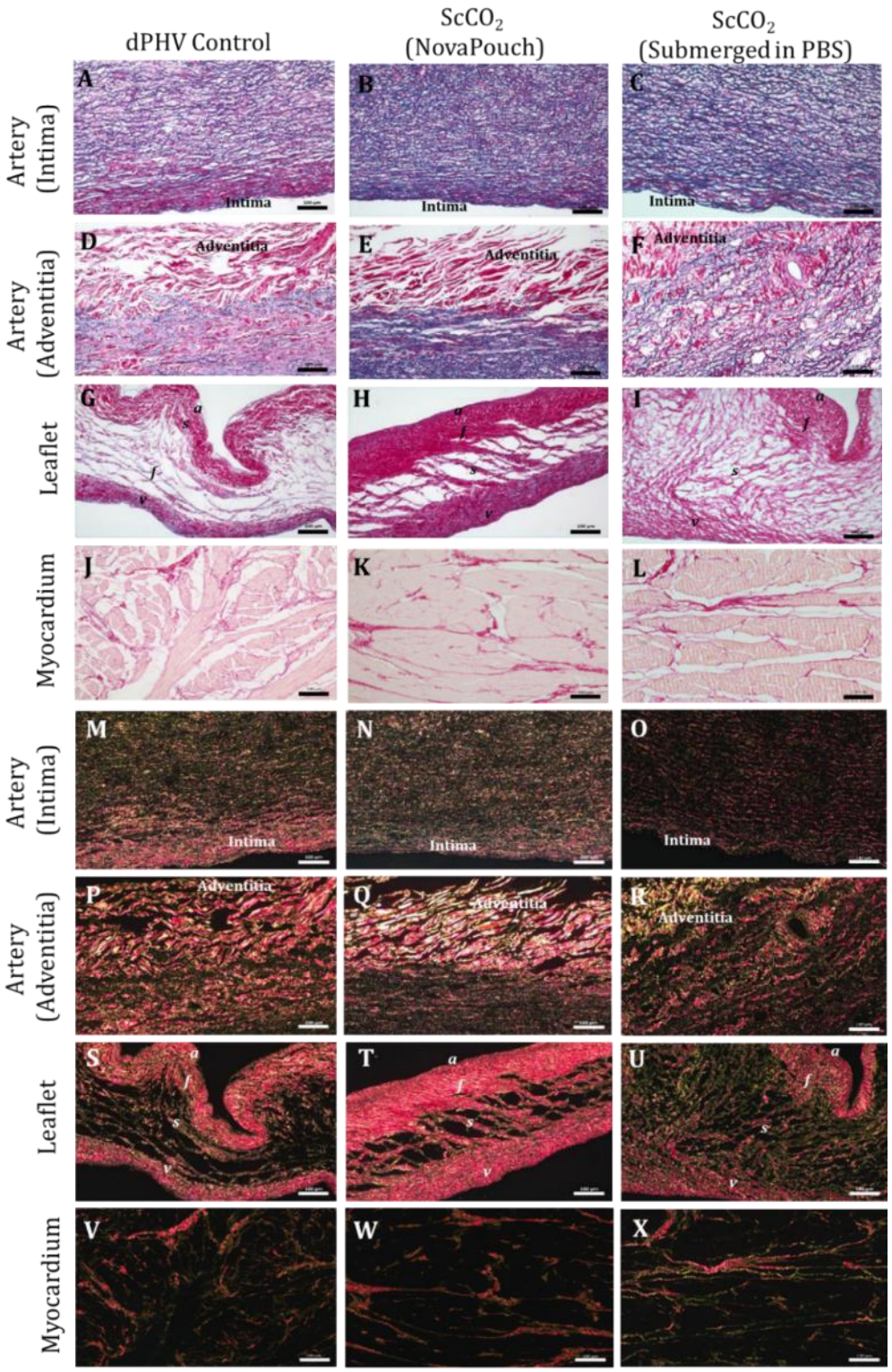


**Figure 5.6 Representative Images of Control, $ScCO_2$ (NovaPouch), and $ScCO_2$ (Submerged in PBS) dPHV Artery Wall Intima, Adventitia, Leaflet, and Myocardium Sections Stained with Picrosirius Red & Miller's Elastin.** Images show control dPHV wall intima (A, M), adventitia (D, P), leaflet (G, S), and myocardium (J, V); $ScCO_2$ (NovaPouch) dPHV wall intima (B, N), adventitia (E, Q), leaflet (H, T) and myocardium (K, W); $ScCO_2$ (Submerged in PBS) dPHV wall intima (C, O), adventitia (F, R), leaflet (I, U) and myocardium (L, X). Images were taken using Köhler illumination (A-L) and polarised light conditions (M-X), using a x 10 objective. *v: ventricularis; s: spongiosa; f: fibrosa; a: arterialis.* Representative images shown, Scale bars 100 μm.

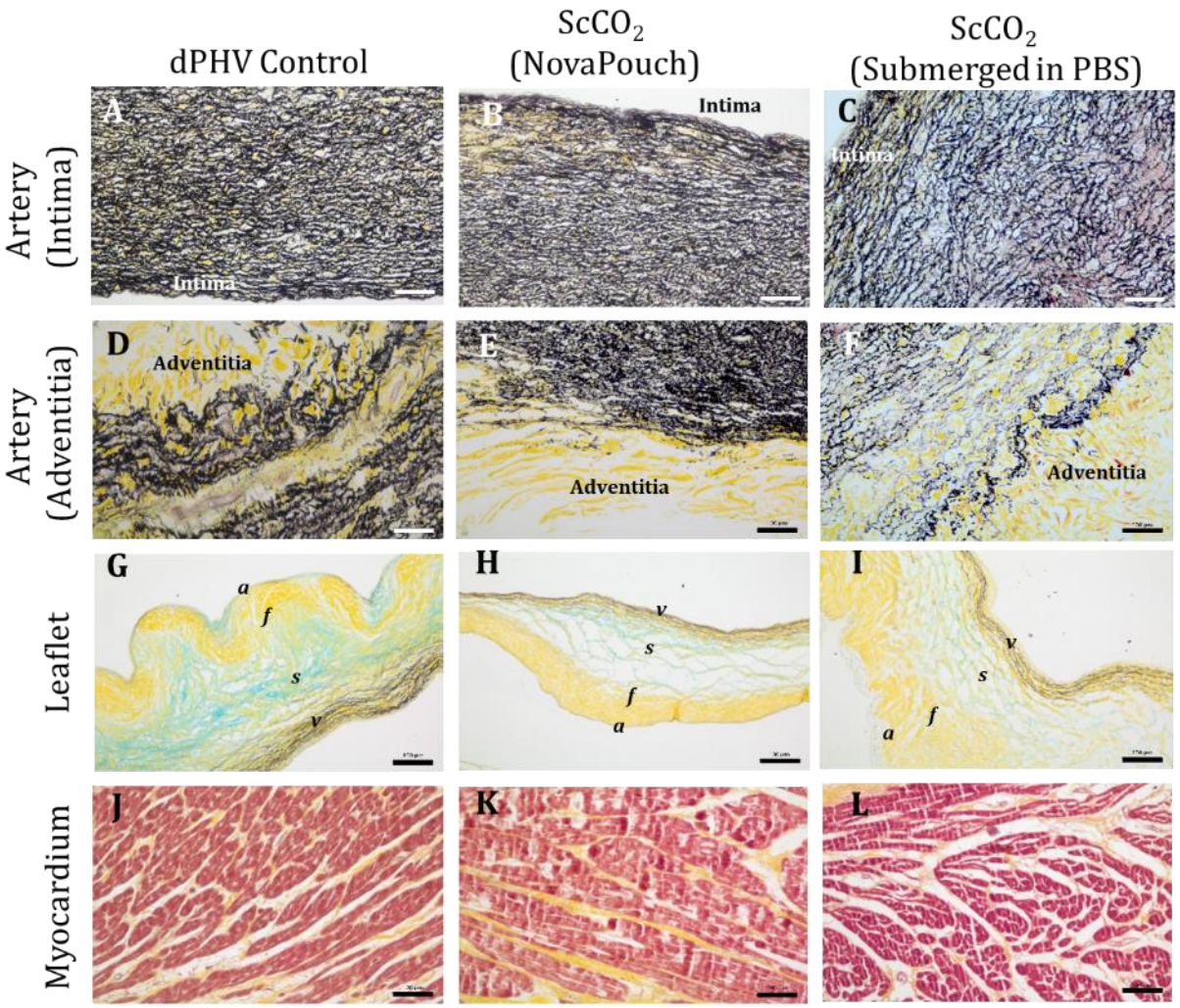


**Figure 5.7 Representative Images of Control, $ScCO_2$ (NovaPouch), and $ScCO_2$ (Submerged in PBS) dPHV Artery Wall Intima, Adventitia, Leaflet, and Myocardium Sections Stained With Movat's Pentachrome.** Images show control dPHV wall intima (A), adventitia (D), leaflet (G), and myocardium (J); $ScCO_2$ (NovaPouch) dPHV wall intima (B), adventitia (E), leaflet (H) and myocardium (K); $ScCO_2$ (Submerged in PBS) dPHV wall intima (C), adventitia (F), leaflet (I) and myocardium (L). Images were taken using Köhler illumination and a x 10 objective. *v: ventricularis; s: spongiosa; f: fibrosa; a: arterialis.* Representative images shown, Scale bars 100 µm.

### 5.5.3 Immunohistochemical Labelling of Collagen IV and Fibronectin

dPHV control, $ScCO_2$ (NovaPouch) and $ScCO_2$ (Submerged in PBS) dPHVs were labelled with monoclonal antibodies against collagen IV and fibronectin.

As shown in Figure 5.8, the intensity of the collagen IV positive labelling was less on the $ScCO_2$ (NovaPouch) artery intima surface in comparison to the dPHV control and was significantly reduced on the $ScCO_2$ (Submerged in PBS) artery intima surface. The loosely organised adventitial surface of the $ScCO_2$ (NovaPouch) pulmonary artery did not display any evidence of the presence of collagen IV. $ScCO_2$ (Submerged in PBS) artery adventitia did display positive staining, particularly in the lining of blood vessels. Both $ScCO_2$ (NovaPouch) and $ScCO_2$ (Submerged in PBS) treated leaflets showed almost no positive collagen IV labelling, except a faint brown line of staining across the *arterialis* surface of the of the $ScCO_2$ (NovaPouch) leaflet. The myocardium displayed a network of defined positive labelling in all 3 groups with greatest intensity in the lining of blood vessels. There was no staining observed in sections stained with the isotype control.

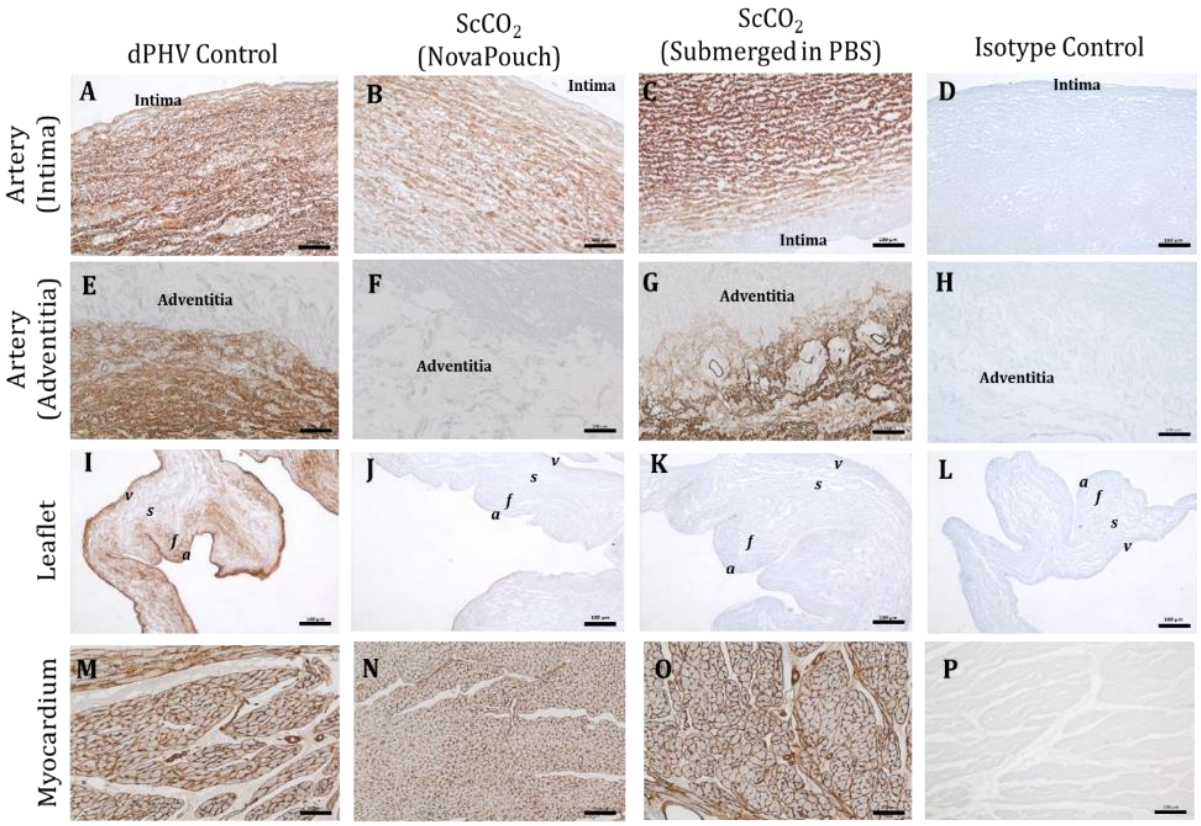


**Figure 5.8 Representative Images of Control, $ScCO_2$ (NovaPouch), and $ScCO_2$ (Submerged in PBS) dPHV Artery Wall Intima, Adventitia, Leaflet, and Myocardium Sections Labelled with Monoclonal Antibodies Against Collagen IV.** Images show control dPHV wall intima (A), adventitia (E), leaflet (I), and myocardium (M); $ScCO_2$ (NovaPouch) dPHV wall intima (B), adventitia (F), leaflet (J) and myocardium (N); $ScCO_2$ (Submerged in PBS) dPHV wall intima (C), adventitia (G), leaflet (K) and myocardium (O); Isotype controls for dPHV wall intima (D), adventitia (H), leaflet (L) and myocardium (P). Images were taken using Köhler illumination and a x 10 objective. *v: ventricularis; s: spongiosa; f: fibrosa; a: arterialis.* Representative images shown, Scale bars 100 µm.

Following fibronectin labelling (Figure 5.9), the results indicate that dPHV control, $ScCO_2$ (NovaPouch) and $ScCO_2$ (Submerged in PBS) dPHVs tissues were stained positive throughout. The artery intima and adventitia tissues displayed similar fibronectin labelling intensities in all 3 groups. The leaflets of all 3 groups also displayed similar intensities, with the darkest colour being observed in the leaflet surfaces. A well-defined network of positive labelling was observed in the myocardium of all 3 groups. Minimal brown staining was observed in undefined areas of sections stained with the isotype control.

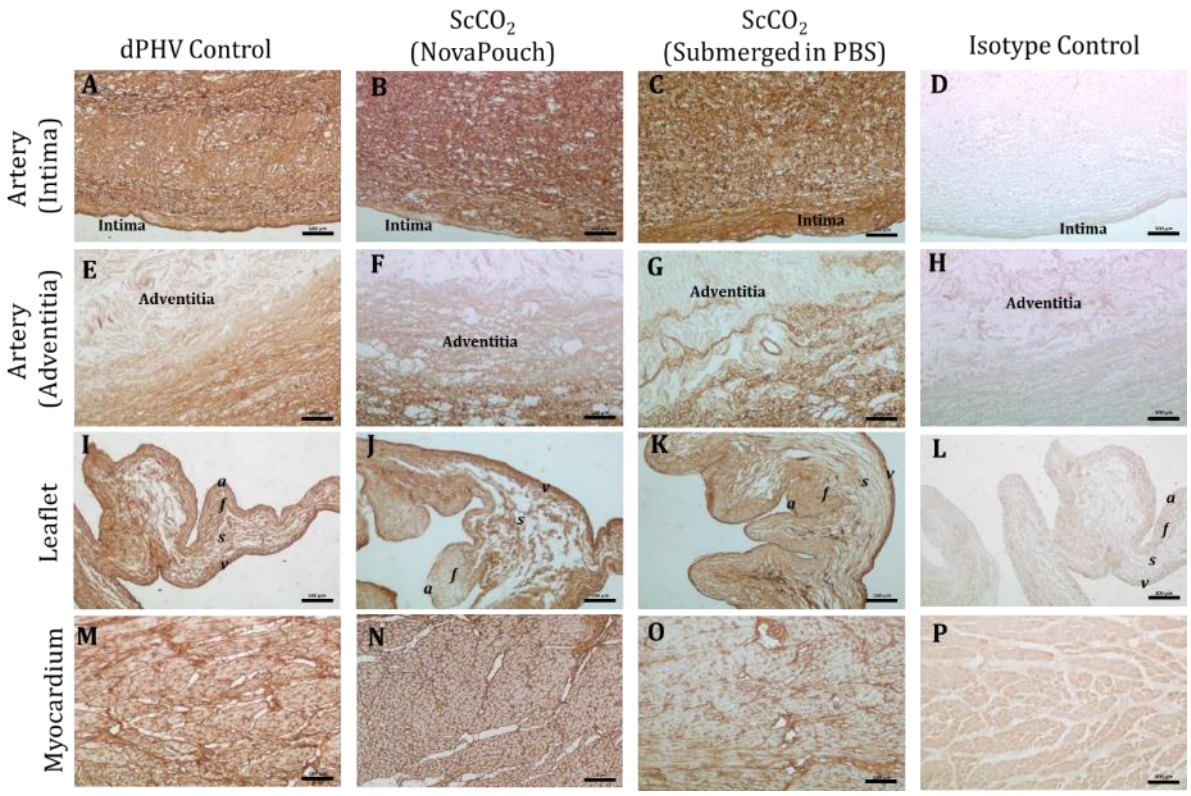


**Figure 5.9 Representative Images of Control, $ScCO_2$ (NovaPouch), and $ScCO_2$ (Submerged in PBS) dPHV Artery Wall Intima, Adventitia, Leaflet, and Myocardium Sections Labelled with Monoclonal Antibodies Against Fibronectin.** Images show control dPHV wall intima (A), adventitia (E), leaflet (I), and myocardium (M); $ScCO_2$ (NovaPouch) dPHV wall intima (B), adventitia (F), leaflet (J) and myocardium (N); $ScCO_2$ (Submerged in PBS) dPHV wall intima (C), adventitia (G), leaflet (K) and myocardium (O); Isotype controls for dPHV wall intima (D), adventitia (H), leaflet (L) and myocardium (P). Images were taken using Köhler illumination and a x 10 objective. *v: ventricularis; s: spongiosa; f: fibrosa; a: arterialis.* Representative images shown, Scale bars 100 µm.

### 5.5.4 Visualisation of Tissue Surface Microscopic Structure

Scanning electron Microscopy (SEM) was used to visualise the impact of $ScCO_2$ (NovaPouch) and $ScCO_2$ (Submerged in PBS) sterilisation on dPHV pulmonary artery wall and leaflet surface microscopic structures (Figure 5.10).

There were no obvious differences observed between dPHV control, $ScCO_2$ (NovaPouch) and $ScCO_2$ (Submerged in PBS) tissues. In all 3 groups, the artery intima displayed a slight cobblestone structure. The artery adventitia displayed loose but organised fibre networks. The leaflet *ventricularis* tissues displayed

undisrupted, slightly cobbled layers of reticular fibres. The leaflet *arterialis* surface displayed small tears within the reticular fibre layers, revealing bundles of arranged collagenous fibres.

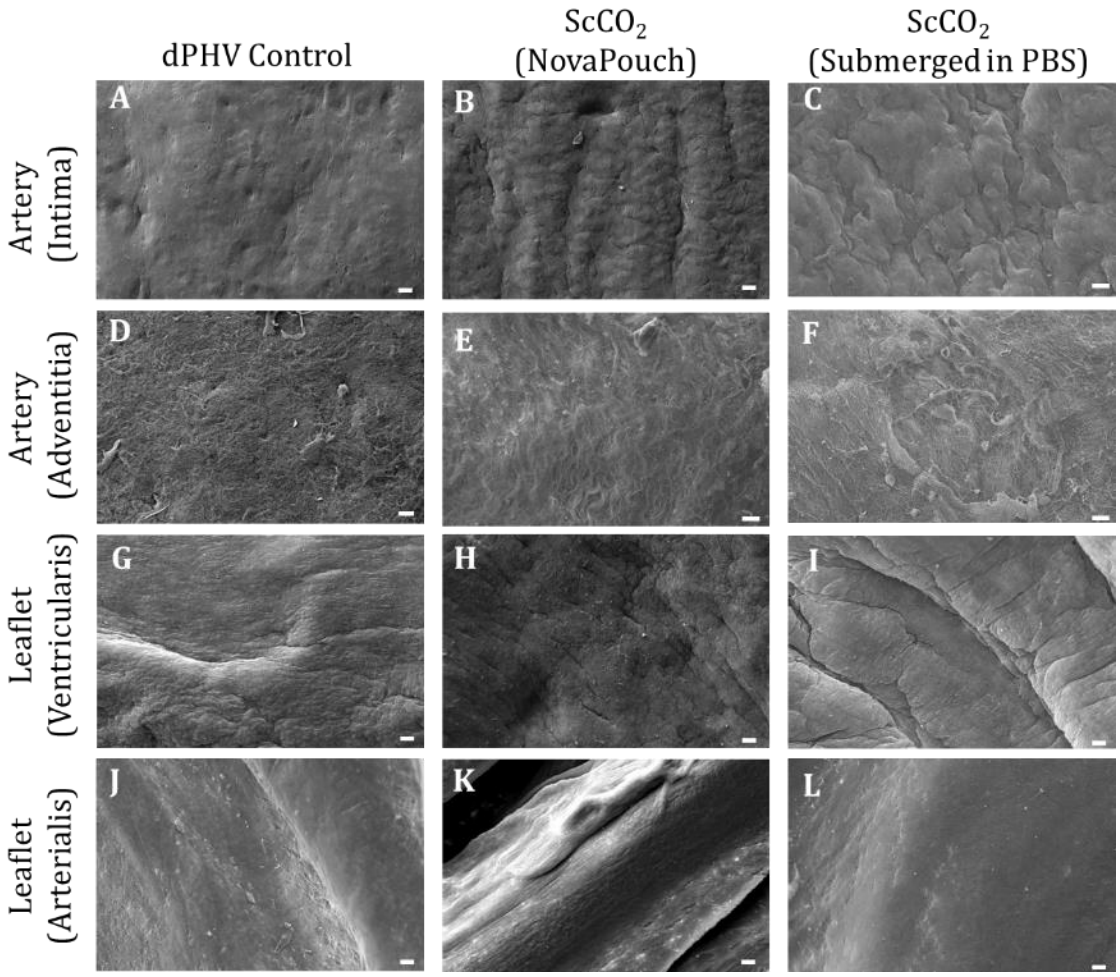


**Figure 5.10 Microscopic Structure of Control, $ScCO_2$ (NovaPouch), and $ScCO_2$ (Submerged in PBS) dPHV Artery Wall Intima, Adventitia, Leaflet Ventricularis, and Leaflet Arterialis Surfaces.** Images show control dPHV wall intima surface (A), adventitia surface (D), leaflet ventricularis surface (G), and leaflet arterialis surface (J); ScCO2 (NovaPouch) dPHV wall intima surface (B), adventitia surface (E), leaflet ventricularis surface (H) and leaflet arterialis surface (K); ScCO2 (Submerged in PBS) dPHV wall intima surface (C), adventitia surface (F), leaflet ventricularis surface (I) and leaflet arterialis surface (L). SEM images were taken using Carl Zeiss EVO MA15, 600 x magnification. Scale bars show 20 µm.

### 5.5.5 Quantification of Collagen Content

To determine the impact of $ScCO_2$ treatment on dPHV collagen content, pulmonary artery wall and leaflet samples were assayed for hydroxyproline content.

There was a significant increase in collagen content of $ScCO_2$ (NovaPouch) artery wall (222.59 ± 41.54 $\mu g.mg^{-1}$) and leaflet (532.89 ± 148.62 $\mu g.mg^{-1}$) samples in comparison to dPHV control wall (161.78 ± 28.77 $\mu g.mg^{-1}$) and leaflet (350.44 ± 89.90 $\mu g.mg^{-1}$) samples ($p<0.05$), as shown in Figure 5.11 A.

There was also a significant increase in collagen content of $ScCO_2$ (submerged in PBS) leaflet samples (874.29 ± 144.89 $\mu g.mg^{-1}$) in comparison to dPHV control leaflet samples (671.26 ± 118.94 $\mu g.mg^{-1}$, $p<0.05$), but no significant difference in the collagen content of the artery wall samples as shown in Figure 5.11 B.

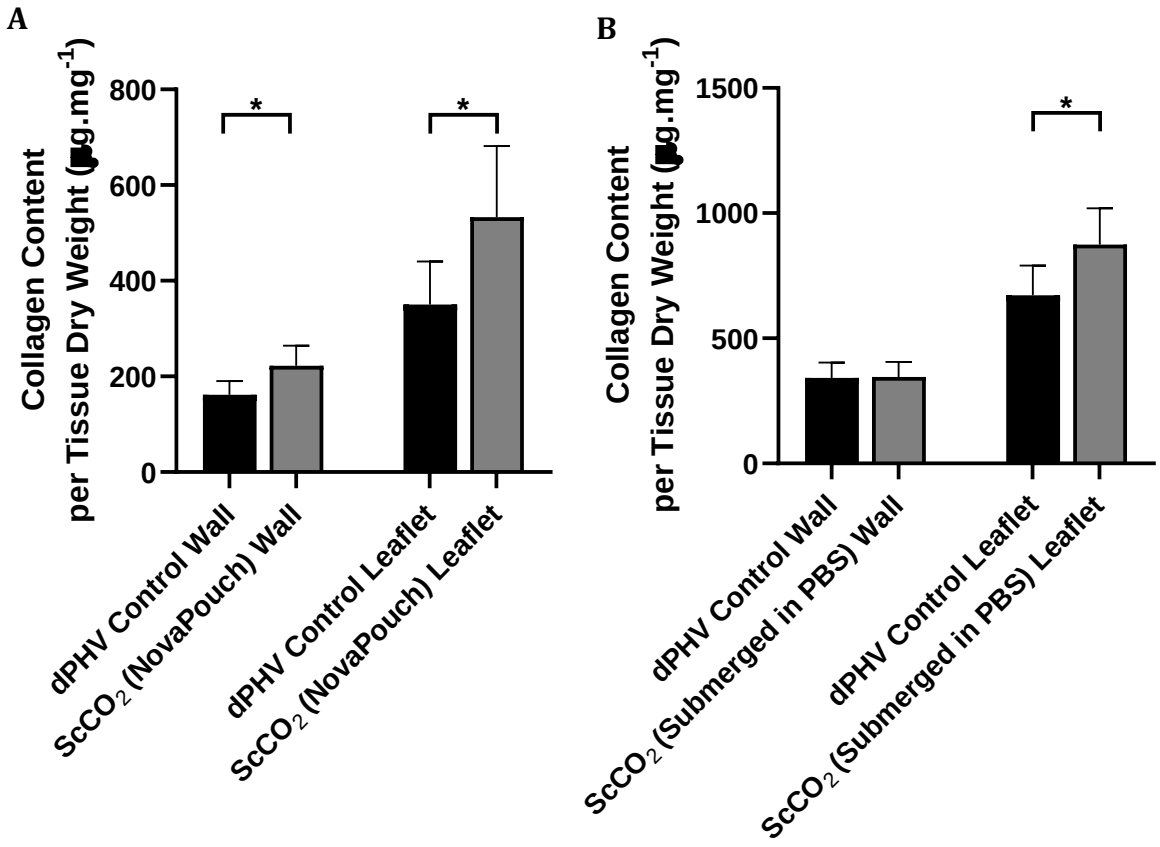


**Figure 5.11 Collagen Content of (A) $ScCO_2$ (NovaPouch) and (B) $ScCO_2$ (Submerged in PBS) dPHV Artery Wall and Leaflet Specimens in Comparison to dPHV Controls.** Data presented as mean (n=6) ± 95% C.I. Data was analysed using unpaired t-test between the two groups in each specimen type. * ($p<0.05$) denotes significant difference between the groups.

### 5.5.6 Quantification of GAG Content

DPHV control, $ScCO_2$ (NovaPouch) and $ScCO_2$ (Submerged in PBS) wall and leaflet samples were digested with papain prior to GAG quantification using the dimethylene blue (DMMB) assay.

Decell, $ScCO_2$ (NovaPouch) and $ScCO_2$ (Submerged in PBS) wall samples were found to have a GAG content of 4 ± 1.57 $\mu g.mg^{-1}$, 3.95 ± 1.13 $\mu g.mg^{-1}$, and 3.44 ± 1.91 $\mu g.mg^{-1}$, respectively. Decell, $ScCO_2$ (NovaPouch) and $ScCO_2$ (Submerged in PBS) leaflet samples were found to have a GAG content of 3.75 ± 1.36 $\mu g.mg^{-1}$, 4.87 ± 1.87 $\mu g.mg^{-1}$, and 3.63 ± 1.3 $\mu g.mg^{-1}$, respectively. There were no significant differences in GAG content found (Figure 5.12).

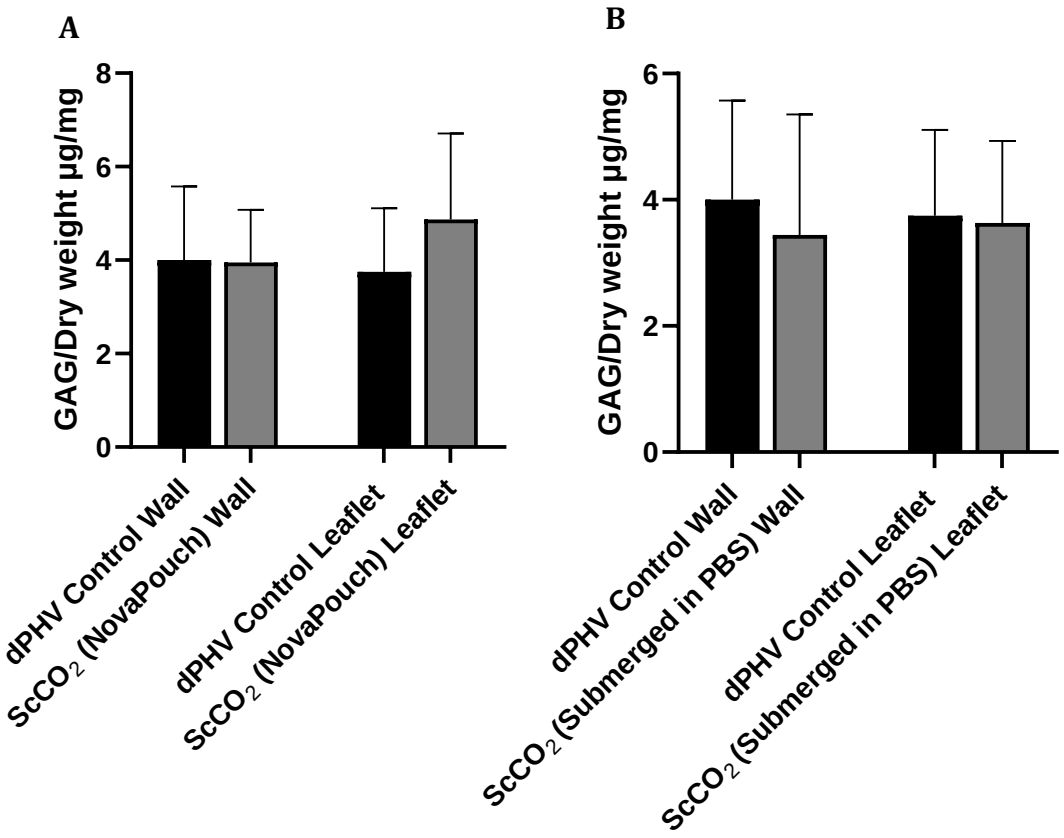


**Figure 5.12 GAG Content of (A) $ScCO_2$ (NovaPouch) and (B) $ScCO_2$ (Submerged in PBS) dPHV Artery Wall and Leaflet Specimens in Comparison to dPHV Controls.** Data presented as mean (n=6) ± 95% C.I. Data was analysed using unpaired t-test between the two groups in each specimen type.

### 5.5.7 DSC Analysis

The collagen denaturation temperatures of dPHV control, $ScCO_2$ (NovaPouch) and $ScCO_2$ (Submerged in PBS) wall and leaflet samples were quantified by measuring heat flow (W/g) in a differential scanning calorimeter.

As shown in Figure 5.13 A, the collagen denaturation temperature of $ScCO_2$ (NovaPouch) wall samples was 62.51 ± 1.09 °C, which was significantly lower than the collagen denaturation temperature of dPHV control wall samples, 68.59 ± 1.07 °C ($p<0.0001$). The collagen denaturation temperature of $ScCO_2$ (NovaPouch) leaflet samples was 63.44 ± 0.32 °C, which was also significantly lower than the collagen denaturation temperature of dPHV control leaflet samples, 67.26 ± 1.21 °C ($p<0.0001$).

As shown in Figure 5.13 B, the collagen denaturation temperature of $ScCO_2$ (Submerged in PBS) wall samples was significantly lower than the collagen denaturation temperature of dPHV control wall samples, at 62.32 ± 1.47 °C and 65.01 ± 0.67 °C, respectively ($p<0.01$). $ScCO_2$ (Submerged in PBS) leaflet samples had a collagen denaturation temperature of 63.33 ± 0.53 °C, which was significantly lower than the collagen denaturation temperature of dPHV control leaflet samples at 65.30 ± 0.48 °C ($p<0.0001$).

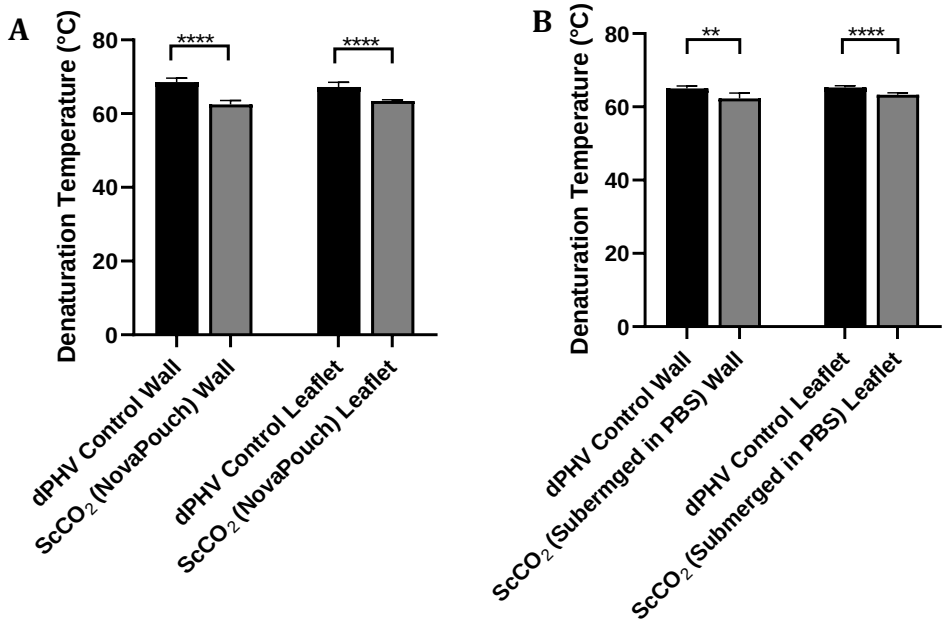


**Figure 5.13 Thermal Stability of (A) $ScCO_2$ (NovaPouch) and (B) $ScCO_2$ (Submerged in PBS) dPHV Artery Wall and Leaflet Specimens in Comparison to dPHV Controls.** Data presented as mean (n=6) ± 95 % C.I. Data was analysed using unpaired t-test between the two groups in each specimen type. ** ($p<0.01$) and ****($p<0.0001$) denotes significant difference between the groups.

### 5.5.8 *In Vitro* Cytocompatibility Assessments

Contact culture of L929 cells with $ScCO_2$ (NovaPouch) and $ScCO_2$ (Submerged in PBS) wall and leaflet samples was used to determine cytocompatibility of the sterilised tissues. The extract cytotoxicity assay was also used to determine if toxins were leached from $ScCO_2$ (NovaPouch) and $ScCO_2$ (Submerged in PBS) wall and leaflet samples.

Prior to conducting contact culture and extract cytotoxicity assays with $ScCO_2$ (NovaPouch) and $ScCO_2$ (Submerged in PBS) wall and leaflet samples, sterility was determined by incubating the tissues in thioglycollate broth (Section 2.2.11.1). The broth remained clear for all samples (N=6 for each specimen type) and negative controls, and only the positive control showed microbial growth (Figure 5.14). Therefore, $ScCO_2$ (NovaPouch) and $ScCO_2$ (Submerged in PBS) wall and leaflet samples were not contaminated.

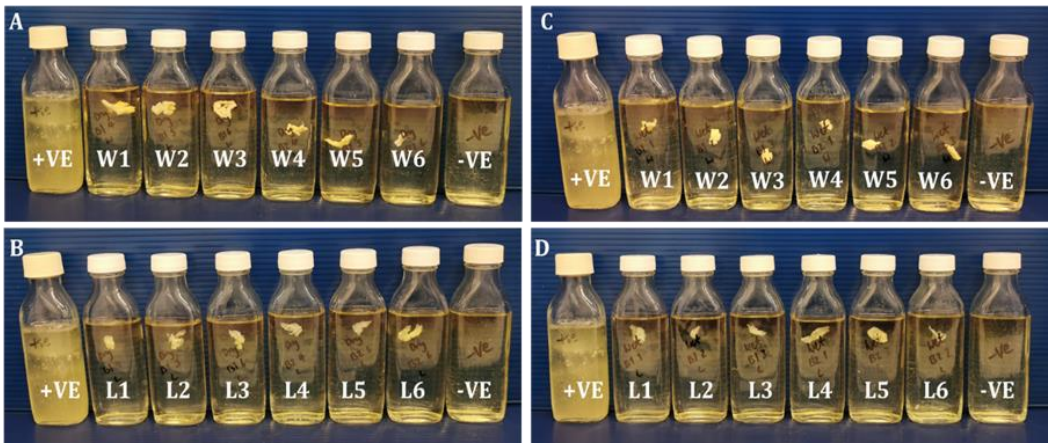


**Figure 5.14 Images of $ScCO_2$ (NovaPouch) and $ScCO_2$ (Submerged in PBS) dPHV Artery Wall (W) and Leaflet (L) Specimen Sterility Tests 48 hours Post Inoculation.** $ScCO_2$ (NovaPouch) dPHV Artery Wall (A) and Leaflet (B) and $ScCO_2$ (Submerged in PBS) dPHV Artery Wall (C) and Leaflet (D) Specimens were incubated. N=6 of wall and leaflet samples were used. Positive controls (+VE) of dermal commensal organisms and negative controls (-VE) of sterile thioglycolate broth were incubated alongside samples.

The contact cytotoxicity assays showed no evidence of $ScCO_2$ treated tissue cytotoxicity (Figure 5.15). L929 cells grew up to and in contact with $ScCO_2$ (NovaPouch) and $ScCO_2$ (Submerged in PBS) dPHV artery wall and leaflet tissue specimens, with no change in the cellular morphology in comparison to the negative steri-strip control. The rounded appearance of dead cells cultured in wells with the positive cyanoacrylate adhesive was absent in cells cultured with $ScCO_2$

(NovaPouch) and $ScCO_2$ (Submerged in PBS) dPHV artery wall and leaflet tissue specimens.

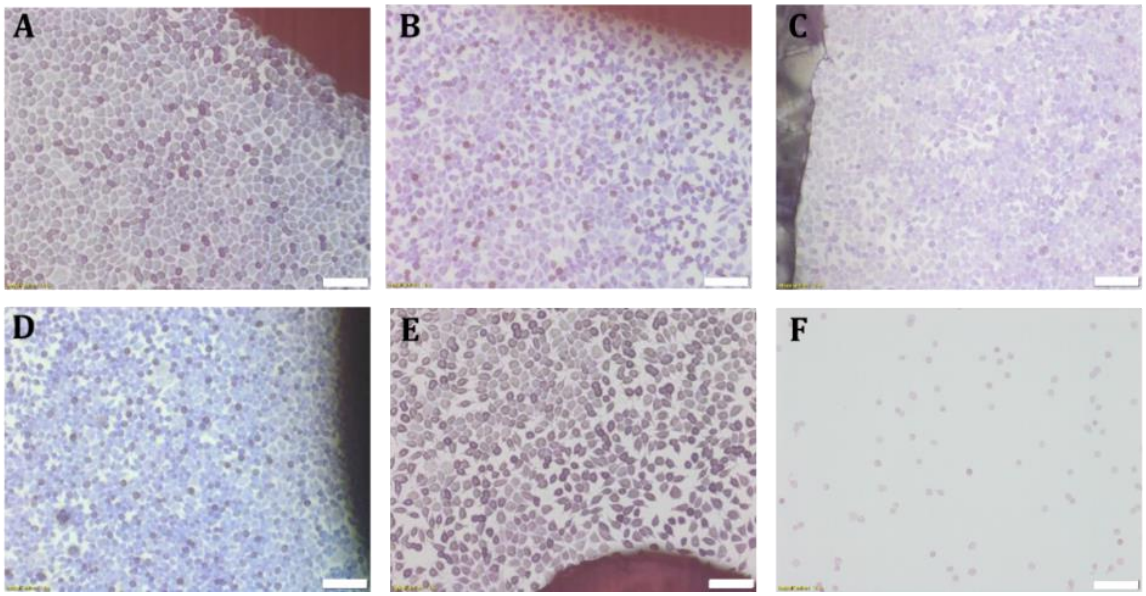


**Figure 5.15 Giemsa Stained Cell Cultures From Contact Cytotoxicity of $ScCO_2$ (NovaPouch) and $ScCO_2$ (Submerged in PBS) dPHV Wall and Leaflet Specimens.** Images show a representative $ScCO_2$ (NovaPouch) dPHV wall specimen (A), leaflet specimen (B), negative control (C), $ScCO_2$ (Submerged in PBS) dPHV wall specimen (D), leaflet specimen (E) and positive control (F). Images were acquired using bright field microscopy using a 10 x objective. Scale bars are 100 µm.

The results from the extract cytotoxicity assay showed no evidence of cytotoxicity (Figure 5.16). ATP levels of cells cultured with $ScCO_2$ (NovaPouch) and $ScCO_2$ (Submerged in PBS) dPHV wall and leaflet control extracts were significantly greater than cells cultured with the positive DMSO control only, and not the negative DMEM control.

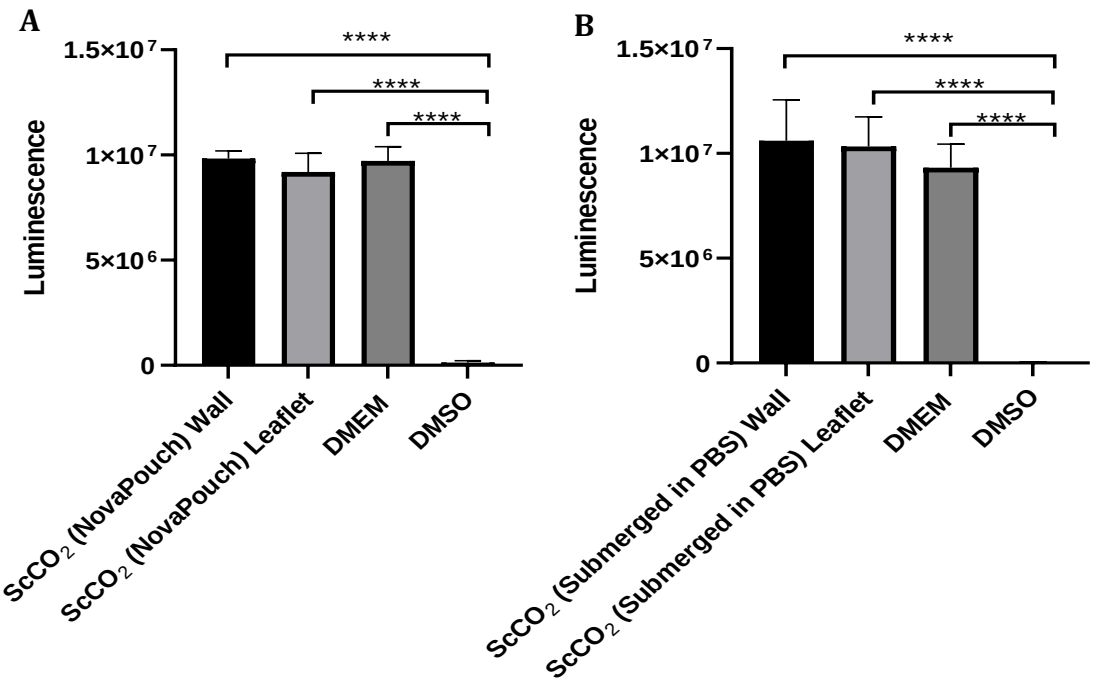


**Figure 5.16 Cell Viability of L929 Cells Cultured With (A) $ScCO_2$ (NovaPouch) and (B) $ScCO_2$ (Submerged in PBS) Wall and Leaflet Tissue Extracts.** Data presented as mean (n=6) ± 95% C.I. Data was analysed using one way ANOVA with Tukey's post-hoc test. **** ($p<0.0001$) denotes significant difference between the groups.

### 5.5.9 Uniaxial Tensile Testing

Uniaxial tensile testing on $ScCO_2$ (NovaPouch) and $ScCO_2$ (Submerged in PBS) dPHV artery wall and leaflet tissue specimens was performed to determine the effects of $ScCO_2$ sterilisation on dPHV tensile material properties.

The stress-strain graphs for all dPHV controls, $ScCO_2$ (NovaPouch) and $ScCO_2$ (Submerged in PBS) dPHV artery wall and leaflet tissue specimens are displayed in Figure 5.17. All graphs demonstrate the typical tri-phasic characteristics. There are no clear differences shown in the stress-strain graphs of $ScCO_2$ (NovaPouch) and $ScCO_2$ (Submerged in PBS) axial and circumferential wall specimens in comparison to their dPHV controls. Similarly, there are no clear differences shown in the stress-strain graphs of $ScCO_2$ (NovaPouch) circumferential leaflet specimens, and $ScCO_2$ (Submerged in PBS) circumferential and radial leaflet specimens in comparison to their dPHV controls. However, tensile leaflet characteristics of $ScCO_2$ (NovaPouch) in radial orientations demonstrated a rise in ultimate tensile strength in comparison to the dPHV controls (**Figure 5.17**).

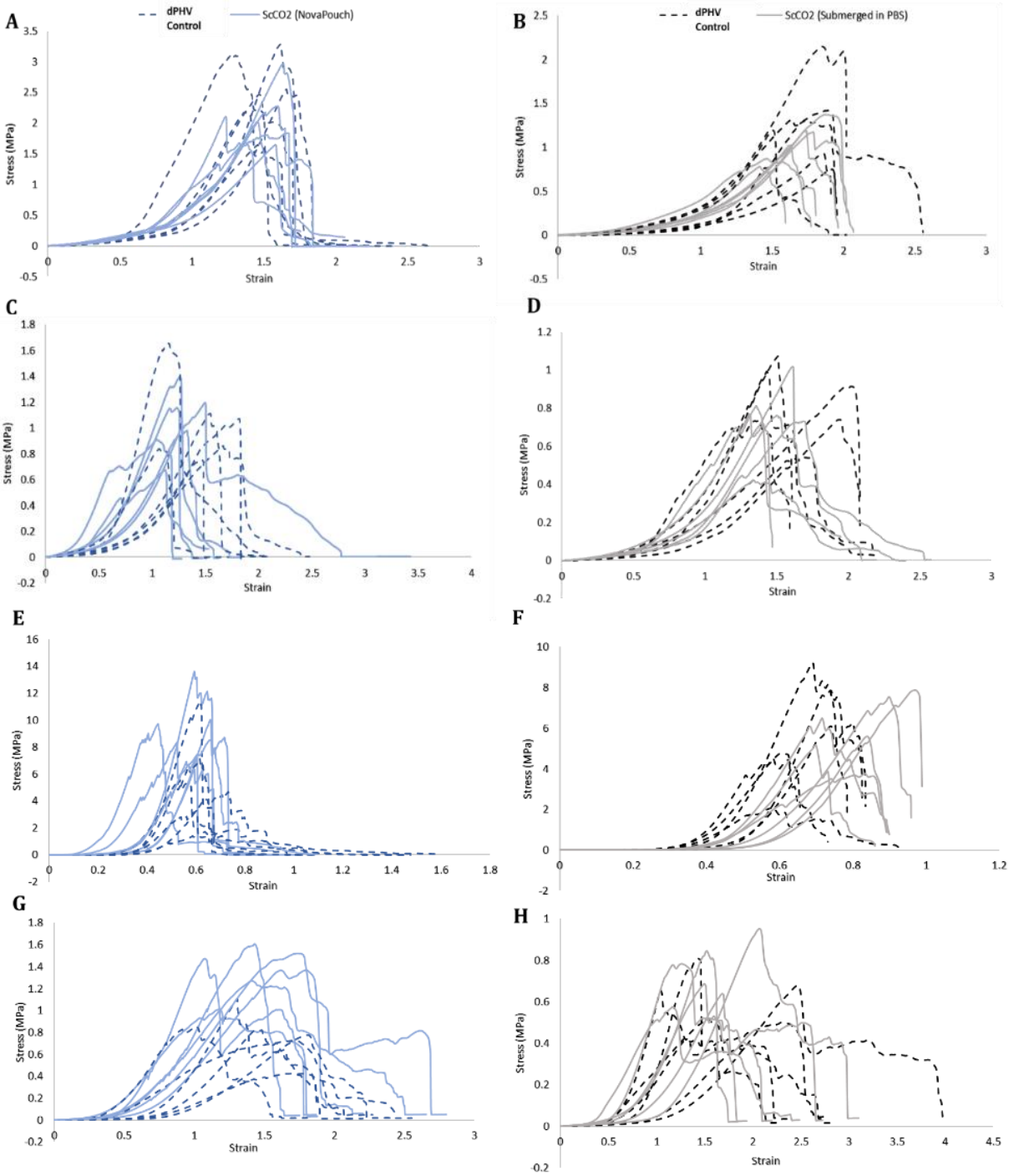


**Figure 5.17 Stress-Strain Graphs of DPHV Control with $ScCO_2$ (NovaPouch) and $ScCO_2$ (Submerged in PBS) dPHV Wall and Leaflet Specimens.** Stress-strain graphs shown for (A) dPHV control and $ScCO_2$ (NovaPouch) and (B) dPHV control and $ScCO_2$ (Submerged in PBS) axial wall; (C) dPHV control and $ScCO_2$ (NovaPouch) and (D) dPHV control and $ScCO_2$ (Submerged in PBS) circumferential wall; (E) dPHV control and $ScCO_2$ (NovaPouch) and (F) dPHV control and $ScCO_2$ (Submerged in PBS) circumferential leaflet; (G) dPHV control and $ScCO_2$ (NovaPouch) and (H) dPHV control and $ScCO_2$ (Submerged in PBS) radial leaflet. N=6 for all specimens.

Graphs displaying the tensile parameters of $ScCO_2$ (NovaPouch) and $ScCO_2$ (Submerged in PBS) dPHV artery wall specimens in comparison to dPHV controls are shown in Figure 5.18. There was a significant increase in the elastin phase slopes of $ScCO_2$ (NovaPouch) circumferential wall (0.18 ± 0.06 MPa) and axial wall (0.13 ± 0.04 MPa) specimens in comparison to the dPHV control circumferential wall (0.10 ± 0.01 MPa) and axial wall (0.08 ± 0.03 MPa) specimens ($p<0.01$ and $<0.05$, respectively). There was also a significant increase in the elastin phase slope of $ScCO_2$ (Submerged in PBS) circumferential wall (0.09 ± 0.03 MPa) in comparison to the dPHV control (0.05 ± 0.02 MPa) ($p<0.05$). There were no significant differences in the collagen phase slopes and ultimate tensile strengths of $ScCO_2$ (NovaPouch) and $ScCO_2$ (Submerged in PBS) dPHV artery wall specimens in comparison to the dPHV controls.

Graphs displaying the tensile parameters of $ScCO_2$ (NovaPouch) and $ScCO_2$ (Submerged in PBS) dPHV Leaflet Specimens in Comparison to dPHV Controls are shown in Figure 5.19. The elastin phase slopes of $ScCO_2$ (NovaPouch) circumferential (0.13 ± 0.05 MPa) and radial (0.05 ± 0.01 MPa) leaflet specimens was significantly greater than the elastin phase slopes of dPHV control circumferential (0.02 ± 0.01 MPa) and radial (0.02 ± 0.02 MPa) leaflet specimens. The elastin phase slope of $ScCO_2$ (Submerged in PBS) radial leaflet specimens (0.04 ± 0.01 MPa) was also significantly greater than the dPHV control radial leaflet specimens (0.02 ± 0.01 MPa). There were no significant differences in the collagen phase slopes of $ScCO_2$ (NovaPouch) and $ScCO_2$ (Submerged in PBS) dPHV leaflet specimens in comparison to the dPHV controls. There were also no significant differences in the UTS of $ScCO_2$ (NovaPouch) and $ScCO_2$ (Submerged in PBS) dPHV leaflet specimens in comparison to the dPHV controls, except an increase in the UTS of $ScCO_2$ (NovaPouch) radial (1.38 ± 0.22 MPa) leaflet specimens in comparison to the UTS of the dPHV control radial (0.78 ± 0.23 MPa) leaflet specimens.

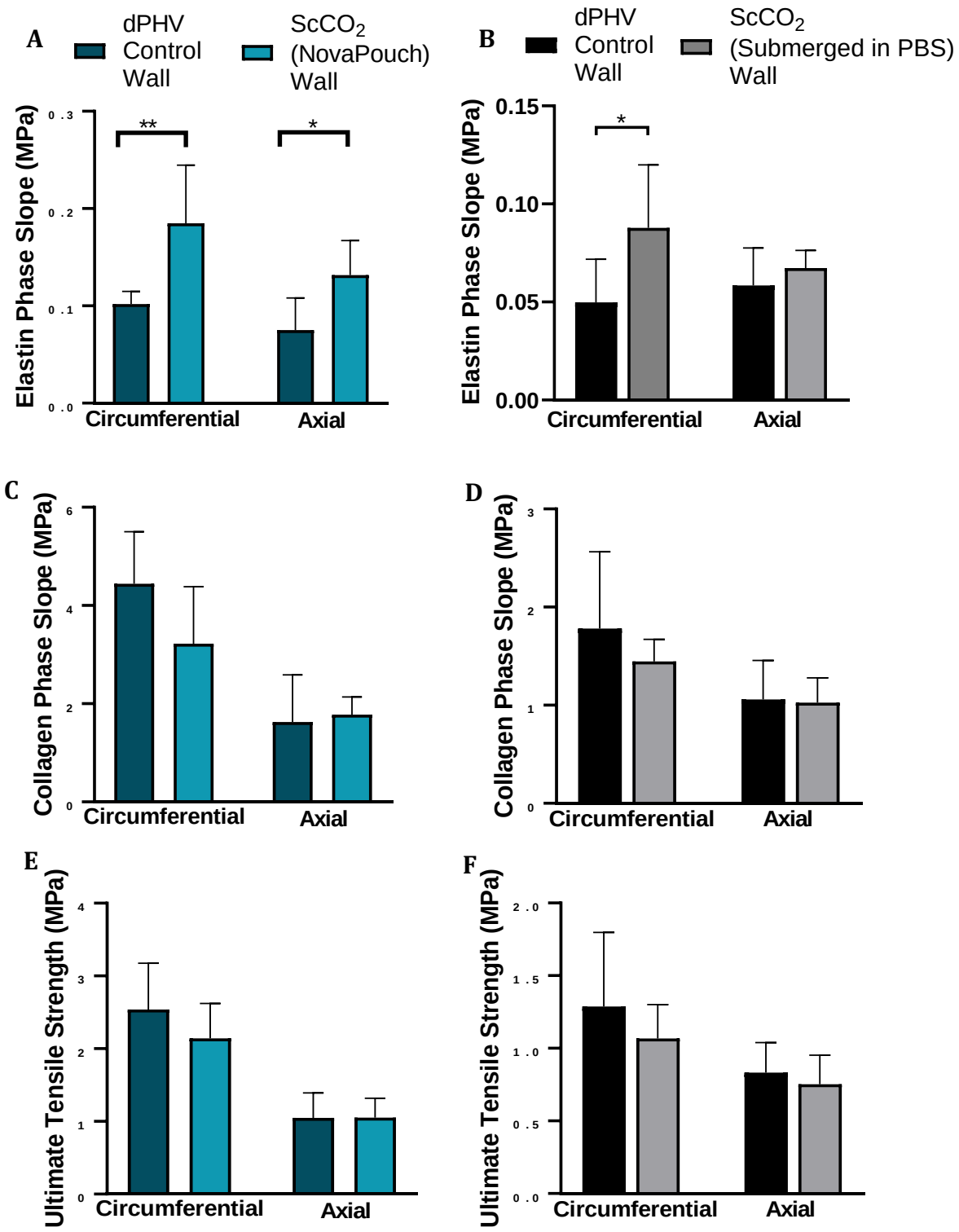


**Figure 5.18 Tensile Parameters of $ScCO_2$ (NovaPouch) and $ScCO_2$ (Submerged in PBS) dPHV Artery Wall Specimens in Comparison to dPHV Controls.** Elastin phase slopes (A,B), collagen phase slopes (C, D) and ultimate tensile strengths (E,F) of dPHV control and $ScCO_2$ (NovaPouch) and dPHV control and $ScCO_2$ (Submerged in PBS) wall specimens. Data presented as mean (n=6) ± 95% C.I. Data was analysed using unpaired t-test between the two groups in each specimen type. Significant differences between groups are represented with * ($p<0.05$) and ** ($p<0.01$).

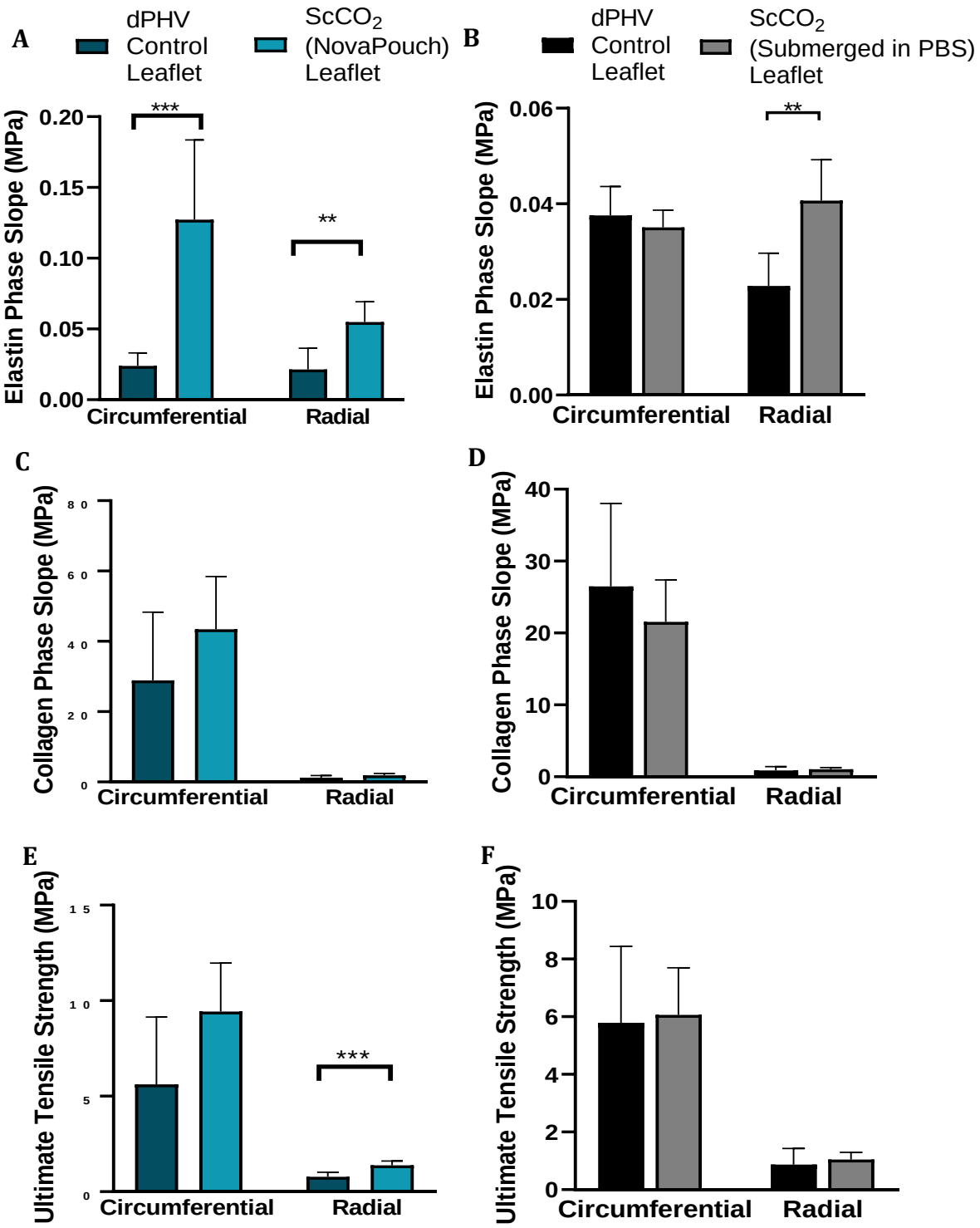


**Figure 5.19 Tensile Parameters of $ScCO_2$ (NovaPouch) and $ScCO_2$ (Submerged in PBS) dPHV Leaflet Specimens in Comparison to dPHV Controls.** Elastin phase slopes (A,B), collagen phase slopes (C, D) and ultimate tensile strengths (E,F) of dPHV control and $ScCO_2$ (NovaPouch) and dPHV control and $ScCO_2$ (Submerged in PBS) leaflet specimens. Data presented as mean (n=6) ± 95% C.I. Data was analysed using unpaired t-test between the two groups in each specimen type. Significant differences between groups are represented with * ($p<0.05$), ** ($p<0.01$) and ***($p<0.001$).

## 5.6 Discussion

An initial macroscopic observation of the dPHVs sterilised with $ScCO_2$ whilst packaged in NovaPouches was that the samples had become compressed and dehydrated within the NovaPouches. This was most likely due to the high pressures required to achieve $CO_2$ in a supercritical state. Although this should not have induced major biological and biomechanical alterations, at this stage it was unknown. This informed the decision to also process dPHV samples whilst submerged in PBS to reduce direct pressure application to the root.

Through staining with H & E, Picrosirius Red & Miller's Elastin, and Movat's Pentachrome, it was shown that $ScCO_2$ treatment did not cause extensive damage to the histoarchitecture of dPHVs, with $ScCO_2$ (submerged in PBS) displaying ECM that resembled dPHV tissue. SEM observations also indicated similarities within the structure of the $ScCO_2$ treated tissue and decellularised control tissue. This demonstrated the non-reactive nature of $CO_2$ in its supercritical state, which exerts its action by increasing intracellular carbonic acid levels and inducing a cytotoxic effect by acidifying intracellular pH (White, A. et al., 2006). Within this study, $ScCO_2$ treatment was facilitated with the addition of oxidising agent containing NovaKill™ additive solution which is required for effective inactivation of microbial bioburden at an industrial level of SAL $10^{-6}$ (Bernhardt et al., 2015). It is well explored within the literature that oxidising agents such as PAA and hydrogen peroxide can induce detrimental changes to ECM components, such as disruption of the collagen structure (Parsons, 2018). However, the collagen structures appeared tight and crimped, and the birefringence of the collagen fibres in Picrosirius red staining displayed similar colour to the untreated control dPHVs. Although the leaflet of $ScCO_2$ (NovaPouch) samples appeared compressed, the interstitial collagen fibres also remained connected and organised. Within the Hennessy *et al.* study, histological techniques were used to assess the presence of cells and microorganisms rather than the histoarchitecture of the heart valve following sterilisation with $ScCO_2$. There were also no histological images of the aortic valve leaflets included within the paper. Balestrini et al. (2016) sterilised decellularised rat lungs with $ScCO_2$ supplemented with NovaKill (13.5–18.5% PAA and 4.5– 6% hydrogen peroxide) at approximately 1440 psi at 35 °C for 2 hours. Despite using a higher $ScCO_2$ operating pressure than that used within the present

study, Balestrini et al. found that the overall microarchitecture of the $ScCO_2$ treated decellularised rat lungs was preserved in comparison to untreated decellularised rat lungs. The storage capacity of $ScCO_2$ sterilised decellularised rat lungs was also demonstrated by the retention of the tissue histoarchitecture after 6 months of storage. Halfwerk et al. (2018) decellularised bovine pericardium with $ScCO_2$ at approximately 1450 psi at 35 °C for 1 hour. Using SEM, it was found that minor disruptive areas were present in comparison to the large disruptive areas shown in the glutaraldehyde treated bovine pericardium.

Antibody labelling of collagen IV revealed a significant reduction of positive staining in both $ScCO_2$ (NovaPouch) and $ScCO_2$ (submerged in PBS) artery intima and leaflet sections. However, the mechanisms underlying these changes are not yet fully elucidated. Similar findings were shown in a study conducted by Granados et al. (2017), where although intact following decellularisation and prior to PAA treatment, there was a complete loss of collagen IV staining in decellularised porcine mitral valve leaflets sterilised with 0.1 % (v/v) PAA for 3 hours at room temperature. It is suggested that the presence of collagen IV is important for scaffold endothelisation (Tudorache et al., 2007; Yurchenco, 2011). It may be possible that collagen IV was still potentially present, but the conformation of the target epitope was modified by the presence of PAA in the NovaKill reagent in such a way that the monoclonal antibody used for collagen IV binding can no longer detect it, resulting in what was shown to be a loss of basement membrane (Luo et al., 2014).

Collagen IV provides an anchor point for cell-attachment proteins such as laminin and fibronectin (Yurchenco, 2011). Although collagen IV could have been removed during $ScCO_2$ processing in the present study, the former reason for the reduction in collagen IV labelling intensity is the most likely, due to the fibronectin labelling intensity being retained in dPHVs following $ScCO_2$ sterilisation. Similar findings were reported by Holland, James D. R. et al. (2021), who found that there was a loss of collagen IV immunolabelling but a retention of fibronectin immunolabelling following treatment of decellularised porcine nerve segments with 0.1 % PAA in PBS (pH 7.2). It was therefore proposed that the complete loss off collagen IV was the unlikely mechanism underlying the absent collagen IV immunolabelling. Fibronectin is an ECM glycoprotein that acts as a chemoattractant for cells to

migrate on and provides a suitable matrix to facilitate cell adhesion and proliferation. Therefore, fibronectin is important in tissue regeneration (Stoffels et al., 2013). This suggests that $ScCO_2$ sterilised dPHVs may have the potential to recellularise, although this has not yet been elucidated. In a study conducted by Chou et al. (2020), the proliferation, growth and differentiation of autologous adipose-derived stem cells (ASCs) seeded onto porcine acellular dermal matrix (ADM) decellularised using $ScCO_2$ was explored. During $ScCO_2$ processing, the porcine dermal matrix was exposed to $H_2O_2$ (10 – 35 %) and NaOH (0.1 - 1 M). The ASCs-$ScCO_2$-treated ADM was then used to treat rats induced with diabetes mellitus that had dorsal skin defects created to evaluate the wound healing efficacy. There was found to be a significant increase in the wound healing rate, epidermal growth factor, and decrease in CD45 (a marker associated with macrophage-mediated chronic inflammation) in comparison to untreated rats. Despite different conditions being used during $ScCO_2$ processing, this study provides evidence that $ScCO_2$ treatment does not impair the anti-inflammation, cell proliferation and regeneration functions of tissue remodelling.

The helical conformation of fibrillar collagen is made up of three α-helix polypeptide chains coiled together (tropocollagen) that are bound together through inter-peptide hydrogen bonds. Amino acids such as Gly, proline, and hydroxyproline are found on the molecule (Brodsky and Shah, 1995; Rich and Crick, 1961). Hydroxyproline is a major fibrillar collagen component that comprises around 14 % of total amino acid content (Cundy et al., 2014). Quantification of collagen content can be determined using the hydroxyproline assay. Within this study, the collagen content of $ScCO_2$ (NovaPouch) wall and leaflet and $ScCO_2$ (Submerged in PBS) leaflet samples was significantly greater than the collagen content found in untreated control dPHVs. The mechanism underlying this change has not yet been elucidated.

Despite there being what seems to be a retention in the collagenous integrity of the $ScCO_2$ treated PHV tissue, there was found to be a significant decrease in the thermal stability of the tissue following treatment, suggesting that there was a rearrangement in the collagen tertiary structure altering the thermal transitions. There is little to no evidence to support that $ScCO_2$ sterilisation treatment may unfavourably alter the tertiary structure of collagen (Ribeiro, N. et al., 2020). The

organisation of the collagen fibres can become altered, either as a result of tissue dehydration or due to the decrease of other large ECM components such as GAGs (Antons et al., 2018; Casali et al., 2018). However, it is well known that ECM components are susceptible to oxidative damage when in the presence of ROS (Scheffler et al., 2008). Within this study, PAA and $H_2O_2$ additives were used to supplement $ScCO_2$ sterilisation by preventing the requirement of harsh treatment conditions such as high temperature and pressure or a prolonged incubation time. PAA is a strong oxidising agent that chemically modifies cell membranes through the transfer of electrons and denatures cell membrane and intracellular components (Clapp et al., 1994). Hydrogen peroxide also relies on its strong oxidising capacity in order to lyse microbial cells and spores (Wardle and Renninger, 1975). Potent superoxide and hydroxyl free radicals are derived from hydrogen peroxide, which then damage protein and lipid components of cell membranes and infiltrate cells to induce extensive damage to nucleic acids. Whilst the presence of these radicals are essential for achieving sterile medical devices, they can also cause oxidative degradation to the tertiary arrangement of collagen. This essentially results in the fragmentation of proteins, and hence an alteration in the tertiary structure of the collagen and therefore a less thermally stable structure (Parsons, 2018). These novel findings cannot be compared to other studies as it is unexplored within the literature. Directly quantifying denatured collagen content would give a better indication of the severity of potential damage induced.

It is not uncommon for the retention of GAGs within ECM scaffolds to be poor following the application of a decellularisation protocol that incorporates sodium dodecyl sulphate (SDS) and similar findings have already been reported by Luo et al. (Luo et al., 2014) on porcine pulmonary heart valves, as well as other studies on different tissue types using SDS as part of the decellularisation protocol (Cheng, H.W. et al., 2009; Stapleton et al., 2008). GAGs are a major component of PHV ECM and play an important role in the mechanical behaviour of tissues. The extended conformation of GAGs occupies a large amount of space within the ECM. Therefore, the resultant looser arrangement of collagen fibres following the loss of GAGs can lead to altered mechanical behaviour. Additionally, GAGs maintain ECM in a hydrated state as they have a high density of negative charges which attracts cations like Na+, which then attracts water (Fenderson, 2008). Within the literature, there is uncertainty about the preservation of GAGs in tissues following

exposure to $ScCO_2$. In a study conducted by Huang, Y.-H. et al. (2017), GAGs were significantly extracted in $ScCO_2$-ethanol treated corneas in comparison to native corneas. Whereas, in a study conducted by Seo et al. (2018), there was no significant difference between the GAG content of heart ECM decellularised using $ScCO_2$-ethanol and native control heart tissue. Within this study, Movat's Pentachrome staining showed the staining of GAGs in $ScCO_2$ treated leaflets was less intense in comparison to the dPHV control leaflets. However, GAG quantification showed no significant reduction in the GAG content between $ScCO_2$ treated tissues and dPHV control tissues.

Uniaxial tensile testing was used to assess the impact of $ScCO_2$ sterilisation on the biomechanical properties of dPHV tissue. The elastin phase slopes, collagen phase slopes, and ultimate tensile strengths of pulmonary artery wall and leaflet specimens were analysed. Generally, $ScCO_2$ sterilisation studies have shown that $ScCO_2$ processing does not cause significant disruptions to tissue mechanical properties. Balestrini et al. (2016) found an increase in the stiffness of $ScCO_2$-treated decellularised rat lung matrices, although only at non-physiological levels of stretch. Irani et al. (2018) found no significant difference in the stiffness and UTS between tendons sterilised with $ScCO_2$ (supplemented with 14.1 % PAA and 4.9 % Hydrogen Peroxide) and non-sterilised tendons. Noble et al. (2022) used uniaxial tensile testing to compare the mechanical performance of decellularised porcine, bovine, and bison pericardial tissues that were sterilised with $ScCO_2$ using the same commercial entity as that used within this study (NovaSterilis, Inc., New York). The mechanical strength of the decellularised sterilised pericardium tissues were comparable to native tissue.

In this study, there was found to be an increase in the elastin phase slope of the $ScCO_2$ (NovaPouch) treated PHV wall samples in both circumferential and axial orientations, as well as the $ScCO_2$ (NovaPouch) treated PHV leaflet samples in both circumferential and radial orientation. There was also an increase in the elastin phase slope of $ScCO_2$ (Submerged in PBS) circumferential wall and radial leaflet specimens. The underlying mechanism(s) for these changes is/are not yet fully known. Halfwerk et al. (2018) investigated the effect of $ScCO_2$ decellularisation on porcine and bovine pericardium, using similar conditions to those observed in this $ScCO_2$ sterilisation study (1450 psi, 35 °C, 25 % $H_2O_2$). It was reported that the

stiffness was significantly higher in $ScCO_2$ processed tissue in comparison to the native tissue (Halfwerk et al., 2018). However, rehydrating the $ScCO_2$–decellularised bovine pericardium restored the elastic modulus from 83 ± 14 MPa to 48 ± 12 MPa. The increase in the tissue elastin stiffness found in this study can therefore potentially be attributed to dehydration, which can often occur during $ScCO_2$ processing as reported by Casali et al. (2018).

There was no significant difference found in the collagen phase slope, but a significant increase in the ultimate tensile strength of $ScCO_2$ (NovaPouch) treated PHV leaflets in the radial orientation. A non-significant ultimate tensile strength increase of $ScCO_2$ (NovaPouch) sterilised dPHV circumferential leaflet specimens was also observed within this study. Similar findings were reported by Hennessy et al. (2017) where there was found to be an increase in the ultimate tensile strength of $ScCO_2$ treated decellularised aortic heart valve leaflets in comparison to non-sterilised decellularised aortic heart valve leaflet controls. However, Hennessy et al. (2017) only reported the results from tests conducted with the collagen fibres circumferentially orientated. Whilst the load bearing collagen fibres are circumferentially aligned, analysis of the leaflet in the radial orientation also provides valuable insight into radial extensibility and therefore leaflet coaptation (Christie, 1992). Efficient leaflet coaptation is required for both aortic and pulmonary heart valves to prevent the backflow of blood into the ventricles during ventricular diastole.

L929 fibroblasts were selected for cytotoxicity testing in accordance to ISO standard 10993-5 (2009), which details cytotoxicity testing using established cell lines that should be applied to medical devices to determine biocompatibility. $ScCO_2$ sterilisation treatment of dPHVs did not negatively impact the growth and morphology of L929 fibroblasts in contact with the $ScCO_2$ sterilised tissue. There was no evidence of toxins leaching from the $ScCO_2$ sterilised tissue as L929 cell proliferation and viability was not impaired following incubation with $ScCO_2$ tissue extracts. Similarly, biocompatibility was observed in decellularised aortic heart valves and decellularised lung matrices after $ScCO_2$-PAA and $H_2O_2$ sterilisation (Balestrini et al., 2016; Hennessy et al., 2017). Huang, Y.-H. et al. (2017) demonstrated neovascularisation, the absence of inflammation and therefore good biocompatibility of porcine corneas decellularised using $ScCO_2$, suggesting that

$ScCO_2$ treatment does not impair tissue scaffolds supporting tissue regeneration *in vivo.* Although appropriate positive and negative controls were used within cytotoxicity testing to determine biocompatibility of $ScCO_2$-treated dPHV tissue, further validation would be required by subjecting untreated dPHV control tissue alongside $ScCO_2$-treated dPHVs to cytotoxicity testing . The observed cytocompatibility in conjunction with fibronectin retention may be an indicator that dPHVs sterilised with $ScCO_2$ may be able to support recellularisation post-implantation.

# Chapter 6 : Further Biomechanical Properties of $ScCO_2$ Sterilised Decellularised Heart Valves

## 6.1 Introduction

Based on the results from the impact of $CuCl_2$ & $H_2O_2$ (Chapter 4) and $ScCO_2$ (Chapter 5) sterilisation on the biological and biomechanical properties of decellularised heart valves, $ScCO_2$ (submerged in PBS) sterilised dPHVs retained the pre-sterilisation dPHV macroscopic structure with minor changes in the biological and biomechanical (uniaxial tensile) properties. Therefore, $ScCO_2$ (submerged in PBS) sterilisation was chosen as the optimum of the sterilisation methods investigated. Thus, dPHVs sterilised with $ScCO_2$ whilst submerged in PBS were subjected to further biomechanical investigations, including functional performance under static pressure and suture retention properties of the wall and myocardium.

Replacement heart valve roots have to be subjected to *in vitro* performance evaluations before clinical translation, as specified by ISO 5840 (2015). However, the *in vitro* performance methods described in ISO 5840 (2015) were developed in conformity with existing mechanical and chemically fixed bioprosthetic heart valves. Similar methods have since been developed and optimised by Desai et al. (2018) to be compatible with (decellularised) heart valve roots.

The static leakage flow evaluation can be used to assess potential valvular regurgitation resulting from valvular insufficiency of the closed valve. A number of studies have used a static leakage flow assessment to evaluate valve competency, with reference to leakage flow rate of the closed valve under a hydrostatic back pressure. Leo et al. (2006) and Loger et al. (2014) evaluated the competency of St. Jude Medical Inc bileaflet mechanical heart valves and transcatheter mechanical heart valve models composed of Nitinol thin film leaflets, respectively. Jennings (2001) also used static leakage flow assessment to evaluate the competency of native and glutaraldehyde fixed porcine aortic and pulmonary heart valve roots.

The circumferential expansion (dilation) of the pulmonary artery forming the PHV root impacts leaflet coaptation following systole, and plays a role in transmitting stress from the leaflets to the pulmonary artery wall during systole. The artery wall therefore aids in the prevention of fatigue and structural failure of the valve

leaflets (Desai et al., 2018; Hopkins, R.A., 2003; Sutton et al., 1995). Therefore, investigating the circumferential expansion of the pulmonary artery under physiological conditions whilst the dPHV root is maintained as a whole structure would give a good indication of arterial stiffness under conditions that mimic the *in vivo* state.

Replacement heart valves are typically sutured to the annulus that remains *in situ* following the removal of the native valve. The failure of the suture attachment, either due to the replacement heart valve material not being strong enough to withstand physiological pressures *in vivo* or due to the suture itself, can lead to severe health complications (Pierce et al., 2016). The separation of the valve from the annulus can cause bacterial endocarditis, aneurysm of the artery, degenerative regurgitation, calcification and failure of the valve (Rizzoli et al., 1984). *In vitro* suture-retention studies have been used by many research groups to quantify heart valve pericardium, annuli and aortic, suture-retention strength, which is the force necessary to pull a suture from the replacement heart valve (McGregor et al., 2016; Pierce et al., 2016; Walraevens et al., 2008).

Successful clinical implementation of sterilised dPHVs will require the maintenance of the biomechanical integrity of all components of the PHV root structure (pulmonary artery, leaflets, and myocardium), which should perform similarly to the native heart valve as a single unit.

The impact of $ScCO_2$ (submerged in PBS) sterilisation on the functional biomechanical properties of heart valves has not yet been reported within the literature. More specifically, exploring the impact of $ScCO_2$ (submerged in PBS) sterilisation on the functional biomechanical properties of dPHVs that have been decellularised using the specifically designed method will give valuable insight into the feasibility of $ScCO_2$ sterilised dPHV roots as a clinical application (Luo et al., 2014).

## 6.2 Aims and Objectives

### 6.2.1 Aim

The aim of the work described in this chapter was to investigate the impact of $ScCO_2$ (Submerged in PBS) sterilisation on the functional biomechanical performance (under static back pressure) and suture retention properties of dPHVs decellularised using a method incorporating 0.1 % SDS, nuclease and protease inhibitors (Luo et al., 2014).

### 6.2.2 Objectives

i. To produce dPHV roots and expose them to $ScCO_2$ treatment whilst submerged in PBS

ii. To determine and compare the functional biomechanical performance of $ScCO_2$ (submerged in PBS) sterilised and untreated control dPHV roots using static leakage assessment

iii. To further determine and compare the functional biomechanical performance of $ScCO_2$ (submerged in PBS) sterilised and untreated control dPHV roots using dilation and suture-retention assessments

## 6.3 Study Experimental Approach

This study was designed to assess the impact of $ScCO_2$ (Submerged in PBS) sterilisation on the functional biomechanical (competency) performance of dPHV roots, and to further characterise the biomechanical (dilation, suture-retention) performance of $ScCO_2$ (Submerged in PBS) in comparison to untreated control dPHV roots.

Decellularised porcine pulmonary heart valves were exposed to NovaProcess™, a $ScCO_2$ process patented and performed by NovaSterilis (NY). Samples were sterilised whilst submerged in PBS, with NovaKill™ proprietary additive added to the PBS surrounding the samples. The hydrodynamic and biomechanical properties of the dPHV roots were characterised as described in Figure 6.1.

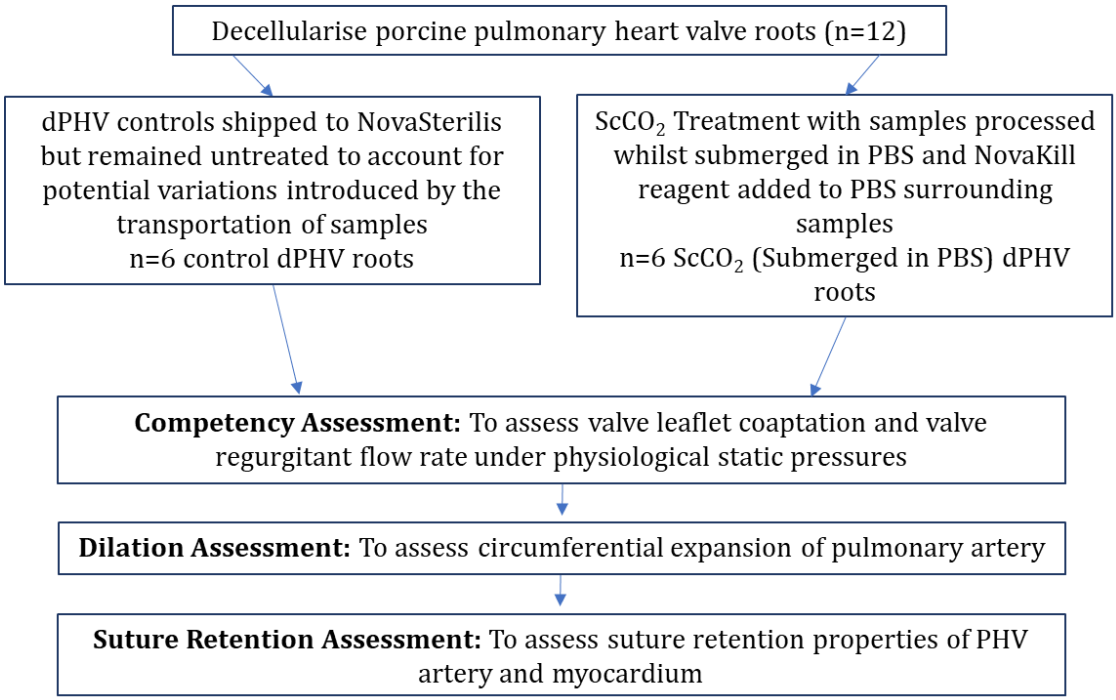


**Figure 6.1 Schematic of the Experimental Approach Adopted to Characterise the Impact of $ScCO_2$ Sterilisation on the Functional Biomechanical Properties of Decellularised Porcine Pulmonary Heart Valves**

## 6.4 Methods

### 6.4.1 Production of Decellularised Porcine Pulmonary Heart Valves

Porcine pulmonary heart valves were acquired and exposed to the Leeds protocol for decellularising heart valves, as described in section 2.2.3 .

### 6.4.2 $ScCO_2$ Sterilisation

dPHV roots were sterilised with $ScCO_2$ whilst submerged in PBS, as described in section 5.4.2.

### 6.4.3 Functional Biomechanical Performance I: Competency Assessment

Competency tests were performed to assess valve leaflet coaptation and to quantify the regurgitant flow rate under hydrostatic physiological back pressures. The static leakage test rig, validation of the test rig, and the process to determine the competency of the samples is described in sections 6.4.3.1, 6.4.3.2, and 6.4.3.3, respectively.

#### 6.4.3.1 Static Leakage Test Rig

A static leakage test rig developed by Jennings (2001) and modified by Desai (2019) was used to assess dPHV competency. The rig consisted of a vertical 1832 millimetre (mm) high cylindrical Perspex column with an internal diameter of 60 mm, with a rectangular Perspex box as the base. The column was marked from 20 mmHg to 120 mmHg at intervals of 200 mmHg which allowed the application of hydrostatic physiological back pressures when the test fluid 0.9 % (w/v) saline was inserted. An outlet drainage pipe at the base of the block allowed drainage of the test fluid. The rig was placed on the floor into a tray to collect the test fluid, and the vertical Perspex column was mounted to a work bench using a G clamp.

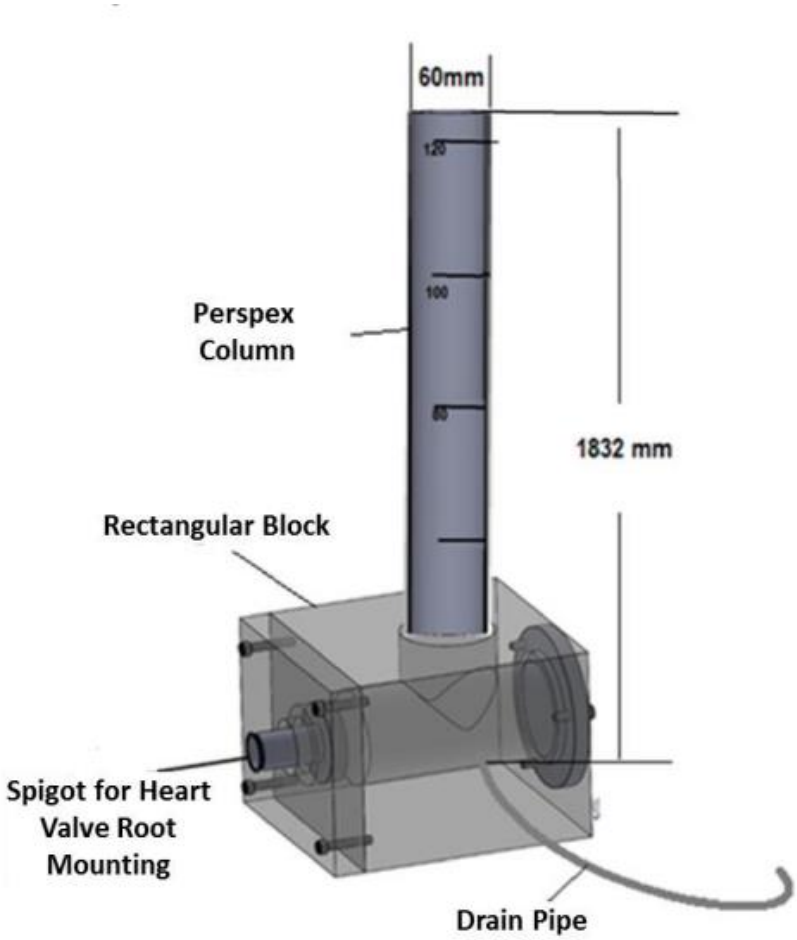


**Figure 6.2 Static Leakage Test Rig Schematic. Figure not drawn to scale. Figure taken from Desai (2019).**

### 6.4.3.2 Validation of Static Leakage Test Rig

The static leakage test rig was validated by recording the time taken for the pressure level of the test fluid to drop from 60 mmHg to 20 mmHg through test fluid leakage from a 1 mm diameter hole (Figure 6.3). This was repeated 6 times. At each time, an externally calibrated Hanhart Mesotron Quartz stop clock (serial number 6558CLK) was used to record the leakage time, and the test fluid volume was recorded. The mean flow rate was calculated using the mean volume of test fluid and leakage time. The static leakage test rig was validated if the individual recorded leakage times, volumes and rates were within a range of ± 5 % of the mean values.

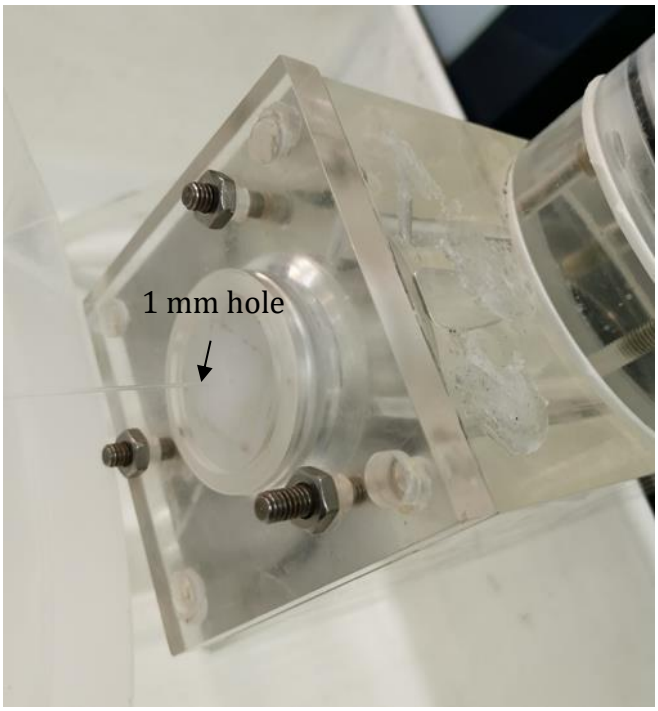


**Figure 6.3 Static Leakage Test Rig Validation**

#### 6.4.3.3 Competency Assessment Procedure

The arterial diameter of all dPHV roots was first measured using custom made obturators. The dPHV root (both control and sterilised) was attached to the rig spigot with a cable tie, and then mounted into the Perspex mounting plate. The Perspex mounting plate and spigot was then attached to the rectangular Perspex block at the base of the static leakage test rig using 3 screws (Figure 6.4).

The maximum applied pressure (systolic pressure) was 60 mmHg, and the minimum pressure (diastolic pressure) was 20 mmHg. The systolic pressure was achieved by filling the Perspex column with 0.9 % (w/v) saline solution up to the 60 mmHg pressure mark on the column. The time taken for the systolic pressure to drop to 20 mmHg was recorded using an externally calibrated Hanhart Mesotron Quartz stop clock (serial number 6558CLK). The test fluid leakage volume was also recorded.

The flow rate was determined using the formula:

$$Flow\ Rate\ (Q) = \frac{Volume\ of\ leaked\ test\ fluid\ (V)}{Leakage\ time\ (t)}$$

The dPHV root was considered competent if the test fluid pressure level did not drop from 60 mmHg to 20 mmHg within a cut-off period of 30 minutes with a leakage flow rate of <0.84 $mL.s^{-1}$. Images of the dPHV roots from an inferior angle were taken during competency testing using a Leica Triple Camera (Wide Angle Lens, f/1.8 aperture and Ultra-Wide Angle Lens, f/2.2 aperture, Huawei P30).

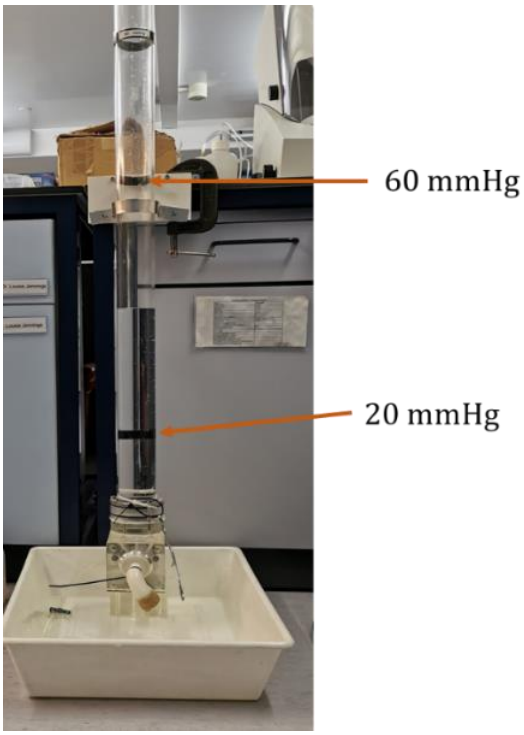


**Figure 6.4 Static Leakage Test Set-Up**

### 6.4.4 Biomechanical Performance II: Expansion Characteristics

The circumferential expansion of the pulmonary artery component of the dPHV roots was determined by measuring the percentage dilation of the artery in response to static back pressures. The method used during this study was developed by Desai (2019).

#### 6.4.4.1 Dilation Test Equipment Set-Up

A schematic diagram of the arrangement of equipment used for dilation test set-up is shown in Figure 6.5. Different sized Cylindrical Perspex tubes were designed to be compatible with dPHV root sizes with diameters ranging from 20 to 32 mm. A stainless steel luer lock 1/4-28 UNF threaded fitting was connected to the narrow end of the cylindrical Perspex tube for a secured connection to external air pressure supply. A three-way connector was attached to this to allow connection of

a digital pressure transducer (S/N: 63204/3, Comark Instruments, Inc.) and pneumatic air regulator. The cylindrical Perspex tube was vertically mounted on a retort stand.

A reference scale was also mounted next to the Cylindrical Perspex tube using a retort stand. A Canon digital SLR 550 D camera was mounted perpendicular to the Perspex column (or dPHV) to take images of the dPHV at each applied pressure increment.

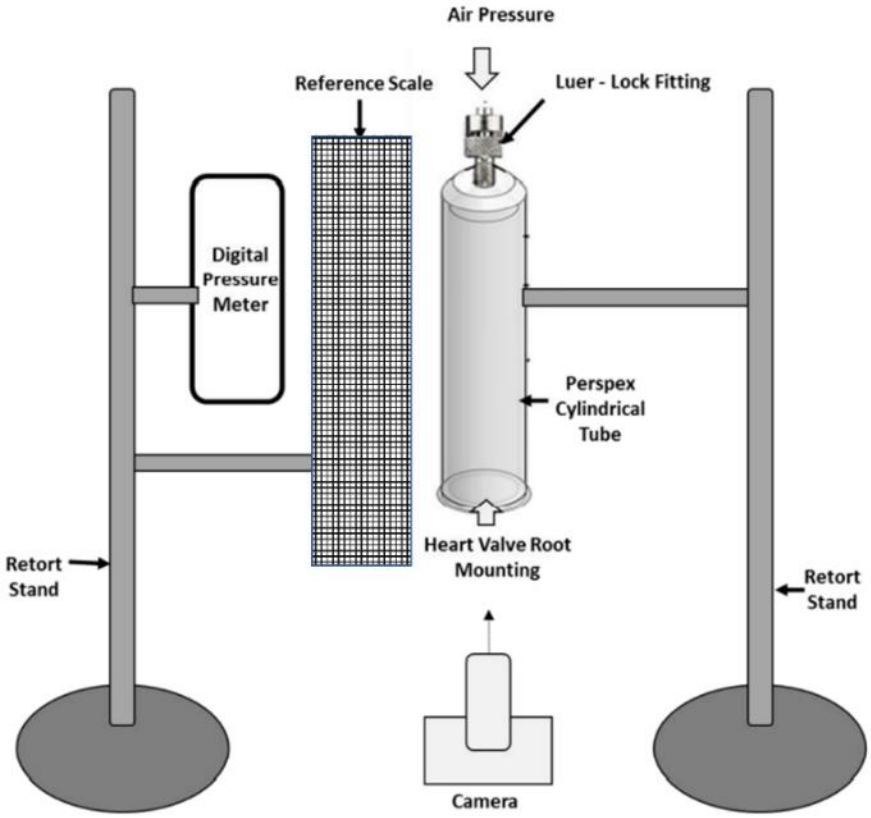


**Figure 6.5 Dilation Testing Equipment Set-Up Schematic. Figure adapted from Desai (2019).**

### 6.4.4.2 Dilation Assessment Procedure

The dPHV root (both sterilised and untreated) was mounted to the wide end of the cylindrical Perspex tube using a cable tie. The open end of the pulmonary artery was mounted, leaving the myocardium to move freely longitudinally. An appropriately sized annulus ring was used to support the dPHV root annulus (Figure 6.6).

The dPHV was marked with a tissue marking dye (Thermo Fisher Scientific, UK), with four reference points at least 5 mm above the sinotubular junction to allow quantification of the artery circumferential expansion upon application of

pressure. PBS was then inserted into the cylindrical perspex tube through the three-way connector, which was pressurised using a pneumatic air regulator. Prior to the application of external pressure, an image was taken to calculate the static pressure ($P_0$) applied to the dPHV root as a result of the PBS solution level in the Perspex column which varied between samples. The scale was calibrated using the reference scale (10 mm) to convert pixels to mm. $P_0$ was then calculated by measuring the height (h) of the PBS in the column (mm) which was then divided by 13.6 to convert the units to mmHg, since mercury is approximately 13.6 times denser than PBS (Desai, 2019).

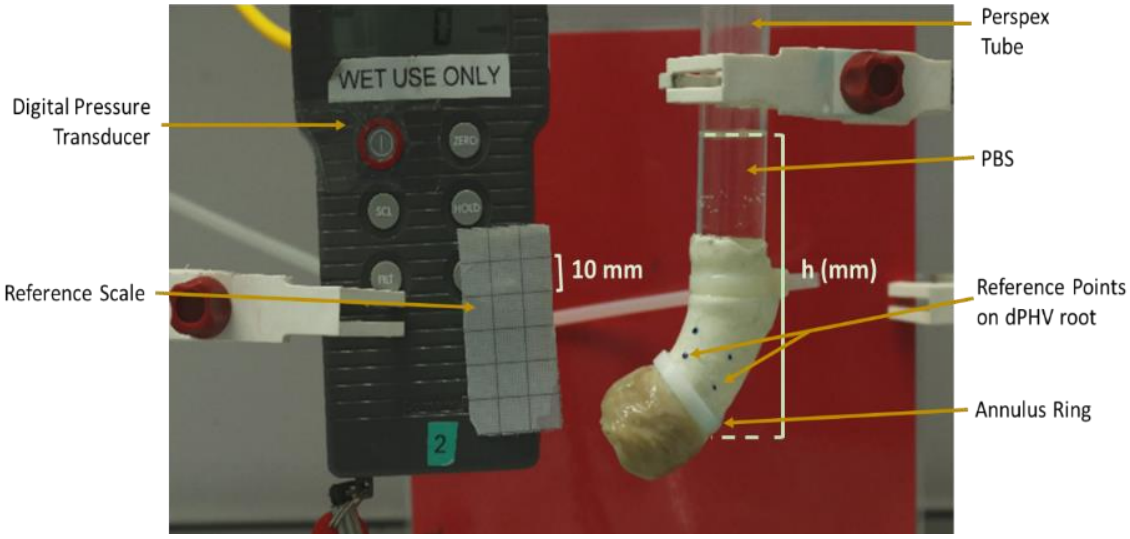


**Figure 6.6 dPHV Dilation Testing Set-Up and Initial Pressure Measurement**

Pressure was then applied in increments of around 5 mmHg until a maximum pressure of 35 mmHg was reached. Images of the dPHV with the digital pressure transducer and reference scale in field of view were taken at each pressure increment. The $P_0$ was added to the applied pressures ($P_a$) to give the final pressure applied ($P_f$). Each dPHV sample had different $P_f$ values applied due to the initial PBS level.

All images were analysed using a Java-based open source image processing software called ImageJ (NIH, Bethesda, MD). Image stacks of each dPHV sample as each pressure increment were aligned on a single canvas an ImageJ plug-in called montage (Figure 6.7). The distance between the reference points ($D_a$) were measured for each applied pressure increment ($P_a$). Similarly, the distance between the reference points ($D_0$) was measured at zero applied pressure ($P_0$). The

percentage dilation at each pressure increment was then calculated using the formula: $Percentange\ Dilation = \frac{Da-D0}{D0} \times 100$

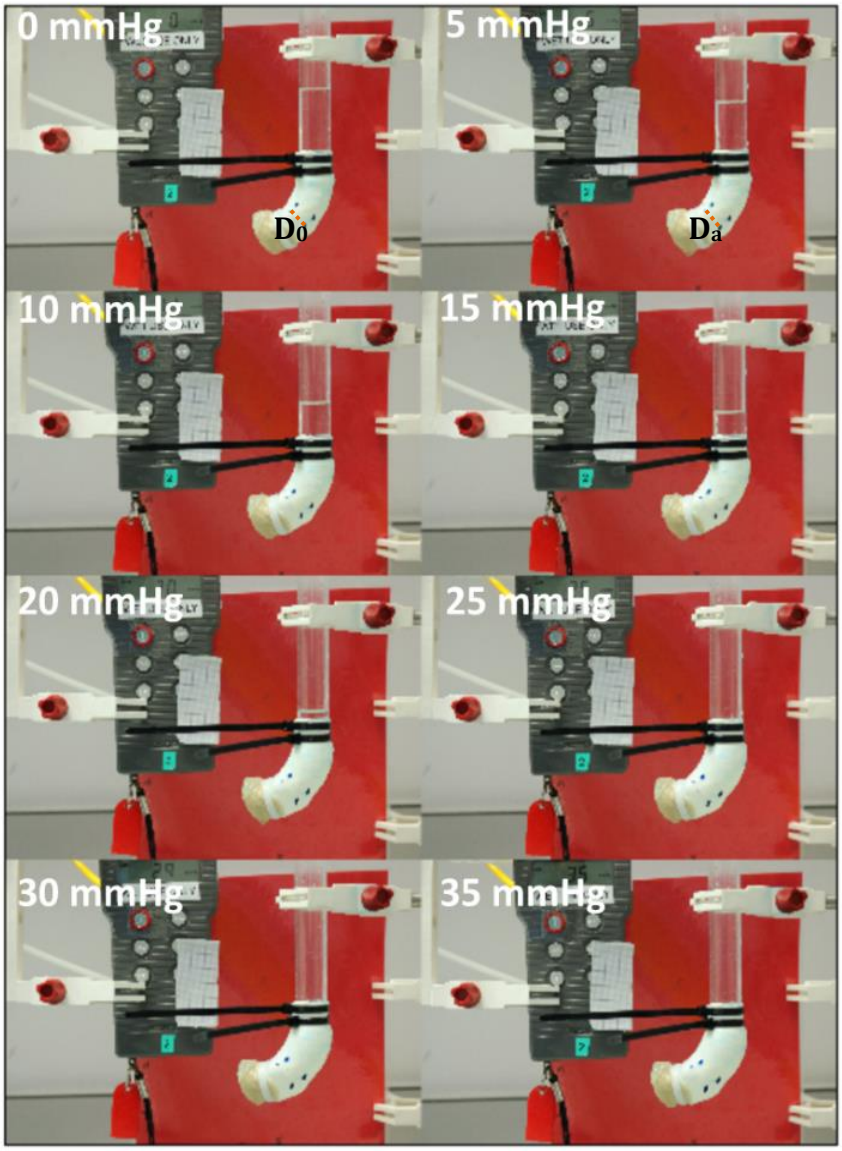


**Figure 6.7 Representative ImageJ Montage of dPHV Dilation Testing.** Image displays D0 at 0 mmHg and Da at 5 mmHg. Da was also applied to images taken at 10, 15, 20, 25, 30, 35 mmHg.

### 6.4.5 Biomechanical Performance: Suture-Retention Assessment

The suture-retention assessment used during this study was adopted from the method described in ISO 7198 (2016) for Cardiovascular implants - Tubular vascular prostheses. Pulmonary artery wall and myocardium specimens were assessed, as these are intended to serve as anchor points when attaching the dPHV *in vivo* when this intervention is clinically translated.

All specimens were taken axially as 20 x 15 mm strips using a custom made tissue-cutter. The width between the two blades of the custom made tissue cutter defined the width of the resultant dissected tissue specimen. The point of suture insertion was 4 mm from the free edge of the specimen and centrally aligned, which was marked with a pen to avoid losing the orientation of the sample during preparation (Figure 6.8). The thickness of the sample at the point of suture insertion was measured six times using a thickness gauge J- 40 V.

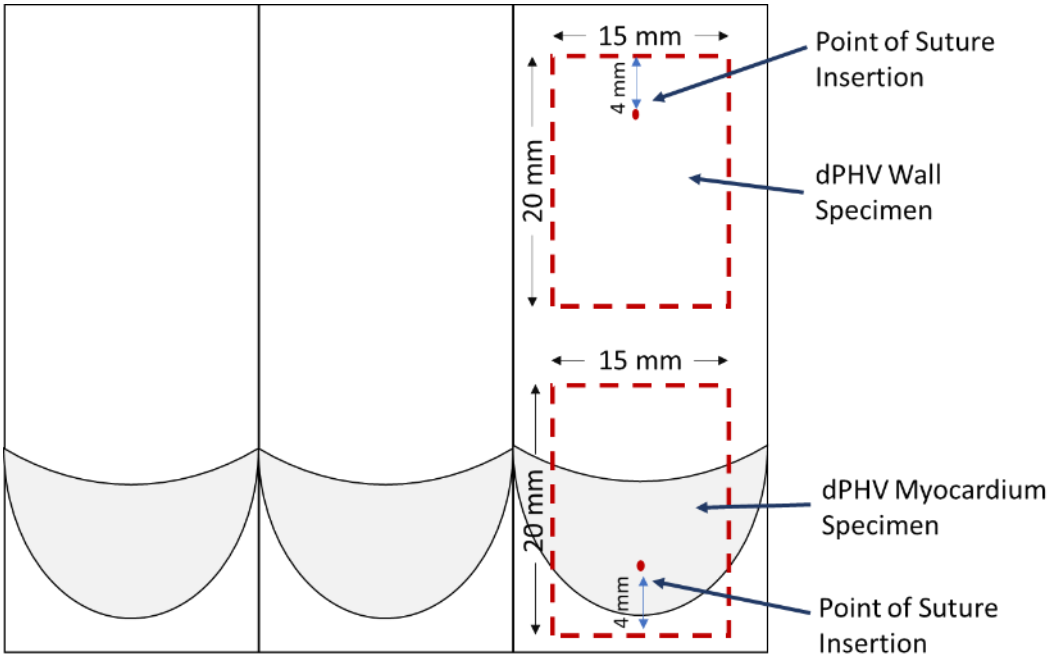


**Figure 6.8 Schematic of Sample Preparation For Suture-Retention Testing**

One end of the specimen was mounted onto a tissue specimen clamping apparatus using custom designed wide grips, as shown in Figure 6.9 (Desai, 2019). A 5 mm suture loop (4-0 non-absorbable monofilament suture with taper needle, Premilene® ) was created using the point of suture insertion reference mark. The suture was then clamped onto the upper grip, and the gauge length was 20 mm. The full tissue specimen clamping apparatus was then mounted into a BioPlus Bath filled with PBS at 37 °C attached to the Instron 3365 apparatus. A 50 N load cell was used and a strain rate of 10 mm/min was applied. The test continued until failure, which was when the suture had pulled out from the specimens.

**Figure 6.9 Representative Images of dPHV Pulmonary Artery (A) and Myocardium (B) Specimens Mounted Tissue Specimen Clamping Apparatus for Suture-Retention Testing**

Observations of the failure were noted during testing. The peak load was reported as the maximum suture pull-out force. Resistance to tearing was also measured using the formula:

$$Resistance\ to\ Tearing\ (N/\text{mm}) = \frac{Maximum\ suture\ pull-out\ force\ (N)}{Specimen\ thickness\ (mm)}$$

### 6.4.6 Statistical Analysis

GraphPad Prism 7 software was used to statistically analyse data within this study. All numerical values are presented as mean ± 95 % confidence limits (C.l). Unpaired t-test was used to compare the means between control dPHVs and $ScCO_2$ (submerged in PBS) sterilised dPHVs. The difference between the means of the groups was considered significant if the p value was less than 0.05.

## 6.5 Results

### 6.5.1 Hydrodynamic Performance I: Competency Assessment

Images of all dPHV roots tested were taken from the inferior angle, as shown in Figure 6.10. The coaptation of the three dPHV leaflets was clearly displayed in control dPHV 1 (Figure 6.10). Due to difficulties in trying to observe and obtain images of the leaflets of all samples during testing, this was not clearly shown in the other samples. As demonstrated by the prominent regurgitant stream of the test solution 0.9 % (w/v) saline, insufficient leaflet coaptation was observed in the control dPHV 4, 5, and 6, as well as $ScCO_2$ (submerged in PBS) sterilised dPHVs 1, 2, 4, 5 and 6 (Figure 6.10). The pulmonary artery of the dPHVs that displayed insufficient leaflet coaptation exhibited slightly transparent protruding bulges around the annuls of the dPHV root.

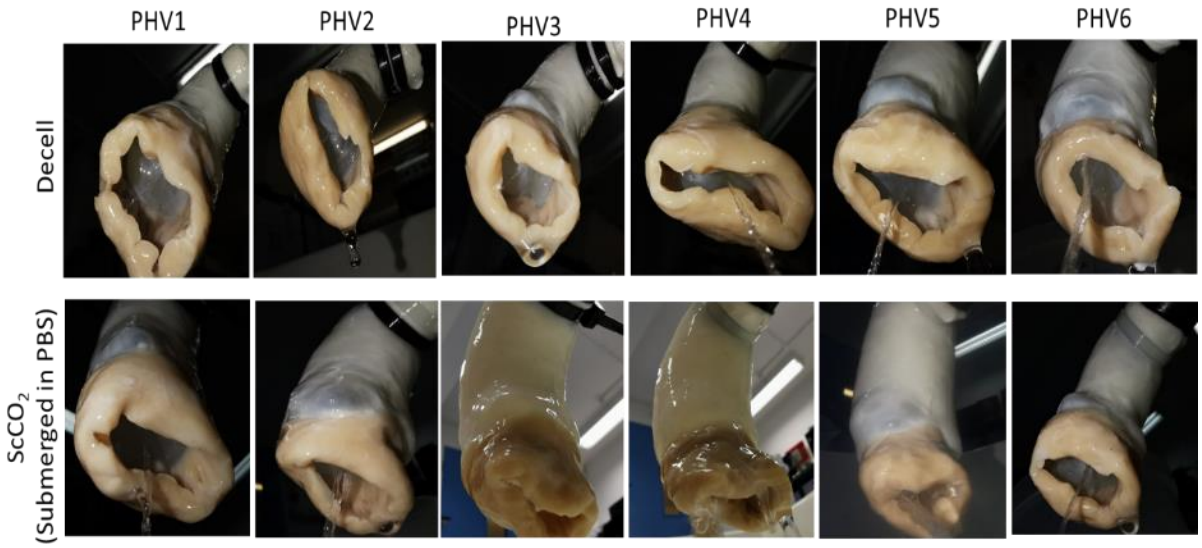


**Figure 6.10 Images of Control and $ScCO_2$ (Submerged in PBS) sterilised dPHVs During Competency Testing.**

The valve competency in terms of leakage flow times and rates for the control and $ScCO_2$ (Submerged in PBS) sterilised dPHVs is shown in Table 6.1. PHV 1, 2 and 3 out of the six control dPHV specimens tested were competent, with leakage flow rates of <0.84 $mL.s^{-1}$. The leakage flow rates of the samples that were not considered competent (PHV 4, 5 and 6) ranged from 1.065-5.395 $mL.s^{-1}$.

Five out of six ScCO2 (Submerged in PBS) sterilised dPHVs were not considered competent, with leakage flow rates ranging from 1.623-15.757 $mL.s^{-1}$. $ScCO_2$

(Submerged in PBS) sterilised dPHV 3 was considered to be competent, with a leakage flow rate of <0.84 $mL.s^{-1}$.

These findings correlated with the observations of the test fluid 0.9 % (w/v) saline regurgitation during testing, whereby the samples that were observed to have a prominent flow of regurgitation were found to have a higher leakage flow rate.

**Table 6.1 Arterial Diameters, Leakage Flow Times, Leakage Flow Rates and Competency of Control and $ScCO_2$ (Submerged in PBS) Sterilised dPHVs**

| Valve Number | Arterial Diameter (mm) | Time (Seconds) | Flow Rate ($mL.s^{-1}$) | Competent? |
|---|---|---|---|---|
| Decell Control dPHV Roots | | | | |
| PHV 1 | 20 | >1800 | <0.84 | Yes |
| PHV 2 | 21 | >1800 | <0.84 | Yes |
| PHV 3 | 20 | >1800 | <0.84 | Yes |
| PHV 4 | 20 | 1442 | 1.065 | No |
| PHV 5 | 23 | 408 | 3.715 | No |
| PHV 6 | 22 | 287 | 5.395 | No |
| $ScCO_2$ (Submerged in PBS) Sterilised dPHV Roots | | | | |
| PHV 1 | 20 | 934 | 1.623 | No |
| PHV 2 | 21 | 643 | 2.357 | No |
| PHV 3 | 20 | >1800 | <0.84 | Yes |
| PHV 4 | 20 | 138 | 10.998 | No |
| PHV 5 | 20 | 96 | 15.757 | No |
| PHV 6 | 20 | 719 | 2.133 | No |

### 6.5.2 Biomechanical Performance II: Expansion Characteristics

The expansion characteristics of the dPHV root pulmonary arteries in terms of percentage dilation in response to applied pressure are shown in Figure 6.11.

It was observed that some samples that were found to be regurgitant during competency testing exhibited a greater percentage dilation in response to applied pressure. As shown in Figure 6.11 A, control dPHVs 5 and 6 trended with a greater percentage dilation with increasing pressure. $ScCO_2$ (Submerged in PBS) dPHVs 1,

3 and 4 also trended with a greater percentage dilation with increasing pressure (Figure 6.11 B).

The starting pressures between all samples tested were different due to the varying levels of PBS at the start of testing. Although pressure was then applied in similar and regular intervals during testing, the final pressure values were different as a result of the differing starting pressures. A true comparison of the percentage dilation of $ScCO_2$ (Submerged in PBS) sterilised and control dPHVs at each pressure level could not be made as a result of the varying final pressures at each increment. Therefore, the trends in the percentage dilation of $ScCO_2$ (Submerged in PBS) sterilised and control dPHVs in response to applied pressures were observed to compare the expansion characteristics between these groups. As shown in Figure 6.12, there were no obvious differences in the pulmonary artery percentage dilations of $ScCO_2$ (Submerged in PBS) sterilised dPHVs in comparison to the dPHV controls.

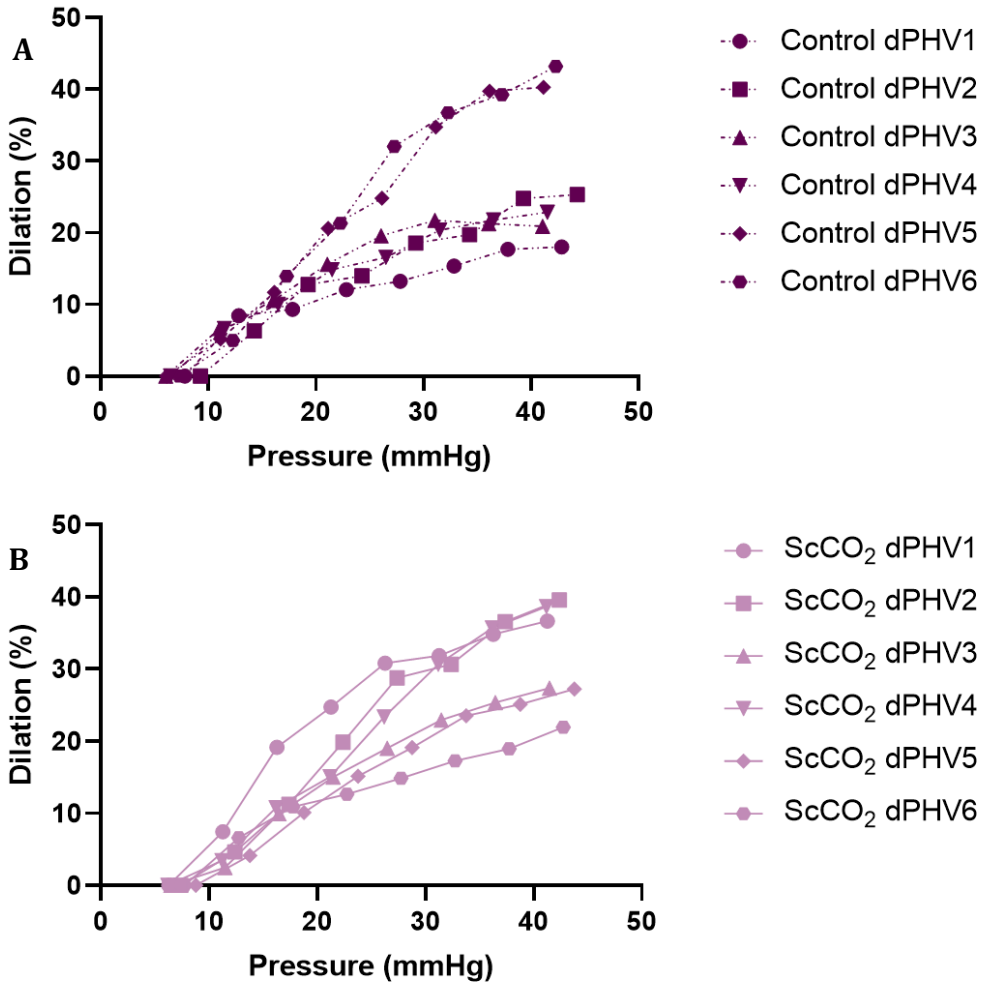


**Figure 6.11 Percentage Dilations of Control (A) and $ScCO_2$ (Submerged in PBS) (B) Individual dPHV Samples**

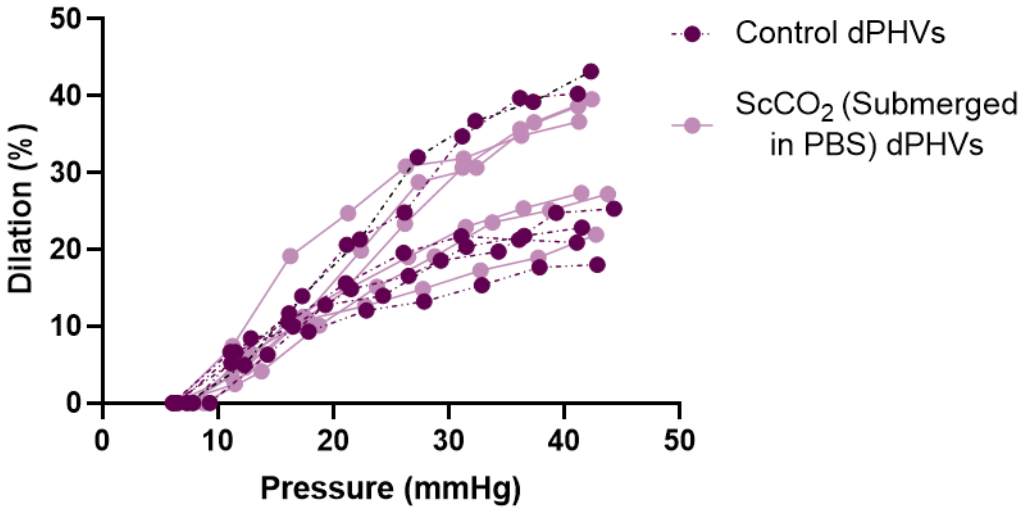


**Figure 6.12 Percentage Dilation Comparison of Control and $ScCO_2$ (Submerged in PBS) dPHVs**

### 6.5.3 Biomechanical Performance: Suture Retention Testing

Suture retention testing of all dPHV wall and myocardium specimens showed failure as a cut spreading from the suture in a circumferential direction (Figure 6.13).

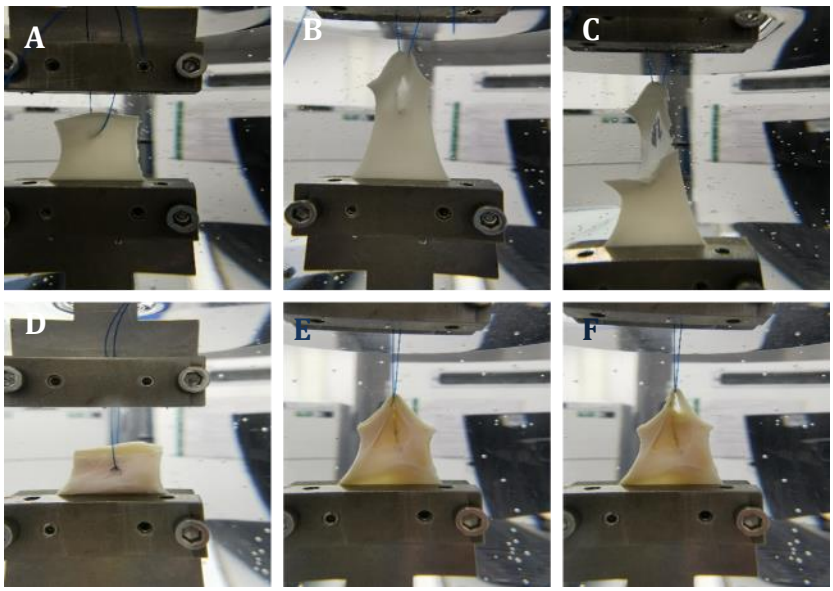


**Figure 6.13 Representative Images of Pulmonary Artery Wall and Myocardium During Suture Pull-Out Testing .** Images show the start (A, D) middle (B, E) and end (C, F) of pulmonary artery wall (A-C) and myocardium (D-F) suture-retention testing.

The maximum suture pull-out force (N) and resistance to tearing (N/mm) of dPHV artery and myocardium specimens are presented in Figure 6.14.

The mean maximum suture pull-out force for control dPHV artery and $ScCO_2$ (Submerged in PBS) artery specimens was 5.99 ± 2.42 N and 6.44 ± 2.96 N (mean ± 95 % C.I), respectively. The mean suture pull-out force for control dPHV myocardium and $ScCO_2$ (Submerged in PBS) myocardium specimens was 4.58 ± 1.50 N and 4.71 ± 1.30 N, respectively. There were no significant differences found between the groups ($p>0.05$).

The mean resistance to tearing for control dPHV artery and $ScCO_2$ (Submerged in PBS) artery specimens was 2.15 ± 0.79N/mm and 2.39 ± 1.14 N/mm, respectively. The mean resistance to tearing for control dPHV myocardium and $ScCO_2$ (Submerged in PBS) myocardium specimens was 0.85 ± 0.31 N/mm and 0.83 ± 0.25 N/mm, respectively. Again, there were no significant differences found between the groups.

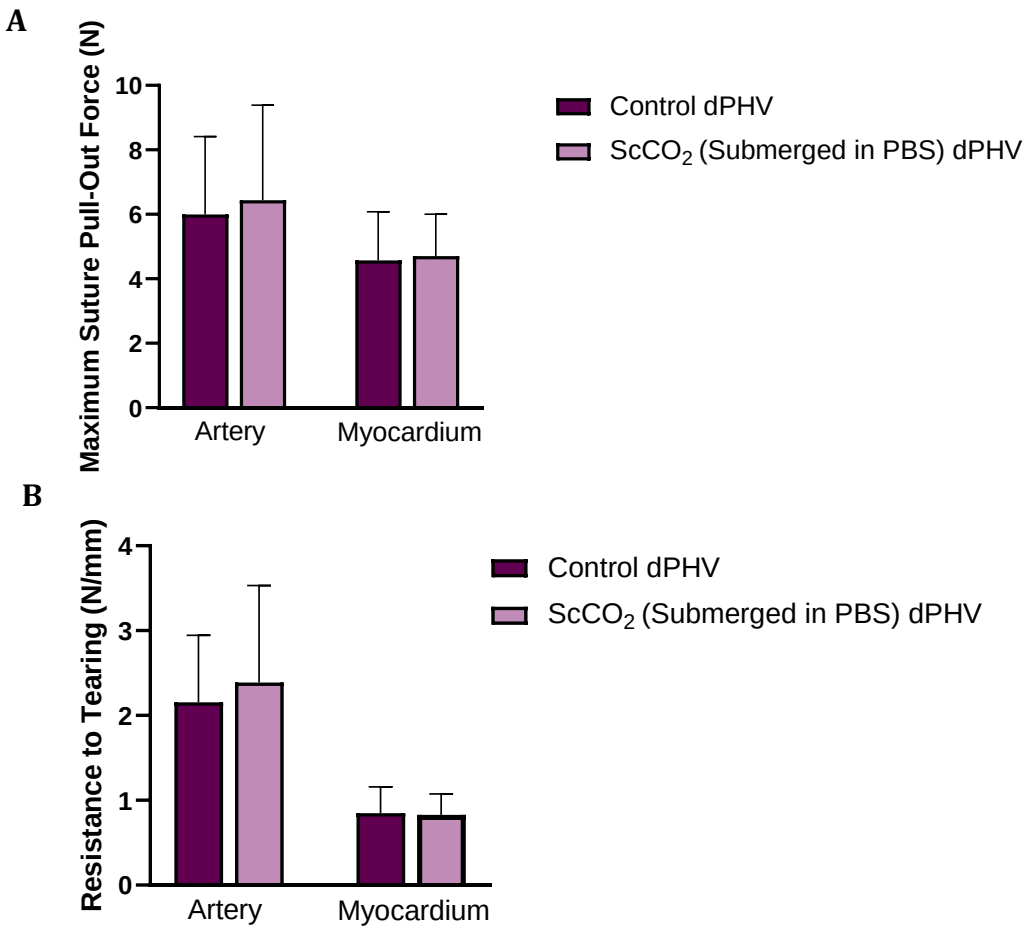


**Figure 6.14 Maximum Suture Pull-Out Force (A) and Resistance to Tearing (B) of Control and ScCO2 (Submerged in PBS) Sterilised dPHV Artery and Myocardium Specimens**

## 6.6 Discussion

$ScCO_2$ (Submerged in PBS) sterilised dPHVs displayed similar suture-retention characteristics to the control dPHVs. This suggested that the dPHV wall and myocardium retains the dPHV mechanical properties following sterilisation with $ScCO_2$. This fits in with the results of control and $ScCO_2$ (Submerged in PBS) sterilised dPHV wall uniaxial tensile testing, where no changes in the tensile parameters in the axial orientation, and only an increase in the elastin phase slope in the circumferential orientation was observed (Chapter 5).

Desai et al. (2018) used the static leakage flow test to investigate the effect of decellularisation on the biomechanical properties of human pulmonary roots. The decellularised tissue was prepared using a specifically designed method as reported by Vafaee et al. (2018), that was also used throughout this study (section 6.4.1). It was found that one out of eight untreated human PHVs were considered fully competent. The competent and incompetent human PHVs had a mean leakage flow rate of ≤ 1.28 $mL.s^{-1}$ and > 1.28 $mL.s^{-1}$, respectively (Desai et al., 2018). All of the human dPHVs tested were not considered competent as they had a mean leakage flow rate of > 1.28 $mL.s^{-1}$. The competency of biological heart valve roots is mediated by the coordinated actions of the annulus, the leaflets, and the artery wall. The pulmonary heart valve root is composed of thin myocardium located on the right side of the heart, and consequentially, the annulus of the pulmonary heart valve root is not fully supported during testing which prevents the full coaptation of leaflets. Thus, it was hypothesisted that the results shown by Desai et al. (2018) was due to the lack of annulus support of the human PHV roots during testing. When repeated with an annulus ring to provide support to the human PHV roots, it was found that five out of eight untreated native PHVs were competent with leakage flow rates ≤ 1.28 $mL.s^{-1}$. From the human dPHV roots retested with annulus support, it was found that only one out of the four human dPHV roots was considered competent, but the mean leakage flow rate of all of the human dPHVs was < 2.5 $mL.s^{-1}$. Therefore, it is clear that the annulus ring provided support to the size and structure of the PHV roots during testing, restoring the physiological geometry of the annulus of the PHV and thus reducing regurgitation. Annulus support was not provided to the dPHV roots during testing in this study, and similar results to those presented in Desai et al. (2018) (without annulus support)

were found, where three out of six control dPHVs and one out of six $ScCO_2$ (Submerged in PBS) dPHVs were considered competent (leakage flow rate < 1.28 $mL.s^{-1}$) . Due to the lack of annulus supported provided to the dPHVs during testing and the novel nature of this research, it was difficult to ascertain whether $ScCO_2$ (Submerged in PBS) sterilisation did impact the functional properties of dPHVs, as opposed to insufficient leaflet coaptation. However, four out of six $ScCO_2$ (Submerged in PBS) sterilised dPHVs had a low leakage flow rate of < 2.5 $mL.s^{-1}$, which was comparable to the control dPHVs, where four out of six dPHVs also had a low leakage flow rate of < 2.5 $mL.s^{-1}$.

In this study, there were no distinct differences in the percentage dilation trends between the two groups. This finding suggests that $ScCO_2$ (Submerged in PBS) sterilisation of dPHVs did not further impact the circumferential expansion properties of dPHV pulmonary arteries. However, samples that were identified as regurgitant during competency assessment in general displayed a greater percentage dilation with increasing pressure. This applied to both control dPHVs and $ScCO_2$ (Submerged in PBS) dPHVs. Desai et al. (2018) also reported similar findings whereby the competency results correlated with the percentage dilation trends of the groups tested, although the results reported were for human PHV tissue. Decellularised human PHVs that were not considered competent displaying an increase in the percentage dilation in comparison to the competent native untreated human dPHVs (Desai et al., 2018). The decellularisation protocol applied requires the removal of excess fat and connective tissue, and scraping of the adventitial layer of the valve root to allow diffusion of 0.1 % SDS, nuclease and protease inhibitors. It is possible that the adventital layer, which is important in providing structural support to the pulmonary artery wall, was disrupted during this procedure which impacted both competency and dilation characteristics. A similar decellularisation protocol was applied to tissue within the present study which could have potnetially disrupted the adventitial layer, impacting both competency and dilation chracteristics of the dPHVs.

It is possible that dPHV hydrodynamic behaviour can be influenced by the circumferential expansion of the pulmonary artery, where excessive dilation of the pulmonary artery wall can lead to PHV regurgitation (Chaturvedi and Redington, 2007). During this study, observations of the dPHV roots during competency

testing were made. Slightly transparent bulges appeared at the annulus, particiularly in the dPHV roots that were not considered competent. This suggests that excess fat and connective tissue was removed from the pulmonary artery inconsistently, disrupting the adventitial layer which had a consequential effect on the competency and dilation biomechanical performance. The excessive dilation of the pulmonary artery due to protruding bulges forming during competeny assessments may have added aditional pressure in the lumen of the dPHV root which the leaflets cannot support, resulting in improper leaflet copation.

Further *in vitro* testing is yet to be performed to assess the impact of $ScCO_2$ (Submerged in PBS) sterilisation on dPHV mechanical properties. Desai (2019) evaluated the functional performance of native and dPHVs under physiological flow conditions, which gives an indication of the dPHV hydrodynamic performance. This was assessed in terms of the transvalvular pressure difference and forward flow performance, which is expressed as valve effective orifice area (EOA), and the regurgitant volumes. In order for the testing of the samples to be successful, the instrumentation was modified to allow secure mounting of the PHV roots to the equipment. The myocardium skirts of the dPHVs used during the study were not trimmed and were therefore used as anchor points for mounting of the dPHV root onto the equipment. The myocardium skirts of the dPHVs used during this study were trimmed, as described in section 2.2.2.3, and therefore were not compatible with the equipment used to assess the functional performance of the $ScCO_2$ (Submerged in PBS) sterilised and control dPHVs.

In a limited number of studies, biaxial tensile tests have also been used to establish the mechanical properties of heart valves. Dynamic biaxial testing is more relevant for the mechanical characterisation of valve leaflets as it is more relevant to their *in vivo* physiological conditions (Hasan et al., 2014). Grashow et al. (2006) detailed a commonly applied biaxial test for valve leaflets. Tensile loads are applied to the specimen at regions of the specimen edges, stretching the specimen in two distinct directions. It was also advised that this procedure should occur whilst the sample is immersed in phosphate buffered saline (PBS) at physiological temperature (Hasan et al., 2014). Huang, H.Y. et al. (2012) conducted a study where biaxial mechanical testing was utilised to characterise the biaxial mechanical responses of porcine aortic and pulmonary valve leaflet tissues. Sample deformation and strain

axes during the mechanical characterisation was also established. The results from this study provided evidence that aortic valves exhibit stronger anisotropic mechanical behaviour than that of the pulmonary valves when less than 18 % strain equibiaxial stretching is applied. In contrast to this, the pulmonary valves exhibit stronger anisotropic mechanical behaviour than that of the aortic valves when more than 28 % strain equibiaxial stretching is applied. The mechanical behaviours were then related to collagen fibre microstructures of the aortic and pulmonary valves used in this study. The orientation of the circumferentially aligned collagen fibres was determined to dictate these highly anisotropic properties of the heart valve tissues. However, a limitation associated with biaxial tensile testing is that damage may be introduced to test specimens during clamping.

Overall, $ScCO_2$ (Submerged in PBS) sterilised dPHVs demonstrated similar functional and biomechanical characteristics to control dPHVs.

# Chapter 7 : Discussion

## 7.1 General Discussion

Heart valve replacement surgery is often a necessity for patients with dysfunctional heart valves. Current valve replacement options include mechanical, bioprosthetic and biological (allograft or autograft) heart valves. The implantation of mechanical heart valves require the life-long use of anticoagulation therapy due to introducing a high thromboembolic risk. Bioprosthetic heart valves may be selected for surgical implantation in the elderly and women of child-bearing age as the need for anticoagulants is averted. However, bioprosthetic heart valves are subject to material fatigue and can also initiate a pro-inflammatory response which can cause progressive calcification, leading to graft failure and therefore, surgical reintervention (Harris et al., 2015). Allograft heart valves have inherent properties ideal for the native-like function of the graft. However, allografts are limited in availability (Lisy et al., 2017). Additionally, mechanical, bioprosthetic and biological heart valve replacement options may eventually require surgical reintervention in paediatric patients as they may outgrow the heart valves as a result of poor structural and functional regenerative capabilities. Thus, there is a clinical requirement for a novel heart valve replacement option that can provide long-term positive clinical outcomes by addressing the limitations of current options.

A decellularisation protocol for xenogeneic heart valves has previously been developed, potentially offering a promising alternative graft material for heart valve replacement (Booth et al., 2002; Luo et al., 2014; Wilcox et al., 2005). Decellularised xenogeneic tissue has characteristics required to perform as an optimum heart valve replacement option, such as durability, non-immunogenicity, non-thrombogenicity, and ability to grow and remodel owed to the inherent native-like ECM structure (Luo et al., 2014; Paniagua Gutierrez et al., 2015; Vafaee et al., 2018). These characteristics enable decellularised xenogeneic heart valves to potentially last the recipient's lifespan. Xenogeneic tissue is also available as an unlimited resource giving it the advantage over allogeneic tissues. Porcine aortic heart valves that were decellularised in a similar manner to the decellularised porcine pulmonary heart valves utilised during this study have demonstrated

regenerative potential when implanted into a sheep model (Paniagua Gutierrez et al., 2015).

Decellularised allograft heart valves currently in clinical use rely on aseptic conditions during procurement and production and antibiotic or chemical disinfection to assume sterility (da Costa, F.D. et al., 2006; Waqanivavalagi et al., 2020). However, medical devices are required to provide a sterility assurance level of at least $10^{-6}$ to prevent the introduction of pathogens when implanted into patients (von Woedtke and Kramer, 2008). Therefore, a sterilisation method suitable for decellularised tissue heart valves needs to be identified to provide the required sterility assurance level (as a medical device), improve production efficiency, ultimately enhancing clinical translation. Treatment processes traditionally employed for the sterilisation of medical devices, or high level disinfection of human tissue grafts include ionising radiation such as gamma radiation and e-beam, and chemical methods such as PAA, glutaraldehyde, and ethylene oxide (Hogg et al., 2015; Luo et al., 2014; Somers et al., 2009). However, such methods have been documented to detrimentally impact proteinaceous tissue material properties (Cao, Q. et al., 2013; Scheffler et al., 2008). Traditional sterilisation methods have thus been disregarded for the processing of decellularised heart valves.

Therefore, the overarching aim of this study was to identify a novel sterilisation method appropriate for use with a previously developed decellularised porcine pulmonary heart valve.

The replicability and consistency of the previously established low concentration detergent based decellularisation method (Luo et al., 2014; Vafaee et al., 2022) was assessed prior to investigating the effects of sterilisation methods on the tissue. This stage was included to ensure consistent inter-operator production of decellularised heart valve conduits, and provide appropriate biological and biomechanical baseline data prior to introduction of alternative sterilisation processes. A batch of decellularised porcine pulmonary heart valves that had less than 50 ng of double stranded DNA per mg of tissue (dry weight), an absence of visible nuclei, retained ECM integrity, *in vitro* biocompatibility, and overall similarity of biomechanical properties in comparison to native tissue were successfully produced, which demonstrated process reproducibility.

Prior to clinical translation, medical devices derived from xenogeneic sources are required to be sterilised to meet the levels defined in BS EN 556-1 (BSI, 2001a). As stated in standard BS EN 556-1, less than 1 in 1 million medical devices that have been sterilised may contain a viable pathogen (BSI, 2001a). The identification and application of a suitable sterilisation process is required for decellularised porcine pulmonary heart valves to meet this sterility assurance requirement of medical devices without compromising the functional properties of the tissue scaffolds. Validation of sterilisation efficacy of the sterilisation methods investigated was beyond the scope of the present study. Therefore, the current study should be deemed a feasibility study to evaluate the compatibility of the chosen sterilisation methods with decellularised heart valves. Current sterilisation methods have been shown to have a detrimental impact on tissue graft microstructure and biomechanical strength (Matuska and McFetridge, 2015). This is due to ECM structural damage induced by oxidative degradation, thermal denaturation and/or cross-linking and chain scission (Deborde et al., 2016; Mazor and Zilberman, 2017). The ECM structural network contains biological cues for cellular infiltration and tissue growth. Retention of the biological composition and biomechanical properties are collectively crucial for the favourable integration and performance of the graft *in vivo*. The impact to these tissue properties must be considered when selecting a sterilisation method. Additionally, the feasibility of the sterilisation method to be applied to the medical device during mass production must also be regarded.

Gamma irradiation sterilisation has been used for the sterilisation of allografts and commercially available decellularised xenografts derived from bone, dermis and cornea (Capella-Monsonís and Zeugolis, 2021). This is because gamma irradiation is a terminal sterilisation method and is widely available in medical device manufacturing as ISO 11137 has been published to support establishing the appropriate gamma irradiation sterilisation dose (Capella-Monsonís and Zeugolis, 2021; ISO, 2006; Song and Ott, 2011). However, there is general consensus that gamma irradiation sterilisation compromises the mechanical stability of collagenous scaffolds (Freytes et al., 2008). The industry standard gamma-irradiation sterilisation dose for devices that come into contact with skin and tissue is 25 kGy (Mazor and Zilberman, 2017). It is of interest to use irradiation doses lower than 25 kGy to retain tissue graft mechanical stability. Helder et al.

(2016) exposed decellularised porcine aortic heart valves to gamma irradiation in doses of 1,500 Gy and 3,000 Gy. *In vitro* investigations revealed evidence of contamination of 1,500 Gy irradiated cusps and significant reduction in stiffness and tensile strength of the decellularised porcine aortic cusps exposed to both doses in comparison to the untreated controls. Despite these findings, *in vivo* experiments were carried out using 3 juvenile sheep which received 1,500 Gy and 3,000 Gy gamma irradiated decellularised porcine aortic heart valve implantation into the right ventricular outflow tract. Both doses showed signs of regurgitation and stenosis following two months and signs of infection were demonstrated by an abundance of neutrophils in the explanted valve irradiated with 1,500 Gy gamma irradiation. Based on these findings, Helder et al. (2016) proposed that a balance cannot be obtained between achieving irradiation mediated sterilisation without inducing detrimental damage to decellularised porcine heart valves. Although, sterility effectiveness of the selected doses should have been investigated in greater depth prior to implantation into the sheep since below commercially relevant doses were being investigated. The current market is also facing a supply shortage of cobalt-60 required for gamma irradiation which cannot meet the growing demand for medical device sterilisation (Wiens, 2018). Therefore, alternative methods of medical device sterilisation need to be explored.

As traditional methods of sterilisation are evidenced to be unsuitable for decellularised heart valves, the novel sterilisation methods $CuCl_2$ and $H_2O_2$, and $ScCO_2$ under standard (packaged and processed in Poly-Tyvek pouches) and submerged conditions were selected as candidate sterilisation methods within this study. Existing research indicates that these sterilisation methods do provide the required sterility level (Leow-Dyke et al., 2017; White, A. et al., 2006) . $CuCl_2$ and $H_2O_2$ is a cost-effective sterilisation method that can potentially be performed on site. Chemical formulations containing a combination of $CuCl_2$ and $H_2O_2$ have not yet been used as a sterilisation agent by tissue banking or tissue engineering despite the well documented bactericidal and virucidal activity of copper ions potentiated by $H_2O_2$ (Sagripanti and Kraemer, 1989; Sagripanti et al., 1993). However, this has recently gained interest by NHS BT tissue bank for decellularised (dCELL) human dermis sterilisation. Investigations conducted by Leow-Dyke et al. (2016, 2017) have shown that $CuCl_2$ and $H_2O_2$ solutions with demonstrated bactericidal and sporicidal activity had no effect on the biological

and biomechanical properties of dCELL human dermis, while biocompatibility was retained. To date, the work conducted by Leow-Dyke et al. (2016, 2017) is the only account of exposing biological tissues to $CuCl_2$ and $H_2O_2$ formulations, providing scope for the potential advantages of exploring this sterilisation method on other tissues. This study provided the basis for the use of $CuCl_2$ and $H_2O_2$ formulations for investigation within the present study as dPHV is also composed of soft, delicate tissue. Although understandably, the ideal formulation specific to dPHV tissue required optimisation within the present study to allow sterilisation to be achieved at less harsh conditions of pH 7, 37 °C.

Within the past few years, $ScCO_2$ has gathered attention due to research continuously providing evidence promoting $ScCO_2$ sterilisation of sensitive biomaterials. When applied with additives such as PAA and $H_2O_2$, $ScCO_2$ can achieve a SAL of $10^{-6}$ in tissues and biomaterials under moderate conditions. The retention of tissue ECM structure, biomechanical properties and good biocompatibility has been demonstrated in porcine heart valves and rat lungs, and the retention of biological cues within ECM hydrogels was reported (Balestrini et al., 2016; Hennessy et al., 2017; White, Lisa J. et al., 2018). $ScCO_2$ has a low viscosity and surface tension which facilitates penetration of complex tissues and porous materials (McHugh and Krukonis, 2013). This feature enables $ScCO_2$ to be considered a terminal sterilisation method which is essential to provide an 'off-the-shelf' packaged graft that is safe for implantation. These advantageous features collectively provided evidence to include $ScCO_2$ sterilisation for investigation within this study.

Initial macroscopic observations indicated that $ScCO_2$ sterilisation carried out under the standard process resulted in the undesired compression of the dPHV valve conduits. This was most likely due to the lack of structural support provided in the presence of high pressure application. Whereas, the gross geometry of the dPHV grafts was preserved following $ScCO_2$ sterilisation under submerged conditions, and $CuCl_2$ and $H_2O_2$ sterilisation. It is possible that the observed change to the macroscopic geometry could have downstream implications on the *in vivo* valve function as the graft tubular structure required for uninhibited blood circulation was lost. The resultant compressed artery can lead to valvular dysfunction, as well as the onset of morbidities such as hypertension and

atherosclerosis (Han, 2012). As described in Chapter 6, the pulmonary artery of the dPHV root plays a role in sufficient leaflet coaptation by transmitting stress from the leaflets to the pulmonary artery during systole (Desai et al., 2018; Hopkins, R.A., 2003; Sutton et al., 1995). The deformed heart valve root can therefore result in incomplete leaflet expansion which may lead to accelerated valve degeneration due to increased flexural strains (Smith, D.B. et al., 1999). Although a potential solution is to insert a cylindrical structure such as a conical tube into the lumen of the graft during standard $ScCO_2$ sterilisation processing, it is not clear how this would further impact the structure as this has not yet been investigated.

The macroscopic observations tied together with the observations from histological examination, which revealed the compression of the leaflet fibrous network treated with $ScCO_2$ under standard conditions in comparison to the decell control. It is plausible that this could potentially inhibit sufficient recellularisation *in vivo* as the interfibrillar pore sizes may be too compact for cells to successfully migrate into (Jana, Soumen et al., 2019). Given the novel nature of $CuCl_2$ & $H_2O_2$ sterilisation, preliminary experiments were conducted to determine the optimum $CuCl_2$ and $H_2O_2$ combination concentration in addition to the optimum time exposure for sufficient sterilisation without inducing major changes to the tissue histoarchitecture. The chosen concentration combination of 1 mg/L $CuCl_2$ and 1 % $H_2O_2$ with 3 hours exposure performed well as a prompt sterilant without inducing major ECM changes in the preliminary experiments and was therefore selected to expose a full batch of dPHVs to in order to conduct further biological and biomechanical analysis. However, upon further analysis $CuCl_2$ and $H_2O_2$ sterilisation treatment induced detrimental damage to the leaflet *ventricularis,* with what appeared to be loose irregular elastin fibres. These results were contrasting to the findings made by Leow-Dyke et al. (2016), who reported that $CuCl_2$ and $H_2O_2$ sterilisation using the aforementioned concentrations did not detrimentally impact dCELL dermis histoarchitecture. SEM analysis also demonstrated damage to the ECM surface microscopic structures which was not observed in tissue exposed to $ScCO_2$ treatment. Oxidative effects of hydroxyl radicals on soft tissue ECM, such as protein cross-linking, are well documented. It is hypothesised that structurally specific oxidative modifications occur via hydroxyl radical and tyrosyl radical mediated pathways. Oxidants react with

collagen, leading to the formation of ditrosyrine as a result of tyrosine residue oxidation. Dityrosine has been demonstrated to cross-link proteins, impacting the protein structure and therefore pose implications on function (Balasubramanian and Kanwar, 2002; Souza et al., 2000). Oxidative stress can lead to increased expression of matrix metalloproteinases which degrade ECM components, release bioactive fragments to the site of degeneration further exacerbating a pro-inflammatory response which can lead to fibrosis, calcification, and eventually graft regeneration (Deborde et al., 2016; Greenberg et al., 2021). Christian et al. (2014) exposed bovine pericardium to *in vitro* oxidising conditions using 1 % $H_2O_2$ which was reported to significantly deteriorate collagen histoarchitecture and increase susceptibility to collagenase degradation after 7 days. Bovine pericardium that was modified via covalent attachment of the oxidant scavenger 3-(4-hydroxy-3,5-di-*tert*-butylphenyl) propyl amine (DBP) was resistant to oxidation-induced structural damage. Therefore, the detrimental impacts of $CuCl_2$ and $H_2O_2$ sterilisation on heart valve histoarchitecture can potentially be refined by exploring the use of oxidant scavengers.

Although $ScCO_2$ processing incorporates oxidising agents to achieve sterility, degradation of ECM components was not apparent following histological examination. However, there was found to be a significant reduction in antibody labelling for collagen IV (a basement membrane constituent) in the leaflet specimens treated with $ScCO_2$ under both conditions in comparison to the $CuCl_2$ and $H_2O_2$ treated specimens. The most-likely mechanism that underlies the observed changes is the presence of residual chemical constituents from the NovaKill additive solution following $ScCO_2$ sterilisation. Similar results were reported by Luo et al. (2014) and Holland, James D. R. et al. (2021). While the nature of the mechanisms underlying these observations remain unknown, it has been hypothesised that PAA treatment was the most likely origin of the collagen IV loss from the basement membrane (Holland, James D. R. et al., 2021; Luo et al., 2014). Following $ScCO_2$ sterilisation under submerged conditions, the dPHV specimens remained submerged in the PBS containing PAA additive solution for up to one week (until the sterilised dPHVs were received back from NovaSterilis). The submerged $ScCO_2$ processing conditions were explored under the hypothesis that the local concentration of oxidising agents would not be too high. PAA supplementary solution was not washed from the tissue after $ScCO_2$ sterilisation

under normal conditions (dPHVs packaged and processed in Poly-tyvek pouches), instead an extraction cycle ($ScCO_2$ treatment at 1,410 psi and 35 °C for 1 hour in the absence of NovaKill additive) was performed to remove PAA. It has since been acknowledged by NovaSterilis that residual PAA may be present despite the performance of an extraction cycle (Bednarski et al., 2020; Bennet et al., 2021). As such, NovaSterilis have recently developed a PAA quantification kit to quantify residual PAA concentrations. Although there were other means of quantifying PAA, it was likely that PAA was present on the specimens following $ScCO_2$ processing as the scent of acetic acid was noticeable. Furthermore, it was not within the scope of the present study to quantify residual PAA concentrations at this stage. $CuCl_2$ and $H_2O_2$ sterilised dPHVs were rinsed and stored in fresh PBS immediately after sterilisation treatment, preventing the non-essential exposure of the tissue to oxidising agents for an elongated time period which ultimately could have protected the basement membrane from oxidative degradation. Quantification of active oxidising agent levels in the dPHVs sterilised with $ScCO_2$ under both conditions and $CuCl_2$ and $H_2O_2$ would provide further insight into the mechanism proposed for the observed ECM degradation.

It is possible that the observed reduction in collagen IV labelling in $ScCO_2$ sterilised dPHVs may propose a detrimental impact the ability of PHVs to regenerate *in vivo*. Collagen IV is believed to play an important role in tissue endothelialisation (Herbst et al., 1988). Collagen IV provides anchor-points for cell-attachment proteins such as laminin and fibronectin. Contrasting to the proposed mechanism for the loss of collagen IV labelling, fibronectin was unaffected following $ScCO_2$ sterilisation under both conditions, similarly to $CuCl_2$ and $H_2O_2$ sterilisation. This suggests that collagen IV was still potentially present, but the conformation of the target epitope was modified by the presence of PAA containing NovaKill reagent in such a way that the antibody used for collagen IV binding can no longer detect it, resulting in what was shown to be a loss of basement membrane. Fibronectin is an multifunctional glycoprotein that aids in the regulation of cell behaviour through interacting with growth factors, cell surface receptors such as integrins and other ECM proteins, as well as providing a fibrillar matrix around cells (Michalski et al., 2020). This suggests that the ability of decellularised PHVs to promote and support regeneration of the ECM *in vivo* may not have been compromised. However, this remains inconclusive as the retention of specific ECM components following $ScCO_2$

sterilisation has not yet been explored within the literature. Vafaee et al. (2018) found that decellularised human aortic and pulmonary wall and leaflet specimens that retained collagen IV, laminin and fibronectin following decellularisation showed evidence of tissue integration and recolonisation *in vivo* using a mouse subcutaneous implant model. Laminin levels in dPHV tissue following sterilisation were not analysed within the present study. However, immunohistochemical labelling of laminin would have provided further insight into the impact of the sterilisation methods on the basement membrane integrity. This would have also provided further evidence into whether ECM oxidative damage occurred following sterilisation, or if the antibody specific target epitopes used for collagen IV labelling were potentially altered by oxidative reactions in such a way that fibronectin and laminin remained unaffected.

Although the collagen IV content appeared reduced following $ScCO_2$ sterilisation, gross collagen concentration was generally greater following $ScCO_2$ sterilisation under both conditions. This is most likely explained by the wider $ScCO_2$ applications, one of which is an extraction method. Non-polar molecules such as residual lipids can be solubilised by $ScCO_2$ in the presence of polar cosolvents such as ethanol, whilst polar ECM proteins remain preserved. The solubility of highly non-polar ECM proteins increase with an increase in treatment pressure required by $CO_2$ to reach supercritical state. These conditions required for optimal non-polar molecular extraction can be manipulated to enhance this function (Gafarova et al., 2020; Wang, C.-H. et al., 2020). As such $ScCO_2$ sterilisation has also been explored by many research groups to be employed as a decellularisation method. Chou et al. (2020) applied $ScCO_2$ at temperatures and pressures up to 40 °C and 5076 psi, respectively, with 75 % ethanol as a cosolvent to successfully extract cellular materials from porcine dermal layers. Thus, the extraction capabilities of $ScCO_2$ treatment may have removed residual soluble ECM molecules that remained following decellularisation. This can account for a difference in the relative proportion of dPHV tissue biological components, resulting in what appears to be an increase in collagen content.

Collagen content remained unaltered following $CuCl_2$ and $H_2O_2$ sterilisation. Similarly, Leow-Dyke et al. (2016) found that $CuCl_2$ concentrations ranging from 0.1 mg/ L – 10 mg/L combined with $H_2O_2$ concentrations ranging from 0.01 % - 1

% were not associated with any hydroxyproline content alterations. In line with intact collagenous network observations, it was suggested that there was no collagen denaturation associated with the $CuCl_2$ and $H_2O_2$ treatments. However, histological analysis revealed $CuCl_2$ and $H_2O_2$ sterilisation did impact the dPHV ECM histoarchitecture, whereas the histoarchitecture of $ScCO_2$ treated tissue remained undamaged.

Differential scanning calorimetry was employed to analyse the dynamic tissue collagen structure following sterilisation treatments. There was found to be a significant reduction in the collagen denaturation temperature of dPHVs following treatment with $ScCO_2$ under both conditions and $CuCl_2$ and $H_2O_2$, although the difference was not greater than 4 °C in comparison to the untreated controls. This suggests that there may have been rearrangements to the collagenous tertiary structure as the thermal energy required to denature and uncoil collagen was altered. A mechanism proposed for these findings is that the collagenous fibre network could become unorganised, either as a result of dehydration or the extraction of other ECM components (Antons et al., 2018; Casali et al., 2018). The susceptibility of ECM components to oxidative degradation is also well known and has been acknowledged within this study. Both sterilisation methods investigated within this study incorporated the use of $H_2O_2$ due to the high oxidising capacity required to inactivate microbial cells and spores (Wardle and Renninger, 1975). Although hydroxyl radicals are actively involved in achieving sterility of tissue grafts, intramolecular hydrogen bonds found between collagen fibrils can become disrupted following hydroxyl radical interactions, destabilising the macromolecular structure (Rabotyagova et al., 2008; Streeter and de Leeuw, 2011). Consistent with the collagen quantification findings and the intact collagen histoarchitecture, it is plausible that the extraction of soluble ECM components and/or residual cellular material could have resulted in a tertiary collagen structural rearrangement following $ScCO_2$ treatment. Hennessy et al. (2017) found that the peak denature temperature of aortic valve leaflets treated with $ScCO_2$ under standard conditions was 69.58 °C which was close to the peak denature temperature of native untreated aortic heart valves at 65.75 °C. However, the statistical significance of this finding cannot be verified as the thermal denaturation temperature of replicate samples was not assessed. With regards to the alterations to tissue thermal stability following $CuCl_2$ and $H_2O_2$ sterilisation,

slight oxidative degradation is the most likely cause as it is known that cuprous and cupric ions can mediate site specific cross-linking, carboxylation and fragmentation of collagen when combined with $H_2O_2$ (Hawkins, C.L. and Davies, 1997). This correlates with the modified histological observations of the leaflet following $CuCl_2$ and $H_2O_2$ treatment. Directly quantifying denatured collagen content following $ScCO_2$ and $CuCl_2$ and $H_2O_2$ sterilisation treatment should be approached in future investigations to give a better indication of the severity of potential damage induced.

Biocompatibility was not adversely impacted by the sterilisation methods investigated within this study. The L929 immortalised mouse fibroblast cell line used in cytotoxicity assessments was selected in accordance to ISO standard 10993-5 (2009), which details cytotoxicity testing using established cell lines that should be applied to medical devices to determine biocompatibility. However, the L929 cell line is not relevant to heart valve tissue. Balestrini et al. (2016) used contact cytotoxicity assessments to demonstrate the biocompatibility of $ScCO_2$-treated decellularised rat lungs with rat microvascular lung endothelial cells and human A549 cells (a type II epithelial-like cell line). Leow-Dyke et al. (2016) also found that 1 mg/L $CuCl_2$ and 1 % $H_2O_2$ treated dermis was biocompatible using *in vitro* contact cytotoxicity assessments with human skin fibroblasts.

In conjunction with the retention of fibronectin, biocompatibility may indicate that the sterilisation methods investigated in the present study may be able to support dPHV recellularisation post-implantation. However, the present study is limited to *in vitro* biocompatibility assessments. Further analysis is essential to investigate the impact of the sterilisation methods on the dPHVs capabilities to support cell attachment and migration, required for graft regeneration *in vivo*.

Uniaxial tensile testing was used to determine the impact of $ScCO_2$ sterilisation under both conditions and $CuCl_2$ and $H_2O_2$ sterilisation on the dPHV wall and leaflet material properties. All sterilisation methods investigated within this study had some impact on the uniaxial tensile testing parameters. $CuCl_2$ and $H_2O_2$ sterilisation was found to have a negative impact on the mechanical strength of dPHVs. It is possible that the disrupted leaflet ECM architecture, as shown by histological analysis, may have been a demonstration of disordered ECM fibre organisation which can disrupt the tissue biomechanical function. $ScCO_2$

processing of dPHVs appeared to preserve the mechanical integrity of the tissue as they showed similar or greater elastin phase slope, collagen phase slope and UTS in comparison to the untreated dPHV controls. Similar findings were reported by Balestrini et al. (2016), Halfwerk et al. (2018) and Hennessy et al. (2017), demonstrating the compatibility of $ScCO_2$ sterilisation of various other tissue types such as lung, pericardium and aortic heart valves, respectively. Balestrini et al. (2016) found no significant difference in the failure strain but an increase in the stiffness of $ScCO_2$-treated decellularised rat lung matrices, although only at non-physiological levels of stretch. Halfwerk et al. (2018) found no significant difference in tensile strength but reported that the stiffness was significantly higher in $ScCO_2$ processed decellularised porcine pericardium in comparison to the native tissue. Hennessy et al. (2017) found an increase in the ultimate tensile strength of $ScCO_2$ treated decellularised porcine aortic heart valve leaflets in comparison to non-sterilised decellularised aortic heart valve leaflet controls. However, the mechanisms underlying these findings remain unclear. It was proposed by Balestrini et al. (2016) that ECM cross-linking may have occurred as a result of the high pressures and chemical environment that tissues are exposed to during $ScCO_2$ sterilisation, which could provide long-term protection to the integrity of $ScCO_2$ treated tissues by preventing hydrolysis often observed during storage (Balestrini et al., 2016).

Although $ScCO_2$ did not reduce the tensile strength of dPHVs, there were still significant increases in some of the uniaxial tensile testing parameters with no indication into how the biomechanical function may be impacted as a result. Due to limitations during this study, $ScCO_2$ processing of dPHVs whilst submerged in PBS was the only sterilisation method selected for further biomechanical analysis. This was justified by the retention of the gross dPHV macroscopic geometry following sterilisation which is essential for physiological performance *in vivo*, the largely retained biological components, and the uniaxial tensile testing parameters were most similar to the untreated dPHVs. Although it was acknowledged that further biomechanical testing on dPHVs sterilised with $ScCO_2$ under standard conditions and $CuCl_2$ and $H_2O_2$ would have provided more depth to this study, and should be the subject of future studies.

Replacement heart valves are typically sutured to the annulus that remains *in situ* following the removal of the native valve. The failure of the suture attachment, which can be due to the replacement heart valve material not being strong enough to withstand physiological pressures *in vivo* can lead to severe health complications (Pierce et al., 2016). Thus, suture-retention characteristics were analysed to further investigate the impact of $ScCO_2$ (Submerged in PBS) sterilisation on the dPHV material properties. $ScCO_2$ (Submerged in PBS) sterilised dPHVs displayed similar suture-retention characteristics to the decell control dPHVs.

Competency testing was performed to assess leaflet coaptation under a static back pressure. The anatomical configurations of the whole heart valve root coordinates the tissue competency, with the leaflets, artery wall and annulus synchronously actioning leaflet coaptation. Therefore, increased elasticity and/or stiffness to the artery wall or leaflets can result in a regurgitant heart valve by impacting correct leaflet coaptation (Desai et al., 2018; Sabbah et al., 1986). The results from the competency testing in the present study were inconclusive and did not add relevant knowledge required to ascertain the impact of $ScCO_2$ sterilisation under submerged conditions on the competency of dPHVs. This was because of a flaw highlighted within the experimental method in that annulus support was not provided to the thin myocardium component of the dPHV root. The conditions used therefore did not resemble the heart valve anatomical configuration *in vivo*. This may have impeded the results by presenting as a confounding factor in the regurgitation rates recorded within this study. Desai et al. (2018) found that human decellularised PHVs had a high leakage rate of > 1.28 mL/s without annulus support which was corrected by the incorporation of an annulus ring on the human decellularised PHVs, after which the human decellularised PHVs competency was comparable to native human PHVs in terms of withstanding the physiological static pressure with minimal back flow. The addition of annulus support can mimic the support to the dPHV provided by the heart. The repetition of competency testing of the sterilised dPHV specimens and the untreated dPHV controls with the addition of annulus support, alongside further *in vitro* functional performance analysis should be investigated in future studies.

The expansion of the pulmonary artery component of the dPHV root is also essential for the physiological function of the dPHV graft when implanted. The expansion characteristics are important to investigate as stress-induced damage to the graft may occur following overexpansion. This study demonstrated that the expansion characteristics of dPHVs sterilised with $ScCO_2$ under PBS submerged conditions were qualitatively similar to the expansion characteristics of untreated dPHVs. However, statistical analysis could not be performed due to the variations in the starting pressures of each specimen. The methodology used to analyse the artery expansion characteristics therefore requires refinement to allow the retrieval of raw data suitable for statistical analysis.

## 7.2 Future Work

The present study demonstrated that all of the sterilisation methods investigated did invoke some alterations to dPHVs. Observations such as changes to the ECM histoarchitecture, reduction in collagen IV labelling intensity, increase in collagen content, decrease in collagen denaturation temperature, and increase or decrease in the biomechanical properties imply that the ECM components were impacted by the sterilisation methods investigated. However, the mechanisms underlying these changes are not yet fully elucidated. Understanding the nature of these changes may provide insight into how well the graft can function *in vivo*, and if necessary how the sterilisation process can be refined to prove better compatibility with the tissue.

While $CuCl_2$ and $H_2O_2$ sterilisation appeared unfavourable for dPHV sterilisation, the potential of this sterilisation method was demonstrated throughout this study. Further refinement of the candidate $CuCl_2$ and $H_2O_2$ concentration combinations may allow the selection of a better suited sterilant for dPHVs that enables the retention of the tissue biological and biomechanical properties whilst sufficiently removing bioburden. Leow-Dyke et al. (2016) identified a range of $CuCl_2$ and $H_2O_2$ concentrations that had proven compatibility with dCELL human dermis as demonstrated by retained morphology, functionality and biocompatibility. It is plausible that this can also be achieved for heart valve tissues by repeating the biological and biomechanical analysis following the exposure of dPHVs to a range of $CuCl_2$ and $H_2O_2$ concentrations.

Confirmation of oxidative damage to the ECM fibrillar collagen following sterilisation could be achieved through qualitative and quantitative denaturation collagen analysis. However, a limitation within the present study was that the intricate sample preparation process, from retrieval of the native porcine PHV root to the decellularisation process completion, made it difficult to produce enough dPHV samples within the same batch for comparative analysis. Hwang et al. (2017) have described the use of a unique and novel collagen hybridising peptide (CHP) that has been proven to specifically bind to denatured collagen. The peptide's biochemical composition and the absence of binding sites renders it incompatible to bind with intact collagen and other ECM biomolecules. In conjunction with immunohistochemistry, SEM and second harmonic generation imaging, the use of CHP has been shown to provide valuable insight into the visualisation, location and intensity of denatured collagen molecules in tissues. This would address the sample size limitation by enabling the analysis of smaller sample sizes. On the other hand, Holland, James D. R. et al. (2021) used an established biochemical assay to quantify denatured collagen content by applying readily available resources. Damaged collagen content was assessed by subjecting tissue specimens to enzymatic digestion using α-chymotrypsin which selectively digests denatured collagen molecules, releasing quantifiable hydroxyproline after acid hydrolysis of the supernatant. However, this method would not have given indication into the location of the denatured collagen in the tissue. Nonetheless, both methods for denaturated collagen content analysis would provide invaluable indication into the impact of the sterilisation methods on ECM collagenous integrity.

Paired comparisons of whole dPHV root biomechanical parameters with and without sterilisation would address the inherent biological variation limitation and give a better indication into how the sterilisation method impacts the biomechanical performance of dPHVs. Desai et al. (2018) found that the paired competency and circumferential dilation comparison of native and decellularised human PHVs were not significantly different, providing evidence that the test methods would not destroy the specimens biomechanical configuration for subsequent testing. Within the present study, affirming sterility of the unprocessed specimens that were produced in aseptic conditions was essential to prevent microbial contamination of specimens which could potentially impact the tissue integrity and therefore function. The mechanical testing of unprocessed dPHVs

should be strategised to ensure that subsequent sterilisation would occur in a short time-frame as to eliminate any potential contaminants before the tissue could be impacted.

The extensive *in vitro* functional performance evaluations that all prosthetic heart valves have to conform to prior to *in vivo* testing has been highlighted in ISO 5840-1 (2021). In accordance to this standard, future studies should be undertaken to further define the *in vitro* hydrodynamic performance, durability and leaflet kinematics of sterilised dPHVs in comparison to untreated dPHVs. Desai et al. (2018) described the use of a pulsatile flow simulator to evaluate the hydrodynamic performance of native and decellularised human heart valve roots. The simulator used allowed the application of physiological ventricular pressure and flow waveforms as well as video recordings of leaflet motion. It was reported that decellularised human pulmonary heart valve roots demonstrated low transvalvular pressure gradients and leaflet kinematics comparable to the native tissue. Cyclic testing of heart valve grafts is essential to determine the lifespan of the tissue under simulated physiological conditions. An *in vitro* real-time fatigue assessment method for biological heart valve roots has been developed, refined and performed by Desai et al. (2022). During the testing, native and decellularised porcine aortic heart valve roots were subject to 120 bpm under physiological cyclic pressures for up to 1.2 million cycles, where no fatigue differences between the two groups was found. This testing allowed the characterisation of the decellularised heart valve long-term performance in line with the requirements highlighted in ISO 5840 (5840-1, 2021). Modifications to the apparatus and physiological conditions used during testing that conform to the distinctions between aortic and pulmonary heart valve roots can potentially allow this test method to be effective for analysing the long-term durability of sterilised decellularised porcine pulmonary heart valve roots. The inclusion of such evaluations in future studies would give indication into how sterilisation can further support long-term durability.

The role of macrophages in decellularised biological scaffold regeneration has been well documented by Brown, B.N. et al. (2012), Paniagua Gutierrez et al. (2015) and Vafaee et al. (2022). It is recognised that macrophages can adopt both the proinflammatory phenotype, known as M1, and reparative anti-inflammatory

phenotype known as M2. Paniagua Gutierrez et al. (2015) found that decellularised porcine aortic heart valves implanted into the RVOT of pigs demonstrated self-regenerative capabilities after 15 months which was paired with the presentation of M2 macrophages in high abundance in the repopulated valves. Vafaee et al. (2022) explored the cellular population of decellularised porcine PHV roots following implantation into the right ventricular outflow tract of sheep. The porcine PHVs were decellularised using a method incorporating low concentration SDS (0.1%) and proteinase inhibitors, similar to that used within this study. At 1-3 months post-implantation, it was found that the repopulation of decellularised tissues with stromal and progenitor cells was orchestrated by MAC 387+ infiltrating macrophages recruited from blood monocytes which then recruited tissue resident CD 163+/MAC 387− M2 macrophages in the tissue remodelling response. A higher M2:M1 ratio has also been associated with positive remodelling outcomes (Brown, B.N. et al., 2012; Brown, B.N. et al., 2009). M1 and M2 phenotypes respectively express CD80/CCR7 and CD163/CD206 cell surface markers, allowing immunohistochemical characterisation of the expression and localisation of pro or anti-inflammatory macrophages (Lock et al., 2019). The immunomodulatory effect of decellularised tissues can also be analysed by using enzyme-linked immunosorbent assay (ELISA) to measure the concentration of pro and/or anti-inflammatory cytokines, chemokines and growth factors released by immune cells in response to the tissue (Brown, B.N. et al., 2012; Lock et al., 2019). Although the immunoreactivity of tissues decellularised using a method similar to that used within this study has been evidenced to demonstrate good immunoreactivity, sterilisation can potentially change the collagen conformation and reveal unrecognised sites that can invoke an adverse immune response (Chakraborty et al., 2020; Paniagua Gutierrez et al., 2015; Vafaee et al., 2018). The aforementioned analytical methods can give insight into this.

Assmann et al. (2013) reported the accelerated autologous *in vivo* recellularisation of decellularised aortic rat conduits conditioned with fibronectin prior to implantation into rat models for 8 weeks. It is reasonable to imply that the retention of dPHV fibronectin labelling intensity following sterilisation was a promising indication of the sterilised dPHV tissue regenerative capabilities. Numerous cell sources such as VICs, VECs, MSCs and SMCs have been used to explore heart valve regeneration (Jana, S. et al., 2016). The *in vitro* recellularisation

potential of porcine heart valve leaflets decellularised using a method comparable to that used within this study was investigated by Wilcox et al. (2005). It was found that α-SMA positive SMCs attached onto and migrated into the leaflet matrix over a 4 week period. α-SMA-positive cells have also been evidenced to be involved in decellularised heart valve tissue remodelling (James et al., 2015). These studies justify the use of SMCs to investigate the *in vitro* recellularisation potential of decellularised heart valve matrices. Future studies should establish an *in vitro* culture system by firstly determining the cytocompatibility and uniform ECM surface adhesion of the optimum SMC primary cell density. A long-term *in vitro* culture system of up to 4 weeks should then be used to establish cell viability and migration using cytotoxicity assays and histological analysis previously described within this study, as well as immunohistochemical labelling of cell specific markers to confirm the cell phenotype throughout the study.

## 7.3 Conclusion

Current heart valve replacement options are associated with numerous limitations that can be addressed by the implementation of a novel decellularised heart valve option that can meet clinical needs. Decellularised porcine heart valves pose an unlimited resource of various sized tissues that may have the ability to promote tissue regeneration and growth along with the patient.

The aim of this study was to identify a novel sterilisation method that would be compatible for use with decellularised porcine pulmonary heart valves. The ideal sterilisation method would minimally impact the ECM components and architectural arrangement, biochemical composition, biocompatibility and biomechanical properties of the decellularised heart valves.

Although $CuCl_2$ and $H_2O_2$ treatment has gained interest by tissue banks for tissue sterilisation applications, $CuCl_2$ and $H_2O_2$ sterilisation cannot be considered a terminal sterilisation method. Sterilisation treatment with 1 mg/L $CuCl_2$ combined with 1 % $H_2O_2$ was not considered a suitable sterilisation method for dPHVs due to histoarchitectural alterations of the leaflets, a reduction in collagen thermal stability in addition to a loss of tissue mechanical strength. However, further

investigation is required to formulate the optimal $CuCl_2$ and $H_2O_2$ sterilant concentration combination that is compatible with dPHV tissue.

The NovaProcess® used during this study was an established methodology that has been refined by NovaSterilis to sufficiently terminally sterilise tissue grafts and biomaterials without adversely impacting the biological and biomechanical properties. $ScCO_2$ sterilisation under standard conditions resulted in the unanticipated compression of the dPHV root macroscopic structure and was therefore not suitable for further biomechanical assessments. Additionally, $ScCO_2$ sterilisation treatment under standard and submerged conditions resulted in a significant reduction in collagen IV immunolabelling along with a reduction in collagen thermal stability. Although, the mechanisms underlying these alterations remain unclear as fibronectin immunolabelling was retained along with the ECM histoarchitecture, biochemical composition and tissue biomechanical properties.

*In vitro* cytotoxicity assessments demonstrated that both sterilisation methods investigated did not induce a cytotoxic response.

In summary, preliminary results reported within this study indicate that $ScCO_2$ processing under submerged conditions may be a promising method for the terminal sterilisation of dPHVs. Further analysis is required to address the discrepancies highlighted within this study, $ScCO_2$ sterilised dPHV immunoreactivity and regenerative capabilities, and further biomechanical characterisation of $ScCO_2$ sterilised dPHVs.

# References

5840-1, I. 2021. *Cardiovascular implants — Cardiac valve prostheses — Part 1: General requirements.*

Acar, C., de Ibarra, J.S. and Lansac, E. 2004. Anterior leaflet augmentation with autologous pericardium for mitral repair in rheumatic valve insufficiency. *J Heart Valve Dis.* **13**(5), pp.741-746.

Ahyayauch, H., Bennouna, M., Alonso, A. and Goñi, F.M. 2010. Detergent effects on membranes at subsolubilizing concentrations: transmembrane lipid motion, bilayer permeabilization, and vesicle lysis/reassembly are independent phenomena. *Langmuir.* **26**(10), pp.7307-7313.

Ali, A., Ershad, M., Vyas, V.K., Hira, S.K., Manna, P.P., Singh, B., Yadav, S., Srivastava, P., Singh, S. and Pyare, R. 2018. Studies on effect of CuO addition on mechanical properties and in vitro cytocompatibility in 1393 bioactive glass scaffold. *Materials Science and Engineering: C.* **93**, pp.341-355.

Ali Mansoori, G., Schulz, K. and Martinelli, E.E. 1988. Bioseparation Using Supercritical Fluid Extraction/Retrograde Condensation. *Bio/Technology.* **6**(4), pp.393-396.

Anderson, R.H. 2007. The surgical anatomy of the aortic root. *Multimedia Manual of Cardiothoracic Surgery : MMCTS.* **2007**(102), pmmcts.2006.002527.

Anderson, R.H., Ho, S.Y. and Becker, A.E. 2000. Anatomy of the human atrioventricular junctions revisited. *The Anatomical Record.* **260**(1), pp.81-91.

Anderson, R.H., Razavi, R. and Taylor, A.M. 2004. Cardiac anatomy revisited. *Journal of Anatomy.* **205**(3), pp.159-177.

Andreas, M., Wiedemann, D., Seebacher, G., Rath, C., Aref, T., Rosenhek, R., Heinze, G., Eigenbauer, E., Simon, P., Ruetzler, K., Hiesmayr, J.M., Moritz, A., Laufer, G. and Kocher, A. 2014. The Ross procedure offers excellent survival compared with mechanical aortic valve replacement in a real-world setting. *Eur J Cardiothorac Surg.* **46**(3), pp.409-413; discussion 413-404.

Antons, J., Marascio, M., Aeberhard, P.A., Weissenberger, G., Hirt-Burri, N., Applegate, L.A., Bourban, P.-E. and Pioletti, D.P. 2018. Decellularised tissues obtained by a CO2-philic detergent and supercritical CO2. *European cells & materials.* **36**, pp.81-95.

Armeniades, C.D., Lake, L.W., Missirlis, Y.F. and Kennedy, J.H. 1973. *Histologic Origin of Aortic Tissue Mechanics, The Role of Collageneous and Elastic Structures.* New York Wiley

Arora, S., Misenheimer, J.A. and Ramaraj, R. 2017. Transcatheter Aortic Valve Replacement: Comprehensive Review and Present Status. *Texas Heart Institute journal.* **44**(1), pp.29-38.

Assmann, A., Delfs, C., Munakata, H., Schiffer, F., Horstkötter, K., Huynh, K., Barth, M., Stoldt, V.R., Kamiya, H., Boeken, U., Lichtenberg, A. and Akhyari, P. 2013. Acceleration of autologous in vivo recellularization of decellularized aortic conduits by fibronectin surface coating. *Biomaterials.* **34**(25), pp.6015-6026.

Athanasiou, L.S., Fotiadis, D.I. and Michalis, L.K. 2017. 1 - Introduction. In: Athanasiou, L.S., et al. eds. *Atherosclerotic Plaque Characterization Methods Based on Coronary Imaging.* Oxford: Academic Press, pp.1-21.

Badria, A.F., Koutsoukos, P.G. and Mavrilas, D. 2020. Decellularized tissue-engineered heart valves calcification: what do animal and clinical studies tell us? *Journal of Materials Science: Materials in Medicine.* **31**(12), p132.

Badylak, S.F., Freytes, D.O. and Gilbert, T.W. 2009. Extracellular matrix as a biological scaffold material: Structure and function. *Acta Biomater.* **5**(1), pp.1-13.

Balasubramanian, D. and Kanwar, R. 2002. Molecular pathology of dityrosine cross-links in proteins: structural and functional analysis of four proteins. *Mol Cell Biochem.* **234-235**(1-2), pp.27-38.

Balestrini, J.L., Liu, A., Gard, A.L., Huie, J., Blatt, K.M., Schwan, J., Zhao, L., Broekelmann, T.J., Mecham, R.P., Wilcox, E.C. and Niklason, L.E. 2016. Sterilization of Lung Matrices by Supercritical Carbon Dioxide. *Tissue Eng Part C Methods.* **22**(3), pp.260-269.

Barbarash, L., Rutkovskaya, N., Barbarash, O., Odarenko, Y., Stasev, A. and Uchasova, E. 2016. Prosthetic heart valve selection in women of childbearing age with acquired heart disease: a case report. *Journal of medical case reports.* **10**, pp.51-51.

Bateman, M.G., Quill, J.L., Hill, A.J. and Iaizzo, P.A. 2013. The Clinical Anatomy and Pathology of the Human Atrioventricular Valves: Implications for Repair or Replacement. *Journal of Cardiovascular Translational Research.* **6**(2), pp.155-165.

Bechtel, J.F., Stierle, U. and Sievers, H.H. 2008. Fifty-two months' mean follow up of decellularized SynerGraft-treated pulmonary valve allografts. *J Heart Valve Dis.* **17**(1), pp.98-104; discussion 104.

Bednarski, D.M., Lantz, E.E., Bobst, C.E., Eisenhut, A.R., Eyles, S.J. and Fey, J.P. 2020. Sterilization of epidermal growth factor with supercritical carbon dioxide and peracetic acid; analysis of changes at the amino acid and protein level. *Biochimica et Biophysica Acta (BBA) - Proteins and Proteomics.* **1868**(2), p140334.

Bennet, D., Harris, A.F., Lacombe, J., Brooks, C., Bionda, N., Strickland, A.D., Eisenhut, T. and Zenhausern, F. 2021. Evaluation of supercritical CO(2) sterilization efficacy for sanitizing personal protective equipment from the coronavirus SARS-CoV-2. *The Science of the total environment.* **780**, pp.146519-146519.

Bernhardt, A., Wehrl, M., Paul, B., Hochmuth, T., Schumacher, M., Schütz, K. and Gelinsky, M. 2015. Improved Sterilization of Sensitive Biomaterials with Supercritical Carbon Dioxide at Low Temperature. *PLoS One.* **10**(6), pe0129205.

Binet, J.P., Carpentier, A., Langlois, J., Duran, C. and Colvez, P. 1965. Implantation of heterogenic valves in the treatment of aortic cardiopathies. *Comptes rendus hebdomadaires des seances de l"Academie des sciences. Serie D: Sciences naturelles.* **261**(25), pp.5733-5734.

Bischoff, J. and Aikawa, E. 2011. Progenitor cells confer plasticity to cardiac valve endothelium. *Journal of Cardiovascular Translation Research.* **4**(6), pp.710-719.

Blot, W.J., Ibrahim, M.A., Ivey, T.D., Acheson, D.E., Brookmeyer, R., Weyman, A., Defauw, J., Smith, J.K. and Harrison, D. 2005. Twenty-Five–Year Experience With the Björk-Shiley Convexoconcave Heart Valve. *Circulation.* **111**(21), pp.2850-2857.

Boethig, D., Horke, A., Hazekamp, M., Meyns, B., Rega, F., Van Puyvelde, J., Hübler, M., Schmiady, M., Ciubotaru, A., Stellin, G., Padalino, M., Tsang, V., Jashari, R., Bobylev, D., Tudorache, I., Cebotari, S., Haverich, A. and Sarikouch, S. 2019. A European study on decellularized homografts for pulmonary valve replacement: initial results from the prospective ESPOIR Trial and ESPOIR Registry data†. *European Journal of Cardio-Thoracic Surgery.* **56**(3), pp.503-509.

Boneva, R.S., Folks, T.M. and Chapman, L.E. 2001. Infectious disease issues in xenotransplantation. *Clinical microbiology reviews.* **14**(1), pp.1-14.

Booth, C., Korossis, S.A., Wilcox, H.E., Watterson, K.G., Kearney, J.N., Fisher, J. and Ingham, E. 2002. Tissue engineering of cardiac valve prostheses I: development and histological characterization of an acellular porcine scaffold. *J Heart Valve Dis.* **11**(4), pp.457-462.

Boudoulas, H. and Wooley, C.F. 2001. Floppy Mitral Valve, Mitral Valve Prolapse, and Mitral Valvular Regurgitation. *Current Treatment Options in Cardiovascular Medicine.* **3**(1), pp.15-24.

Boudoulas, K.D., Borer, J.S. and Boudoulas, H. 2013. Etiology of valvular heart disease in the 21st century. *Cardiology.* **126**(3), pp.139-152.

Bowdish, M.E., Kumar, S.R. and Starnes, V.A. 2016. The Ross procedure: an excellent option in the right hands. *Annals of translational medicine.* **4**(23), pp.471-471.

Bowen, J., Boudoulas, H. and Wooley, C.F. 1987. Cardiovascular disease of connective tissue origin. *The American Journal of Medicine.* **82**(3), pp.481-488.

Brand, N.J., Roy, A., Hoare, G., Chester, A. and Yacoub, M.H. 2006. Cultured interstitial cells from human heart valves express both specific skeletal muscle and non-muscle markers. *The International Journal of Biochemistry & Cell Biology.* **38**(1), pp.30-42.

Brinston, R.M. and Wilson, B.K. 1993. Converting to gamma-radiation sterilization: an overview for medical device manufacturers. *Med Device Technol.* **4**(4), pp.18-22.

Brodsky, B. and Shah, N.K. 1995. The triple-lielix motif in proteins. *The FASEB Journal.* **9**(15), pp.1537-1546.

Broom, N.D. 1978. The observation of collagen and elastin structures in wet whole mounts of pulmonary and aortic leaflets. *The Journal of Thoracic and Cardiovascular Surgery.* **75**(1), pp.121-130.

Brown, B.N., Ratner, B.D., Goodman, S.B., Amar, S. and Badylak, S.F. 2012. Macrophage polarization: an opportunity for improved outcomes in biomaterials and regenerative medicine. *Biomaterials.* **33**(15), pp.3792-3802.

Brown, B.N., Valentin, J.E., Stewart-Akers, A.M., McCabe, G.P. and Badylak, S.F. 2009. Macrophage phenotype and remodeling outcomes in response to biologic scaffolds with and without a cellular component. *Biomaterials.* **30**(8), pp.1482-1491.

Brown, J., Ruzmetov, M., Eltayeb, O., Rodefeld, M. and Turrentine, M. 2011. Performance of SynerGraft Decellularized Pulmonary Homograft in Patients Undergoing a Ross Procedure. *The Annals of thoracic surgery.* **91**, pp.416-422; discussion 422.

BSI. 2001a. BS EN 556-1. Sterilization of medical devices-Requirements for medical devices to be designated" STERILE"-Part 1: Requirements for terminally sterilized medical devices. *London: British Standards Institution.*

BSI. 2001b. *Sterilization of medical devices. Requirements for medical devices to be designated "STERILE". Requirements for terminally sterilized medical devices. .* BSI: British Standards Institution

Butcher, J.T., Mahler, G.J. and Hockaday, L.A. 2011. Aortic valve disease and treatment: the need for naturally engineered solutions. *Advanced Drug Delivery Reviews.* **63**(4-5), pp.242-268.

Butcher, J.T. and Nerem, R.M. 2004. Porcine aortic valve interstitial cells in three-dimensional culture: comparison of phenotype with aortic smooth muscle cells. *The Journal of Heart Valve Disease.* **13**(3), pp.478-485; discussion 485-476.

Butcher, J.T. and Nerem, R.M. 2006. Valvular endothelial cells regulate the phenotype of interstitial cells in co-culture: effects of steady shear stress. *Tissue Engineering.* **12**(4), pp.905-915.

Butterworth, B.E. and Chapman, J.R. 2007. Exposure of hematopoietic stem cells to ethylene oxide during processing represents a potential carcinogenic risk for transplant recipients. *Regulatory Toxicology and Pharmacology.* **49**(3), pp.149-153.

Cai, Z., Gu, Y., Xiao, Y., Wang, C. and Wang, Z. 2021. Porcine carotid arteries decellularized with a suitable concentration combination of Triton X-100 and sodium dodecyl sulfate for tissue engineering vascular grafts. *Cell and Tissue Banking.* **22**(2), pp.277-286.

Campo, G.M., D'Ascola, A., Avenoso, A., Campo, S., Ferlazzo, A.M., Micali, C., Zanghì, L. and Calatroni, A. 2004. Glycosaminoglycans reduce oxidative damage induced by copper (Cu+2), iron (Fe+2) and hydrogen peroxide (H2O2) in human fibroblast cultures. *Glycoconj J.* **20**(2), pp.133-141.

Cao, B., Zheng, Y., Xi, T., Zhang, C., Song, W., Burugapalli, K., Yang, H. and Ma, Y. 2012. Concentration-dependent cytotoxicity of copper ions on mouse fibroblasts in

vitro: effects of copper ion release from TCu380A vs TCu220C intra-uterine devices. *Biomedical Microdevices.* **14**(4), pp.709-720.

Cao, Q., Tao, L., Liu, M., Yin, M. and Sun, K. 2013. The effect of vacuum freeze-drying and radiation on allogeneic aorta grafts. *Mol Med Rep.* **7**(1), pp.144-148.

Capella-Monsonís, H. and Zeugolis, D.I. 2021. Decellularized xenografts in regenerative medicine: From processing to clinical application. *Xenotransplantation.* **28**(4), pe12683.

Carapetis, J.R., Steer, A.C., Mulholland, E.K. and Weber, M. 2005. The global burden of group A streptococcal diseases. *Lancet Infectious Diseases.* **5**(11), pp.685-694.

Carmeliet, P. and Jain, R.K. 2000. Angiogenesis in cancer and other diseases. *Nature.* **407**(6801), pp.249-257.

Carpentier, A., Deloche, A., Relland, J., Fabiani, J.N., Forman, J., Camilleri, J.P., Soyer, R. and Dubost, C. 1974. Six-year follow-up of glutaraldehyde-preserved heterografts. With particular reference to the treatment of congenital valve malformations. *J Thorac Cardiovasc Surg.* **68**(5), pp.771-782.

Carpentier, A., Lemaigre, G., Robert, L., Carpentier, S. and Dubost, C. 1969. Biological factors affecting long-term results of valvular heterografts. *Journal of Thoracic and Cardiovascular Surgery.* **58**(4), pp.467-483.

Casali, D.M., Handleton, R.M., Shazly, T. and Matthews, M.A. 2018. A novel supercritical CO2-based decellularization method for maintaining scaffold hydration and mechanical properties. *The Journal of Supercritical Fluids.* **131**, pp.72-81.

CDC. 2018. *Prion Diseases* [Online]. Available from: https://www.cdc.gov/prions/index.html

Cebotari, S., Tudorache, I., Jaekel, T., Hilfiker, A., Dorfman, S., Ternes, W., Haverich, A. and Lichtenberg, A. 2010. Detergent decellularization of heart valves for tissue engineering: toxicological effects of residual detergents on human endothelial cells. *Artif Organs.* **34**(3), pp.206-210.

Chaikof, E.L. 2007. The development of prosthetic heart valves--lessons in form and function. *The New England journal of medicine.* **357**(14), pp.1368-1371.

Chakraborty, J., Roy, S. and Ghosh, S. 2020. Regulation of decellularized matrix mediated immune response. *Biomater Sci.* **8**(5), pp.1194-1215.

Chaturvedi, R.R. and Redington, A.N. 2007. Pulmonary regurgitation in congenital heart disease. *Heart (British Cardiac Society).* **93**(7), pp.880-889.

Checinska, A., Fruth, I.A., Green, T.L., Crawford, R.L. and Paszczynski, A.J. 2011. Sterilization of biological pathogens using supercritical fluid carbon dioxide containing water and hydrogen peroxide. *Journal of Microbiological Methods.* **87**(1), pp.70-75.

Cheng, H.W., Tsui, Y.K., Cheung, K.M., Chan, D. and Chan, B.P. 2009. Decellularization of chondrocyte-encapsulated collagen microspheres: a three-dimensional model to study the effects of acellular matrix on stem cell fate. *Tissue Eng Part C Methods.* **15**(4), pp.697-706.

Cheng, J., Li, J., Cai, Z., Xing, Y., Wang, C., Guo, L. and Gu, Y. 2021. Decellularization of porcine carotid arteries using low-concentration sodium dodecyl sulfate. *The International Journal of Artificial Organs.* **44**(7), pp.497-508.

Chetta, G.E. and Lloyd, J.R. 1980. The design, fabrication and evaluation of a trileaflet prosthetic heart valve. *J Biomech Eng.* **102**(1), pp.34-41.

Cheung, D.T., Perelman, N., Tong, D. and Nimni, M.E. 1990. The effect of gamma-irradiation on collagen molecules, isolated alpha-chains, and crosslinked native fibers. *J Biomed Mater Res.* **24**(5), pp.581-589.

Chou, P.-R., Lin, Y.-N., Wu, S.-H., Lin, S.-D., Srinivasan, P., Hsieh, D.-J. and Huang, S.-H. 2020. Supercritical Carbon Dioxide-decellularized Porcine Acellular Dermal Matrix combined with Autologous Adipose-derived Stem Cells: Its Role in Accelerated Diabetic Wound Healing. *International journal of medical sciences.* **17**(3), pp.354-367.

Christian, A.J., Lin, H., Alferiev, I.S., Connolly, J.M., Ferrari, G., Hazen, S.L., Ischiropoulos, H. and Levy, R.J. 2014. The susceptibility of bioprosthetic heart valve leaflets to oxidation. *Biomaterials.* **35**(7), pp.2097-2102.

Christie, G.W. 1992. Anatomy of aortic heart valve leaflets: the influence of glutaraldehyde fixation on function. *Eur J Cardiothorac Surg.* **6 Suppl 1**, pp.S25-32; discussion S33.

Ciolacu, D.E., Nicu, R. and Ciolacu, F. 2022. Natural Polymers in Heart Valve Tissue Engineering: Strategies, Advances and Challenges. *Biomedicines.* **10**(5).

Ciubotaru, A., Cebotari, S., Tudorache, I., Beckmann, E., Hilfiker, A. and Haverich, A. 2013. Biological heart valves. *Biomedizinische Technik. Biomedical engineering.* **58**(5), pp.389-397.

Clapp, P.A., Davies, M.J., French, M.S. and Gilbert, B.C. 1994. The bactericidal action of peroxides; an E.P.R. spin-trapping study. *Free Radic Res.* **21**(3), pp.147-167.

Cochran, R.P. and Kunzelman, K.S. 1989. Cryopreservation does not alter antigenic expression of aortic allografts. *J Surg Res.* **46**(6), pp.597-599.

Converse, G.L., Armstrong, M., Quinn, R.W., Buse, E.E., Cromwell, M.L., Moriarty, S.J., Lofland, G.K., Hilbert, S.L. and Hopkins, R.A. 2012. Effects of cryopreservation, decellularization and novel extracellular matrix conditioning on the quasi-static and time-dependent properties of the pulmonary valve leaflet. *Acta Biomater.* **8**(7), pp.2722-2729.

Cooper, A.I. 2000. Polymer synthesis and processing using supercritical carbon dioxide. *Journal of Materials Chemistry.* **10**(2), pp.207-234.

Coulthard, C. and Sykes, G. 1936. The germicidal effect of alcohol with special reference to its action on bacterial spores. . *Pharmaceutical Journal* **137**, pp.79-81

Cox, B. and Emili, A. 2006. Tissue subcellular fractionation and protein extraction for use in mass-spectrometry-based proteomics. *Nat Protoc.* **1**(4), pp.1872-1878.

Coyan, G.N., D'Amore, A., Matsumura, Y., Pedersen, D.D., Luketich, S.K., Shanov, V., Katz, W.E., David, T.E., Wagner, W.R. and Badhwar, V. 2019. In vivo functional assessment of a novel degradable metal and elastomeric scaffold-based tissue engineered heart valve. *J Thorac Cardiovasc Surg.* **157**(5), pp.1809-1816.

Crapo, P.M., Gilbert, T.W. and Badylak, S.F. 2011. An overview of tissue and whole organ decellularization processes. *Biomaterials.* **32**(12), pp.3233-3243.

Cunanan, C.M., Cabiling, C.M., Dinh, T.T., Shen, S., Tran-Hata, P., Rutledge, J.H., III and Fishbein, M.C. 2001. Tissue characterization and calcification potential of commercial bioprosthetic heart valves. *The Annals of Thoracic Surgery.* **71**(5), pp.S417-S421.

Cundy, T., Reid, I.R. and Grey, A. 2014. CHAPTER 31 - Metabolic bone disease. In: Marshall, W.J., et al. eds. *Clinical Biochemistry: Metabolic and Clinical Aspects (Third Edition).* Churchill Livingstone, pp.604-635.

da Costa, F., Dohmen, P., Vieira, E., Lopes, S.V., Colatusso, C., Pereira, E.W., Matsuda, C.N. and Cauduro, S. 2007. Ross Operation with decellularized pulmonary allografts: medium-term results. *Rev Bras Cir Cardiovasc.* **22**(4), pp.454-462.

da Costa, F.D., Costa, A.C., Prestes, R., Domanski, A.C., Balbi, E.M., Ferreira, A.D. and Lopes, S.V. 2010. The early and midterm function of decellularized aortic valve allografts. *Ann Thorac Surg.* **90**(6), pp.1854-1860.

da Costa, F.D., Dohmen, P.M., Duarte, D., von Glenn, C., Lopes, S.V., Filho, H.H., da Costa, M.B. and Konertz, W. 2005. Immunological and echocardiographic evaluation of decellularized versus cryopreserved allografts during the Ross operation. *Eur J Cardiothorac Surg.* **27**(4), pp.572-578.

da Costa, F.D., Pereira, E.W., Barboza, L.E., Haggi Filho, H., Collatusso, C., Gomes, C.H., Lopes, S.A., Sardetto, E.A., Ferreira, A.D., da Costa, M.B. and da Costa, I.A. 2006. Ten-year experience with the Ross operation. *Arq Bras Cardiol.* **87**(5), pp.583-591.

da Costa, F.D., Takkenberg, J.J., Fornazari, D., Balbi Filho, E.M., Colatusso, C., Mokhles, M.M., da Costa, A.B., Sagrado, A.G., Ferreira, A.D., Fernandes, T. and Lopes, S.V. 2014. Long-term results of the Ross operation: an 18-year single institutional experience. *Eur J Cardiothorac Surg.* **46**(3), pp.415-422; discussion 422.

da Costa, F.D.A., Costa, A.C.B.A., Prestes, R., Domanski, A.C., Balbi, E.M., Ferreira, A.D.A. and Lopes, S.V. 2010. The Early and Midterm Function of Decellularized Aortic Valve Allografts. *The Annals of Thoracic Surgery.* **90**(6), pp.1854-1860.

da Costa, F.D.A., Etnel, J.R.G., Charitos, E.I., Sievers, H.H., Stierle, U., Fornazari, D., Takkenberg, J.J.M., Bogers, A. and Mokhles, M.M. 2018. Decellularized Versus Standard Pulmonary Allografts in the Ross Procedure: Propensity-Matched Analysis. *Ann Thorac Surg.* **105**(4), pp.1205-1213.

Dai, Z., Ronholm, J., Tian, Y., Sethi, B. and Cao, X. 2016. Sterilization techniques for biodegradable scaffolds in tissue engineering applications. *Journal of tissue engineering.* **7**, pp.2041731416648810-2041731416648810.

Dalecki, A.G., Crawford, C.L. and Wolschendorf, F. 2017. Copper and Antibiotics: Discovery, Modes of Action, and Opportunities for Medicinal Applications. *Adv Microb Physiol.* **70**, pp.193-260.

Damar, S. and Balaban, M.O. 2006. Review of Dense Phase CO2 Technology: Microbial and Enzyme Inactivation, and Effects on Food Quality. *Journal of Food Science.* **71**(1), pp.R1-R11.

Dasi, L.P., Simon, H.A., Sucosky, P. and Yoganathan, A.P. 2009. Fluid mechanics of artificial heart valves. *Clinical and experimental pharmacology & physiology.* **36**(2), pp.225-237.

de Vlaming, A., Sauls, K., Hajdu, Z., Visconti, R.P., Mehesz, A.N., Levine, R.A., Slaugenhaupt, S.A., Hagège, A., Chester, A.H., Markwald, R.R. and Norris, R.A. 2012. Atrioventricular valve development: new perspectives on an old theme. *Differentiation; research in biological diversity.* **84**(1), pp.103-116.

Deborde, C., Simionescu, D.T., Wright, C., Liao, J., Sierad, L.N. and Simionescu, A. 2016. Stabilized Collagen and Elastin-Based Scaffolds for Mitral Valve Tissue Engineering. *Tissue engineering. Part A.* **22**(21-22), pp.1241-1251.

Delgado, L.M., Pandit, A. and Zeugolis, D.I. 2014. Influence of sterilisation methods on collagen-based devices stability and properties. *Expert Review of Medical Devices.* **11**(3), pp.305-314.

Delmo Walter, E.M., de By, T.M.M.H., Meyer, R. and Hetzer, R. 2012. The future of heart valve banking and of homografts: perspective from the Deutsches Herzzentrum Berlin. *HSR proceedings in intensive care & cardiovascular anesthesia.* **4**(2), pp.97-108.

Desai, A. 2019. *Extended Duration Simulation and Testing of Cellular and Decellularised Heart Valve Roots*. Doctoral thesis, University of Leeds, UK.

Desai, A., Ingham, E., Berry, H.E., Fisher, J. and Jennings, L.M. 2022. The effect of decellularisation on the real time mechanical fatigue of porcine aortic heart valve roots. *PLoS One.* **17**(4), pe0265763.

Desai, A., Vafaee, T., Rooney, P., Kearney, J.N., Berry, H.E., Ingham, E., Fisher, J. and Jennings, L.M. 2018. In vitro biomechanical and hydrodynamic characterisation of decellularised human pulmonary and aortic roots. *Journal of the Mechanical Behavior of Biomedical Materials.* **79**, pp.53-63.

Dong, X., Tang, M., Sun, Q. and Zhang, S. 2018. Anatomical relevance of ablation to the pulmonary artery root: Clinical implications for characterizing the pulmonary sinus of Valsalva and coronary artery. *Journal of Cardiovascular Electrophysiology.* **29**(9), pp.1230-1237.

Duan, B., Hockaday, L.A., Kang, K.H. and Butcher, J.T. 2013. 3D bioprinting of heterogeneous aortic valve conduits with alginate/gelatin hydrogels. *Journal of biomedical materials research. Part A.* **101**(5), pp.1255-1264.

Duarte, M.M., Silva, I.V., Eisenhut, A.R., Bionda, N., Duarte, A.R.C. and Oliveira, A.L. 2022. Contributions of supercritical fluid technology for advancing decellularization and postprocessing of viable biological materials. *Materials Horizons.*

Eagle, M.J., Man, J., Rooney, P., Hogg, P. and Kearney, J.N. 2015. Assessment of an improved bone washing protocol for deceased donor human bone. *Cell Tissue Bank.* **16**(1), pp.83-90.

Eagle, M.J., Rooney, P., Lomas, R. and Kearney, J.N. 2005. Validation of radiation dose received by frozen unprocessed and processed bone during terminal sterilisation. *Cell Tissue Bank.* **6**(3), pp.221-230.

Edwards, J.V., Prevost, N.T., Santiago, M., von Hoven, T., Condon, B.D., Qureshi, H. and Yager, D.R. 2018. Hydrogen Peroxide Generation of Copper/Ascorbate Formulations on Cotton: Effect on Antibacterial and Fibroblast Activity for Wound Healing Application. *Molecules (Basel, Switzerland).* **23**(9), p2399.

Eikelboom, J.W., Connolly, S.J., Brueckmann, M., Granger, C.B., Kappetein, A.P., Mack, M.J., Blatchford, J., Devenny, K., Friedman, J., Guiver, K., Harper, R., Khder, Y., Lobmeyer, M.T., Maas, H., Voigt, J.-U., Simoons, M.L. and Van de Werf, F. 2013. Dabigatran versus Warfarin in Patients with Mechanical Heart Valves. *New England Journal of Medicine.* **369**(13), pp.1206-1214.

Elenes, E.Y. and Hunter, S.A. 2014. Soft-tissue allografts terminally sterilized with an electron beam are biomechanically equivalent to aseptic, nonsterilized tendons. *J Bone Joint Surg Am.* **96**(16), pp.1321-1326.

Elkins, R.C., Dawson, P.E., Goldstein, S., Walsh, S.P. and Black, K.S. 2001. Decellularized human valve allografts. *The Annals of Thoracic Surgery.* **71**(5), pp.S428-S432.

Emery, R.W., Arom, K.V., Kshettry, V.R., Kroshus, T.J., Von, R., Kersten, T.E., Lillehei, T.J., Nicoloff, D.M. and Erickson, C.A. 2002. Decision-making in the choice of heart valve for replacement in patients aged 60-70 years: twenty-year follow up of the St. Jude Medical aortic valve prosthesis. *The Journal of heart valve disease.* **11 Suppl 1**, pp.S37-44.

Emmanouilides, G.C., Linde, L.M. and Crittenden, I.H. 1964. PULMONARY ARTERY STENOSIS ASSOCIATED WITH DUCTUS ARTERIOSUS FOLLOWING MATERNAL RUBELLA. *Circulation.* **29**, pp.Suppl:514-522.

Espírito Santo, C., Taudte, N., Nies, D.H. and Grass, G. 2008. Contribution of copper ion resistance to survival of Escherichia coli on metallic copper surfaces. *Appl Environ Microbiol.* **74**(4), pp.977-986.

Farrington, M., Wreghitt, T., Matthews, I., Scarr, D., Sutehall, G., Hunt, C.J., Santiago, T., Gruys, E., Voorhout, W., Ramos, T. and Pegg, D.E. 2002. Processing of cardiac

valve allografts: 2. Effects of antimicrobial treatment on sterility, structure and mechanical properties. *Cell Tissue Bank.* **3**(2), pp.91-103.

Faulk, D.M., Carruthers, C.A., Warner, H.J., Kramer, C.R., Reing, J.E., Zhang, L., D'Amore, A. and Badylak, S.F. 2014a. The effect of detergents on the basement membrane complex of a biologic scaffold material. *Acta Biomater.* **10**(1), pp.183-193.

Faulk, D.M., Carruthers, C.A., Warner, H.J., Kramer, C.R., Reing, J.E., Zhang, L., D'Amore, A. and Badylak, S.F. 2014b. The effect of detergents on the basement membrane complex of a biologic scaffold material. *Acta Biomaterialia.* **10**(1), pp.183-193.

Fenderson, B. 2008. Molecular Biology of the Cell,5th Edition. *Medicine & Science in Sports & Exercise.* **40**(9).

Fenoglio, J.J., Jr., Tuan Duc, P., Wit, A.L., Bassett, A.L. and Wagner, B.M. 1972. Canine mitral complex. Ultrastructure and electromechanical properties. *Circulation Research.* **31**(3), pp.417-430.

Ferng, A.S., Connell, A.M., Marsh, K.M., Qu, N., Medina, A.O., Bajaj, N., Palomares, D., Iwanski, J., Tran, P.L., Lotun, K., Johnson, K. and Khalpey, Z. 2017. Acellular porcine heart matrices: whole organ decellularization with 3D-bioscaffold & vascular preservation. *Journal of clinical and translational research.* **3**(2), pp.260-270.

Fidalgo, C., Iop, L., Sciro, M., Harder, M., Mavrilas, D., Korossis, S., Bagno, A., Palù, G., Aguiari, P. and Gerosa, G. 2018. A sterilization method for decellularized xenogeneic cardiovascular scaffolds. *Acta Biomaterialia.* **67**, pp.282-294.

Filip, D.A., Radu, A. and Simionescu, M. 1986. Interstitial cells of the heart valves possess characteristics similar to smooth muscle cells. *Circulation Research.* **59**(3), pp.310-320.

Finnegan, M., Linley, E., Denyer, S.P., McDonnell, G., Simons, C. and Maillard, J.Y. 2010. Mode of action of hydrogen peroxide and other oxidizing agents: differences between liquid and gas forms. *J Antimicrob Chemother.* **65**(10), pp.2108-2115.

Flameng, W., Hermans, H., Verbeken, E. and Meuris, B. 2015. A randomized assessment of an advanced tissue preservation technology in the juvenile sheep model. *The Journal of Thoracic and Cardiovascular Surgery.* **149**(1), pp.340-345.

Freytes, D.O., Stoner, R.M. and Badylak, S.F. 2008. Uniaxial and biaxial properties of terminally sterilized porcine urinary bladder matrix scaffolds. *Journal of Biomedical Materials Research Part B: Applied Biomaterials.* **84B**(2), pp.408-414.

Gafarova, E.R., Grebenik, E.A., Lazhko, A.E., Frolova, A.A., Kuryanova, A.S., Kurkov, A.V., Bazhanov, I.A., Kapomba, B.S., Kosheleva, N.V., Novikov, I.A., Shekhter, A.B., Golubeva, E.N., Soloviova, A.B. and Timashev, P.S. 2020. Evaluation of Supercritical CO2-Assisted Protocols in a Model of Ovine Aortic Root Decellularization. **25**(17), p3923.

Gallegos, R.P., Gudbjartsson, T. and Aranki, S. 2011. Cardiac Surgery in the Adult Heart In: Cohn, L. ed. *Mitral Valve Replacement* Fourth ed. New York: McGraw-Hill, pp.1032-1068.

Garba, I.H., Ubom, G.A. and Ejiogu, N.B. 2006. Serum copper concentration in adults with acute, uncomplicated falciparum malaria infection. *Biol Trace Elem Res.* **113**(2), pp.125-130.

Gardner, E.M.H., VonderHeide, N., Fisher, R., Brooker, G. and Yates, P.J. 2013. Effect of hydrogen peroxide on human tendon allograft. *Cell and Tissue Banking.* **14**(4), pp.667-671.

Ghanbari, H., Viatge, H., Kidane, A.G., Burriesci, G., Tavakoli, M. and Seifalian, A.M. 2009. Polymeric heart valves: new materials, emerging hopes. *Trends in Biotechnology.* **27**(6), pp.359-367.

Gilbert, T.W., Freund, J.M. and Badylak, S.F. 2009. Quantification of DNA in biologic scaffold materials. *The Journal of surgical research.* **152**(1), pp.135-139.

Gilbert, T.W., Sellaro, T.L. and Badylak, S.F. 2006. Decellularization of tissues and organs. *Biomaterials.* **27**(19), pp.3675-3683.

Giles, C., Lamont-Friedrich, S.J., Michl, T.D., Griesser, H.J. and Coad, B.R. 2018. The importance of fungal pathogens and antifungal coatings in medical device infections. *Biotechnol Adv.* **36**(1), pp.264-280.

Goissis, G., Suzigan, S., Parreira, D.R., Maniglia, J.V., Braile, D.M. and Raymundo, S. 2000. Preparation and Characterization of Collagen-Elastin Matrices From Blood Vessels Intended as Small Diameter Vascular Grafts. *Artificial Organs.* **24**(3), pp.217-223.

Gonzalez-Lavin, L., Geens, M., Somerville, J. and Ross, D.N. 1970. Autologous pulmonary valve replacement of the diseased aortic valve. *Circulation.* **42**(5), pp.781-785.

Gott, V.L., Alejo, D.E. and Cameron, D.E. 2003. Mechanical heart valves: 50 years of evolution. *The Annals of Thoracic Surgery.* **76**(6), pp.S2230-S2239.

Granados, M., Morticelli, L., Andriopoulou, S., Kalozoumis, P., Pflaum, M., Iablonskii, P., Glasmacher, B., Harder, M., Hegermann, J., Wrede, C., Tudorache, I., Cebotari, S., Hilfiker, A., Haverich, A. and Korossis, S. 2017. Development and Characterization of a Porcine Mitral Valve Scaffold for Tissue Engineering. *Journal of Cardiovascular Translational Research.* **10**(4), pp.374-390.

Grashow, J.S., Sacks, M.S., Liao, J. and Yoganathan, A.P. 2006. Planar biaxial creep and stress relaxation of the mitral valve anterior leaflet. *Annals of Biomedical Engineering.* **34**(10), pp.1509-1518.

Grauss, R.W., Hazekamp, M.G., van Vliet, S., Gittenberger-de Groot, A.C. and DeRuiter, M.C. 2003. Decellularization of rat aortic valve allografts reduces leaflet destruction and extracellular matrix remodeling. *J Thorac Cardiovasc Surg.* **126**(6), pp.2003-2010.

Greenberg, H.Z.E., Zhao, G., Shah, A.M. and Zhang, M. 2021. Role of oxidative stress in calcific aortic valve disease and its therapeutic implications. *Cardiovascular Research.* **118**(6), pp.1433-1451.

Gross, L. and Kugel, M.A. 1931. Topographic Anatomy and Histology of the Valves in the Human Heart. *The American journal of pathology.* **7**(5), pp.445-474.447.

Gu, X. and Masters, K.S. 2010. Regulation of valvular interstitial cell calcification by adhesive peptide sequences. *Journal of Biomedical Materials Reserach. Part A.* **93**(4), pp.1620-1630.

Guo, R., Zhou, Y., Liu, S., Li, C., Lu, C., Yang, G., Nie, J., Wang, F., Dong, N.-G. and Shi, J. 2021. Anticalcification Potential of POSS-PEG Hybrid Hydrogel as a Scaffold Material for the Development of Synthetic Heart Valve Leaflets. *ACS Applied Bio Materials.* **4**(3), pp.2534-2543.

Halfwerk, F.R., Rouwkema, J., Gossen, J.A. and Grandjean, J.G. 2018. Supercritical carbon dioxide decellularised pericardium: Mechanical and structural characterisation for applications in cardio-thoracic surgery. *Journal of the Mechanical Behavior of Biomedical Materials.* **77**, pp.400-407.

Hamdan, A., Guetta, V., Konen, E., Goitein, O., Segev, A., Raanani, E., Spiegelstein, D., Hay, I., Di Segni, E., Eldar, M. and Schwammenthal, E. 2012. Deformation Dynamics and Mechanical Properties of the Aortic Annulus by 4-Dimensional Computed Tomography: Insights Into the Functional Anatomy of the Aortic Valve Complex and Implications for Transcatheter Aortic Valve Therapy. *Journal of the American College of Cardiology.* **59**(2), pp.119-127.

Han, H.-C. 2012. Twisted blood vessels: symptoms, etiology and biomechanical mechanisms. *Journal of vascular research.* **49**(3), pp.185-197.

Hans, M., Mathews, S., Mücklich, F. and Solioz, M. 2016. Physicochemical properties of copper important for its antibacterial activity and development of a unified model. *Biointerphases.* **11**(1), p018902.

Haraguchi, Y., Shimizu, T., Yamato, M. and Okano, T. 2012. Concise review: cell therapy and tissue engineering for cardiovascular disease. *Stem cells translational medicine.* **1**(2), pp.136-141.

Harris, C., Croce, B. and Cao, C. 2015. Tissue and mechanical heart valves. *Annals of Cardiothoracic Surgery.* **4**(4), p399.

Hasan, A., Ragaert, K., Swieszkowski, W., Selimovic, S., Paul, A., Camci-Unal, G., Mofrad, M.R. and Khademhosseini, A. 2014. Biomechanical properties of native and tissue engineered heart valve constructs. *Journal of Biomechanics* **47**(9), pp.1949-1963.

Hastings, C.E., Jr., Martin, S.A., Heath, J.R., 3rd, Mark, D.E., Mansfield, J.L. and Hollinger, J.O. 1990. The effects of ethylene oxide sterilization on the in vitro cytotoxicity of a bone replacement material. *Toxicol In Vitro.* **4**(6), pp.757-762.

Hawkins, C.L. and Davies, M.J. 1997. Oxidative damage to collagen and related substrates by metal ion/hydrogen peroxide systems: random attack or site-specific damage? *Biochim Biophys Acta.* **1360**(1), pp.84-96.

Hawkins, J.A., Bailey, W.W., Dillon, T. and Schwartz, D.C. 1992. Midterm results with cryopreserved allograft valved conduits from the right ventricle to the pulmonary arteries. *J Thorac Cardiovasc Surg.* **104**(4), pp.910-916.

Helder, M.R.K., Hennessy, R.S., Spoon, D.B., Tefft, B.J., Witt, T.A., Marler, R.J., Pislaru, S.V., Simari, R.D., Stulak, J.M. and Lerman, A. 2016. Low-Dose Gamma Irradiation of Decellularized Heart Valves Results in Tissue Injury In Vitro and In Vivo. *The Annals of Thoracic Surgery.* **101**(2), pp.667-674.

Hennessy, R.S., Jana, S., Tefft, B.J., Helder, M.R., Young, M.D., Hennessy, R.R., Stoyles, N.J. and Lerman, A. 2017. Supercritical carbon dioxide-based sterilization of decellularized heart valves. *JACC. Basic to translational science.* **2**(1), pp.71-84.

Herbst, T.J., McCarthy, J.B., Tsilibary, E.C. and Furcht, L.T. 1988. Differential effects of laminin, intact type IV collagen, and specific domains of type IV collagen on endothelial cell adhesion and migration. *The Journal of cell biology.* **106**(4), pp.1365-1373.

Hickey, G.L., Bridgewater, B., Grant, S.W., Deanfield, J., Parkinson, J., Bryan, A.J., Dalrymple-Hay, M., Moat, N., Buchan, I. and Dunning, J. 2017. National Registry Data and Record Linkage to Inform Postmarket Surveillance of Prosthetic Aortic Valve Models Over 15 Years. *JAMA Internal Medicine.* **177**(1), pp.79-86.

Hinton, R.B., Adelman-Brown, J., Witt, S., Krishnamurthy, V.K., Osinska, H., Sakthivel, B., James, J.F., Li, D.Y., Narmoneva, D.A., Mecham, R.P. and Benson, D.W. 2010. Elastin haploinsufficiency results in progressive aortic valve malformation and latent valve disease in a mouse model. *Circulation Research.* **107**(4), pp.549-557.

Hinton, R.B. and Yutzey, K.E. 2011. Heart valve structure and function in development and disease. *Annual review of physiology.* **73**, pp.29-46.

Hoerstrup, S.P., Sodian, R., Daebritz, S., Wang, J., Bacha, E.A., Martin, D.P., Moran, A.M., Guleserian, K.J., Sperling, J.S., Kaushal, S., Vacanti, J.P., Schoen, F.J. and Mayer, J.E. 2000. Functional Living Trileaflet Heart Valves Grown In Vitro. *Circulation.* **102**(suppl_3), pp.Iii-44-Iii-49.

Hogg, P., Rooney, P., Leow-Dyke, S., Brown, C., Ingham, E. and Kearney, J.N. 2015. Development of a terminally sterilised decellularised dermis. *Cell Tissue Bank.* **16**(3), pp.351-359.

Holland, J.D.R. 2019. *Development of sterilisation strategies for decellularised peripheral nerve grafts*. Doctor of Philosophy thesis, University of Leeds.

Holland, J.D.R., Webster, G., Rooney, P., Wilshaw, S.-P., Jennings, L.M. and Berry, H.E. 2021. Effects of Chemical and Radiation Sterilisation on the Biological and Biomechanical Properties of Decellularised Porcine Peripheral Nerves. *Frontiers in bioengineering and biotechnology.* **9**, pp.660453-660453.

Holland, J.D.R., Webster, G., Rooney, P., Wilshaw, S.P., Jennings, L.M. and Berry, H.E. 2021. Effects of Chemical and Radiation Sterilisation on the Biological and Biomechanical Properties of Decellularised Porcine Peripheral Nerves. *Front Bioeng Biotechnol.* **9**, p660453.

Hopkins, R. 2006. From cadaver harvested homograft valves to tissue-engineered valve conduits. *Progress in Pediatric Cardiology.* **21**(2), pp.137-152.

Hopkins, R.A. 2003. Aortic valve leaflet sparing and salvage surgery: evolution of techniques for aortic root reconstruction. *European Journal of Cardio-Thoracic Surgery.* **24**(6), pp.886-897.

Hsiao, C.-Y., Liu, S.-J., Wen-Neng Ueng, S. and Chan, E.-C. 2012. The influence of γ irradiation and ethylene oxide treatment on the release characteristics of biodegradable poly(lactide-co-glycolide) composites. *Polymer Degradation and Stability.* **97**(5), pp.715-720.

Huang, G. and Rahimtoola, S.H. 2011. Prosthetic heart valve. *Circulation.* **123**(22), pp.2602-2605.

Huang, H.Y., Balhouse, B.N. and Huang, S. 2012. Application of simple biomechanical and biochemical tests to heart valve leaflets: implications for heart valve characterization and tissue engineering. *Proceedings of the Institution of Mechanical Engineers. Part H, journal of engineering in medicine* **226**(11), pp.868-876.

Huang, Q., Dawson, R.A., Pegg, D.E., Kearney, J.N. and Macneil, S. 2004. Use of peracetic acid to sterilize human donor skin for production of acellular dermal matrices for clinical use. *Wound Repair Regen.* **12**(3), pp.276-287.

Huang, Y.-H., Tseng, F.-W., Chang, W.-H., Peng, I.C., Hsieh, D.-J., Wu, S.-W. and Yeh, M.-L. 2017. Preparation of acellular scaffold for corneal tissue engineering by supercritical carbon dioxide extraction technology. *Acta Biomaterialia.* **58**, pp.238-243.

Hussein, K.H., Park, K.M., Teotia, P.K., Hong, S.H., Yang, S.R., Park, S.M., Ahn, C. and Woo, H.M. 2013. Sterilization using electrolyzed water highly retains the biological properties in tissue-engineered porcine liver scaffold. *Int J Artif Organs.* **36**(11), pp.781-792.

Hwang, J., San, B.H., Turner, N.J., White, L.J., Faulk, D.M., Badylak, S.F., Li, Y. and Yu, S.M. 2017. Molecular assessment of collagen denaturation in decellularized tissues using a collagen hybridizing peptide. *Acta Biomaterialia.* **53**, pp.268-278.

Icardo, J.M. and Colvee, E. 1995. Atrioventricular valves of the mouse: II. Light and transmission electron microscopy. *The Anatomical Record.* **241**(3), pp.391-400.

Inoue, K., Owaki, T., Nakamura, T., Kitamura, F. and Miyamoto, N. 1984. Clinical application of transvenous mitral commissurotomy by a new balloon catheter. *J Thorac Cardiovasc Surg.* **87**(3), pp.394-402.

Ionescu, M.I. and Ross, D.N. 1969. Heart-valve replacement with autologous

fascia lata. *Lancet* pp.335-338

Ionescu, M.I., Tandon, A.P., Mary, D.A. and Abid, A. 1977. Heart valve replacement with the Ionescu-Shiley pericardial xenograft. *The Journal of thoracic and cardiovascular surgery.* **73**(1), pp.31-42.

Irani, M., Lovric, V. and Walsh, W.R. 2018. Effects of supercritical fluid CO2 and 25 kGy gamma irradiation on the initial mechanical properties and histological appearance of tendon allograft. *Cell and Tissue Banking.* **19**(4), pp.603-612.

ISO. 2006. *Sterilization of health care products — Radiation — Part 1: Requirements for development, validation and routine control of a sterilization process for medical devices.*

ISO. 2009. *Sterilization of Health Care Products — General Requirements for Characterization of a Sterilizing Agent and the Development, Validation and Routine Control of a Sterilization Process for Medical Devices,.*

Jackson, D.W., Windler, G.E. and Simon, T.M. 1990. Intraarticular reaction associated with the use of freeze-dried, ethylene oxide-sterilized bone-patella tendon-bone allografts in the reconstruction of the anterior cruciate ligament. *Am J Sports Med.* **18**(1), pp.1-10; discussion 10-11.

James, I.A., Yi, T., Tara, S., Best, C.A., Stuber, A.J., Shah, K.V., Austin, B.F., Sugiura, T., Lee, Y.U., Lincoln, J., Trask, A.J., Shinoka, T. and Breuer, C.K. 2015. Hemodynamic Characterization of a Mouse Model for Investigating the Cellular and Molecular Mechanisms of Neotissue Formation in Tissue-Engineered Heart Valves. *Tissue Eng Part C Methods.* **21**(9), pp.987-994.

Jana, S., Bhagia, A. and Lerman, A. 2019. Optimization of polycaprolactone fibrous scaffold for heart valve tissue engineering. *Biomedical Materials.* **14**, p065014.

Jana, S. and Lerman, A. 2019. Behavior of valvular interstitial cells on trilayered nanofibrous substrate mimicking morphologies of heart valve leaflet. *Acta Biomater.* **85**, pp.142-156.

Jana, S., Tranquillo, R.T. and Lerman, A. 2016. Cells for tissue engineering of cardiac valves. *J Tissue Eng Regen Med.* **10**(10), pp.804-824.

Jennings, L.M. 2001. *The Pulmonary Bioprosthetic Valve* Doctoral thesis, University of Leeds, UK.

Jonas, S.N., Kligerman, S.J., Burke, A.P., Frazier, A.A. and White, C.S. 2016. Pulmonary Valve Anatomy and Abnormalities: A Pictorial Essay of Radiography, Computed Tomography (CT), and Magnetic Resonance Imaging (MRI). *Journal of Thoracic Imaging.* **31**(1), pp.W4-W12.

Junqueira, L.C., Bignolas, G. and Brentani, R.R. 1979. Picrosirius staining plus polarization microscopy, a specific method for collagen detection in tissue sections. *Histochem J.* **11**(4), pp.447-455.

Kamihira, M., Taniguchi, M. and Kobayashi, T. 1987. Sterilization of Microorganisms with Supercritical Carbon Dioxide. *Agricultural and Biological Chemistry.* **51**(2), pp.407-412.

Kapadia, S.R., Leon, M.B., Makkar, R.R., Tuzcu, E.M., Svensson, L.G., Kodali, S., Webb, J.G., Mack, M.J., Douglas, P.S., Thourani, V.H., Babaliaros, V.C., Herrmann, H.C., Szeto, W.Y., Pichard, A.D., Williams, M.R., Fontana, G.P., Miller, D.C., Anderson, W.N., Akin, J.J., Davidson, M.J. and Smith, C.R. 2015. 5-year outcomes of transcatheter aortic valve replacement compared with standard treatment for patients with inoperable aortic stenosis (PARTNER 1): a randomised controlled trial. *Lancet.* **385**(9986), pp.2485-2491.

Karimi, R., Zhu, T., Bouma, B.E. and Mofrad, M.R. 2008. Estimation of nonlinear mechanical properties of vascular tissues via elastography. *Cardiovascular Engineering (Dordrecht, Netherlands).* **8**(4), pp.191-202.

Kasimir, M.T., Rieder, E., Seebacher, G., Silberhumer, G., Wolner, E., Weigel, G. and Simon, P. 2003. Comparison of different decellularization procedures of porcine heart valves. *Int J Artif Organs.* **26**(5), pp.421-427.

Keane, T.J., Swinehart, I.T. and Badylak, S.F. 2015. Methods of tissue decellularization used for preparation of biologic scaffolds and in vivo relevance. *Methods.* **84**, pp.25-34.

Kearney, J.N., Bojar, R. and Holland, K.T. 1993. Ethylene oxide sterilisation of allogenic bone implants. *Clin Mater.* **12**(3), pp.129-135.

Kearney, J.N., Franklin, U.C., Aguirregoicoa, V. and Holland, K.T. 1989. Evaluation of ethylene oxide sterilization of tissue implants. *J Hosp Infect.* **13**(1), pp.71-80.

Khatoon, Z., McTiernan, C.D., Suuronen, E.J., Mah, T.F. and Alarcon, E.I. 2018. Bacterial biofilm formation on implantable devices and approaches to its treatment and prevention. *Heliyon.* **4**(12), pe01067.

Kheir, E., Stapleton, T., Shaw, D., Jin, Z., Fisher, J. and Ingham, E. 2011. Development and characterization of an acellular porcine cartilage bone matrix for use in tissue engineering. *J Biomed Mater Res A.* **99**(2), pp.283-294.

King, W.L. and Gould, G.W. 1969. Lysis of bacterial spores with hydrogen peroxide. *J Appl Bacteriol.* **32**(4), pp.481-490.

Kishore, N.K., Emani, S.S., Maiti, T.K. and Bisht, G.S. 2007. Studies on Pulsed Electric Field applications for food sterilization. In: *2007 International Conference on Industrial and Information Systems, 9-11 Aug. 2007*, pp.497-502.

Klebe, R.J. 1974. Isolation of a collagen-dependent cell attachment factor. *Nature.* **250**(463), pp.248-251.

Konuma, T., Devaney, E.J., Bove, E.L., Gelehrter, S., Hirsch, J.C., Tavakkol, Z. and Ohye, R.G. 2009. Performance of CryoValve SG decellularized pulmonary allografts compared with standard cryopreserved allografts. *Ann Thorac Surg.* **88**(3), pp.849-854; discussion 554-845.

Korossis, S. 2018. Structure-Function Relationship of Heart Valves in Health and Disease. *Structural Insufficiency Anomalies in Cardiac Valves.*

Korossis, S.A., Wilcox, H.E., Watterson, K.G., Kearney, J.N., Ingham, E. and Fisher, J. 2005. In-vitro assessment of the functional performance of the decellularized intact porcine aortic root. *J Heart Valve Dis.* **14**(3), pp.408-421; discussion 422.

Laue, M., Han, H., Dittmann, C. and Setlow, P. 2018. Intracellular membranes of bacterial endospores are reservoirs for spore core membrane expansion during spore germination. *Scientific Reports.* **8**.

Lawrence, S. 2016. *The Cardiovascular System.* [Online]. Available from: https://slideplayer.com/slide/14393195/

Leikina, E., Mertts, M.V., Kuznetsova, N. and Leikin, S. 2002. Type I collagen is thermally unstable at body temperature. *Proc Natl Acad Sci U S A.* **99**(3), pp.1314-1318.

Leo, H.L., Simon, H.A., Dasi, L.P. and Yoganathan, A.P. 2006. Effect of hinge gap width on the microflow structures in 27-mm bileaflet mechanical heart valves. *J Heart Valve Dis.* **15**(6), pp.800-808.

Leow-Dyke, S.F., Rooney, P. and Kearney, J.N. 2016. Evaluation of Copper and Hydrogen Peroxide Treatments on the Biology, Biomechanics, and Cytotoxicity of Decellularized Dermal Allografts. *Tissue Eng Part C Methods.* **22**(3), pp.290-300.

Leow-Dyke, S.F., Rooney, P. and Kearney, J.N. 2017. The efficacy and sterilisation of human decellularised dermal allografts with combinations of cupric ions and hydrogen peroxide. *Cell Tissue Bank.* **18**(4), pp.561-572.

Levy, R.J., Schoen, F.J., Levy, J.T., Nelson, A.C., Howard, S.L. and Oshry, L.J. 1983. Biologic determinants of dystrophic calcification and osteocalcin deposition in glutaraldehyde-preserved porcine aortic valve leaflets implanted subcutaneously in rats. *The American journal of pathology.* **113**(2), pp.143-155.

Liao, K., Seifter, E., Hoffman, D., Yellin, E.L. and Frater, R.W. 1992. Bovine pericardium versus porcine aortic valve: comparison of tissue biological properties as prosthetic valves. *Artif Organs.* **16**(4), pp.361-365.

Lin, H.-M., Yang, Z. and Chen, L.-F. 1992. Inactivation of Saccharomyces cerevisiae by Supercritical and Subcritical Carbon Dioxide. *Biotechnology Progress.* **8**(5), pp.458-461.

Lindblom, D., Rodriguez, L. and Bjork, V.O. 1989. Mechanical failure of the Bjork-Shiley valve. Updated follow-up and considerations on prophylactic rereplacement. *The Journal of thoracic and cardiovascular surgery.* **97**(1), pp.95-97.

Linley, E., Denyer, S.P., McDonnell, G., Simons, C. and Maillard, J.Y. 2012. Use of hydrogen peroxide as a biocide: new consideration of its mechanisms of biocidal action. *J Antimicrob Chemother.* **67**(7), pp.1589-1596.

Liochev, S.I. and Fridovich, I. 2002. The Haber-Weiss cycle -- 70 years later: an alternative view. *Redox Rep.* **7**(1), pp.55-57; author reply 59-60.

Lisy, M., Kalender, G., Schenke-Layland, K., Brockbank, K.G., Biermann, A. and Stock, U.A. 2017. Allograft Heart Valves: Current Aspects and Future Applications. *Biopreserv Biobank.* **15**(2), pp.148-157.

Liu, A.C., Joag, V.R. and Gotlieb, A.I. 2007. The emerging role of valve interstitial cell phenotypes in regulating heart valve pathobiology. *The American journal of pathology.* **171**(5), pp.1407-1418.

Lock, A., Cornish, J. and Musson, D.S. 2019. The Role of In Vitro Immune Response Assessment for Biomaterials. *J Funct Biomater.* **10**(3).

Loger, K., Miranda, R., Engel, A., Marczynski-Bühlow, M., Lutter, G. and Quandt, E. 2014. Fabrication and Evaluation of Nitinol Thin Film Heart Valves. *Cardiovascular Engineering and Technology.* **5**, pp.308-316.

Lomas, R.J., Jennings, L.M., Fisher, J. and Kearney, J.N. 2004. Effects of a peracetic acid disinfection protocol on the biocompatibility and biomechanical properties of human patellar tendon allografts. *Cell Tissue Bank.* **5**(3), pp.149-160.

Luo, J., Korossis, S.A., Wilshaw, S.P., Jennings, L.M., Fisher, J. and Ingham, E. 2014. Development and characterization of acellular porcine pulmonary valve scaffolds for tissue engineering. *Tissue Eng Part A.* **20**(21-22), pp.2963-2974.

Ma, L., Gao, C., Mao, Z., Zhou, J., Shen, J., Hu, X. and Han, C. 2003. Collagen/chitosan porous scaffolds with improved biostability for skin tissue engineering. *Biomaterials.* **24**(26), pp.4833-4841.

Mack, M.J., Leon, M.B., Smith, C.R., Miller, D.C., Moses, J.W., Tuzcu, E.M., Webb, J.G., Douglas, P.S., Anderson, W.N., Blackstone, E.H., Kodali, S.K., Makkar, R.R., Fontana, G.P., Kapadia, S., Bavaria, J., Hahn, R.T., Thourani, V.H., Babaliaros, V., Pichard, A., Herrmann, H.C., Brown, D.L., Williams, M., Akin, J., Davidson, M.J. and Svensson, L.G. 2015. 5-year outcomes of transcatheter aortic valve replacement or surgical aortic valve replacement for high surgical risk patients with aortic stenosis (PARTNER 1): a randomised controlled trial. *Lancet.* **385**(9986), pp.2477-2484.

Mahmood, F., Matyal, R., Mahmood, F., Sheu, R.D., Feng, R. and Khabbaz, K.R. 2018. Intraoperative Echocardiographic Assessment of Prosthetic Valves: A Practical Approach. *J Cardiothorac Vasc Anesth.* **32**(2), pp.823-837.

Mahmoud, M. 2018. *External features of the heart.* [Online]. Available from: https://www.slideshare.net/DrMohammadMahmoud/2-external-features-of-the-heart

Manji, R.A., Lee, W. and Cooper, D.K.C. 2015. Xenograft bioprosthetic heart valves: Past, present and future. *International Journal of Surgery.* **23**, pp.280-284.

Marron, K., Yacoub, M.H., Polak, J.M., Sheppard, M.N., Fagan, D., Whitehead, B.F., de Leval, M.R., Anderson, R.H. and Wharton, J. 1996. Innervation of human atrioventricular and arterial valves. *Circulation.* **94**(3), pp.368-375.

Masters, K.S., Shah, D.N., Leinwand, L.A. and Anseth, K.S. 2005. Crosslinked hyaluronan scaffolds as a biologically active carrier for valvular interstitial cells. *Biomaterials.* **26**(15), pp.2517-2525.

Matthews, P.B., Azadani, A.N., Jhun, C.S., Ge, L., Guy, T.S., Guccione, J.M. and Tseng, E.E. 2010. Comparison of porcine pulmonary and aortic root material properties. *Ann Thorac Surg.* **89**(6), pp.1981-1988.

Matuska, A.M. and McFetridge, P.S. 2015. The effect of terminal sterilization on structural and biophysical properties of a decellularized collagen-based scaffold; implications for stem cell adhesion. *Journal of biomedical materials research. Part B, Applied biomaterials.* **103**(2), pp.397-406.

Mavrilas, D. and Missirlis, Y. 1991. An approach to the optimization of preparation of bioprosthetic heart valves. *Journal of Biomechanics* **24**(5), pp.331-339.

Mazor, E. and Zilberman, M. 2017. Effect of gamma-irradiation sterilization on the physical and mechanical properties of a hybrid wound dressing. *Polymers for Advanced Technologies.* **28**(1), pp.41-52.

Mbithi, J.N., Springthorpe, V.S. and Sattar, S.A. 1990. Chemical disinfection of hepatitis A virus on environmental surfaces. *Applied and environmental microbiology.* **56**(11), pp.3601-3604.

McEvoy, B. and Rowan, N.J. 2019. Terminal sterilization of medical devices using vaporized hydrogen peroxide: a review of current methods and emerging opportunities. *Journal of Applied Microbiology.* **127**(5), pp.1403-1420.

McGregor, C., Byrne, G., Rahmani, B., Chisari, E., Kyriakopoulou, K. and Burriesci, G. 2016. Physical equivalency of wild type and galactose α 1,3 galactose free porcine pericardium; a new source material for bioprosthetic heart valves. *Acta Biomater.* **41**, pp.204-209.

McHugh, M. and Krukonis, V. 2013. *Supercritical fluid extraction: principles and practice.* Elsevier.

Mendibil, U., Ruiz-Hernandez, R., Retegi-Carrion, S., Garcia-Urquia, N., Olalde-Graells, B. and Abarrategi, A. 2020. Tissue-Specific Decellularization Methods: Rationale and Strategies to Achieve Regenerative Compounds. *International journal of molecular sciences.* **21**(15), p5447.

Mendoza-Novelo, B., Avila, E.E., Cauich-Rodríguez, J.V., Jorge-Herrero, E., Rojo, F.J., Guinea, G.V. and Mata-Mata, J.L. 2011. Decellularization of pericardial tissue and its impact on tensile viscoelasticity and glycosaminoglycan content. *Acta Biomaterialia.* **7**(3), pp.1241-1248.

Mercer, J.L., Benedicty, M. and Bahnson, H.T. 1973. The geometry and construction of the aortic leaflet. *Journal of Thoracic and Cardiovascular Surgery.* **65**(4), pp.511-518.

Michalski, D., Spielvogel, E., Puchta, J., Reimann, W., Barthel, H., Nitzsche, B., Mages, B., Jäger, C., Martens, H., Horn, A.K.E., Schob, S. and Härtig, W. 2020. Increased Immunosignals of Collagen IV and Fibronectin Indicate Ischemic Consequences for the Neurovascular Matrix Adhesion Zone in Various Animal Models and Human Stroke Tissue. *Frontiers in Physiology.* **11**.

Misfeld, M. and Sievers, H.-H. 2007. Heart valve macro- and microstructure. *Philosophical transactions of the Royal Society of London. Series B, Biological sciences.* **362**(1484), pp.1421-1436.

Moffat, D., Ye, K. and Jin, S. 2022. Decellularization for the retention of tissue niches. *Journal of Tissue Engineering.* **13**, p20417314221101151.

Mohapatra, S. 2017. Sterilization and Disinfection. pp.929-944.

Montero, D.A., Arellano, C., Pardo, M., Vera, R., Gálvez, R., Cifuentes, M., Berasain, M.A., Gómez, M., Ramírez, C. and Vidal, R.M. 2019. Antimicrobial properties of a novel copper-based composite coating with potential for use in healthcare facilities. *Antimicrobial Resistance & Infection Control.* **8**(1), p3.

Mostow, E.N., Haraway, G.D., Dalsing, M., Hodde, J.P. and King, D. 2005. Effectiveness of an extracellular matrix graft (OASIS Wound Matrix) in the treatment of chronic leg ulcers: a randomized clinical trial. *J Vasc Surg.* **41**(5), pp.837-843.

Mueller, N.J. 2022. Porcine cytomegalovirus: A very unwelcome stowaway. *Xenotransplantation.* **29**(3), pe12769.

Murata, K. 1981. Acidic glycosaminoglycans in human heart valves. *Journal of Molecular and Cellular Cardiology.* **13**(3), pp.281-292.

Neves, J.P., Gulbenkian, S., Ramos, T., Martins, A.P., Caldas, M.C., Mascarenhas, R., Guerreiroa, M., Matoso-Ferreira, A., Santos, R. and Monteiro, C. 1997. Mechanisms underlying degeneration of cryopreserved vascular homografts. *The Journal of Thoracic and Cardiovascular Surgery.* **113**(6), pp.1014-1021.

Nguyen, H., Morgan, D.A.F. and Forwood, M.R. 2007. Sterilization of allograft bone: effects of gamma irradiation on allograft biology and biomechanics. *Cell and Tissue Banking.* **8**(2), pp.93-105.

Nichols, A., Burns, D. and Christopher, R. 2009. Studies on the Sterilization of Human Bone and Tendon Musculoskeletal Allograft Tissue Using Supercritical Carbon Dioxide. *Journal of Orthopaedics.* **6**.

Nicodemus, G.D. and Bryant, S.J. 2008. Cell encapsulation in biodegradable hydrogels for tissue engineering applications. *Tissue engineering. Part B, Reviews.* **14**(2), pp.149-165.

Noble, C., Morse, D., Lerman, A. and Young, M. 2022. Evaluation of Pericardial Tissues from Assorted Species as a Tissue-Engineered Heart Valve Material. *Medical & Biological Engineering & Computing.* **60**(2), pp.393-406.

Noyce, J.O., Michels, H. and Keevil, C.W. 2006. Use of copper cast alloys to control Escherichia coli O157 cross-contamination during food processing. *Appl Environ Microbiol.* **72**(6), pp.4239-4244.

O'Brien, M.F., Goldstein, S., Walsh, S., Black, K.S., Elkins, R. and Clarke, D. 1999. The SynerGraft valve: a new acellular (nonglutaraldehyde-fixed) tissue heart valve for

autologous recellularization first experimental studies before clinical implantation. *Semin Thorac Cardiovasc Surg.* **11**(4 Suppl 1), pp.194-200.

Oh, J.K., Appleton, C.P., Hatle, L.K., Nishimura, R.A., Seward, J.B. and Tajik, A.J. 1997. The noninvasive assessment of left ventricular diastolic function with two-dimensional and Doppler echocardiography. *Journal of the American Society of Echocardiography : official publication of the American Society of Echocardiography* **10**(3), pp.246-270.

Otto, C.M. 2001. Clinical practice. Evaluation and management of chronic mitral regurgitation. *The New England Journal of Medicine.* **345**(10), pp.740-746.

Otto, C.M., Lind, B.K., Kitzman, D.W., Gersh, B.J. and Siscovick, D.S. 1999. Association of Aortic-Valve Sclerosis with Cardiovascular Mortality and Morbidity in the Elderly. *New England Journal of Medicine.* **341**(3), pp.142-147.

Paniagua Gutierrez, J.R., Berry, H., Korossis, S., Mirsadraee, S., Lopes, S.V., da Costa, F., Kearney, J., Watterson, K., Fisher, J. and Ingham, E. 2015. Regenerative potential of low-concentration SDS-decellularized porcine aortic valved conduits in vivo. *Tissue engineering. Part A.* **21**(1-2), pp.332-342.

Park, S., Lee, D.R., Nam, J.S., Ahn, C.W. and Kim, H. 2018. Fetal bovine serum-free cryopreservation methods for clinical banking of human adipose-derived stem cells. *Cryobiology.* **81**, pp.65-73.

Parsons, B.J. 2018. Free radical studies of components of the extracellular matrix: contributions to protection of biomolecules and biomaterials from sterilising doses of ionising radiation. *Cell and Tissue Banking.* **19**(2), pp.201-213.

Petersen, T.H., Calle, E.A., Zhao, L., Lee, E.J., Gui, L., Raredon, M.B., Gavrilov, K., Yi, T., Zhuang, Z.W., Breuer, C., Herzog, E. and Niklason, L.E. 2010. Tissue-engineered lungs for in vivo implantation. *Science.* **329**(5991), pp.538-541.

Petersen, T.H., Calle, E.A., Zhao, L., Lee, E.J., Gui, L., Raredon, M.B., Gavrilov, K., Yi, T., Zhuang, Z.W., Breuer, C., Herzog, E. and Niklason, L.E. 2010. Tissue-engineered lungs for in vivo implantation. *Science (New York, N.Y.).* **329**(5991), pp.538-541.

Piazza, N., de Jaegere, P., Schultz, C., Becker, A.E., Serruys, P.W. and Anderson, R.H. 2008. Anatomy of the aortic valvar complex and its implications for transcatheter implantation of the aortic valve. *Circulation. Cardiovascular Interventions.* **1**(1), pp.74-81.

Pierce, E.L., Siefert, A.W., Paul, D.M., Wells, S.K., Bloodworth, C.H.t., Takebayashi, S., Aoki, C., Jensen, M.O., Gillespie, M.J., Gorman, R.C., Gorman, J.H., 3rd and Yoganathan, A.P. 2016. How Local Annular Force and Collagen Density Govern Mitral Annuloplasty Ring Dehiscence Risk. *Ann Thorac Surg.* **102**(2), pp.518-526.

Pollock, J.D. and Makaryus, A.N. 2018. Physiology, Cardiac Cycle. *StatPearls.* Treasure Island (FL).

Prodan, Z., Mroczek, T., Sivalingam, S., Bennink, G., Asch, F.M., Cox, M., Carrel, T., Yakub, M.A., Nagy, Z., Skalski, J., Svanidze, O., Schutte, E., Verhees, L., Klersy, C.,

Virmani, R. and Sreeram, N. 2022. Initial Clinical Trial of a Novel Pulmonary Valved Conduit. *Seminars in Thoracic and Cardiovascular Surgery.* **34**(3), pp.985-991.

Qiu, Q.-Q., Leamy, P., Brittingham, J., Pomerleau, J., Kabaria, N. and Connor, J. 2009. Inactivation of bacterial spores and viruses in biological material using supercritical carbon dioxide with sterilant. *Journal of Biomedical Materials Research Part B: Applied Biomaterials.* **91B**(2), pp.572-578.

Quan, Y., Choi, K.D., Chung, D. and Shin, I.S. 2010. Evaluation of bactericidal activity of weakly acidic electrolyzed water (WAEW) against Vibrio vulnificus and Vibrio parahaemolyticus. *Int J Food Microbiol.* **136**(3), pp.255-260.

Rabotyagova, O.S., Cebe, P. and Kaplan, D.L. 2008. Collagen Structural Hierarchy and Susceptibility to Degradation by Ultraviolet Radiation. *Materials science & engineering. C, Materials for biological applications.* **28**(8), pp.1420-1429.

Rahman, S.M.E., Khan, I. and Oh, D.-H. 2016. Electrolyzed Water as a Novel Sanitizer in the Food Industry: Current Trends and Future Perspectives. *Comprehensive Reviews in Food Science and Food Safety.* **15**(3), pp.471-490.

Rajamannan, N.M., Evans, F.J., Aikawa, E., Grande-Allen, K.J., Demer, L.L., Heistad, D.D., Simmons, C.A., Masters, K.S., Mathieu, P., O'Brien, K.D., Schoen, F.J., Towler, D.A., Yoganathan, A.P. and Otto, C.M. 2011. Calcific aortic valve disease: not simply a degenerative process: A review and agenda for research from the National Heart and Lung and Blood Institute Aortic Stenosis Working Group. Executive summary: Calcific aortic valve disease-2011 update. *Circulation.* **124**(16), pp.1783-1791.

Rajamannan, N.M., Nealis, T.B., Subramaniam, M., Pandya, S., Stock, S.R., Ignatiev, C.I., Sebo, T.J., Rosengart, T.K., Edwards, W.D., McCarthy, P.M., Bonow, R.O. and Spelsberg, T.C. 2005. Calcified rheumatic valve neoangiogenesis is associated with vascular endothelial growth factor expression and osteoblast-like bone formation. *Circulation.* **111**(24), pp.3296-3301.

Ramachandran, G.N., Bansal, M. and Bhatnagar, R.S. 1973. A hypothesis on the role of hydroxyproline in stabilizing collagen structure. *Biochimica et biophysica acta.* **322**(1), pp.166-171.

Rauh, J., Despang, F., Baas, J., Liebers, C., Pruss, A., Gelinsky, M., Günther, K.P. and Stiehler, M. 2014. Comparative biomechanical and microstructural analysis of native versus peracetic acid-ethanol treated cancellous bone graft. *Biomed Res Int.* **2014**, p784702.

Redington, A.N. 2006. Determinants and assessment of pulmonary regurgitation in tetralogy of Fallot: practice and pitfalls. *Cardiology Clinics* **24**(4), pp.631-639, vii.

Reing, J.E., Brown, B.N., Daly, K.A., Freund, J.M., Gilbert, T.W., Hsiong, S.X., Huber, A., Kullas, K.E., Tottey, S., Wolf, M.T. and Badylak, S.F. 2010. The effects of processing methods upon mechanical and biologic properties of porcine dermal extracellular matrix scaffolds. *Biomaterials.* **31**(33), pp.8626-8633.

Rendic, S. and Guengerich, F.P. 2012. Summary of information on the effects of ionizing and non-ionizing radiation on cytochrome P450 and other drug metabolizing enzymes and transporters. *Curr Drug Metab.* **13**(6), pp.787-814.

Reul, H. and Talukder, N. 1989. *Heart valve mechanics* New York, NY:McGraw Hill The Heart

Ribeiro, N., Soares, G.C., Santos-Rosales, V., Concheiro, A., Alvarez-Lorenzo, C., García-González, C.A. and Oliveira, A.L. 2020. A new era for sterilization based on supercritical CO2 technology. *Journal of Biomedical Materials Research Part B: Applied Biomaterials.* **108**(2), pp.399-428.

Ribeiro, N., Soares, G.C., Santos-Rosales, V., Concheiro, A., Alvarez-Lorenzo, C., García-González, C.A. and Oliveira, A.L. 2020. A new era for sterilization based on supercritical CO(2) technology. *J Biomed Mater Res B Appl Biomater.* **108**(2), pp.399-428.

Rich, A. and Crick, F.H. 1961. The molecular structure of collagen. *J Mol Biol.* **3**, pp.483-506.

Rieder, B., Weihs, A.M., Weidinger, A., Szwarc, D., Nürnberger, S., Redl, H., Rünzler, D., Huber-Gries, C. and Teuschl, A.H. 2018. Hydrostatic pressure-generated reactive oxygen species induce osteoarthritic conditions in cartilage pellet cultures. *Scientific Reports.* **8**(1), p17010.

Rieder, E., Kasimir, M.-T., Silberhumer, G., Seebacher, G., Wolner, E., Simon, P. and Weigel, G. 2004. Decellularization protocols of porcine heart valves differ importantly in efficiency of cell removal and susceptibility of the matrix to recellularization with human vascular cells. *The Journal of Thoracic and Cardiovascular Surgery.* **127**(2), pp.399-405.

Rizzoli, G., Russo, R., Valente, S., Mazzucco, A., Valfré, C., Brumana, T., Aru, G., Rubino, M., Rocco, F. and Gallucci, V. 1984. Dehiscence of aortic valve prostheses: analysis of a ten-year experience. *Int J Cardiol.* **6**(2), pp.207-221.

Roberts, C.R., Roughley, P.J. and Mort, J.S. 1989. Degradation of human proteoglycan aggregate induced by hydrogen peroxide. Protein fragmentation, amino acid modification and hyaluronic acid cleavage. *Biochem J.* **259**(3), pp.805-811.

Rooney, P., Eagle, M., Hogg, P., Lomas, R. and Kearney, J. 2008. Sterilisation of skin allograft with gamma irradiation. *Burns.* **34**(5), pp.664-673.

Rosario, D.J., Reilly, G.C., Ali Salah, E., Glover, M., Bullock, A.J. and Macneil, S. 2008. Decellularization and sterilization of porcine urinary bladder matrix for tissue engineering in the lower urinary tract. *Regen Med.* **3**(2), pp.145-156.

Rossi, M.A. and Carillo, S.V. 1991. Cardiac hypertrophy due to pressure and volume overload: distinctly different biological phenomena? *Int J Cardiol.* **31**(2), pp.133-141.

Roy, S., Khanna, S., Nallu, K., Hunt, T.K. and Sen, C.K. 2006. Dermal wound healing is subject to redox control. *Molecular therapy : the journal of the American Society of Gene Therapy.* **13**(1), pp.211-220.

Rozeik, M., Wheatley, D. and Gourlay, T. 2014. The aortic valve: structure, complications and implications for transcatheter aortic valve replacement. *Perfusion.* **29**(4), pp.285-300.

Russell, N., Rives, A., Pelletier, M.H., Wang, T. and Walsh, W.R. 2015. The effect of supercritical carbon dioxide sterilization on the anisotropy of bovine cortical bone. *Cell Tissue Bank.* **16**(1), pp.109-121.

Russo, M., Taramasso, M., Guidotti, A., Pozzoli, A., K Von Segesser, L., Nietlispach, F. and Maisano, F. 2017. *The evolution of surgical valves.*

Sabbah, H.N., Hamid, M.S. and Stein, P.D. 1986. Mechanical Stresses on Closed Cusps of Porcine Bioprosthetic Valves: Correlation with Sites of Calcification. *The Annals of Thoracic Surgery.* **42**(1), pp.93-96.

Sacks, M.S. and Yoganathan, A.P. 2007. Heart valve function: a biomechanical perspective. *Philosophical Transactions of the Royal Society B: Biological Sciences.* **362**(1484), pp.1369-1391.

Sagripanti, J.L. and Kraemer, K.H. 1989. Site-specific oxidative DNA damage at polyguanosines produced by copper plus hydrogen peroxide. *J Biol Chem.* **264**(3), pp.1729-1734.

Sagripanti, J.L., Routson, L.B. and Lytle, C.D. 1993. Virus inactivation by copper or iron ions alone and in the presence of peroxide. *Appl Environ Microbiol.* **59**(12), pp.4374-4376.

Sampaio, R.O., Silva, F.C., Jr., Oliveira, I.S., Padovesi, C.M., Soares, J.A., Silva, W.M., Samorano Lde, P., Tarasoutchi, F., Spina, G.S. and Grinberg, M. 2009. Postoperative outcome of patients with prosthetic valve leak. *Arquivos brasileiros de cardiologia* **93**(3), pp.283-289.

Saremi, F., Gera, A., Yen Ho, S., Hijazi, Z.M. and Sánchez-Quintana, D. 2014. CT and MR Imaging of the Pulmonary Valve. *RadioGraphics.* **34**(1), pp.51-71.

Sattar, S., Springthorpe, V. and Rochon, M. 1998. A product based on accelerated and stabilized hydrogen peroxide: Evidence for broad-spectrum germicidal activity. *Canadian Journal of Infection Control* pp.123-130

Sawada, K., Terada, D., Yamaoka, T., Kitamura, S. and Fujisato, T. 2008. Cell removal with supercritical carbon dioxide for acellular artificial tissue. *Journal of Chemical Technology & Biotechnology: International Research in Process, Environmental & Clean Technology.* **83**(6), pp.943-949.

Schaner, P.J., Martin, N.D., Tulenko, T.N., Shapiro, I.M., Tarola, N.A., Leichter, R.F., Carabasi, R.A. and DiMuzio, P.J. 2004. Decellularized vein as a potential scaffold for vascular tissue engineering. *Journal of Vascular Surgery.* **40**(1), pp.146-153.

Scheffler, S.U., Gonnermann, J., Kamp, J., Przybilla, D. and Pruss, A. 2008. Remodeling of ACL allografts is inhibited by peracetic acid sterilization. *Clin Orthop Relat Res.* **466**(8), pp.1810-1818.

Schiros, C.G. 2012. *Biventricular Active Mesh Model of the Heart and Analysis of Morphologic Changes Toward Physiology and Pathologies*. thesis, Auburn University.

Schlein, J., Simon, P., Wollenek, G., Base, E., Laufer, G. and Zimpfer, D. 2021. Aortic valve replacement in pediatric patients: 30 years single center experience. *Journal of Cardiothoracic Surgery.* **16**(1), p259.

Schoen, F.J. 2008. Evolving concepts of cardiac valve dynamics: the continuum of development, functional structure, pathobiology, and tissue engineering. *Circulation.* **118**(18), pp.1864-1880.

Schoen, F.J. and Levy, R.J. 1999. Tissue heart valves: Current challenges and future research perspectives. *Journal of Biomedical Materials Research.* **47**(4), pp.439-465.

Seddon, A.M., Curnow, P. and Booth, P.J. 2004. Membrane proteins, lipids and detergents: not just a soap opera. *Biochimica et Biophysica Acta (BBA) - Biomembranes.* **1666**(1), pp.105-117.

Seo, Y., Jung, Y. and Kim, S.H. 2018. Decellularized heart ECM hydrogel using supercritical carbon dioxide for improved angiogenesis. *Acta Biomaterialia.* **67**, pp.270-281.

Setlow, P. 2006. Spores of Bacillus subtilis: their resistance to and killing by radiation, heat and chemicals. *J Appl Microbiol.* **101**(3), pp.514-525.

Sharony, R., Grossi, E.A., Saunders, P.C., Schwartz, C.F., Ciuffo, G.B., Baumann, F.G., Delianides, J., Applebaum, R.M., Ribakove, G.H., Culliford, A.T., Galloway, A.C. and Colvin, S.B. 2003. Aortic valve replacement in patients with impaired ventricular function. *Ann Thorac Surg.* **75**(6), pp.1808-1814.

Shearer, H., Ellis, M.J., Perera, S.P. and Chaudhuri, J.B. 2006. Effects of common sterilization methods on the structure and properties of poly(D,L lactic-co-glycolic acid) scaffolds. *Tissue Eng.* **12**(10), pp.2717-2727.

Sheridan, W.S., Duffy, G.P. and Murphy, B.P. 2012. Mechanical characterization of a customized decellularized scaffold for vascular tissue engineering. *Journal of the Mechanical Behavior of Biomedical Materials.* **8**, pp.58-70.

Shi, M., Chen, Z., Farnaghi, S., Friis, T., Mao, X., Xiao, Y. and Wu, C. 2016. Copper-doped mesoporous silica nanospheres, a promising immunomodulatory agent for inducing osteogenesis. *Acta biomaterialia.* **30**, pp.334-344.

Shin, S.Y., Calvisi, E.G., Beaman, T.C., Pankratz, H.S., Gerhardt, P. and Marquis, R.E. 1994. Microscopic and thermal characterization of hydrogen peroxide killing and lysis of spores and protection by transition metal ions, chelators, and antioxidants. *Appl Environ Microbiol.* **60**(9), pp.3192-3197.

Silindir Gunay, M. and Ozer, Y. 2009. *Sterilization methods and the comparison of E-Beam sterilization with gamma radiation sterilization.*

Silver, M.D., Lam, J.H., Ranganathan, N. and Wigle, E.D. 1971. Morphology of the human tricuspid valve. *Circulation.* **43**(3), pp.333-348.

Simmons, C.A., Grant, G.R., Manduchi, E. and Davies, P.F. 2005. Spatial heterogeneity of endothelial phenotypes correlates with side-specific vulnerability to calcification in normal porcine aortic valves. *Circulation Research.* **96**(7), pp.792-799.

Simon, P., Kasimir, M.T., Seebacher, G., Weigel, G., Ullrich, R., Salzer-Muhar, U., Rieder, E. and Wolner, E. 2003. Early failure of the tissue engineered porcine heart valve SYNERGRAFT in pediatric patients. *Eur J Cardiothorac Surg.* **23**(6), pp.1002-1006; discussion 1006.

Sloth, E., Houlind, K.C., Oyre, S., Kim, W.Y., Pedersen, E.M., Jorgensen, H.S. and Hasenkam, J.M. 1994. Three-dimensional visualization of velocity profiles in the human main pulmonary artery with magnetic resonance phase-velocity mapping. *American Heart Journal.* **128**(6 Pt 1), pp.1130-1138.

Smith, C.R., Leon, M.B., Mack, M.J., Miller, D.C., Moses, J.W., Svensson, L.G., Tuzcu, E.M., Webb, J.G., Fontana, G.P., Makkar, R.R., Williams, M., Dewey, T., Kapadia, S., Babaliaros, V., Thourani, V.H., Corso, P., Pichard, A.D., Bavaria, J.E., Herrmann, H.C., Akin, J.J., Anderson, W.N., Wang, D. and Pocock, S.J. 2011. Transcatheter versus surgical aortic-valve replacement in high-risk patients. *N Engl J Med.* **364**(23), pp.2187-2198.

Smith, D.B., Sacks, M.S., Pattany, P.M. and Schroeder, R. 1999. Fatigue-induced changes in bioprosthetic heart valve three-dimensional geometry and the relation to tissue damage. *J Heart Valve Dis.* **8**(1), pp.25-33.

Smith, J.D., Ogino, H., Hunt, D., Laylor, R.M., Rose, M.L. and Yacoub, M.H. 1995. Humoral immune response to human aortic valve homografts. *The Annals of Thoracic Surgery.* **60**, pp.S127-S130.

Somers, P., Cuvelier, C.A., Somer, F.D., Cornelissen, M., Cox, E., Verloo, M., Chiers, K. and van Nooten, G. 2009. Gamma radiation alters the ultrastructure in tissue-engineered heart valve scaffolds. *Tissue Eng Part A.* **15**(11), pp.3597-3604.

Song, J.J. and Ott, H.C. 2011. Organ engineering based on decellularized matrix scaffolds. *Trends in Molecular Medicine.* **17**(8), pp.424-432.

Souza, J.M., Giasson, B.I., Chen, Q., Lee, V.M. and Ischiropoulos, H. 2000. Dityrosine cross-linking promotes formation of stable alpha -synuclein polymers. Implication of nitrative and oxidative stress in the pathogenesis of neurodegenerative synucleinopathies. *J Biol Chem.* **275**(24), pp.18344-18349.

Spilimbergo, S. and Bertucco, A. 2003. Non-thermal bacterial inactivation with dense CO(2). *Biotechnol Bioeng.* **84**(6), pp.627-638.

Stamm, C., Anderson, R.H. and Ho, S.Y. 1998. Clinical anatomy of the normal pulmonary root compared with that in isolated pulmonary valvular stenosis. *Journal of the American College of Cardiology* **31**(6), pp.1420-1425.

Stapleton, T.W., Ingram, J., Katta, J., Knight, R., Korossis, S., Fisher, J. and Ingham, E. 2008. Development and characterization of an acellular porcine medial meniscus for use in tissue engineering. *Tissue Eng Part A.* **14**(4), pp.505-518.

Starr, A., Herr, R. and Wood, J.A. 1969. *Accumulated experience with the Starr-Edwards prosthesis 1960-1968.* Springfield, IL: L.A. Brewer III (Ed.).

Stassen, O., Muylaert, D.E.P., Bouten, C.V.C. and Hjortnaes, J. 2017. Current Challenges in Translating Tissue-Engineered Heart Valves. *Curr Treat Options Cardiovasc Med.* **19**(9), p71.

Stewart, S., Cianciotta, D., Hicks, G.L. and DeWeese, J.A. 1988. The Lillehei-Kaster aortic valve prosthesis. Long-term results in 273 patients with 1253 patient-years of follow-up. *The Journal of thoracic and cardiovascular surgery.* **95**(6), pp.1023-1030.

Stoffels, J.M., Zhao, C. and Baron, W. 2013. Fibronectin in tissue regeneration: timely disassembly of the scaffold is necessary to complete the build. *Cell Mol Life Sci.* **70**(22), pp.4243-4253.

Stradins, P., Lacis, R., Ozolanta, I., Purina, B., Ose, V., Feldmane, L. and Kasyanov, V. 2004. Comparison of biomechanical and structural properties between human aortic and pulmonary valve. *European Journal of Cardiothoracic Surgery : official journal of the European Association for Cardio-thoracic Surgery* **26**(3), pp.634-639.

Streeter, I. and de Leeuw, N.H. 2011. A molecular dynamics study of the interprotein interactions in collagen fibrils. *Soft matter.* **7**(7), pp.3373-3382.

Sutton, J.P., 3rd, Ho, S.Y. and Anderson, R.H. 1995. The forgotten interleaflet triangles: a review of the surgical anatomy of the aortic valve. *Ann Thorac Surg.* **59**(2), pp.419-427.

Swanson, M. and Clark, R.E. 1974. Dimensions and geometric relationships of the human aortic valve as a function of pressure. *Circulation Research.* **35**(6), pp.871-882.

Tao, M., Ao, T., Mao, X., Yan, X., Javed, R., Hou, W., Wang, Y., Sun, C., Lin, S., Yu, T. and Ao, Q. 2021. Sterilization and disinfection methods for decellularized matrix materials: Review, consideration and proposal. *Bioact Mater.* **6**(9), pp.2927-2945.

Theodoridis, K., Müller, J., Ramm, R., Findeisen, K., Andrée, B., Korossis, S., Haverich, A. and Hilfiker, A. 2016. Effects of combined cryopreservation and decellularization on the biomechanical, structural and biochemical properties of porcine pulmonary heart valves. *Acta Biomater.* **43**, pp.71-77.

Tortora, G.J. and Derrikson, B. 2011. *Principles of anatomy and physiology.* John Wiley and Sons Ltd.

Tudorache, I., Cebotari, S., Sturz, G., Kirsch, L., Hurschler, C., Hilfiker, A., Haverich, A. and Lichtenberg, A. 2007. Tissue engineering of heart valves: biomechanical and morphological properties of decellularized heart valves. *J Heart Valve Dis.* **16**(5), pp.567-573; discussion 574.

Tudorache, I., Horke, A., Cebotari, S., Sarikouch, S., Boethig, D., Breymann, T., Beerbaum, P., Bertram, H., Westhoff-Bleck, M., Theodoridis, K., Bobylev, D., Cheptanaru, E., Ciubotaru, A. and Haverich, A. 2016. Decellularized aortic homografts for aortic valve and aorta ascendens replacement. *Eur J Cardiothorac Surg.* **50**(1), pp.89-97.

Tweddell, J.S., Pelech, A.N., Frommelt, P.C., Mussatto, K.A., Wyman, J.D., Fedderly, R.T., Berger, S., Frommelt, M.A., Lewis, D.A., Friedberg, D.Z., Thomas, J.P., Jr., Sachdeva, R. and Litwin, S.B. 2000. Factors affecting longevity of homograft valves used in right ventricular outflow tract reconstruction for congenital heart disease. *Circulation.* **102**(19 Suppl 3), pp.Iii130-135.

Underwood, M.J., El Khoury, G., Deronck, D., Glineur, D. and Dion, R. 2000. The aortic root: structure, function, and surgical reconstruction. *Heart.* **83**(4), p376.

Uygun, B.E., Soto-Gutierrez, A., Yagi, H., Izamis, M.-L., Guzzardi, M.A., Shulman, C., Milwid, J., Kobayashi, N., Tilles, A., Berthiaume, F., Hertl, M., Nahmias, Y., Yarmush, M.L. and Uygun, K. 2010. Organ reengineering through development of a transplantable recellularized liver graft using decellularized liver matrix. *Nature Medicine.* **16**(7), pp.814-820.

Vafaee, T., Thomas, D., Desai, A., Jennings, L.M., Berry, H., Rooney, P., Kearney, J., Fisher, J. and Ingham, E. 2018. Decellularization of human donor aortic and pulmonary valved conduits using low concentration sodium dodecyl sulfate. *J Tissue Eng Regen Med.* **12**(2), pp.e841-e853.

Vafaee, T., Walker, F., Thomas, D., Roderjan, J.G., Veiga Lopes, S., da Costa, F.D., Desai, A., Rooney, P., Jennings, L.M., Fisher, J., Berry, H.E. and Ingham, E. 2022. Repopulation of decellularised porcine pulmonary valves in the right ventricular outflow tract of sheep: Role of macrophages. *J Tissue Eng.* **13**, p20417314221102680.

Vasan, R.S., Shrivastava, S., Vijayakumar, M., Narang, R., Lister, B.C. and Narula, J. 1996. Echocardiographic evaluation of patients with acute rheumatic fever and rheumatic carditis. *Circulation.* **94**(1), pp.73-82.

VeDepo, M.C., Buse, E.E., Quinn, R.W., Williams, T.D., Detamore, M.S., Hopkins, R.A. and Converse, G.L. 2017. Species-specific effects of aortic valve decellularization. *Acta Biomater.* **50**, pp.249-258.

Ventura, R.D., Padalhin, A.R., Park, C.M. and Lee, B.T. 2019. Enhanced decellularization technique of porcine dermal ECM for tissue engineering applications. *Materials Science and Engineering: C.* **104**, p109841.

Vesely, I. 1998. The role of elastin in aortic valve mechanics. *Journal of Biomechanics* **31**(2), pp.115-123.

Vincent, M., Duval, R.E., Hartemann, P. and Engels-Deutsch, M. 2018. Contact killing and antimicrobial properties of copper. *Journal of Applied Microbiology.* **124**(5), pp.1032-1046.

Vincent, M., Hartemann, P. and Engels-Deutsch, M. 2016. Antimicrobial applications of copper. *Int J Hyg Environ Health.* **219**(7 Pt A), pp.585-591.

Vogt, P.R., Stallmach, T., Niederhäuser, U., Schneider, J., Zünd, G., Lachat, M., Künzli, A. and Turina, M.I. 1999. Explanted cryopreserved allografts: a morphological and immunohistochemical comparison between arterial allografts and allograft heart valves from infants and adults1. *European Journal of Cardio-Thoracic Surgery.* **15**(5), pp.639-645.

von Woedtke, T. and Kramer, A. 2008. The limits of sterility assurance. *GMS Krankenhaushygiene interdisziplinar.* **3**(3), pp.Doc19-Doc19.

Walraevens, J., Willaert, B., De Win, G., Ranftl, A., De Schutter, J. and Sloten, J.V. 2008. Correlation between compression, tensile and tearing tests on healthy and calcified aortic tissues. *Med Eng Phys.* **30**(9), pp.1098-1104.

Wang, C.-H., Hsieh, D.-J., Periasamy, S., Chuang, C.-T., Tseng, F.-W., Kuo, J.-C. and Tarng, Y.-W. 2020. Regenerative porcine dermal collagen matrix developed by supercritical carbon dioxide extraction technology: Role in accelerated wound healing. *Materialia.* **9**, p100576.

Wang, H., Tibbitt, M.W., Langer, S.J., Leinwand, L.A. and Anseth, K.S. 2013. Hydrogels preserve native phenotypes of valvular fibroblasts through an elasticity-regulated PI3K/AKT pathway. *Proceedings of the National Academy of Sciences of the United States of America.* **110**(48), pp.19336-19341.

Waqanivavalagi, S.W.F.R., Bhat, S., Ground, M.B., Milsom, P.F. and Cornish, J. 2020. Clinical performance of decellularized heart valves versus standard tissue conduits: a systematic review and meta-analysis. *Journal of Cardiothoracic Surgery.* **15**(1), p260.

Wardle, M.D. and Renninger, G.M. 1975. Bactericidal effect of hydrogen peroxide on spacecraft isolates. *Applied microbiology.* **30**(4), pp.710-711.

Watanabe, N., Mizuno, M., Matsuda, J., Nakamura, N., Otabe, K., Katano, H., Ozeki, N., Kohno, Y., Kimura, T., Tsuji, K., Koga, H., Kishida, A. and Sekiya, I. 2019. Comparison of High-Hydrostatic-Pressure Decellularized Versus Freeze-Thawed Porcine Menisci. *Journal of Orthopaedic Research.* **37**(11), pp.2466-2475.

Watanabe, T., Furukawa, S., Hirata, J., Koyama, T., Ogihara, H. and Yamasaki, M. 2003. Inactivation of Geobacillus stearothermophilus spores by high-pressure carbon dioxide treatment. *Appl Environ Microbiol.* **69**(12), pp.7124-7129.

Waxler, B. and Rabito, S.F. 2003. Aprotinin: a serine protease inhibitor with therapeutic actions: its interaction with ACE inhibitors. *Curr Pharm Des.* **9**(9), pp.777-787.

Weaver, L., Michels, H.T. and Keevil, C.W. 2008. Survival of Clostridium difficile on copper and steel: futuristic options for hospital hygiene. *J Hosp Infect.* **68**(2), pp.145-151.

Weiss, S.J. 1989. Tissue destruction by neutrophils. *N Engl J Med.* **320**(6), pp.365-376.

Wells, D.L., Hopfensperger, D.J., Arden, N.H., Harmon, M.W., Davis, J.P., Tipple, M.A. and Schonberger, L.B. 1991. Swine influenza virus infections. Transmission from ill pigs to humans at a Wisconsin agricultural fair and subsequent probable person-to-person transmission. *Jama.* **265**(4), pp.478-481.

White, A., Burns, D. and Christensen, T.W. 2006. Effective terminal sterilization using supercritical carbon dioxide. *J Biotechnol.* **123**(4), pp.504-515.

White, L.J., Keane, T.J., Smoulder, A., Zhang, L., Castleton, A.A., Reing, J.E., Turner, N.J., Dearth, C.L. and Badylak, S.F. 2018. The impact of sterilization upon extracellular matrix hydrogel structure and function. *Journal of Immunology and Regenerative Medicine.* **2**, pp.11-20.

White, L.J., Taylor, A.J., Faulk, D.M., Keane, T.J., Saldin, L.T., Reing, J.E., Swinehart, I.T., Turner, N.J., Ratner, B.D. and Badylak, S.F. 2017. The impact of detergents on the tissue decellularization process: A ToF-SIMS study. *Acta Biomater.* **50**, pp.207-219.

Wiens, R.A. 2018. *Ensuring a reliable global Cobalt-60 supply for the next generation.* India: National Association for Applications of Radioisotopes and Radiation in Industry.

Wilcox, H.E., Korossis, S.A., Booth, C., Watterson, K.G., Kearney, J.N., Fisher, J. and Ingham, E. 2005. Biocompatibility and recellularization potential of an acellular porcine heart valve matrix. *J Heart Valve Dis.* **14**(2), pp.228-236; discussion 236-227.

Wiltz, D.C., Arevalos, C.A., Balaoing, L.R., Blancas, A.A., Sapp, M.C., Zhang, X. and Grande-Allen, K.J. 2013. Extracellular Matrix Organization, Structure, and Function. In.

Xu, H., Wan, H., Sandor, M., Qi, S., Ervin, F., Harper, J.R., Silverman, R.P. and McQuillan, D.J. 2008. Host response to human acellular dermal matrix transplantation in a primate model of abdominal wall repair. *Tissue Eng Part A.* **14**(12), pp.2009-2019.

Xue, Y., Sant, V., Phillippi, J. and Sant, S. 2017. Biodegradable and biomimetic elastomeric scaffolds for tissue-engineered heart valves. *Acta Biomaterialia.* **48**, pp.2-19.

Yacoub, M.H. and Cohn, L.H. 2004. Novel approaches to cardiac valve repair: from structure to function: Part I. *Circulation.* **109**(8), pp.942-950.

Yacoub, M.H. and Takkenberg, J.J. 2005. Will heart valve tissue engineering change the world? *Nature Clinical Practice. Cardiovascular Medicine.* **2**(2), pp.60-61.

Yang, B., Zhang, Y., Zhou, L., Sun, Z., Zheng, J., Chen, Y. and Dai, Y. 2010. Development of a porcine bladder acellular matrix with well-preserved extracellular bioactive factors for tissue engineering. *Tissue Eng Part C Methods.* **16**(5), pp.1201-1211.

Yanik, K., Karadag, A., Unal, N., Odabasi, H., Esen, S. and Gunaydin, M. 2015. An ınvestigation into the in-vitro effectiveness of electrolyzed water against various microorganisms. *International journal of clinical and experimental medicine.* **8**(7), pp.11463-11469.

Yarmush, M.L., Golberg, A., Serša, G., Kotnik, T. and Miklavčič, D. 2014. Electroporation-Based Technologies for Medicine: Principles, Applications, and Challenges. *Annual Review of Biomedical Engineering.* **16**(1), pp.295-320.

Yazici, E.Y. and Deveci, H. 2010. Factors affecting decomposition of hydrogen peroxide. In: *Proceedings of the XIIth international mineral processing symposium*: Mining Engineering Department, Hacettepe University Ankara, pp.609-616.

Yurchenco, P.D. 2011. Basement membranes: cell scaffoldings and signaling platforms. *Cold Spring Harb Perspect Biol.* **3**(2).

Zazo, J., Pliego, G., Blasco, S., Casas, J. and Rodriguez, J. 2010. Intensification of the Fenton Process by Increasing the Temperature. *Industrial & Engineering Chemistry Research.* **50**.

Zhang, X., Heinonen, S. and Levänen, E. 2014. Applications of supercritical carbon dioxide in materials processing and synthesis. *RSC Advances.* **4**(105), pp.61137-61152.

Zhang, Y., Ouyang, H., Lim, C.T., Ramakrishna, S. and Huang, Z.-M. 2005. Electrospinning of gelatin fibers and gelatin/PCL composite fibrous scaffolds. *Journal of Biomedical Materials Research Part B: Applied Biomaterials.* **72B**(1), pp.156-165.

Zheng, M.H., Chen, J., Kirilak, Y., Willers, C., Xu, J. and Wood, D. 2005. Porcine small intestine submucosa (SIS) is not an acellular collagenous matrix and contains porcine DNA: possible implications in human implantation. *J Biomed Mater Res B Appl Biomater.* **73**(1), pp.61-67.

Zou, Y. and Zhang, Y. 2012. Mechanical evaluation of decellularized porcine thoracic aorta. *J Surg Res.* **175**(2), pp.359-368.

# Appendix A: Equipment and Materials

**Supplementary Table 1. Chemicals and Reagents Used Throughout This Study.**

| Chemical/Reagent | Supplier |
|---|---|
| 1,9 dimethylene blue | Sigma-Aldrich |
| Absolute ethanol (200 Proof), molecular biology grade | Thermo Fisher Scientific Ltd. |
| Alpha (α) chymotrypsin | Sigma-Aldrich |
| Alternative: SDS powder | Sigma-Aldrich |
| Aprotinin (10000 KIU.mL-1) | Nordic Pharma |
| ATPLite-M assay | Perkin-Elmer |
| Benzonase® Nuclease HC, Purity > 90 % | Merck Chemicals |
| Calcium chloride (dihydrate) | Sigma-Aldrich |
| Calf thymus DNA (5 mg lyophilized) | Sigma-Aldrich |
| Chloramine T hydrate | Sigma-Aldrich |
| Chondroitin sulphate B | Sigma-Aldrich |
| Citric acid (monohydrate) | VWR International |
| Collagen gel | N/A |
| Cyanoacrylate contact adhesive | Sigma |
| Dako Fluorescence mounting medium | Dako |
| DAPI stain (4',6-Diamidino-2-phenylindole Dihydrochloride) | Sigma-Aldrich |
| Diaminoethanetetra-acetic acid disodium salt (EDTA) | Fisher Scientific Ltd |

| | |
|---|---|
| Dimethyl sulfoxide (DMSO) | Sigma-Aldrich |
| Disodium ethylenediaminetetraacetic acid (EDTA) | Thermo Fisher Scientific |
| Disodium ethylenediaminetetraacetic acid (Na2 EDTA) | Thermo Fisher Scientific |
| di-sodium hydrogen orthophosphate (anhydrous) | Millipore |
| DNeasy kit | Qiagen |
| DPX mountant | Atom Scientific |
| Dulbecco's PBS with Ca2+ & Mg2+ | Sigma |
| Dulbecco's PBS without Ca2+ & Mg2+ | Sigma |
| Dulbecco's Modified Eagle Medium (DMEM) | Sigma |
| Eosin Y | Merck Millipore |
| Ethanol | Fisher Scientific |
| Ethanol | Thermo Fisher Scientific Ltd. |
| Ethylene diamine tetra-acetic acid (EDTA) disodium salt | Thermo Fisher Scientific |
| Ethylenediaminetetraacetic acid | Thermo Fisher Scientific |
| Foetal bovine serum | Seralab |
| Foetal bovine serum (FBS) | Sera Lab |
| Formic acid 95-97% (w/v) | Sigma-Aldrich |
| Gentamycin solution | Sigma |
| Giemsa solution | Sigma |

| | |
|---|---|
| Glacial acetic acid | VWR International |
| Glasgows Minimal Essential Medium (GMEM) | Sigma |
| Hydrochloric acid | VWR International |
| Hydrochloric acid (6 M) | VWR International |
| L-Cysteine hydrochloride (10 G) | Sigma-Aldrich |
| L-cysteine hydrochloride anhydrous | Sigma-Aldrich |
| L-Glutamine (200mM) | Sigma |
| Low melting point agarose | Invitrogen |
| Magnesium chloride hexahydrate | VWR |
| Mayer's Haematoxylin | Atom Scientific |
| Neutral buffered formalin | Atom Scientific |
| Papain | Applichem |
| PBS (Dulbecco 'A' ) tablets | Oxoid |
| p-dimethylaminobenzaldehyde | Sigma-Aldrich |
| Penicillin (5000U/ml) / Streptomycin (5mg/ml) | Sigma |
| Peracetic acid (38 – 40 %) | Merck |
| Perchloric acid (60 %) | VWR International |
| PBS containing calcium and magnesium | Sigma-Aldrich |
| Propan-1-ol | VWR International |
| RNase A (17,500 U) | Qiagen |

| | |
|---|---|
| Scott's tap water substitute 10x concentrate | Atom Scientific |
| Sodium acetate (trihydrate) | Thermo Fisher Scientific Ltd |
| Sodium chloride | Thermo Fisher Scientific Ltd. |
| Sodium di-hydrogen orthophosphate monohydrate | VWR International |
| Sodium dodecyl sulphate (SDS) Solution (10 %) | Invitrogen |
| Sodium formate | Alfa Aesar |
| Sodium hydroxide | Thermo Fisher Scientific Ltd |
| Sodium hydroxide (6 M) | VWR International |
| Sodium hydroxide pellets | Sigma-Aldrich |
| Steri-Strip SkinClosure 3x75mm | Medisave |
| Thioglycollate medium USP | Oxoid |
| Trans-4-hydroxy-L-proline | Alfa Aesar |
| Trizma base (Tris) | Sigma-Aldrich |
| Trypsin | Sigma |
| Trypsin inhibitor | Sigma |
| Tryptose Phosphate broth | Sigma |
| UltraPure DNase/ RNase free distilled water | Invitrogen |
| Xylene | Atom Scientific |

**Supplementary Table 2. Equipment Used Throughout This Study.**

| Equipment | Supplier |
|---|---|
| Automatic pipettes | Any |
| Balance | Any |
| Block Heater | Labnet International Inc. |
| Centrifuge | MSR |
| Class II safety cabinet | N/A |
| Dissection kit | N/A |
| Freeze dryer | Thermo Scientific |
| Heater-stirrer | various |
| Histology water bath | Barnstead Electrothermal |
| Hog hair brush (approx. 15 mm) | Any |
| Hot wax oven | Raymond A Lamb |
| Hotplate | R.A. Lamb |
| Incubator | various |
| Incubator | Panasonic |
| Inverted microscope | Olympus UK |
| Magnetic stirrer | Stuart scientific |
| Micro plate spectrophotometer | Thermo Scientific |
| Microtome | Leica |
| Nalgene 500 mL PP wide mouth jar | Thermo Fisher Scientific Ltd. |
| Nanodrop spectrophotometer | Labtech |

| | |
|---|---|
| Orbital shaker (10 mm orbit) | Grant-bio |
| pH meter | Jenway |
| Plate reader | Hidex |
| Shaking oven | Stuart Scientific |
| Small vacuum autoclave | Priorclave Ltd |
| Stainless steel sieve | Any |
| Table shaker | IKA |
| Tissue processor | Leica |
| Water bath | Grant |
| Wax dispenser | Raymond A Lamb |
| Whirly mixer | Thermo Fisher Scientific |

**Supplementary Table 3. Labware and Consumables Used Throughout This Study.**

| Material | Supplier |
|---|---|
| Bijou tubes | Scientific Laboratory Supplies |
| Cotton Wool | Any |
| Duran bottles (0.25, 0.5, 1 and 2 L) | Scientific Laboratory Supplies |
| Feather S35 microtome blade | Fisher Scientific |
| Fine tip stainless steel forceps | R.A. Lamb |
| Flat bottomed 96 well plate | Scientific laboratory supplies |
| Histology moulds | Raymond A Lamb |

| | |
|---|---|
| Long hair brush No6 | R.A. Lamb |
| Micro tube 1.5ml, loop cap - Simport | VWR International |
| Narrow neck 60 mL glass medicine bottles with metal lid | FBS media stores |
| Para film | Fisher Scientific |
| Pipette man | Various |
| Plastic histology cassettes | Thermo Fisher Scientific Ltd. |
| Polypropylene universal (sure seal, 30 mL) | Scientific Laboratory Supplies |
| Qualitative filter paper circles | N/A |
| Serological pipette (25 mL) | Sarstedt |
| Single use filter unit 0.22 μm 33 mm | Merck Millipore |
| Six well tissue culture plates | Thermo Fisher Scientific Ltd. |
| Sterile containers (60, 150 and 250 mL) | Scientific Laboratory Supplies |
| Sterile syringe (50 mL) | Terumo |
| Superfrost Microscope Slide | SLS |
| Superfrost Plus Microscope Slide | SLS |
| Syringe filter unit (0.22 μm) | Millipore |
| Tissue culture plate (6 well) | Nunc |
| TopSeal 96 well plate | Perkin Elmer |
| White, 96 well Optiplate | Perkin Elmer |